

References

1. R.K. Ibrahim, M. Hayyan, M.A. Alsaadi, A.H. Shaliza, *Environ. Sci. Pollut. Res.*, **223**, **2016**, 13754-13788.
2. T. Hussain, A. Wahab, *J. Clean. Prod.*, **198**, **2018**, 806-819.
3. S. Mandal, A. Kuhikrishnan, N.S. Bolan, H. Wijesekara, R. Naidu, *Environmental Materials and Waste*, ed. M.N.V. Prasad, K. Shih, Elsevier, **2016**, vol., ch. 4, pp.73-89.
4. A.L. Srivastav, M. Ranjan, *Inorganic Pollutants in Water*, ed. P. Devi, P. Singh, S.K. Kansal, Elsevier, **2020**, ch. 1, pp. 1-15.
5. S. Velusamy, A. Roy, S. Sundaram, T.K. Mallick, *Chem Rec.*, **21**, **2021**, 1570-1610.
6. B. Leillis, C.Z. Favaro-Polonia, J.A. Pamphile, J.C. Polonio, *Biotechnol. Res. Innov.*, **3**, **2019**, 275-290.
7. A. Azanaw, B. Birlie, B. Teshome, M. Jemberie, *Case Stud. Chem. Environ.*, **6**, **2022**, 100230.
8. B. Pizzicato, S. Pacifico, D. Cayuela, G. Mijas, M. Riba-Moliner, *Molecules.*, **28**, **2023**, 5954.
9. T. Sudare, S. Tamura, H. Tanaka, F. Hayashi, K. Teshima, *Inorg. Chem.*, **58**, **2019**, 15710-15719.
10. G. Rathee, S. Kohli, S. Panchal, N. Singh, A. Awasthi, S. Singh, A. Singh, S. Hooda, R. Chandra, *ACS Omega.*, **5**, **2020**, 23967-23974.
11. T. Jiang, C. Liu, L. Liu, J. Hong, M. Dong, X. Deng, *RSC Adv.*, **6**, **2016**, 91720-91727.
12. S. Yu, G. Choi, J.H. Choy, *Nanomaterials.*, **13**, **2023**, 1102.
13. N. Dewangan, W.M. Hui, S. Jayaprakash, A.R. Bawah, A.J. Poerjoto, T. Jie, A. Jangam, K. Hidajat, S. Kawi, *Catal. Today.*, **356**, **2020**, 490-513.
14. L. Vigna, A. Nigro, A. Verna, I.V. Ferrari, S.L. Marasso, S. Bocchini, M. Fontana, A. Chiodoni, C.F. Pirri, M. Cocuzza, *ACS Omega.*, **6**, **2021**, 20205-20217.
15. A. Mohammad, H. Abdolvand, S.A.A. Najafabadi, F. Najaddehbashi, S. Beigi-Boroujeni, P. Makvandi, H. Daemi, *Appl. Bio Mater.*, **5**, **2022**, 5800-5815.
16. S.K. Pillai, P. Kleyi, M.D. Beer, P. Mudaly, *Appl Clay Sci.*, **199**, **2020**, 105868.
17. P. Lyu, L. Li, X. Huang, G. Wang, C. Zhu, *Sci. Total Environ.*, **823**, **2022**, 153743.
18. U.A. Mohanty, D.P. Sahoo, L. Paramanik, K. Parida, *Sustainable Energy & Fuels*, **7**, **2023**, 1145-1186.
19. S.V. Vassiley, D. Baxter, L.K. Andersen, C.G. Vassileva, *Fuel.*, **105**, **2013**, 40-76.
20. F.C. Silva, N.C. Cruz, L.A.C. Tarelho, S.M. Rodrigues, *J. Clean. Prod.*, **214**, **2019**, 112-124.
21. N.S. Samanta, P.P. Das, P. Mondal, M. Changmai, M.K. Purkait, *J. Indian Chem. Soc.*, **99**, **2022**, 100761.
22. G. Yadav, N. Yadav, M. Ahmaruzzaman, *RSC Adv.*, **13**, **2023**, 23197-23210.
23. O.J. Olatoyan, M.A. Kareem, A.U. Adebajo, S.O.A. Olawale, K.T. Alao, *Hybrid Advances.*, **4**, **2023**, 100076.
24. M. Zubair, H.A. Aziz, I. Ihsanullah, M.A. Ahmad, M.A. Al-Harhi, *Chemosphere*, **307**, **2022**, 136054.
25. H. Bian, M. Wang, J. Han, X. Hu, H. Xia, L. Wang, C. Fang, C. Shen, Y.B. Man, M.H. Wong, S. Shan, J. Zhang, *Chemosphere*, **324**, **2023**, 138333.
26. S. Sonal, B.K. Mishra, *Chem. Eng. J.*, **424**, **2021**, 130509.
27. Z. Milavanovic, S. Lazarevic, I. Jankovic-Castvan, Z. Radovanovic, S. Cvetkovic, D. Janackovic, R. Petrovic, *Water*, **15**, **2023**, 2376.

28. M.A. Khan, *Groundw. Sustain. Dev.*, 11, **2020**, 100427.
29. A. Grover, R. Kaur, I. Mohiuddin, A.K. Malik, J.S. Aulakh, Y.F. Tsang, K.H. Kim, *Environ Res.*, 177, **2019**, 108605.
30. A. Kumar, U. Dixit, K. Singh, S.P. Gupta, M.S.J. Beg, *Dyes and Pigments-Novel Applications and Waste Treatment*, ed. R. Papadakis, Intech open, **2021**, ch. 1, pp. 1-3.
31. J.A. Rippon, D.J. Evans, *Handbook of Natural Fibres-Processing and Applications*, ed. R.M. Kozlowski, Elsevier, **2012**, vol. 2, ch. 3, pp. 63-140.
32. E. Hagan, J. Poulin, *Herit. Sci.*, 9, **2021**, 33.
33. S.S. Affat, *University of Thi-Qar Journal of Science*, 8, **2021**, 130-135.
34. A. Gurses, M. Acikyildiz, K. Gunes, M.S. Gurses, *Dyes and Pigments, Springer briefs in Molecular Science*, Springer Cham, **2016**, ch. 2, 13-29.
35. H. Mustroph, *Dyes and Pigments.*, 208, **2023**, 110783.
36. R. Khanum, R.A.S. Ali, H.R. Rangaswamy, S.R.S. Kumar, A.G. Prashantha, A.S. Jagadisha, *Results Chem.*, 5, **2023**, 100890.
37. L.D.S. Yadav, *Organic Spectroscopy*, Springer Dordrecht, **2005**, ch. 2, pp. 7-51.
38. IARC Monographs on the Evaluation of Carcinogenic Risks to Humans, **2010**, Vol. 99.
39. M. Hagos, M. Redi-Abshiro, B.S. Chandravanshi, E.E. Yaya, *Int J Anal Chem.*, 2022, **2022**, 9363692.
40. S. Benkhaya, S. M' rabbet, A. E. Harfi, *Inorg. Chem. Commun.*, 115, **2020**, 107891.
41. A. Gurses, M. Acikyildiz, K. Gunes, M.S. Gurses, *Dyes and Pigments, Springer briefs in Molecular Science*, Springer Cham, **2016**, ch. 3, 31-45.
42. N. Sekar, *Handbook of Textile and Industrial Dyeing-Principles Processes and Types of Dyes*, ed. M. Clark, Elsevier, **2011**, vol. 1, ch. 15, pp. 486-514.
43. W.R. Remington, E.K. Gladding, *J. Am. Chem. Soc.*, 72, **1950**, 2553-2559.
44. R. Al-Tohamy, S.S. Ali, F. Li, K.M. Okasha, Y.A.G. Mahmoud, T. Elsamahy, H. Jiao, Y. Fu, J. Sun, *Ecotoxicol. Environ. Saf.*, 231, **2022**, 113160.
45. A. Zannat, M.N. Uddin, S.T. Mahmud, R. Mia, T. Ahmed, *Renewable Dyes and Pigments*, ed. S.U. Islam, Elsevier, **2023**, ch. 13, 271-287.
46. K.H. Prabhu, A.S. Bhute, *J. Nat. Prod. Plant Resour.*, 2, **2012**, 649-664.
47. J. Robinson, *J. Soc. Dye.*, 111, **1995**, 172-175.
48. J.J. Lee, W.S. Shim, I.S. Kim, J.P. Kim, *Fibres and Polym.*, 6, **2005**, 244-249.
49. U.H. Siddiqua, S. Ali, M. Iqbal, T. Hussain, *J. Mol. Liq.*, 241, **2017**, 839-844.
50. D.M. Lewis, *Handbook of Textile and Industrial Dyeing-Principles Processes and Types of Dyes*, ed. M. Clark, Elsevier, **2011**, vol.1, ch. 9, 303-364.
51. J. Koh, *Textile Dyeing*, ed. P. Hauser, Intechopen, **2011**, ch.10, 195-220.
52. A.K. Roy Choudhury, *Handbook of Textile and Industrial Dyeing-Applications of Dyes*, ed. M. Clark, Elsevier, **2011**, vol. 2, ch. 2, 40-128.
53. V.K. Garg, M. Amita, R. Kumar, R. Gupta, *Dyes and Pigm.*, 63, **2004**, 243-250.
54. M.M.H. Elzahar, M. Bassyouni, *Sci. Rep.*, 13, **2023**, 15750.
55. T. Hussain, A. Wahab, *J. Clean Prod.*, 198, **2018**, 806-819.
56. D.A. Yaseen, M. Scholz, *International Journal of Environmental Science and Technology.*, 16, **2019**, 1193-1226.
57. S. Khan, A. Malik, *Environmental Deterioration and Human Health*, ed. A. Malik, E. Grohmann, R. Akhtar, Springer, Dordrecht, **2014**, ch. 4, 55-71.

58. D. Sivakumar, D. Shankar, A.J.R.V. Prathima, M. Valarmathi, *Int. J. Environ. Sci.*, 3, **2013**, 1223.
59. P.A. Carneiro, G.A. Umbuzeiro, D. P. Oliveira, M.V.B. Zanoni, *J. Hazard. Mater.*, 174, **2010**, 694-699.
60. D. Bhatia, N.R. Sharma, R. Kanwar, J. Singh, *Appl. Water Sci.*, 8, **2018**, 1-12.
61. T.M. Farook, S. Manderia, K. Manderia, *Int. Res. J. Environment Sci.*, 1, **2012**, 41-45.
62. M.A.S. Jiku, A. Singha, M. Faruquee, M.A. Rahaman, M.A. Alam, M. Ehsanullah, *Acta Ecol. Sin.*, 41, **2021**, 358-364.
63. E.S. Armengol, A.B. Kerezsi, F. Laffleur, *Int. Immunopharmacol.*, 110, **2022**, 109043.
64. J. Sharma, S. Sharma, V. Soni, *Reg. Stud. Mar. Sci.*, 62, **2023**, 102911.
65. S. Velusamy, A. Roy, S. Sundaram, T.K. Mallick, *Chem Rec.*, 21, **2021**, 1570-1610.
66. D.M. Leme, F.L. Primo, G.G. Gobo, C.R.V. da Costa, A.C. Tedesco, D.P. de Oliveira, *Journal Toxicol Environ Health A.*, 78, **2015**, 466-480.
67. S. Sudarshan, V.S. Bharti, S. Harikrishnan, S.P. Sukla, G.R. Bhuvanewari, *Arch. Microbiol.*, 204, **2022**, 658.
68. O.V. Ayebidun, A.O. Ajibare, *Bulletin of the National Research Centre.*, 47, **2023**, 86.
69. R. Sinha, R. Jindal, C. Faggio, *Appl. Sci.*, 11, **2021**, 3507.
70. M. Alaguprathana, M. Poonkothai, *Environ. Sci. Pollut. Res.*, 28, **2021**, 17602-17612.
71. H.B. Siama, A.C. Bouket, Z. Pourhassan, F.N. Alenezi, A. Silini, H. Cherif-Silini, T. Oszako, L. Luptakova, P. Golinska, L. Belbahri, *Appl. Sci.*, 11, **2021**, 6255.
72. L. Pereira, M. Alves, *Environmental Protection Strategies for Sustainable Development, Strategies for Sustainability*, ed. A. Malik, E. Grohmann, Springer, Dordrecht, **2011**, ch. 4, pp. 111-162.
73. P. Saharan, V. Kumar, I. Kaushal, A. Mittai, S.K. Shukla, D. Kumar, A.K. Sharma, H. Om, *Environ. Sci. Pollut. Res.*, 30, **2023**, 45677-45700.
74. S. Ahuja, *Separation Science and Technology*, ed. S. Ahuja, **2019**, Elsevier, vol. 11, ch. 1, pp. 1-12.
75. Commission Regulation (EC) No 552/2009 OF 22 June 2009 amending Regulation (EC) No 1907/2006 of the European Parliament and of the Council on the Registration, Evaluation, Authorisation and Restriction of Chemicals (REACH) as regards Annex XVII, *Official Journal of European Union*, 164, **2009**, 7-31.
76. I. Jasmin, P. Mallikarjuna, *Environ. Monit. Assess.*, 186, **2014**, 935-948.
77. K. Xu, G. Tian, *Int J Environ Res Public Health.*, 19, **2022**, 9978.
78. U. Nimkar, *Curr. Opin. Green Sustain. Chem.*, 9, **2018**, 13-17.
79. *Textile Industry Wastewater Discharge Quality Standards: Literature Review-Zero Discharge of Hazardous Chemicals Programme*, **2015**.
80. M. Roy, R. Saha, *Intelligent Environmental Data Monitoring for Pollution Management*, ed. S. Bhattacharyya, N.K. Mondal, P. Kromer, Elsevier, **2021**, ch. 6, pp. 127-160.
81. E. Idaka, T. Ogawa, H. Horitsu, C. Yatome, *Eur. J. Appl. Microbiol.*, 15, **1982**, 141-143.
82. R. Majumdar, W.K. Shaikh, S. Chakraborty, S. Chowdhury, *Microbial Biodegradation and Bioremediation-Techniques and Case Studies for Environmental Pollution.*, ed. S. Das, H.R. Dash, Elsevier, **2021**, ch. 12, 241-261.
83. M.M. El-Sheekh, M.M. Gharieb, G.W. Abou-El-Souod, *International Biodeterioration & Biodegradation.*, 63, **2009**, 699-704.

84. J.M. Khaled, S.A. Alyahya, R. Govindan, C.K. Chelliah, M. Maruthupandy, N.S. Alharbi, S. Kadaikunnan, R. Issac, S. Murugan, W.J. Li, *Environ. Res.*, 207, **2022**, 112211.
85. L. Xu, J. Sun, M.A. Qaria, L. Gao, D. Zhu, *Catalysts.*, 11, **2021**, 955.
86. R.V. Khandare, S.P. Govindwar, *Biotechnol. Adv.*, 33, **2015**, 1697-1714.
87. A. Movafeghi, A.R. Khataee, Z. Moradi, F. Vafaei, *Int. J. Phytoremediation.*, 18, **2016**, 337-347.
88. G. Bal, A. Thakur, *Mater Today: Proc.*, 50, **2022**, 1575-1579.
89. X.R. Xu, H.B. Li, W.H. Wang, J.D. Gu, *Chemosphere*, 59, **2005**, 893-898.
90. L. Bilinska, K. Blus, M. Bilinska, M. Gmurek, *Catalysts.*, 10, **2022**, 611.
91. P.V. Nidheesh, R. Gandhimathi, S.T. Ramesh, *Environ. Sci. Pollut. Res.*, 20, **2013**, 2099-2132.
92. B. Viswanathan, *Current Catalysis.*, 7, **2018**, 99-121.
93. S. Ammar, M. Asma, N. Oturan, *Curr. Org. Chem.*, 16, **2012**, 1978-1985.
94. S. Singh, V.C. Srivastava, I.D. Mall, *J. Phys. Chem. C.*, 117, **2013**, 15229-15240.
95. M.M. Hassan, C.M. Carr, *Chemosphere.*, 209, 2018, 201-219.
96. S.S. Moghaddam, M.R.A. Maghaddam, A. Arami, *J. Hazard. Mater.*, 175, **2010**, 651-657.
97. A.K. Badawi, M.A. Elkodous, G.A.M. Ali, *RSC Adv.*, 11, **2021**, 36528-36553.
98. P. Moradihamedani, *Polym. Bull.*, 79, **2022**, 2603-2631.
99. M. Suzuki, *Fundamentals of Adsorption*, ed. M.D. Levan, Springer, Boston, MA, **1996**, vol. 356, ch. 1, pp. 3-15.
100. W.J. Thomas, B. Crittenden, *Adsorption Technology & Design*, Elsevier, **1998**, ch. 1, 1-7.
101. E. Robens, *Stud. Surf. Sci. Catal.*, 87, **1994**, 109-118.
102. S. Dutta, B. Gupta, S.K. Srivastava, A.K. Gupta, *Mater. Adv.*, 2, **2021**, 4497-4531.
103. P. Pourhakkak, A. Taghizadeh, M. Taghizadeh, M. Ghaedi, S. Haghdoost, *Interface Science and Technology.*, Elsevier, **2021**, vol. 33, ch. 1, pp. 1-70.
104. H.B. Patterson, *Bleaching and Purifying Fats and Oils-Theory and Practice*, ed. G.R. List, Elsevier, **2009**, ch. 2, pp. 53-67.
105. T.A. Saleh, *Adsorption technology and surface science*, Elsevier, **2022**, vol. 34, ch. 2, pp. 39-64.
106. J. He, M. Wei, B. Li, Y. Kang, D.G. Evans, X. Duan, *Layered Double Hydroxides*, ed. X. Duan, D.G. Evans, Springer, Berlin, Heidelberg, **2005**, vol. 119, ch. 1, pp. 89-119.
107. G. Arrabito, A. Bonasera, G. Prestopino, A. Orsini, A. Mattocchia, E. Martinelli, B. Pignataro, P.G. Medaglia, *Crystals*, 9, **2019**, 361.
108. G. Mishra, B. Dash, S. Pandey, *Appl Clay Sci.*, 153, **2018**, 172-186.
109. Z. Chen, Q. Fan, M. Huang, H. Colfen, *CrystEngComm.*, 24, **2022**, 4639-4655.
110. L. Jin, X. Zhou, F. Wang, X. Ning, Y. Wen, B. Song, C. Yang, D. Wu, X. Ke, L. Peng, *Nat. Commun.*, 13, **2022**, 6093.
111. X. Fang, C. Chen, H. Jia, Y. Li, J. Liu, Y. Wang, Y. Song, T. Du, L. Liu, *J. Ind. Eng. Chem.*, 95, **2021**, 16-27.
112. D. Tonelli, I. Gualandi, E. Musella, E. Scavetta, *Nanomaterials.*, 11, **2021**, 725.
113. Z. Jiang, J. Wu, X. Liu, H. Yu, C. Jiao, J. Shen, Y. Pei, *New J. Chem.*, 45, **2021**, 14580-14588.
114. Z. Liu, R. Ma, M. Osada, N. Iyi, Y. Ebina, K. Takada, T. Sasaki, *J. Am. Chem. Soc.*, 128, 2006, 4872-4880.
115. L. Dubnova, R. Danhel, V. Meinhardova, V. Korolova, L. Smolakova, T. Kondratowicz, O. Kiktyanin, L. Capek, *Front Chem.*, 9, **2021**, 803764.
116. A. Inayat, M. Klumpp, W. Schwieger, *Appl Clay Sci.*, 51, **2011**, 452-459.

117. Z.P. Xu, G.Q. Lu, *Chem. Mater.*, 17, **2005**, 1055-1062.
118. Z. Yang, F. Wang, C. Zhang, G. Zeng, Z. Yu, Y. Zhong, H. Wang, F. Cui, *RSC Adv.*, 6, **2016**, 79415-79436.
119. N. Almoisheer, F.A. Alseroury, R. Kumar, M. Aslam, M.A. Barakat, *RSC Adv.*, 9, **2019**, 560-568.
120. G. Darmograi, B. Prelot, G. Layrac, D. Tichit, G. Martin-Gassin, F. Salles, J. Zajac, *J. Phys. Chem. C.*, 119, **2015**, 23388-23397.
121. D. Yuan, L. Zhou, D. Fu, *Appl. Phys. A.*, 123, **2017**, 146.
122. J. Nie, D. Zhi, Y. Zhou, *Sorbents Materials for Controlling Environmental Pollution- Current State and Trends*, ed. A. Nunez-Delgado, Elsevier, **2021**, ch. 8, pp. 163-187.
123. I. Haziri, D. Chebli, A. Bouguettoucha, S. Rohani, A. Amrane, *Arab. J. Sci. Eng.*, 44, **2019**, 5245-5261.
124. M. Shamim, K. Dana, *Int J Environ Sci Technol.*, 15, **2018**, 1275-1284.
125. R.M.M. dos Santos, R.G.L. Goncalves, V.R.L. Constantino, C.V. Santilli, P.D. Borges, J. Tronto, F.G. Pinto, *Appl. Clay Sci.*, 140, **2017**, 132-139.
126. N.D. Setti, N. Jouini, Z. Derriche, *J. Phys. Chem. Solids.*, 71, **2010**, 556-559.
127. C. Lei, M. Pi, P. Kuang, Y. Guo, F. Zhang, *J. Colloid Interface Sci.*, 496, **2017**, 158-166.
128. D. Bharali, R.C. Deka, *Colloids Surf A: Physicochem. Eng. Asp.*, 525, **2017**, 64-76.
129. B. Zhang, Z. Dong, D. Sun, T. Wu, Y. Li, *J. Indus. Eng. Chem.*, 49, **2017**, 208-218.
130. S. Lei, S. Wang, B. Gao, Y. Zhan, Q. Zhao, S. Jin, G. Song, X. Lyu, Y. Zhang, Y. Tang, *J. Colloid Interface Sci.*, 557, **2020**, 181-190.
131. M. Bouraada, M. Lafjah, M.S. Ouali, L.C. de Menorval, *J. Hazard. Mater.*, 153, **2008**, 911-918.
132. M. Bouraada, M. Lafjah, M.S. Ouali, L.C. de Menorval, *J. Hazard. Mater.*, 163, **2009**, 463-467.
133. D. Zhang, M.Y. Zhu, J.G. Yu, H.W. Meng, F.P. Jiao, *Trans. Nonferrous Met. Soc. China.*, 27, **2017**, 2673-2681.
134. H. Starukh, S. Levytska, *Appl. Clay Sci.*, 180, **2019**, 105183.
135. A. Kheradmand, M. Negarestani, S. Kazemi, H. Shayesteh, S. Javanshir, H. Ghiasinejad, *Sci. Rep.*, 12, **2022**, 14623.
136. M. Zubair, I. Ihsanullah, H.A. Aziz, M.A. Ahmad, M.A. Al-Harhi, *Bioresour. Technology.*, 319, **2021**, 124128.
137. M. Zubair, M.S. Manzar, N.D. Muazu, I. Anil, N.I. Blaisi, M.A. Al-Harhi, *Appl. Clay Sci.*, 190, **2020**, 105587.
138. M. Zubair, I. Ihsanullah, H.A. Aziz, M.A. Ahmad, M.A. Al-Harhi, *Environ. Technol. Innov.*, 23, **2021**, 101614.
139. L. Meili, P.V. Lins, C.L.P.S. Zanta, J.I. Soletti, L.M.O. Ribeiro, C.B. Dornelas, T.L. Silva, M.G.A. Vieira, *Appl. Clay Sci.*, 168, **2019**, 11-20.
140. N.R. Palapa, T. Taher, B.R. Rahayu, R. Mohadi, A. Rachmat, A. Lesbani, *Bull. Chem. React. Eng.*, 15, **2020**, 525-537.
141. J. Missau, D.A. Bertuol, E.H. Tanabe, *Appl. Clay Sci.*, 214, **2021**, 106297.
142. X.F. Li, R.X. Li, K.X. Wang, *J. Ind. Eng. Chem.*, 126, **2023**, 270-282.
143. H. Wang, W. Zhao, Y. Chen, Y. Li, *Bioresour. Technol.*, 315, **2020**, 123834.
144. S. Natarajan, V. Anitha, G.P. Gajula, V. Thiagarajan, *ACS Omega.*, 5, **2020**, 3181-3193.

145. R. Tabatabaeian, M. Dinari, H.M. Aliabadi, *Carbohydr. Polym.*, 257, **2021**, 117628.
146. Q. Yan, Z. Zhang, Y. Zhang, A. Umar, Z. Guo, D. O'Hare, Q. Wang, *Eur. J. Inorg. Chem.*, 2015, **2015**, 4182-4191.
147. T. Taher, R. Putra, N.R. Palapa, A. Lesbani, *Chem. Phys. Lett.*, 777, **2021**, 138712.
148. Q. Sun, M. Tang, P.V. Hendriksen, B. Chen, *J. Alloys Compd.*, 829, **2020**, 154552.
149. L. Adlnasab, M. Ezoddin, M.A. Karimi, N. Hatamikia, *Res. Chem. Intermed.*, 44, **2018**, 3249-3265.
150. N. Ghanbari, H. Ghafuri, *Environ. Technol. Innov.*, 26, **2022**, 102377.
151. M. Abbasi, M.M. Sabzehmeidani, M. Ghaedi, R. Jannesar, A. Shokrollahi, *Mater. Sci. Eng. B.*, 267, **2021**, 115086.
152. F. Mohamed, M.R. Abukhadra, M. Shaban, *Sci. Total Environ.*, 640-641, **2018**, 352-363.
153. J. Zhao, Q. Huang, M. Liu, Y. Dai, J. Chen, H. Huang, Y. Wen, X. Zhu, X. Zhang, Y. Wei, *J Colloid Interface Sci.*, 505, **2017**, 168-177.
154. R. Khalili, M. Ghaedi, M. Parvinnia, M.M. Sabzehmeidani, *Surf. Interfaces.*, 23, **2021**, 100976.
155. S. Benhaya, S. M' rabbet, S, A.E. Harfi, *Inorg. Chem. Commun.*, 115, **2020**, 107891.
156. K. Abdellaoui, I. Pavlovic, C. Barriga, *ChemEngineering.*, 3, **2019**, 41.
157. R. Krishnamoorthy, A. Roy Choudhury, P. Arul Jose, K. Suganya, M. Senthikumar, J. Prabhakaran, N.O. Gopal, J. Choi, K. Kim, R. Anandham, T. Sa, *Appl. Sci.*, 11, **2021**, 379.
158. T. Shindhal, P. Rakholiya, S. Varjani, A. Pandey, H.H. Ngo, W. Guo, H.Y. Ng, M.J. Taherzadeh, *Bioengineered.*, 12, **2020**, 70-87.
159. W. Konicki, D. Sibera, U. Narkiewicz, *Sep Sci Technol.*, 53, **2018**, 1295-1306.
160. S.K. Sela, A.K.K. Nayab-Ul-Hossain, S.Z. Hussain, N. Hasan, *Clean. Eng. Technol.*, 1, **2020**, 100021.
161. B. Lellis, C.Z. Favaro-Polonio, J.A. Pamphile, J.C. Polonio, *Biotechnol. Res. Innov.*, 3, **2019**, 275-290.
162. J.N. Wekoye, W.C. Wanyonyi, P.T. Wangila, M.K. Tonui, *Environmental Chemistry and Ecotoxicology.*, 2, **2020**, 24-31.
163. S. Farhadi, F. Manteghi, R. Tondfehr, *Monatshe. Chem.*, 150, **2019**, 193-205.
164. B. Sherino, S.N.A. Halim, S. Shahabuddin, S. Mohamad, *S. Sep Sci Technol.*, 56, **2021**, 330-343.
165. N. Ali, A. Said, F. Ali, F. Raziq, Z. Ali, M. Bilal, L. Reinert, T. Begum, H.M.N. Iqbal, *Water Air Soil Pollut.*, 231, **2020**, 1-16.
166. M.R. Gadekar, M.M. Ahammed, *Appl. Sci.*, 10, **2020**, 1-8.
167. S. Natarajan, V. Anitha, G.P. Gajula, V. Thiagarajan, *ACS Omega.*, 5, **2020**, 3181-3193.
168. K. Ikehata, Y. Zhao, H.V. Kulkarni, Y. Li, S.A. Snyder, K.P. Ishida, M.A. Anderson, *Environ. Sci. Technol.*, 52, **2018**, 8588-8595.
169. Q. Wang, A. Tang, L. Zhong, X. Wen, P. Yan, J. Wang, *Powder Technol.*, 339, **2018**, 872-881.
170. R. Lafi, L. Gzara, R.H. Lajimi, A. Hafiane, *Chem. Eng. Process.: Process Intensif.*, 132, **2018**, 105-113.
171. N. Elhadiri, M. Benchanaa, R. Chikri, *J. Chem.*, 2020, **2020**, 2096834.
172. G. Moussavi, M. Mahmoudi, *J. Hazard. Mater.*, 168, **2019**, 806-812.
173. M.R. Abukhadra, A.S. Mohamed, *Silicon.*, 11, **2019**, 1635-1647.
174. X.S. Hu, R. Liang, G. Sun, *J. Mater. Chem. A.*, 6, **2018**, 17612-17624.

175. B. Mao, B. Sidhureddy, A.R. Thirupathi, P.C. Wood, A. Chen, *New J. Chem.*, 44, **2020**, 4519-4528.
176. M. Munir, M.F. Nazar, M.N. Zafar, M. Zubair, M. Asfaq, A. Hosseini-Bandegharai, S.U. Khan, A. Ahmad, *ACS Omega.*, 5, **2020**, 16711-16721.
177. M. Mohapi, J.S. Sefadi, M.J. Mochane, S.I. Magagula, K. Lebelo, *Crystals*, 10, **2020**, 957
178. M. Daud, A. Hai, F. Banat, M.B. Wazir, M. Habib, G. Bharath, M.A. Al-Harathi, *J. Mol. Liq.*, 288, **2019**, 110989.
179. R.K. Mahmoud, M. Taha, A. Zaher, R.M. Amin, *Sci. Rep.*, 11, 2021, 1-19.
180. S. Sonal, B.K. Mishra, *Chem. Eng. J.*, 424, **2021**, 130509.
181. R. Torres-Caban, C.A. Vega-Olivencia, N. Mina-Camilde, *Appl. Sci.*, 9, **2019**, 4531.
182. J.M. Jabar, Y.A. Odusote, K.A. Alabi, I.B. Ahmed, *Appl. Water Sci.*, 10, **2020**, 1-11.
183. I. Langmuir, *J. Am. Chem. Soc.*, 40, **1918**, 1361-1403.
184. S. Das, S.K. Dash, K.M. Parida, *ACS Omega.*, 3, **2018**, 2532-2545.
185. H.M.F. Freundlich, *J. Phys. Chem.*, 57, **1906**, 385-471.
186. M.I. Temkin, *Adv. Catal.*, 28, **1979**, 173-291.
187. O. Redlich, D.L. Peterson, *J. Phys. Chem.*, 63, **1959**, 1024-1024.
188. S. Sonal, P. Prakash, B.K. Mishra, G.C. Nayak, *RSC Adv.*, 10, **2020**, 13783-13798.
189. Y.S. Ho, G. McKay, *Process biochem.*, 34, **2020**, 451-465.
190. W.J. Weber, J.C. Morris, *J. Sanit. Eng. Div.*, 89, **1963**, 31-59.
191. M. Benjelloun, Y. Miyah, G.A. Evrendilek, F. Zerrouq, S. Lairini, *Arab. J. Chem.*, 14, **2021**, 103031.
192. S. Vahidhabanu, A.I. Adeogun, B.R. Babu, *ACS Omega.*, 4, **2019**, 2425-2436.
193. R. Benhiti, A.A. Ichou, A. Zaghoul, R. Aziam, G. Carja, M. Zerbet, F. Sinan, M. Chiban, *Environ. Sci. Pollut. Res.*, 27, **2020**, 45767-45774.
194. A. Nuryadin, T. Imai, *Glob. J. Environ. Sci.*, 7, **2021**, 485-502.
195. J. Poonosamy, F. Brandt, M. Stekiel, P. Kegler, M. Klinkenberg, B. Winkler, V. Vinograd, *Appl. Clay Sci.*, 151, **2018**, 54-65.
196. A.K. Avila-Martinez, J.H. Roque-Ruiz, J. Torres-Perez, N.A. Medellin-Castillo, S.Y. Reyes-Lopez, *Environ. Technol. Innov.*, 18, **2020**, 100760.
197. R. Shabbir, A. Gu, J. Chen, M.M. Khan, P. Wang, Y. Jiao, Z. Zhang, Y. Liu, Y. Yang, *Int J Environ Anal Chem.*, **2020**, 1-18.
198. O.S. Travkina, M.R. Agliullin, R.Z. Kuvatova, I.N. Pavlova, N. Narender, B.I. Kutepov, *J. Porous Mater.*, 26, **2018**, 995-1004.
199. B. Priyadarshini, T. Patra, T.R. Sahoo, *J Magnes. Alloys.*, 9, **2021**, 478-488.
200. V.R. Magri, A. Duarte, G.F. Perotti, V.R.L. Constantino, *Chemengineering*, 3, **2019**, 55.
201. S. Naseem, B. Gevers, R. Boldt, F.J.W.J. Labuschagne, A. Leuteritz, *RSC Adv.*, 9, **2019**, 3030-3040.
202. C. Hobbs, S. Jaskaniec, E.K. McCarthy, C. Downing, K. Opelt, K. Guth, A. Shmeliov, M.C.D. Mourad, K. Mandel, V. Nicolosi, *NPJ 2D Mater. Appl.*, 2, **2018**, 1-10.
203. J. Zhu, Z. Zhu, H. Zhang, H. Lu, Y. Qiu, *RSC Adv.*, 9, **2019**, 2284-2291.
204. P. Lackner, Z. Zou, S. Mayr, U. Diebold, M. Schmid, *Phys. Chem. Chem. Phys.*, 21, **2019**, 17613-17620.
205. Z. Azdad, L. Marot, L. Moser, R. Steiner, E. Meyer, E. *Sci. Rep.*, 8, **2018**, 1-6.
206. G. Rathee, A. Awasthi, D. Sood, R. Tomar, V. Tomar, R. Chandra, *Sci. Rep.*, 9, **2019**, 1-14.

207. A.E. Khanchaoui, M. Sajieddine, M. Mansori, A. Essoumhi, *Int J Environ Anal Chem.*, 102, **2020**, 1-19.
208. S. Popa, M.E. Radulescu-Grad, A. Perdivara, G. Mosoarca, *Sci. Rep.*, 11, **2021**, 1-9.
209. A. Sharma, Z.M. Siddiqui, S. Dhar, P. Mehta, D. Pathania, *Sep. Sci. Technol.*, 54, **2019**, 916-929.
210. Y. Lv, L. Gao, S. Feng, S.; Wang, Y. Qiao, Q. Li, *Sep. Sci. Technol.*, 54, **2019**, 2625-2637.
211. N.I. Blaisi, M. Zubair, Ihsanullah, S. Ali, T.S. Kazeem, M.S. Manzar, W. Al-Kutti, M.A. Al Harthi, *Environ. Sci. Pollut. Res.*, 25, **2018**, 34319-34331.
212. N.K. Gupta, M. Saifuddin, S. Kim, K.S. Kim, *J. Mol. Liq.*, 297, **2020**, 111935.
213. Y. Chen, C. Jing, X. Zhang, D. Jiang, X. Liu, B. Dong, L. Feng, Li.; S. Li, Y. Zhang, *J. Colloid Interface Sci.*, 548, **2019**, 100-109.
214. G.Y. Abo El-Reesh, A.A. Farghali, M. Taha, R.K. Mahmoud, *Sci. Rep.*, 10, **2020**, 1-20.
215. S. Dutta, B. Gupta, S.K. Srivastava, A.K. Gupta, *Mater. Adv.*, 2, **2021**, 4497-4531.
216. R. Gopinathan, A. Bhowal, C. Garlapati, *J. Chem. Eng. Data*, 64, **2019**, 2320-2328.
217. D. Bharali, R.C. Deka, *J. Environ. Chem. Eng.*, 5, **2017**, 2056-2067.
218. L. Jiang, Y. Liu, S. Liu, X. Hu, G. Zeng, X. Hu, S. Liu, S. Liu, B. Huang, M. Li, *Chem. Eng. J.*, 308, **2017**, 597-605.
219. P.K. Singh, S. Banerjee, A.L. Srivastava, Y.C. Sharma, *RSC Adv.*, 5, **2015**, 35365-35376.
220. X. Zheng, X. Li, J. Li, L. Wang, W. Jin, J. Liu, Y. Pei, K. Tang, *Int. J. Biol. Macromol.*, 107, **2018**, 283-289.
221. V.O. Shikuku, R. Zanella, C.O. Kowenje, F.F. Donato, N.M.G. Bandeira, O.D. Prestes, *Appl. Water Sci.*, 8, **2018**, 1-12.
222. Y. Li, H.Y. Bi, Y.S. Jin, X.Q. Shi, *RSC Adv.*, 4, **2014**, 58307-58314.
223. D.N. Ahmed, L.A. Naji, A.A.H. Faisal, N. Al-Ansari, M. Naushad, *Sci. Rep.*, 10, **2020**, 1-12.
224. E. Rapo, S. Tonk, *Molecules.*, 26, **2021**, 5419.
225. D. Brahma, H. Saikia, *Chem. Thermodyn. Therm. Anal.*, 7, **2022**, 100067.
226. H. Bensalah, S.A. Younssi, M. Ouammou, A. Gurlo, M.F. Bekheet, *J. Environ. Chem. Eng.*, 8, **2020**, 103807.
227. Q. Sun, B. Chen, *Ind. Eng. Chem. Res.*, 59, **2020**, 16838-16850.
228. J.O. Eniola, R. Kumar, A.A. Al-Rashdi, M.O. Ansari, M.A. Barakat, *ACS Omega.*, 4, **2019**, 18268-18278.
229. Y. Zheng, B. Cheng, W. You, J. Yu, W. Ho, *J. Hazard. Mater.*, 369, **2019**, 214-225.
230. F. Lu, D. Astruc, *Coord. Chem. Rev.*, 356, **2018**, 147-164.
231. A.A. Peláez-Cid, A.M. Herrera-González, M. Salazar-Villanueva, A. Bautista-Hernández, *J. Env. Manag.*, 181, **2016**, 269-278.
232. L. Wang, A. Wang, *J. Hazard. Mater.*, 147, **2007**, 979-85.
233. A.S. Özcan, B. Erdem, A. Özcan, *Colloids Surf. A Physicochem. Eng.* 266, **2005**, 73-81.
234. Y. Badr, M.G. Abd El-Wahed, M.A. Mahmoud, *J. Hazard. Mater.*, 154, **2008**, 245-53.
235. B. Lellis, C.Z. Fávaro-Polonio, J.A. Pamphile, J.C. Polonio, *Biotechnology. Res. Innov.*, 3, **2019**, 275-90.
236. Z. Yang, F. Wang, C. Zhang, G. Zeng, X. Tan, Z. Yu, H. Wang, F. Cui, *RSC Adv.*, 6, **2016**, 79415-79436.
237. A.Y. Zahrim, N. Hilal, *Water Resource. Ind.*, 3, **2013**, 3, 23-34.
238. C. Sahoo, A.K. Gupta, A. Pal, *Desalination.*, 181, **2005**, 91-100.
239. Q. Wang, A. Tang, L. Zhong, X. Wen, P. Yan, *Powder Technol.*, 339, **2018**, 872-881.

240. N. Al-Bastaki, *Chem. Eng. Process.*, 43, **2004**, 1561-1567.
241. A.Y. Zahrim, C. Tizaoui, N. Hilal, *Sep Sci Technol.*, 46, **2011**, 883-892.
242. I.M. Ahmed, M.S. Gasser, *Appl. Surf. Sci.*, 259, **2012**, 259, 650-656.
243. Z. Zaheer, A.A. Aisha, E.S. Aazam, *J. Mol. Liq.*, 283, **2019**, 283, 287-298.
244. A.S. Eltaweil, E.M. Abd El-Monaem, G.M. El-Subruiti, M.M. Abd El-Latif, A.M. Omer, *RSC Adv.* 10, **2020**, 19008-19019.
245. G. Mishra, B. Dash, S. Pandey, *Appl. Clay. Sci.*, 153, **2018**, 172-186.
246. Y.X. Chen, R. Zhu, Z.L. Xu, Q.F. Ke, Q. Zhang, Y.P. Guo, *J. Mater. Chem. B.*, 5, **2017**, 2245-2253.
247. Y. Jiang, Z. Hao, H. Luo, Z. Shao, Q. Yu, M. Sun, Y. Ke, Y. Chen, *RSC Adv.*, 8, **2018**, 11078-11086.
248. P. Wu, T. Wu, W. He, L. Sun, Y. Li, D. Sun, *Colloids Surf. A Physicochem. Eng. Asp.*, 436, **2013**, 436, 726-731.
249. B. Zhang, Z. Dong, D. Sun, T. Wu, Y.J. Li, *J. Ind. Eng. Chem.*, 49, **2017**, 208-218.
250. J. Li, S. Zhang, Y. Chen, C. Liu, X. Zhang, M. Yi, *RSC Adv.*, 46, **2017**, 29051-29057.
251. J. Qu, X. He, Z. Lei, Q. Zhang, X. Liu, *Solid State Sci.*, 74, **2017**, 125-130.
252. M. Meyn, K. Beneke, G. Lagaly, *Inorg. Chem.*, 29, **1990**, 5201-5207.
253. N. Iyi, K. Tamura, H. Yamada, *J. Colloid Interface Sci.*, 340, **2009**, 67-73.
254. S. Berner, P. Araya, J. Govan, H. Palza, *J. Ind. Eng. Chem.*, 59, **2018**, 134-140.
255. M.A.M. El-Mansy, I.S. Yahia, *Spectrochim. Acta A.*, 130, **2014**, 59-63.
256. G. Rathee, N. Singh, R. Chandra, *ACS Omega.*, 5, **2020**, 2368-2377.
257. Y. Chen, C. Jing, X. Zhang, D. Jiang, X. Liu, B. Dong, L. Feng, S. Li, Y. Zhang, *J. Colloid Interface Sci.*, 548, **2019**, 100-109.
258. S. Natarajan, R. Naresh, V. Thiagarajan, *Chemistry Select.*, 5, **2020**, 4165-4174.
259. I. Mindru, D. Gingasu, L. Patron, G. Marinescu, J.M. Calderon-Moreno, S. Preda, O. Oprea, N. Sultana, *Ceram. Int.*, 42, **2016**, 154-164.
260. S. Lei, S. Wang, B. Gao, Y. Zhan, Q. Zhao, S. Jin, G. Song, X. Lyu, Y. Zhang, Y. Tang, *J. Colloid Interface Sci.*, 577, **2020**, 181-190.
261. B.A. Fil, *Part. Sci. Technol.*, 34, **2016**, 118-126.
262. J. Khatri, P.V. Nidheesh, T.S.A. Singh, M.S. Kumar, *Chem. Eng. J.*, 348, **2018**, 67-73.
263. L. D. Ardila-Leal, R. A. Poutou-Pinales, A.M. Pedroza-Rodriguez, B. E. Quevedo-Hidalgo, *Molecules.*, 26, **2021**, 3813.
264. S. Srivastava, R. Sinha, D. Roy, *Aquat. Toxicol.* 66, **2004**, 319-329.
265. N. Hidayah, F.A. Bakar, N.A. Mahyudin, S. Faridah, M.S. Nur-Azura, M.Z. Zaman, *Int. Food Res. J.*, 20, **2013**, 1511.
266. P. S. David, A. Karunanithi, N. N. Fathima, *Environ. Sci. Pollut. Res.*, 27, **2020**, 45629-45638.
267. A.M. Saad, M. R. Abukhadra, A. K. Ahmed, A.M. Elzanaty, A.H. Mady, M.A. Betiha, J. J. Shim, A.M. Rabie, *J. Environ. Manage.*, 258, **2020**, 110043.
268. M.G. Abrile, M.L. Fiasconaro, M.E. Lovato, *SN Appl. Sci.*, 2, **2020**, 995.
269. V.S. Watwe, S.D. Kulkarni, P.S Kulkarni, *ACS Omega.*, 6, **2021**, 27288-27296.
270. K. Ikehata, Y. Zhao, H.V. Kulkarni, Y. Li, S.A. Snyder, K.P. Ishida, M.A. Anderson, *Environ. Sci. Technol.*, 52, **2018**, 8588-8595.
271. S.S. Mohanty, A. Kumar, *Sci. Rep.*, 11, **2021**, 1-5.
272. M.R. Gadekar, M.M. Ahammed, *Appl. Water Sci.* 10, **2020**, 1-8.
273. L.J. Martis, N. Parushuram, Y. Sangappa, *Environ. Sci.: Adv.*, 1, **2022**, 285-296.
274. S. Moosavi, C.W. Lai, S. Gan, G. Zamini, O.A. Pivehzhani, M.R. Johan, *ACS Omega.*, 5, **2020**, 20684-20697.
275. S. Yu, H. Pang, S. Huang, H. Tang, S. Wang, M. Qiu, Z. Chen, H. Yang, G. Song, D. Fu, B. Hu, X. Wang, *Sci. Total Environ.*, 800, **2021**, 149662.

276. S. Zhang, J. Wang, Y. Zhang, J. Ma, L. Huang, S. Yu, L. Chen, G. Song, M. Qiu, X. Wang, *Environ. Pollut.*, 291, **2021**, 118076.
277. M.E. Alouani, S. Alehyen, H.E. Hadki, H. Saufi, A. Elhalil, O.K. Kabbaj, M. Taibi, *Surf. Interfaces.*, 24, **2021**, 101136.
278. M.M. Sabzehmeidani, H. Karimi, M. Ghaedi, *New J. Chem.*, 44, **2020**, 5033-5048.
279. H. Abbasi-Asl, M.M. Sabzehmeidani, M. Ghaedi, *J. Environ. Chem. Eng.* **2021**, 9, 105963.
280. M.M. Sabzehmeidani, H. Karimi, M. Ghaedi, *Arab. J. Chem.*, 13, **2020**, 7583-7597.
281. L. Liang, F. Xi, W. Tan, X. Meng, B. Hu, X. Wang, *Biochar*. 3, **2021**, 255-281.
282. A. Machrouhi, M. Farnane, A. Elhalil, R. Elmoubarki, M. Abdennouri, S. Qourzal, H. Tounsadi, N. Barka, *J. Water Reuse Desalin.*, 8, **2018**, 522-531.
283. S. Yu, H. Tang, D. Zhang, S. Wang, M. Qiu, G. Song, D. Fu, B. Hu, X. Wang, *Sci. Total Environ.*, 811, **2022**, 152280.
284. R. Elmoubarki, W. Boumya, F.Z. Mahjoubi, A. Elhalil, M. Sadiq, N. Barka, *Mater. Today: Proc.*, 37, **2021**, 3871-3875.
285. J. Yu, Q. Wang, D. O'Hare, L. Sun, *Chem. Soc. Rev.* 46, **2017**, 5950-5974.
286. L. Yan, S. Gonca, G. Zhu, W. Zhang, X. Chen, *J. Mater. Chem. B.*, 7, **2019**, 5583-5601.
287. M. Zubair, H. A. Aziz, I. Ihsanullah, M.A. Ahmad, M.A. Al-Harhi, *Environ. Technol. Innov.*, 23, **2021**, 101614.
288. L. Zhang, S. Tang, C. Jiang, X. Jiang, Y. Guan, *ACS Appl. Mater. Interfaces.*, 10, **2018**, 43013-43030.
289. W. Qu, T. Yuan, G. Yin, S. Xu, Q. Zhang, H. Su, *Fuel.*, 249, **2019**, 45-53.
290. L. Meili, P.V. Lins, C.L.P.S. Zanta, J.I. Soletti, L.M.O. Ribeiro, C.B. Dornelas, T.L. Silva, M.G.A. Vieira, *Appl. Clay Sci.*, 168, **2019**, 11-20.
291. L. Mishra, G. Basu, *Handbook of Natural Fibres*, ed. R.M. Kozlowski, M. Mackiewicz-Talarczyk, Elsevier, **2020**, vol. 1, ch. 8, pp. 231-255.
292. R.K. Ahmad, S.A. Sulaiman, S. Yusup, S.S. Dol, M. Inayat, H.A. Umar, *Ain Shams Eng. J.*, 13, **2022**, 101499.
293. A. Kundu, B.S. Gupta, M.A. Hashim, G. Redzwan, *J. Clean. Prod.*, 105, **2015**, 420-427.
294. I. Langmuir, *J. Am. Chem. Soc.*, 40, **1918**, 1361-1403.
295. S. Das, S.K. Dash, K.M. P, *ACS Omega.*, 3, **2018**, 2532-2545.
296. H.M.F. Freundlich, *J. Phys. Chem.*, 57, **1906**, 385-471.
297. M.I. Temkin, *Adv. Catal.*, 28, **1979**, 173-291.
298. C.R. Lee, H.S. Kim, I.H. Jang, J.H. Im, N.G. Park, *ACS Appl. Mater. Interfaces.*, 3, **2011**, 1953-1957.
299. Y.S. Ho, G. Mckay, *Process Biochem.*, 34, **1999**, 451-465.
300. W.J. Weber, J.C. Morris, *Journal of the sanitary engineering division.*, 89, **1963**, 31-59.
301. F.C. Wu, R. L. Tseng, R.S. J, *Chem. Eng. J.*, 150, **2009**, 366-373.
302. S. Rani, R.K. Mahajan, *Arab. J. Chem.*, 9, **2016**, 1464-1477.
303. Z. Lu, W. Zhu, X. Lei, G.R. Williams, D. O'Hare, Z. Chang, X. Sun, Xue. D, *Nanoscale.*, 4, **2012**, 3640-3643.
304. M.F. Anuar, Y.W. Fen, M.H.M. Zaid, K.A. Matori, R.E.M. Khaidir, *Results Phys.*, 11, **2018**, 1-4.
305. Z.P. Diao, Y.X. Zhang, X.D. Hao, Z.Q. Wen, *Ceram. Int.*, 40, **2014**, 2115-2120.
306. L.Zhang, L.Y. Tu, Y. Liang, Q. Chen, Z.S. Li, C.H. Li, Z.H. Wang, W. Li, *RSC Adv.*, 8 **2018**, 42280-42291.
307. Y. Chen, C. Jing, X. Zhang, D. Jiang, X. Liu, B. D, L. Feng, S. Li, Y. Zhang, *J. Colloid Interface Sci.*, 548, **2019**, 100-109.
308. O.S. Bello, K.A. Adegoka, S.O. Fagbenro, O.S. Lameed. *Appl. Water Sci.*, 9, **2019**, 1-15.
309. L. Meili, P.V. Lins, C.L.P.S. Zanta, J.I. Soletti, L.M.O. Ribeiro, C.B. Dornelas, T.L. Silva, M.G.A. Vieira, *Appl. Clay Sci.*, 168, **2019**, 11-20.

310. M.F. Anuar, Y.W. Fen, M.H.M. Zaid, K.A. Matori, R.E.M. Khaidir, *Appl. Sci.*, 10, **2020**, 2128.
311. R. S. Piriya, R.M. Jayabalakrishnan, M. Maheshwari, K. Boomiraj, S. Qumabady, *Water Sci. Technol.*, 83, **2021**, 1167-1182.
312. Z. Hu, M.P. Srinivasan, *Microporous Mesoporous Mater.*, 27, **1999**, 11-18.
313. S. Kundu, M.K. Naskar, *Materials Advances.*, 2, **2021**, 3600-3612.
314. H. Ma, Z. Xu, W. Wang, X. Gao, H. Ma, *RSC Adv.*, 9, **2019**, 39282-39293.
315. G.Y. Abate, A.N. Alene, A.T. Habte, D.M. Getahun, *Environ. Syst. Res.*, 9, **2020**, 1-13.
316. N.A. Rahmat, A.A. Ali, N. Hussain, M.S. Muhamad, R.A. Kristanti, T. Hadibarata, *Water Air Soil Pollut.*, 227, 2016, 1-11.
317. N.K. Mondal, S. K, *Appl. Water Sci.*, 8, **2018**, 1-12.
318. L. Ai, C. Zhang, F. Liao, Y. Wang, M. Li, L. Meng, J. Jiang, *J. Hazard. Mater.*, 198, **2011**, 282-290.
319. K.G. Alpomie, F.A. Dawodu, K.O. Adebowale, *Alex. Eng. J.*, 54, **2015**, 757-767.
320. F. Ali, S. Bibi, N. Ali, Z. Ali, A. Said, Z.U. Wahab, M. Bilal, H.M.N. Iqbal, *Case Studies in Chemical and Environmental Engineering.*, 2, **2020**, 100025.
321. V.P. Dinh, T.D.T. Huynh, H.M. Le, V.D. Nguyen, V.A. Dao, N.Q. Hung, L.A. Tuyen, S. Lee, J. Yi, T.D. Nguyen, L.V. Tan, *RSC Adv.* 9, **2019**, 25847-25860.
322. I. Savva, O. Marinica, C.A. Papatryfonos, L. Vekas, T. Krasia-Christoforou, *RSC Adv.*, 5, **2015**, 16484-16496.
323. G. Rathee, A. Awasthi, D. Sood, R. Tomar, R. Chandra, *Sci. Rep.*, 9, **2019**, 1-14.
324. Y.T. Gebreslassie, *J. Anal. Methods Chem.*, 2020, **2020**, 7384675.
325. M.A. Ahmad, R. Alrozi, *Chem. Eng. J.*, 171, **2011**, 510-516.
326. V.O. Shikuku, R. Zanella, C.O. Kowenje, F.F. Donato, N.M.G. Bandeira, O.D. Prestes, *Appl. Water Sci.*, 8, **2018**, 1-12.
327. J.H. Potgieter, C. Pardesi, S. Pearson, *Environ. Geochem. Health.*, 43, **2021**, 2539-2550.
328. M. Maruthapandi, V.B. Kumar, J.H.T. Luong, A. Gedanken, *ACS Omega.*, 3, **2018**, 7196-7203.
329. K. Sharma, H.K. Sadhanala, Y. Mastai, Z. Porat, A. Gedanken, *Langmuir.*, 37, **2021**, 9927-9938.
330. E. Sterenzon, V.K. Vadivel, Y. Gerchman, T. Luxbacher, R. Narayanan, H. Mamane, *ACS Omega.*, 7, **2022**, 118-128.
331. F.C. Wu, R.L. Tseng, R.S. Juang, *Chem. Eng. J.*, 153, **2009**, 153, 1-8.
332. I. Ali, C. Peng, T. Ye, I. Naz, *RSC Adv.*, 8, **2018**, 8878-8897.
333. A.E. Ofomaja, E.B. Naidoo, A. Pholosi, *S. Afr. J. Chem. Eng.*, 32, **2020**, 39-55.
334. J.A. Mattson, H.B. Mark Jr, M.D. Malbin, W.J. Weber Jr, J.C. Crittenden, *J. Colloid Interface Sci.* 31, **1969**, 116-130.
335. R.W. Coughlin, F.S. Ezra, *Environ. Sci. Technol.*, 2, **1968**, 291-297.
336. T.G. Ambaye, M. Vaccari, E.D. V. Hullebusch, A. Amrane, S. Rtimi, *Int J Environ Sci Technol.*, 18, 2021, 3273-3294.
337. H. N. Tran, Y.F. Wang, S.J. You, H.P. Chao, *Process Saf. Environ. Prot.*, 107, **2017**, 168-180.
338. S. Fan, J. Tang, Y. Wang, H. Li, H. Zhang, J. Tang, Z. Wang, X. Li, *J. Mol. Liq.* 220, **2016**, 432-441.
339. M. Abbasi, M.M. Sabzehmeidani, M. Ghaedi, R. Jannesar, A. Shokrollahi, *Appl. Clay Sci.*, 203, **2021**, 105946.
340. R. Bagheri, M. Ghaedi, A. Asfaram, E.A. Dil, H. Javadian, *Polyhedron.*, 171, **2019**, 464-472.
341. R.K. Mahmoud, M. Taha, A. Zaher, R.M. Amin, *Sci. Rep.*, 11, **2021**, 1-19.
342. N.R. Palapa, N. Juleanti, N. Normah, T. Taher, A. Lesbani, *Bull. Chem. React. Eng. Catal.*, 15, **2020**, 653-661.
343. M.A. Nazir, M.A. Bashir, T. Najam, M.S. Javed, S. Suleman, S. Hussain, O.P. Kumar, S.S.A. Shah, *Microchem. J.*, 164, **2021**, 105973.

344. M.A. Nazir, T. Najam, M.S. Bashir, M.S. Javed, M.A. Bashir, M. Imran, U. Azhar, S.S.A. Shah, A.U. Rehman, *Korean J Chem Eng.*, 39, **2022**, 216-226.
345. A.F. Badri, P.M.S.B.N Siregar, N.R. Palapa, R. Mohadi, *Bull. Chem. React. Eng. Catal.*, 16, **2021**, 149-160.
346. A.A. Ahmad, M.A. Ahmad, N.K.E. Yahaya, J. Karim, *Arab. J. Chem.*, 14, **2021**, 103104
347. D. Brahma, H. Nath, D. Borah, M. Debnath, H. Saikia, *Inorg. Chem. Commun.*, 144, **2022**, 109878.
348. H. Halepoto, T. Gong, H. Memon, *Front. Environ. Sci.*, 10, **2022**, 1042256.
349. R. Al-Tohamy, S.S. Ali, F. Li, K.M. Okasha, Y.A.G. Mahmoud, T. Elsamahy, H. Jiao, Y. Fu, J. Sun, *Ecotoxicol Environ. Saf.*, 231, **2022**, 113160.
350. P.O. Oladoye, T.O. Ajiboye, E.O. Omotola, O.J. Oyewola, *Results Eng.*, 16, **2022**, 100678.
351. I. Khan, K. Saeed, I. Zekker, B. Zhang, A.H. Hendi, A. Ahmad, S. Ahmad, N. Zada, H. Ahmad, L.A. Shah, T. Shah, I. Khan, *Water.*, 14, **2022**, 242.
352. J. Clifton II, J.B. Leikin, *Am. J. Ther.*, 10, **2003**, 289.
353. F. Mashkoo, A. Nasar, *Cellulose.*, 27, **2020**, 2613.
354. M. Khodale, N. Ghasemi, B. Moradi, M. Rahimi, *J. Chem.*, **2013**, 383985.
355. D. Brahma, H. Nath, D. Borah, M. Debnath, H. Saikia, *Inorg Chem Commun.*, 144, **2022**, 109878.
356. Z.M. Lazim, T. Hadibarata, M. Puteh, Z. Yusop, *Water Air Soil Pollut.*, 226, **2015**, 34.
357. B.R. Freitas, J.O. Bragg, M.P. Orlandi, B.P. da Silva, I.V. Aoki, V.F.C. Lins, F. Cotting, *J. Mater. Res. Technol.*, 19, **2022**, 1332.
358. S. Suman, S. Gautam, *Energy Sources, Part A: Recovery, Utilization, and Environmental Effects.*, 39, **2017**, 761.
359. M.F. Anuar, Y.W. Fen, M.H.M. Zaid, K.A. Matori, R.E.M. Khaidir, *Results Phys.*, 11, **2018**, 1.
360. B.S. Yadav, S. Dasgupta, *Inorg Chem Commun.*, 137, **2022**, 109203.
361. P.S. Kumar, P.S.A. Fernando, R.T. Ahmed, R. Srinath, M. Priyadharshini, A.M. Vignesh, A. Thanjiappan, *Chem Eng Commun.*, 201, **2014**, 1526.
362. A.F. Hassan, G.A. El-Naggar, G. Esmail, W.A. Shaltout, *Appl. Surf. Sci. Adv.*, 13, **2023**, 100388.
363. U.J. Etim, S.A. Umoren, U.M. Eduok, *J. Saudi Chem. Soc.*, 20, **2016**, s-67.
364. M.Y. Chong, Y.J. Tam, *SN Appl. Sci.*, 2, **2020**, 187.
365. P. Sharma, R. Kaur, C. Baskar, W.J. Chung, *Desalination.*, 259, **2010**, 249.
366. M.H. Isa, L.S. Lang, F.A.H. Asaari, H.A. Aziz, N.A. Ramli, J.P.A. Dhas, *Dyes Pigm.*, 74, **2007**, 446.
367. S. Dogar, S. Nayab, M.Q. Farooq, A. Said, R. Kamran, H. Duran, B. Yameen, *ACS Omega.*, 5, **2020**, 15850.
368. N.T. Dinh, L.N.H. Vo, N.T.T. Tran, T.D. Phan, D.B. Nguyen, *RSC Adv.*, 11, **2021**, 20292.
369. S. Sultana, K. Islam, M.A. Hasan, H.M.J. Khan, M.A.R. Khan, A. Deb, M.A. Raihan, M.W. Rahman, *Environ. Nanotechnol.*, 17, **2022**, 100651.
370. O.S. Bello, K.A. Adegoke, S.O. Fagbenro, O.S. Lameed, *Appl. Water Sci.*, 9, **2019**, 189.
371. V.P. Singh, A. Susaniya, S.C. Jain, R. Vaish, *J. Chem. Educ.*, 98, **2021**, 3288.
372. T. Hongo, M. Moriura, Y. Hatada, H. Abiko, *ACS Omega.*, 6, **2021**, 21604.
373. O.M. Paska, C. Pacurariu, S.G. Muntean, *RSC Adv.*, 4, **2014**, 62621.
374. G.B. Balji, A. Surya, P. Govindaraj, G.M. Ponsakthi, *Inorg Chem Commun.*, 143, **2022**, 109708.
375. H.N. Tran, Y.F. Wang, S.J. You, H.P. Chao, *Process Saf. Environ.*, 107, **2017**, 168.
376. G.M. Ziarani, R. Moradi, N. Lashgari, H.G. Kruger, *Metal-Free Synthetic Organic Dyes*, Elsevier, **2018**, ch. 4, pp. 47-93.

377. D. Iark, A.J. dos Reis Buzzo, J.A.A. Garcia, V.G. Correa, C.V. Helm, R.C.G. Correa, R.A. Peralta, R.F.P.M. Moreira, A. Bracht, R.M. Peralta, *Bioresource Technology.*, 289, **2019**, 121655.
378. S.S. Yang, J.H. Kang, T.R. Xie, D.F. Xing, N.Q. Ren, S.H. Ho, W.M. Wu, *Journal of Cleaner Production.*, 227, **2019**, 33.
379. C.Y. Teh, P.M. Budiman, K.P.Y. Shak, T.Y. Wu, *Ind. Eng. Chem. Res.*, 55, **2016**, 4363.
380. A.B. Fradj, A. Boubakri, A. Hafiane and S.B. Hamouda, *Results in Chemistry.*, 2, **2020**, 100017.
381. S. Venkatesh, K. Venkatesh, A.R. Quaff, *Journal of applied research and technology.*, 15, **2017**, 340.
382. S.Y. Lee, D. Kang, S. Jeong, H.T. Do, J.H. Kim, *ACS Omega.*, 5, **2020**, 4233.
383. A.K. Badawi, M.A. Elkodous, G.A.M. Ali, *RSC Adv.*, 11, **2021**, 36528.
384. Y. Tanimoto, S.I. Noro, *RSC Adv.*, 11, **2021**, 23707.
385. R.A.E.G. Mansour, M.G. Sameda, A.A. Zaatout, *RSC Adv.*, 11, **2021**, 7851.
386. W. Huang, S. Wang, D. Li, *Sustainable Polymer Composites and Nanocomposites*, e.d Inamuddin, S. Thomas, R.K. Mishra, A.M. Asiri, Springer Cham, **2019**, pp. 519-556.
387. S. Radoor, J. Karayil, A. Jayakumar, D. Nandi, J. Parameswaranpillai, J. Lee, J.M. Shivanna, R. Nithya, S. Siengchin, *J. Polym. Environ.*, 30, **2022**, 3279.
388. P. Huang, J. Liu, F. Wei, Y. Zhu, X. Wang, C. Cao, W. Song, *Mater. Chem. Front.*, 1, **2017**, 1550.
389. M. Khorshidi, S. Asadpour, N. Sarmast and M. Dinari, *J. Mol. Liq.*, 348, **2022**, 118399.
390. M. Daud, A. Hai, F. Banat, M.B. Wazir, M. Habib, G. Bharath, M.A.A. Harthi, *J. Mol. Liq.*, 288, **2019**, 110989.
391. L.J. Foruzin, Z. Rezvani, B. Habibi, *Appl. Clay Sci.*, 188, **2020**, 105511.
392. G. Rathee, N. Singh, R. Chandra, *ACS Omega.*, 5, **2020**, 2368.
393. T.R.R. Timoteo, C.G. de Melo, L.J. de Alencar Danda, L.C.P.B.B. Silva, D.A.F. Fontes, P.C.D. Silva, C.S.B. Aguilera, L. da Paixao Siqueira, L.A. Rolim, P.J.R. Neto, *Appl. Clay Sci.*, 180, **2019**, 105197
394. D. Bharali, R.C. Deka, *J. Environ. Chem. Eng.*, 5, **2017**, 2056.
395. S.S. R, A. Jana and S. De, *J. Hazard. Mater.*, 373, **2019**, 791.
396. M.A. Iqbal, L. Sun and M. Fedel, *SN Appl. Sci.*, 1, **2010**, 1415.
397. Z. Wang, L. Zhang, P. Fang, L. Wang, W. Wang, *ACS Omega.*, 5, **2020**, 21805.
398. H. Lv, H. Rao, Z. Liu, Z. Zhou, Y. Zhao, H. Wei, Z. Chen, *J Energy Storage.*, 52, **2022**, 104940.
399. I. Langmuir, *J. Am. Chem. Soc.*, 40, **1918**, 1361.
400. H. Freundlich, *J. Phys. Chem.*, 57, **1906**, 385.
401. M.I. Temkin, V. Pyzhev, *Acta Physicochimica URSS.*, 12, **1940**, 327.
402. M.K. Raman, G. Muthuraman, *Asian J. Chem.*, 31, **2019**, 1255.
403. S. Lagergren, *Kungl. Svenska Vetenskapskad. Handl.*, 24, **1898**, 1.
404. Y.S. Ho, G. Mckay, *Chem. Eng. J.*, 70, **1998**, 115.
405. W.J. Weber, J.C. Morris, *J. Sanit. Eng. Div.*, 89, **1963**, 31.
406. J.M. Jabar, Y.A. Odusote, K.A. Alabi, I.B. Ahmed, *Appl. Water Sci.*, 10, **2020**, 136.
407. F.C. Wu, R.L. Tseng, R.S. Juang, *Chem. Eng. J.*, 153, **2009**, 1.
408. H.T.N. Thi, D.C. Nguyen, T.T. Nguyen, V.T. Tran, H.V. Nguyen, L.G. Bach, D.V.N. Vo, D.H. Nguyen, D.V. Thuan, S.T. Do, T.D. Nguyen, *Key Engineering Materials.*, 814, **2019**, 463.
409. D. Maiti, S. Mukhopadhyay, P.S. Devi, *ACS Sustainable Chem. Eng.*, 5, **2017**, 11255.
410. A. Li, H. Deng, C. Ye, Y. Jiang, *ACS Omega.*, 5, **2020**, 15152
411. B. Priyadarshini, T. Patra, T.R. Sahoo, *J. Magnes. Alloy.*, 9, **2021**, 478.
412. R. Lafi, K. Charradi, M.A. Djebbi, A.B.H. Amara, A. Hafiane, *Adv. Powder Technol.*, 27, **2016**, 232.
413. J. Li, H. Yu, X. Zhang, R. Zhu, L. Yan, *Front. Environ. Sci. Eng.*, 14, **2020**, 52.

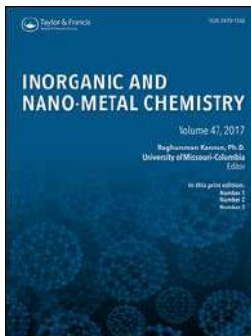
414. H.A. Tabti, B. Medjahed, M. Boudinar, A. Kadeche, N. Bouchikhi, A. Ramdani, S. Taleb, M. Adjdir, *Res. Chem. Intermed.*, 48, **2022**, 2683.
415. S. Chilukoti, T. Thangavel, *Inorg. Chem. Commun.*, 100, **2019**, 107.
416. I.M. Ahmed, M.S. Gasser, *Appl. Surf. Sci.*, 259, **2012**, 650.
417. T. Taher, R. Putra, N.R. Palapa, A. Lesbani, *Chem. Phys. Lett.*, 777, **2021**, 138712.
418. C. Suppaso, N. Pongkan, S. Intachai, M. Ogawa, N. Khaorapapong, *Appl. Surf. Sci.*, 213, **2021**, 106115.
419. P. Chakraborty, R. Nagarajan, *Appl. Surf. Sci.*, 118, **2015**, 308.
420. D. Brahma, K.P. Nath, M. Patgiri, H. Saikia, *Asian J. Chem.*, 35, 2022, 3215-3223.

List of publications/seminar presentation

1. Brahma, D.; Saikia, H.; (2022) Synthesis of ZrO₂/MgAl-LDH composites and evaluation of its isotherm, kinetics and thermodynamic properties in the adsorption of congo red dye. *Chemical Thermodynamics and Thermal Analysis*, 7: 100067, (Elsevier)
2. Brahma, D.; Nath, H.; Borah, D.; Debnath, M.; Saikia, H.; (2022) Coconut Husk Fabricated CoAl-Layered Double Hydroxide Composite for the Enhanced Sorption of Malachite Green Dye: Isotherm, Kinetics and Thermodynamic Studies, *Inorganic Chemistry Communications*, 144: 109878. (Elsevier)
3. Brahma, D.; Saikia, H.; (2023) Surfactants assisted synthesis of CuAl-sodium dodecyl sulfate layered double hydroxide and its adsorptive removal methyl red dye from aqueous solution, *Inorganic and Nano-Metal Chemistry*, (Taylor & Francis)
4. Brahma, D.; Nath, K.P.; Borah, Patgiri, M.; Saikia, H.; (2022) Synthesis of ternary CaNiAl-Layered Double Hydroxide as a potential adsorbent and its effective removal of Congo red dye, *Asian Journal of Chemistry*, 34: 3215-3223. (Asian Publication Corporation)

National and International Conferences

1. Surfactants assisted synthesis of CuAl-sodium dodecyl sulfate layered double hydroxide and its adsorptive removal of methyl red dye from aqueous solution. National Conferences on Advances in Sustainable Chemistry and Material Science (ASCMS-2022), Bodoland University, 29-30th April, 2022.
2. Synthesis of ternary CaNiAl-Layered Double Hydroxide as a potential adsorbent and its effective removal of Congo red dye from aqueous solution. International Conference on Emerging Trends in Nanomaterials Science and Technology, Department of Science and Humanities, NIT Nagaland, 27-29th January, 2022.
3. Synthesis of LDH derived CuAlO mixed metal oxide. International e-poster Conference on Current Outlook in Material Science and Engineering (COMSE-2K20), Department of Chemistry, Bodoland University, 15-16th May, 2020.
4. Synthesis of ZrO₂/MgAl-LDH composites and evaluation of its isotherm, kinetics and thermodynamic properties in the adsorption of congo red dye. National Conference on Science and Technology for Sustainable Development (STSD-2022), Science College, 9-10th September 2022.
5. Coconut Husk Ash Modified CoAl-Layered Double Hydroxide Composite and its application in Dye Remediation from Aqueous Solution. International Conferences on Current Trends in Chemical Sciences for Sustainable Living, Shyam Lal College, 4th April, 2024.



Surfactants assisted synthesis of CuAl-sodium dodecyl sulfate layered double hydroxide and its adsorptive removal of methyl red dye from aqueous solution

Deepmoni Brahma & Hemaprobha Saikia

To cite this article: Deepmoni Brahma & Hemaprobha Saikia (2023): Surfactants assisted synthesis of CuAl-sodium dodecyl sulfate layered double hydroxide and its adsorptive removal of methyl red dye from aqueous solution, Inorganic and Nano-Metal Chemistry, DOI: [10.1080/24701556.2023.2166074](https://doi.org/10.1080/24701556.2023.2166074)

To link to this article: <https://doi.org/10.1080/24701556.2023.2166074>



Published online: 19 Jan 2023.



Submit your article to this journal [↗](#)



View related articles [↗](#)



View Crossmark data [↗](#)



Surfactants assisted synthesis of CuAl-sodium dodecyl sulfate layered double hydroxide and its adsorptive removal of methyl red dye from aqueous solution

Deepmoni Brahma and Hemaprobha Saikia

Department of Chemistry, Bodoland University, Kokrajhar, Assam, India

ABSTRACT

The versatile nature of layered double hydroxide (LDH) has made it the most widely used potential adsorbent for the decontamination of azo dye-polluted wastewater. Recently, the assembling of organic molecules on LDH structure to improve its physicochemical characteristics is given more attention by researchers. In this present work, the adsorption property of the CuAl-LDH was enhanced by modification with anionic surfactants sodium dodecyl sulfate and the synthesized materials were applied for the examination of methyl red removal from its aqueous solution. Both the pristine and surfactants modified LDH were synthesized by a facile co-precipitation method and characterized by X-ray diffraction, Brauner-Emmet-Teller surface area, thermogravimetric analysis, infrared spectroscopy, scanning emission microscopy, and energy dispersive x-ray spectroscopy. The obtained experimental data were analyzed by different isotherm and kinetics models and it shows higher degree of coefficient correlation with Langmuir isotherm and pseudo-second-order kinetic model. However, the study of thermodynamic parameters reveals that the adsorption process is spontaneous and endothermic in nature for both the adsorbents. The adsorption efficiency of surfactant fabricated CuAl/SDS-LDH was increased compared to pristine LDH and the maximum monolayer adsorption capacity q_{max} (mg g^{-1}) for CuAl-LDH and CuAl/SDS-LDH were 209.9 mg g^{-1} and 411.47 mg g^{-1} , respectively. The reusability of the materials indicates impressive results and can be repeated for up to four cycles. The synthesized sorbents CuAl-LDH and CuAl/SDS-LDH can significantly remove the target organic pollutant over a broad range of dye concentrations.

ARTICLE HISTORY

Received 22 September 2021
Accepted 29 December 2022

KEYWORDS

CuAl/SDS; surfactants; methyl red; layered double hydroxide; adsorption; dye removal

Introduction

Water pollution has become a global environmental problem due to the development of rapidly growing modern industry, increasing population and climate change. The increased water pollution caused by various consumers has significantly contributed and adversely intensified the contamination of scarce and freshwater resources.^[1] Recently, the major water contaminants are the organic azo dyes which are utilized in various industries, including textile, paper, cosmetics and food industries for coloring and dyeing purposes.^[2] Subsequently, a large amount of wastewater are generated which is directly drained over the natural water bodies like lakes, seas, oceans rivers etc. Since, dyes are generally complex organic compounds and chemically inactive which are synthesized to overcome degradation from various contacts like sunlight, water, detergents.^[3] Therefore, it is difficult to remove it easily and can influence the environment by creating short- and long-term effects.^[4] In addition, these organic pollutants for instance the anionic methyl red dye that contain $-\text{N}=\text{N}-$ group in the structure are responsible for various health issues including respiratory tract damage and mucous membrane irritation, gastrointestinal disturbances and liver damage, which had posed a threat to

the global environment.^[5] The serious consequences like carcinogenicity and biotoxicity due to dye-polluted effluents observed in aquatic plants and animals are also reported.^[6] Therefore, the extraction of organic azo dye pollutants from wastewater is very crucial.

In order to mitigate the problems now a day researchers have adopted various methods for removing azo-dye contaminants from effluent which may include adsorption,^[7] filtration,^[8] photocatalytic degradation,^[9] magnetic separation,^[10] reverse osmosis,^[11] and flocculation.^[12] Among the different techniques employed, adsorption is one of the most efficient processes for the treatment of toxic contaminants. Due to the less expensive, more convenient and less generation of waste products, it is considered to be more appropriate compared to other techniques. Another advantage of this method relies on the reversible characteristics between adsorbate-adsorbent systems, which can facilitate the easy regeneration of the adsorbent material for repeated usage. As a result, adsorption can also be regarded as the most extensively used and promising method for developing nations.^[13] Some of the previously reported materials applied for detoxification of aqueous media include metal organic framework, biogenic nanocomposite, activated carbon-nanocomposite, bentonite, biochar and mixed metal oxides.^[14,15] However, owing to less

adsorption capacity and reusability of these sorbents, currently a large number of researchers are interested in modification or fabrication of the material structure for increasing the monolayer adsorption capacity and effective elimination of dyestuffs from its aqueous media.

Layered double hydroxides are anionic clays generally constructed by the brucite type layers, which comprise divalent M^{2+} and trivalent M^{3+} cations along with intergallery anions like A^{2-} lying between the brucite layers. In addition, the high-density positively charged layers are balanced by the intergallery anions and the metal cations are coordinated octahedrally by the hydroxyl group. In general, the molecular formula of LDH is represented by $[M_{1-x}^{2+}M_x^{3+}(\text{OH})_2]^{x+}(A^{m-})_{x/m}\cdot n\text{H}_2\text{O}$ where M^{2+} and M^{3+} are divalent and trivalent cations and A is a counter anion with a negative charge m.^[16] Accounting to its unique nature, LDH is not only confined to the field of catalysis, but also to the ability to tune its hetero architecture by isomorphous substitution, intercalation and surface modification which makes it versatile, having potential applications in miscellaneous fields including catalysis, drug delivery, flame retardants, environmental remediations.^[17,18] Concerning the high efficient and multi-dye removal adsorbent, the search for a better synthetic protocol for altering the surface of LDH with organic surfactants or molecules is extensively under study. Usually, in the traditional methods of LDH synthesis due to the presence of hydrated interlayer ions such as Cl^- , NO_3^- and CO_3^{2-} , it imparts hydrophilic properties to the LDH particle. As a result, it does not preferentially adsorb cationic dyes and non-ionic organic molecules.^[19] Therefore, fabrication with organic sodium dodecyl sulfate molecules can provide hydrophobic nature to the resultant LDH material which is essential for the removal of hydrophobic organic dye pollutants from wastewater. The surface alteration with surfactants in the previous work reported by Zhang et al. can significantly enhance the adsorption behavior of LDH during removal of methyl orange dye. All these modified LDH have a broad range of utilization in the environmental remediation field.^[20]

In this study, we have investigated the decontamination of dye polluted water with surfactants fabricated LDH and compared with its parent pristine LDH. The synthesized adsorbents CuAl-LDH and CuAl-SDS-LDH are characterized and used for investigating its adsorption performance for the removal of Methyl Red dye from an aqueous solution. Under the study, we have reported the effect of various physical parameters such as contact time, adsorbent dosages, pH, temperature, and reusability. From our literature study till now, no reports regarding the sorption of methyl red by LDH are available. However, the results shown by the current materials are impressive. The possible mechanisms involved in kinetics and isotherm studies during the reaction are also illustrated.

Experimental

Materials and methods

The precursor materials are copper nitrate trihydrate ($\text{Cu}(\text{NO}_3)_2\cdot 3\text{H}_2\text{O}$), aluminum nitrate nonahydrate ($\text{Al}(\text{NO}_3)_3\cdot 9\text{H}_2\text{O}$), sodium hydroxide (NaOH), sodium dodecyl

sulfate ($\text{CH}_3(\text{CH}_2)_{11}\text{SO}_4\text{Na}$), and methyl red ($\text{C}_{15}\text{H}_{15}\text{N}_3\text{O}_2$, M.W-269.3g/mol). All the chemicals are of analytical grade and purchased from Merck India, and utilized for the synthesis of materials without any further purification. In addition, under all experimental conditions, the required solution was prepared by using distilled water.

Synthesis

The sample represented as CuAl-LDH was prepared by a simple co-precipitation method where the ratios of divalent and trivalent cation M^{2+}/M^{3+} were maintained at 2:1 with the slight modification from the previously reported literature. The first metal precursor solution A was obtained by mixing 0.2 M $\text{Al}(\text{NO}_3)_3\cdot 9\text{H}_2\text{O}$ and 0.4 M $\text{Cu}(\text{NO}_3)_2\cdot 3\text{H}_2\text{O}$ in an aqueous solution of 100 ml. The second solution B contains 0.2 M NaOH in 150 ml distilled water. Subsequently, solution B is then added slowly dropwise to solution A up to 30 minutes under vigorous stirring at room temperature with simultaneous maintenance of pH at (9–10). Furthermore, the reaction mixture is allowed to stir continuously for 24 h. The blue color slurry is obtained, which is then centrifuged and washed with distilled water for several times until the pH of the filtrate is neutral. The resulting product is obtained by drying in an oven at 50 °C for 12 h and crushed with mortar to get powdered form.

For the synthesis of surfactant-assisted CuAl/SDS-LDH, similar procedures have been carried out, except 0.5 g of sodium dodecyl sulfate that has been added to solution B and the remaining steps are performed under identical conditions as in the case of earlier pristine CuAl-LDH material.

Adsorption experiment

The adsorption experiments were performed by adopting a batch equilibrium adsorption method under a constant temperature of 28 °C. For the study of adsorption isotherm, a series of methyl red dye solutions containing a total volume of 20 mL each with a different concentration ranging from 25 to 350 mg/L was taken in 150 mL conical glass bottle. Subsequently, 22 mg of the adsorbent was added in the dye solution, which is then allowed to shake in a thermostatic shaker machine for a timeperiod of 6 h to reach equilibrium adsorption. After completion of shaking the solution was filtered, and the concentration of dye remaining in the filtrate was measured by using UV-spectrophotometer (EI-3315) at 432 nm. The amount of methyl red dye adsorbed on the adsorbent was evaluated by the formula:

$$q_e = \frac{(C_0 - C_e) V}{W} \quad (1)$$

The percentage of dye uptake was evaluated as:

$$\% \text{ of dye uptake} = \frac{(C_0 - C_e) \times 100}{C_0} \quad (2)$$

where C_0 and C_e are the initial concentration and equilibrium concentration of methyl red dye, respectively. V is the

volume of the solutions in litres (L) and W is the weight of the adsorbent used in grams (g).

For the adsorption kinetics experiment, 44 mg of the adsorbent was mixed with 50 mL of the methyl red dye solution having an initial concentration of 60 mg/L, and then the resulting solution was shaken. After a definite time interval, the solution was withdrawn from the conical flask and the residual dye concentration was measured. The variation in the amount of dye adsorbed at different time intervals was studied for 0 to 4 h. The amount of dye adsorbed with time was calculated by:

$$q_t = \frac{(C_0 - C_t) V}{W} \quad (3)$$

where C_0 and C_t are the initial concentration of dye solution and concentration at time t , respectively. q_t is the amount of dye adsorbed at time t . However, in order to obtain better reproducibility, all the experiments are carried out thrice.

Characterization techniques

X-ray diffraction analysis was conducted with Rigaku Ultima-IV powder X-ray diffractometer at the Bragg's angle ranging between 5 and 70° by employing $\text{CuK}\alpha$ ($\lambda = 1.54\text{\AA}$) radiation. Fourier transform infrared spectroscopy FT-IR was recorded on SHIMADZU-IR Affinity-1 at a frequency range of 300–4000 cm^{-1} by using the KBr background. The microstructure morphology of the sample was investigated by Gemini Carl Zeiss Sigma 300, and the elemental composition was studied by EDX. The thermal degradation of the sample was investigated in between the temperature ranging from 29 to 900 °C by using TGA under the ramping rate of 20° C/min. The textural properties of the as-synthesized CuAl-LDH, including specific surface area, pore size, and pore volume, were analyzed in an instrument Quantachrome Novawin version 11.05 by performing adsorption-desorption of the N_2 gas at 77.3 K. Initially, the sample was outgassed at 150 °C for 6 h. The BET (Brunauer-Emmett-Teller) method was used for the evaluation of specific surface area whereas for pore size and pore volume the BJH (Brunauer-Joyner-Hallenda) method is employed. The measurement in the concentration of the unknown dye solution was made in UV-Spectrophotometer-3375 (Electronics India).

Results and discussions

Characterization of adsorbents

The analysis of structure and crystalline size of the adsorbent material was investigated with the help of powdered XRD technique. The measurement of crystallite size was performed by using the Debye-Scherrer equation, $D = B\lambda/\beta_{1/2} \cos\theta$ where $\beta_{1/2}$ denotes full-width at half-maximum (FWHM), B indicates Scherrer constant, λ signifies wavelength of the X-ray, and θ is the diffracted angle. The XRD diffraction pattern is presented in Figure 1. The synthesized CuAl-LDH shows sharp reflections corresponding to indexed plane 003, 006, 009, 015, 018, 110, and 113 which infers the formation of well crystallized layered structure

with a basal space of 7.4 Å (d_{003}). The lattice cell parameters evaluated from the position of diffraction plane 110 ($a = 2d_{110}$) and 003 ($c = 3d_{003}$) are 2.22 nm and 0.3 nm, respectively. These values are consistent with the previously reported literature.^[21] However, modification with surfactants in LDH structure leads to shifting of the peaks at a lower angle that results in increasing interlayer distance of CuAl/SDS-LDH and the theoretically calculated length of basal spacing was found to be 14 Å. The observed results suggest intercalation of sodium dodecyl sulfate molecule on the inter lamellar region as well as assemblage on the external surface of LDH. Accounting for LDH thickness (0.48 nm) and the length of SDS chain which is taken as 1.78 nm, the possible alignment of SDS inside the layer sheets is tilted with respect to LDH sheets. The diffraction peaks of CuAl/SDS-LDH at higher angles are quite similar to parent LDH which indicates the retainment of LDH structure whereas the initially observed peaks corresponding to reflection plane 015, 018 vanish which may be attributed to the lowering in the stacking order of LDH sheets.^[22–24] Nevertheless, the appearance of 001 plane at $2\theta < 7$ from which the basal spacing value are evaluated is observed in most organo modified LDH, which is obvious in the currently studied material.

The FT-IR spectrum of CuAl-LDH, CuAl/SDS-LDH before and after adsorption of methyl red dye is displayed in Figure 2. In CuAl-LDH, the observed bands are highlighted at the stretching frequency of 3447 cm^{-1} , 1626 cm^{-1} , 1383 cm^{-1} , 827 cm^{-1} , and 639 cm^{-1} . The broad band at 3447 cm^{-1} indicates the presence of interlayer water molecules corresponding to the ν -OH stretch of free and H-bonded OH groups. The broadness of such band increases with number of increasing H-bonding which could be possible among interlayer NO_3^- , H_2O , OH^- ions. Another absorption at 1626 cm^{-1} is due to O-H bending vibration of water molecules present in the interlayer region of LDH.

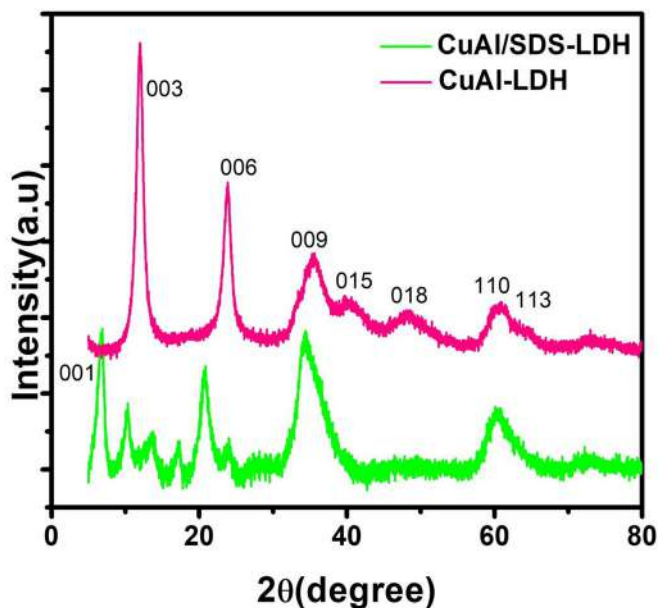


Figure 1. XRD patterns of pristine CuAl-LDH and surfactants modified CuAl/SDS-LDH.

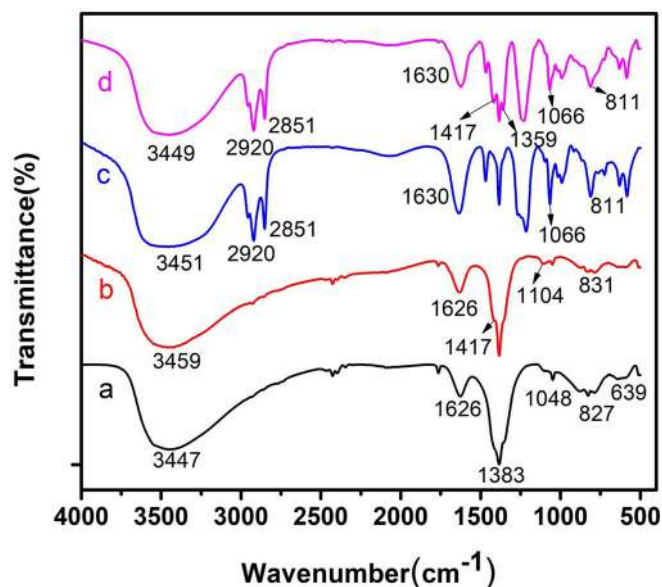


Figure 2. FT-IR spectrum before and after adsorption of methyl red dye (a) CuAl-LDH (b) CuAl-LDH-methyl red (c) CuAl/SDS-LDH (d) CuAl/SDS-LDH-methyl red.

Furthermore, the presence of NO_3^- is also revealed at 1383 cm^{-1} and 827 cm^{-1} which is assigned to antisymmetric stretching mode and non-planar bending mode vibration, respectively. And the less intense band at 639 cm^{-1} can be attributed to the M-OH stretching vibration.^[21,25] After modification with the surfactant molecules the bands manifested at 2851 cm^{-1} , 2920 cm^{-1} , 1066 cm^{-1} , and 811 cm^{-1} can be related to $\delta\text{-CH}_2$ symmetric stretch, $\delta\text{-CH}_2$ asymmetric stretch, S-O-C bond stretch and out of plane SO_3^{2-} stretch, respectively.^[20] The new additional weak and sharp band at 1417 cm^{-1} and 1359 cm^{-1} arises in CuAl/SDS-LDH after incorporation of methyl red which is corresponding to $-\text{CH}_3$ deformation and C-N stretching vibration of dye molecules. The appearance of a weak band at 1417 cm^{-1} and 1104 cm^{-1} in CuAl-LDH after adsorption also accounts for $-\text{CH}_3$ deformation and C-H in plane bending vibration of adsorbate. The obtained results confirm the presence of target dye pollutant on both adsorbents.^[26]

To illustrate the surface characteristics, the N_2 adsorption-desorption isotherm and pore size distribution curves of the adsorbent are presented in Figure 3(a, b), respectively. The specific surface area of CuAl-LDH and CuAl/SDS-LDH was determined to be 65.146 and $74.055\text{ m}^2/\text{g}$, respectively. The presence of mesopores (9.086 nm) distribution can be anticipated from the analysis which is shown in the insets of Figure 3(a, b). In addition from the N_2 adsorption-desorption curves of both materials, it manifests type IV isotherm with H3 hysteresis loop as per the IUPAC classification and signifies mesoporous materials.^[27,28] Moreover, the measured pore volume of CuAl-LDH and CuAl/SDS-LDH are 0.289 cc/g and 0.178 cc/g , respectively. After the introduction of surfactants, it is apparent that the relatively higher surface area and mesoporous characteristics of CuAl/SDS-LDH provide it with a larger adsorption site and make it more suitable for the adsorption performance of these materials.

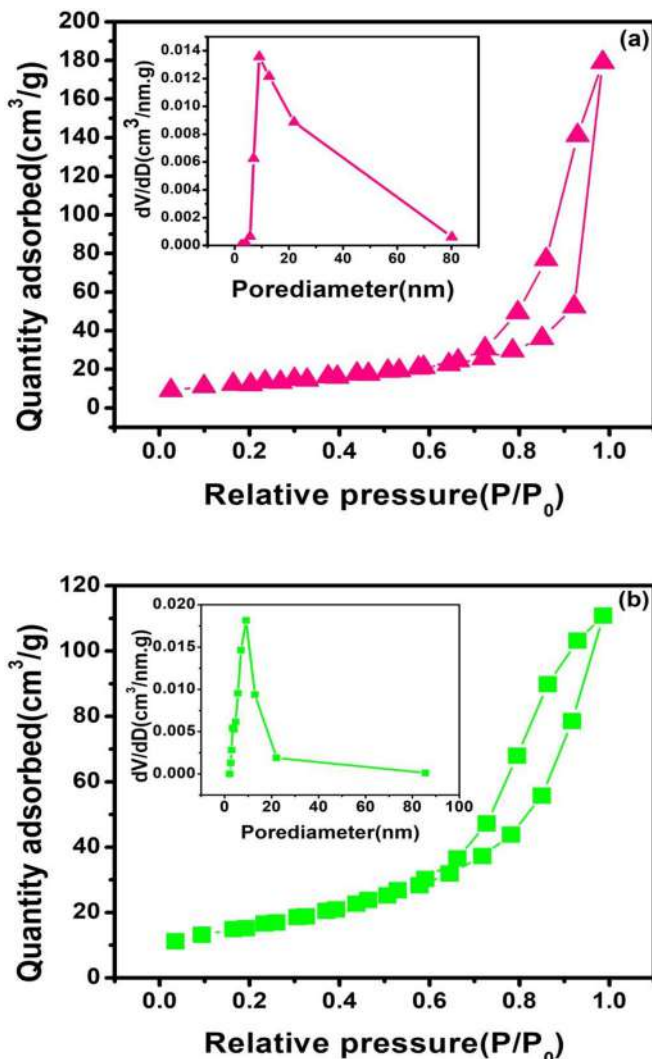


Figure 3. N_2 adsorption-desorption isotherm and pore size distribution of (a) CuAl-LDH and (b) CuAl/SDS-LDH.

The thermal stability of the synthesized CuAl-LDH and CuAl/SDS-LDH was studied by thermo gravimetric analysis which is displayed in Figure 4(a, b). From the TGA curve of CuAl-LDH, two distinct regions of weight loss can be identified. The mass loss of 9.67% noticed at a temperature below 210°C can be ascribed to the evaporation of adsorbed water molecules, while the weight loss of 28.16% between 230 and 450°C is due to the removal of intergallery ions and the hydroxyl group of the LDH sheets.^[29,30] In contrast the CuAl/SDS-LDH showed weight loss of 9.11% , 32.31% and 19.64% at three different stages. The weight loss of 9.11% corresponding to the first step is similarly related to the removal of physical surface adsorbed water molecules. The major amount of 32.31% weight loss has been observed between the temperature $165\text{--}260^\circ\text{C}$ which is associated with the decomposition of surfactants molecule embedded on LDH. In addition, the final step of mass decomposition can be accounted for elimination of intercalated inorganic anions and breakdown of LDH sheets.^[31] For CuAl-LDH, after the decomposition temperature of 435°C , the curve tends to be constantly straight, which indicates no further weight loss, whereas in CuAl/SDS-LDH, it was achieved

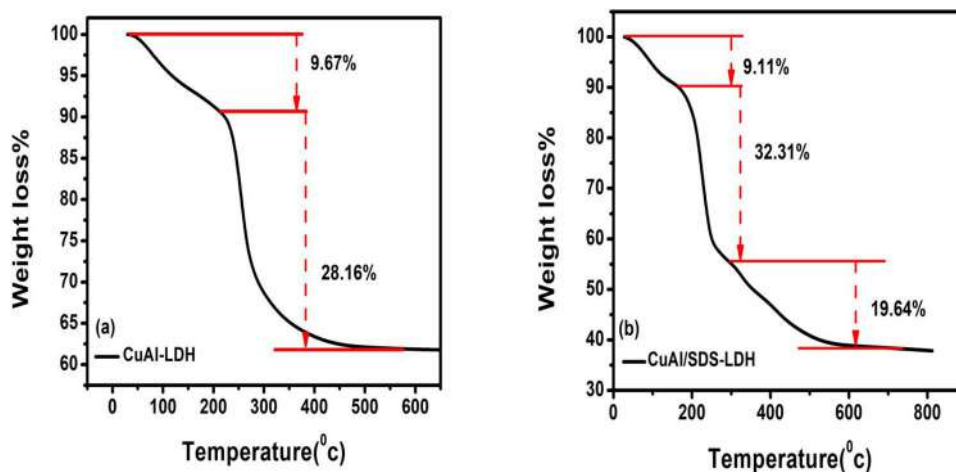


Figure 4. TGA curves of (a) CuAl-LDH and (b) CuAl/SDS-LDH.

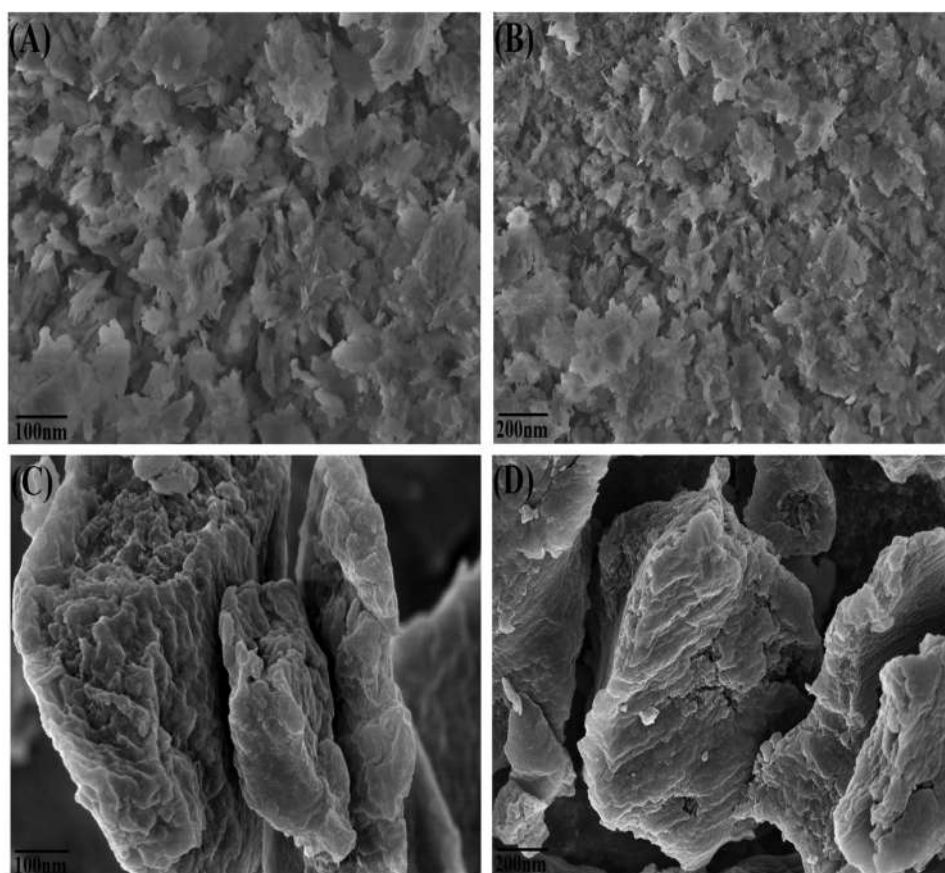


Figure 5. SEM images of CuAl-LDH (A, B) and CuAl/SDS-LDH (C, D).

after 580 °C and the complete destruction of material structure is obtained beyond this temperature.

The SEM micrographs pattern of CuAl-LDH and CuAl/SDS-LDH are depicted in Figure 5(a–d). The study of surface morphology shows the formation of porous and thin sharp sheet-like structure having a dimension below 100 nm in CuAl-LDH which may be attributed to the irregular and non-uniform arrangement of layer structures. It is also evident from Figure 5(a) that the LDH particles are highly dispersed and found stacked with each other. After fabrication with surfactants, the SEM image of CuAl/SDS-LDH

illustrates the reduction in sharpness of LDH sheets and the growth in thickness of particle size due to the expansion of interlayer region.^[21,32]

The elemental analysis spectrum of the CuAl-LDH and CuAl/SDS-LDH is presented in Figure 6(A, B). The chemical constituents of the synthesized LDH were determined by an energy dispersive x-ray method which indicates the formation of LDH with an expected molar ratio of $\text{Cu}^{2+}/\text{Al}^{3+}$ (2:1) is close to 2, as shown in Table 1. The observed atomic percentage of the elements Cu, Al, and O are 18.23%, 10.71%, and 71%, respectively. Similarly, the EDX spectrum

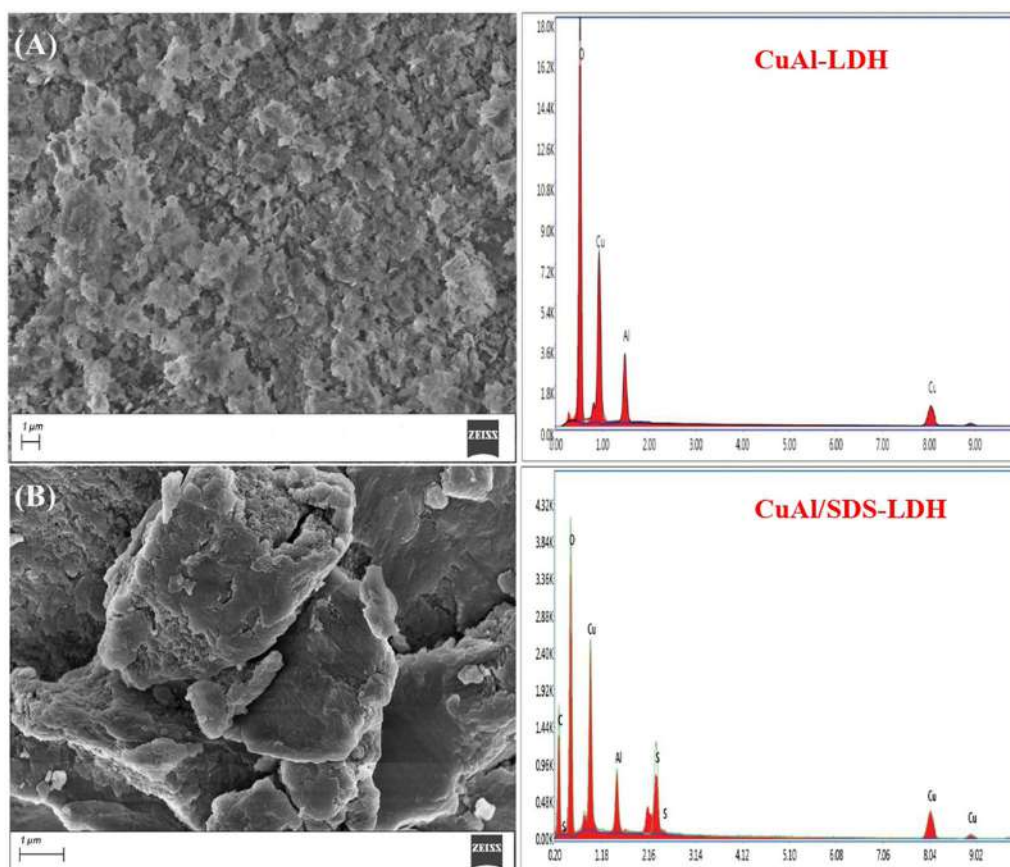


Figure 6. (A) SEM-EDX spectra of CuAl-LDH at 1 μm resolution. (B) SEM-EDX spectra of CuAl/SDS-LDH at 1 μm resolution.

Table 1. Atomic percentage of the constituent elements present in the proposed adsorbent determined by EDX analysis.

Adsorbents	Cu%	Al%	C%	O%	S%
CuAl-LDH	18.23	10.76	–	71	–
CuAl/SDS-LDH	6.87	3.35	42.77	42.78	4.24

of CuAl/SDS-LDH also confirms the presence of all constituent elements. Moreover, the presence of other impurity elements of the precursor solutions like alkali metals are not detected, thereby confirming efficient synthetic procedure and resulting in pure form of the sample.

Adsorption isotherm

In order to have detailed information considering the affinity of targeted anionic dyes toward the proposed adsorbent materials, the distribution of dye molecules between solid and liquid phases after reaching the equilibrium stage can be best understood from the study of adsorption isotherm. With the help of the isotherm study, it is also possible for interpreting the qualitative nature of adsorbate-adsorbent system. For a clear illustration of the adsorption behavior and its underlying mechanisms, three models including Langmuir, Freundlich, and Temkin are employed. These model isotherms can easily explain the relation among the quantity of dye adsorbed with equilibrium concentration.^[33]

Langmuir isotherm

It is a monolayer adsorption model which assumes, if the complete saturation of homogeneous vacant site of the adsorbent surface is reached, then there is no further additional occupation of those sites by the adsorbate molecules.^[34] The non-linear form of the Langmuir equation is represented as:

$$q_e = \frac{q_m C_e K_L}{1 + K_L C_e} \quad (4)$$

where q_m , C_e , q_e , and K_L represent highest monolayer adsorption capacity, final equilibrium concentration of dye solution (mg/g), quantity of dye adsorbed at equilibrium (mg/L), and Langmuir constant, respectively.

Figure 7(a–d) shows different isotherm model plots for removal of methyl red dye. With the help of the Langmuir isotherm plot, the highest monolayer adsorption capacity q_{max} value for the adsorbents CuAl/SDS-LDH (411.47 mg/g) and CuAl-LDH (209.97 mg/g) was evaluated. The favorability of the adsorption process was determined by a factor R_L , which is calculated from the equation:

$$R_L = \frac{1}{1 + K_L C_0} \quad (5)$$

where C_0 and K_L are the initial dye concentration and Langmuir constant, respectively. Moreover, if the equilibrium parameter $R_L > 1$ then the adsorption process is

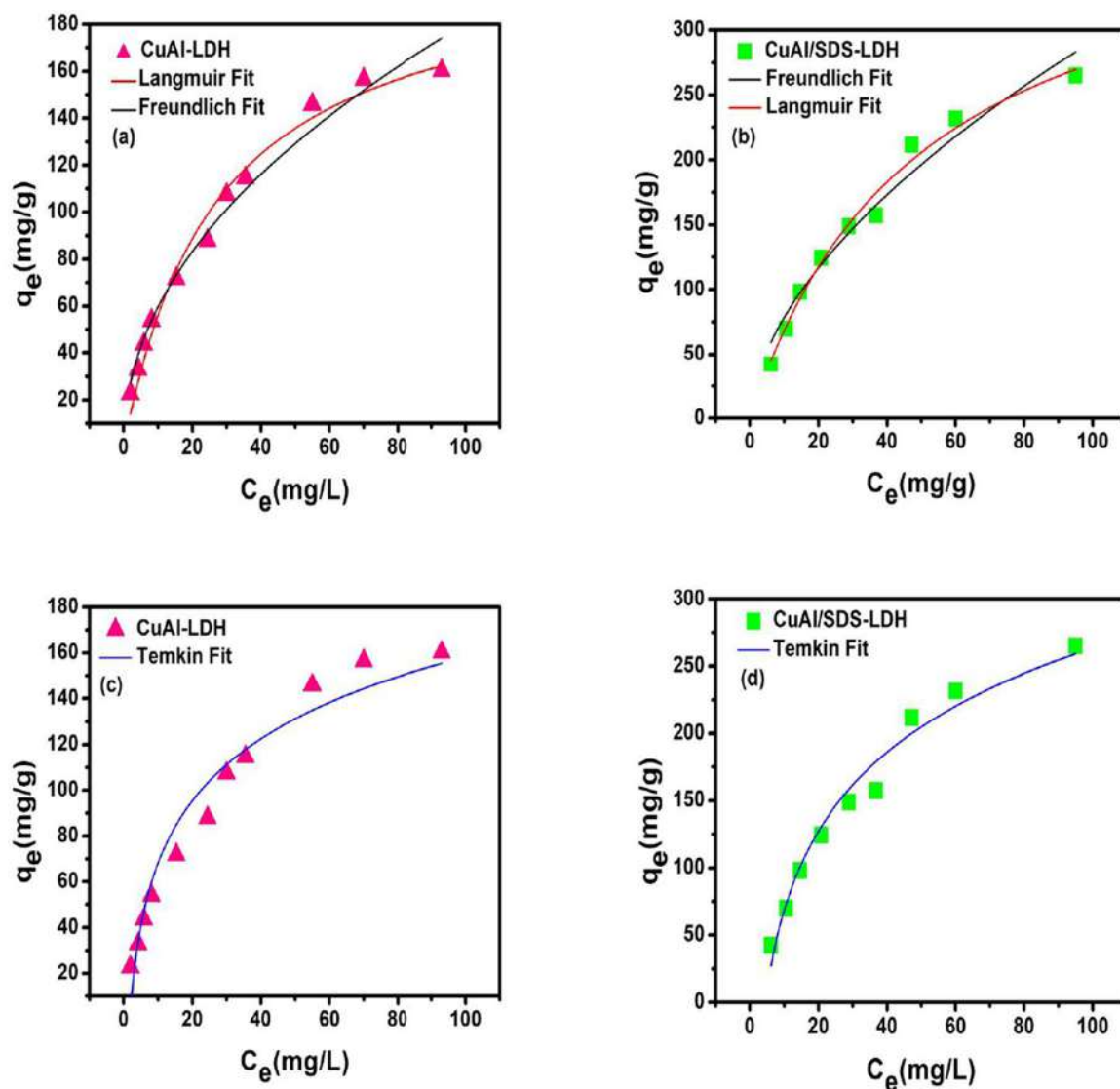


Figure 7. Non-linear plot of adsorption isotherm by using Langmuir, Freundlich and Temkin model for adsorption of methyl red dye on CuAl-LDH (a, c) and CuAl/SDS-LDH (b, d).

unfavorable and for the values of R_L in between 0 and 1 it indicates favorable process, while for irreversible process $R_L = 0$. The obtained results shown in Figure 8(a, b) indicate that for both adsorbents at different initial dye concentrations, R_L values lie in the range from 0 to 1 that infers the feasibility of the adsorption process.^[35]

Freundlich isotherm

Freundlich isotherm is an empirical equation representing the relation between quantities of solute adsorbed per unit mass of solid adsorbent. This model is more suitable for studying the adsorption in the heterogeneous surface of the adsorbent.^[36] The equation for Freundlich isotherm is given as:

$$q_e = K_f C_e^{1/n} \quad (6)$$

where q_e and C_e have their usual meaning, K_f and n are constants that provide information regarding capacity and intensity of adsorption, respectively.

Temkin isotherm

Concerning the interaction between adsorbate-adsorbent system Temkin isotherms considers that heat of adsorption of all the molecules present on the surface of LDH sheets get reduced linearly with surface coverage and the nature of the adsorption is best described by the orderly arrangement of binding energies until a certain maximum value.^[37] The non-linear equation of Temkin isotherm is given as:

$$q_e = B_T \ln(K_T C_e) \quad (7)$$

where B_T (kJ/mol) and K_T (L/mg) represent the heat of adsorption and equilibrium binding constant, respectively.

The various adsorption isotherm parameters are summarized in Table 2. The observed results from the adsorption isotherm data after nonlinear fitting showed a greater coefficient of correlation regression R^2 for Langmuir fitting in comparison to Freundlich and Temkin fitting which implies that the Langmuir model can be best accounted for the adsorption mechanism. Consequently, the surfaces of the applied adsorbent are closer to homogeneous than

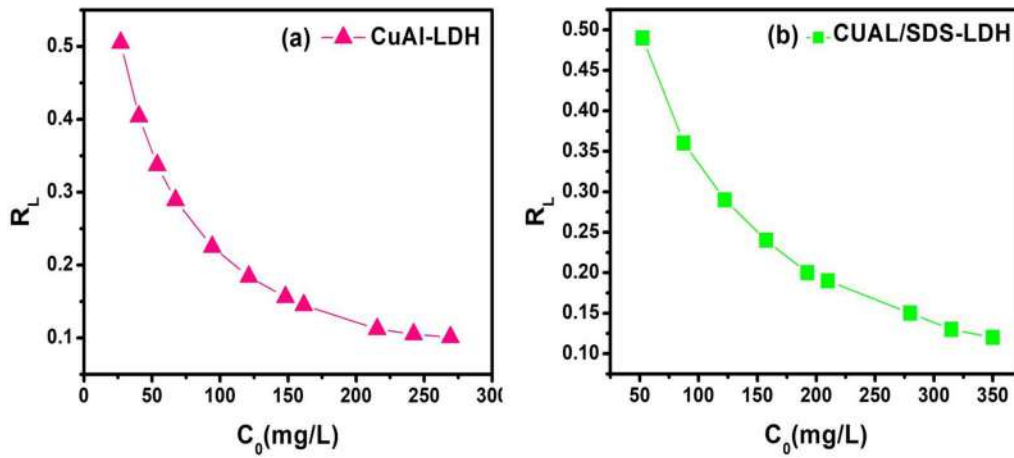


Figure 8. Plot of R_L vs C_0 for adsorption of methyl red dye over two adsorbents (a) CuAl-LDH and (b) CuAl/SDS-LDH.

Table 2. Isotherm parameters for adsorption of methyl red on CuAl-LDH and CuAl/SDS-LDH.

Isotherm model	Constants	Adsorbents	
		CuAl-LDH	CuAl/SDS-LDH
Langmuir	K_f (L/mg)	0.0365 ± 0.004	0.0200 ± 0.002
	q_{max} (mg/g)	209.97 ± 11.46	411.47 ± 15.22
	R^2	0.981	0.985
Freundlich	n	2.0825 ± 0.12	1.756 ± 0.14
	K_f	19.744 ± 2.17	21.180 ± 3.90
	R^2	0.978	0.961
Temkin	B_T	39.088 ± 2.82	84.635 ± 5.15
	K_T	0.5733 ± 0.10	0.2249 ± 0.02
	R^2	0.950	0.971

heterogeneous. The K_f values for CuAl-SDS LDH and CuAl-LDH were determined to be 21.18 and 19.74, respectively. In addition, the values of constant n greater than 1 in both adsorbents suggest that the adsorbate gets suitably adsorbed on the material surface under the studied experimental conditions.

In order to assess the adsorption performance of the currently proposed LDH, it is compared with the previously reported material, which is displayed in Table 3. It highlights the maximum adsorption capacity and optimum experimental conditions of several adsorbents for the elimination of methyl red dye from an aqueous medium. It is clear from Table 3 that the dye adsorption capacity of the proposed LDH material is comparatively higher than some of the adsorbents such as biogenic Ag@Fe nanocomposite, MIL-53(Fe), Pd-NP-AC while other adsorbents showed greater monolayer adsorption capacity. However, few of these materials involve harsh and complicated synthetic methods. In contrast, synthesis of pristine and surfactant LDH involves simple and less toxic reactions which is an advantage in the materials. Therefore, it can be concluded that CuAl-LDH and CuAl/SDS-LDH can be considered promising material for removal of methyl red dye in terms of less toxic, low cost, and good adsorption performances.

Adsorption kinetics

The evaluation of various kinetic parameters can have essential practical value for technological utilization. In the present study,

in order to estimate the rate of dye adsorption and to have detailed information about the regulated mechanism, a kinetic study was performed and the two different most widely used kinetic models, namely pseudo-first order and pseudo-second order was adopted for the determination of kinetic parameters. Based on the physical adsorption pseudo-first-order kinetic model considers that the rate of dye intake is proportionate to the ratio of the concentration of dye and the quantity of adsorbent used. On the contrary, the pseudo-second order kinetics depends on chemisorptions where the chemical bond either covalent or ionic holds the adsorbate-adsorbent system.^[44,45] The linear form of pseudo-first order, second-order kinetic and intraparticle diffusion equation is formulated as

$$\log(q_e - q_t) = \log q_e - \frac{K_1 t}{2.303} \quad (8)$$

$$\frac{t}{q_t} = \frac{1}{K_2 q_e^2} + \frac{t}{q_e} \quad (9)$$

$$q_t = K_1 t^{0.5} + C \quad (10)$$

where q_e and q_t represent the quantity of adsorbate taken up by an adsorbent under equilibrium and time t (min), respectively. As shown in Figure 9(a), the linear plot of $\log(q_e - q_t)$ vs t gives a straight line from which the obtained slope and intercept values are used in the determination of first-order rate constant K_1 and q_{e1} amount of dye adsorbed at equilibrium, respectively. Nevertheless, from Figure 9(b), the plot of (t/q_t) vs t evaluates pseudo-second-order rate constant K_2 and quantity of dye adsorbed at equilibrium q_{e2} .

The detailed kinetic parameters are depicted in Table 4. From the obtained results, it can be anticipated that the experimental data fit well with a pseudo-second-order kinetic model having a greater correlation coefficient ($R^2 > 0.994$) value in comparison to the first-order kinetic model. Moreover, it is also evident that the pseudo-second-order rate constant for CuAl-LDH and CuAl/SDS-LDH are $5.77 \times 10^{-4} \text{ g.mg}^{-1} \text{ min}^{-1}$ and $4.29 \times 10^{-4} \text{ g.mg}^{-1} \text{ min}^{-1}$, respectively, which implies that the sorption rate of methyl red dye on CuAl-LDH is faster than CuAl/SDS-LDH. Besides, the higher experimental q_e value for CuAl-SDS (69.48 mg.g^{-1}) compare to CuAl-LDH

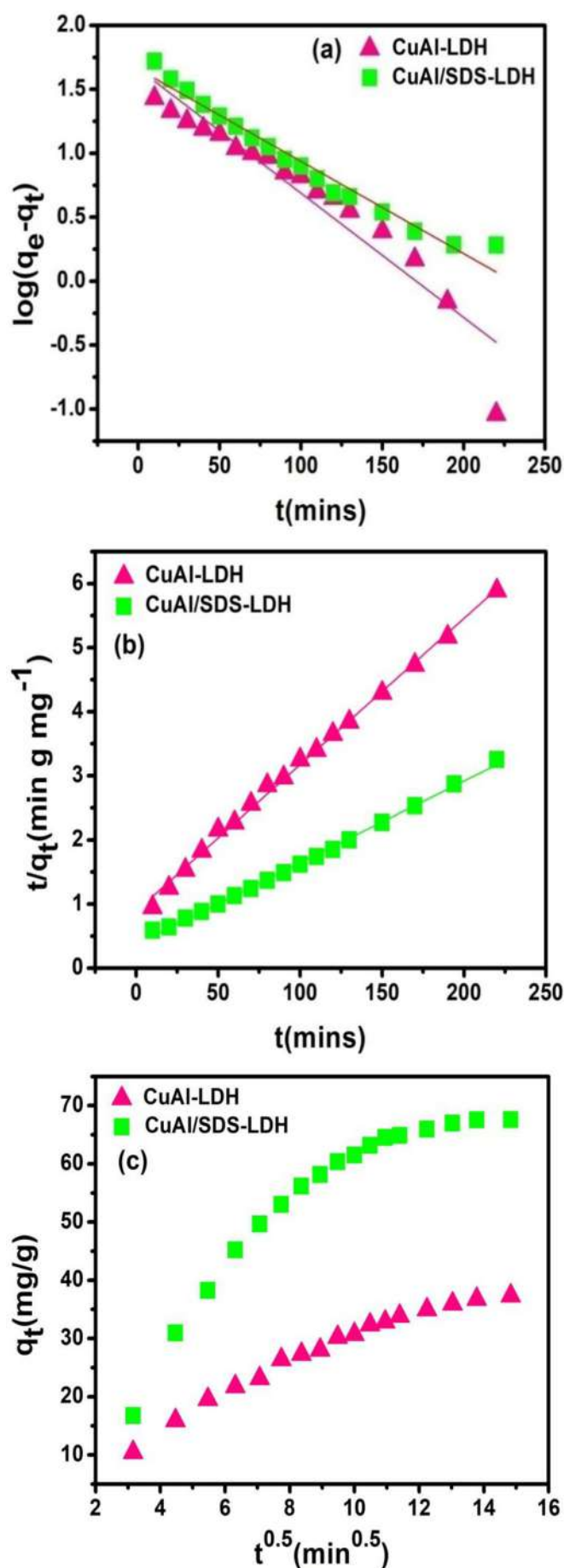


Figure 9. (a) Pseudo-first-order kinetic plot for adsorption of methyl red on CuAl-LDH and CuAl/SDS-LDH. (b) Pseudo-second-order kinetic plot. (c) Intraparticle diffusion kinetics plot.

(37.44 mg.g^{-1}) further conveys enhancement in the adsorption capacity of surfactant-assisted LDH. In the adsorption process of methyl red dye, the relatively closer values of pseudo-second-order q_{e2} with q_e in both adsorbents infers that during the studied experimental condition for the initial dye concentration 50 mg/L and contact time from 0 to 220 minutes, the adsorption behavior can be best described by pseudo-second-order mechanism. In addition, the values of calculated q_{e1} from pseudo-first-order in both adsorbents do not agree with experimental q_e . Thus, it confirms that the rate-determining step in the adsorption process may be due to chemisorption.

The mechanism of the diffusion process during the adsorption of methyl red dye has been described by employing the intraparticle diffusion model (Equation 10). From Figure 9(c), the plot of q_t vs $t^{0.5}$ clearly manifests the appearances of multiple step processes in both the adsorption system. The initial region observed in Figure 9(c) indicates sorption on the external surface of the adsorbents while the middle region represents the occupation of dye molecules inside the pores, and the third region implies completion of the equilibrium stage of adsorption due to a lack of available vacant sites.^[46] The value of intraparticle diffusion constants k_i and the thickness of the boundary layer C were determined from the slope and intercept of the linear plot q_t vs $t^{0.5}$ which is demonstrated in Table 4.

Effect of temperature

Temperature is another important parameter affecting the adsorption of organic dye molecules on the surface of the substrate or LDH. In order to have a broad insight about the adsorption process with the change in temperature the various parameters ΔG , ΔH and ΔS were evaluated. The experimental reactions with varying temperatures at 301 K, 313 K and 323 K were performed on 90 mg/L of methyl red with 0.0220 g adsorbent dosages for a contact time of 1 h. The equations for the calculation of the thermodynamic parameters are given as:

$$\ln K_d = \frac{\Delta S}{R} - \frac{\Delta H}{RT} \quad (11)$$

$$\Delta G = -RT \ln K_d \quad (12)$$

where ΔG , K_d , R , and T indicate standard free energy, adsorption distribution coefficient, universal gas constant, and temperature (K), respectively.^[47]

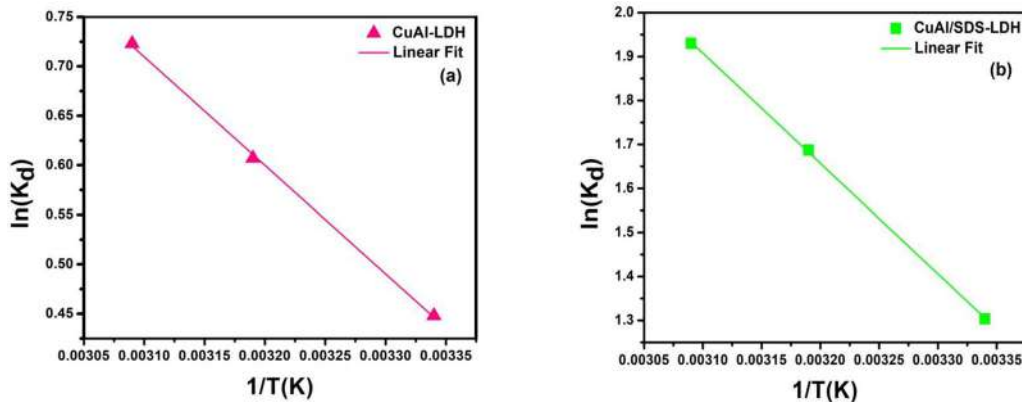
From the Vant Hoff plot ($\ln K_d$ vs $1/T$) is shown in Figure 10(a, b). The values of enthalpy ΔH and entropy ΔS are determined from the slope ($\Delta H/R$) and intercept ($\Delta S/R$), respectively. The results obtained from the thermodynamic parameters represented in Table 5 revealed the negative value of ΔG in both materials CuAl-LDH and CuAl/SDS-LDH, which infers the feasibility of the adsorption process. With increasing temperature from 301 K to 323 K, ΔG value decreases from -1.12 to -1.94 kJ/mol (CuAl-LDH) and -3.26 to -5.18 kJ/mol (CuAl/SDS-LDH). The value of enthalpy change ΔH provides information to interpret if the nature of dye intake in the adsorption system is either physical or chemical. Moreover, values of ΔH lying between (-20 to 40) kJ/mole indicates the physical nature of

Table 3. Comparison of various adsorbents used for the removal of methyl red dye.

Adsorbents	q_{\max} (mg/g)	pH	Time(min)	Dosages (g)	Isotherm	References
Biogenic Ag@Fe nanocomposite	125	5	160	0.042	Langmuir	[14]
Natural raw Clay Anb	397	7	5	0.25	Langmuir	[38]
Pd-NP-AC activated carbon	133.33	2	15	0.01	Langmuir	[39]
Fe ₃ O ₄ @MIL-100(Fe)	625	4	360	0.01	Langmuir	[40]
Custard apple derived activated carbon AC	434.78	5	50	0.15	Langmuir	[41]
Durian seed derived activated carbon AC	384.62	6	180	0.10	Langmuir	[42]
MIL-53(Fe)	183.5	4	120	0.05	Langmuir	[43]
CuAl-LDH	209.97	7	360	0.022	Langmuir	This work
CuAl/SDS-LDH	411.47	7	360	0.022	Langmuir	This work

Table 4. Parameters of two kinetic model for the adsorption of 50 mg/L methyl red by CuAl-LDH and CuAl/SDS-LDH.

Adsorbents	Pseudo-first order				Pseudo-second order			Intraparticle diffusion		
	$q_e(\text{exp})$ mg. g ⁻¹	$q_{e1}(\text{cal})$	$K_1(10^{-3}) \text{ min}^{-1}$	R ²	$q_{e2}(\text{cal})$ mg. g ⁻¹	$K_2(10^{-4})$ g. mg ⁻¹ min ⁻¹	R ²	K_i	C	R ²
CuAl/LDH	37.44 ± 0.39	45.90 ± 0.06	22.36 ± 0.09	0.90	43.95 ± 0.35	5.77 ± 0.16	0.99	2.28 ± 0.02	6.92 ± 0.14	0.95
CuAl/SDS-LDH	69.48 ± 1.07	46.08 ± 1.42	16.65 ± 0.95	0.96	78.74 ± 1.59	4.29 ± 0.20	0.99	4.05 ± 0.04	17.08 ± 0.71	0.84

**Figure 10.** Vant Hoff plot for the adsorption behavior of the methyl red by the adsorbents (a) CuAl-LDH (b) CuAl/SDS-LDH (Initial dye concentration = 90 mg/L, dosages = 22 mg, volume = 20 mL, contact time = 1 h).**Table 5.** Thermodynamic parameters for the adsorption of methyl red on CuAl-LDH and CuAl/SDS-LDH.

Adsorbent	$+\Delta H$ (kJ/mol)	$+\Delta S$ (J/mol)	$-\Delta G$ (kJ/mol)		
			301 K	313 K	323 K
CuAl-LDH	9.11	34.16	1.12	1.58	1.94
CuAl/SDS-LDH	20.86	80.55	3.26	4.39	5.18

adsorption, whereas the value within (-400 to -80) kJ/mol refers to the chemical nature. The positive values of ΔH and ΔS correspond to the endothermic and spontaneity of the process. The obtained ΔH value for CuAl-LDH and CuAl/SDS-LDH are $+9.11$ kJ/mol and $+20.86$ kJ/mol, respectively, which indicates the physical nature of the process. Again the entropy change ΔS value signifies the randomness of molecules in the solid-liquid interfaces.^[48] However, there is a slight enhancement in the adsorption process with increasing temperature in both adsorbents thereby revealing that the adsorption process takes place through endothermic reactions. The obtained result shows that surfactant-assisted CuAl-LDH has greater adsorption for methyl red dye compared to pristine CuAl-LDH which is achieved at higher temperature 323 K. Initially, the positively charged external surface and intergallery region of the

materials are saturated with dye molecules due to the coulombic force and other interactions possibly H-bonding, vander waals, etc. After filling up external surfaces the dye molecule then gets attached to surfactants loaded LDH via weak interactions.^[20] From the experimental data, it suggests that surfactants can improve the capacity of dye removal. Therefore, CuAl-LDH and CuAl/SDS-LDH prove to be promising and effective adsorbents in the removal of anionic dyes.

Effect of initial dye concentration

The effect of initial dye concentration on the adsorption efficiency is depicted in Figure 11(a, b). The removal efficiency of methyl red dye over CuAl-LDH and CuAl/SDS-LDH decreases with increasing initial dye concentration. It can be attributed to the less number of free sorption site on the adsorbent surfaces. Moreover, the type of adsorption process becomes monolayer at the initial low concentration which then further extends to multilayer after the complete saturation level is achieved at the higher concentration of methyl red solution. As expected, it is not surprising that the time required to attain equilibrium is less at low initial concentration which is relatively higher in case of high

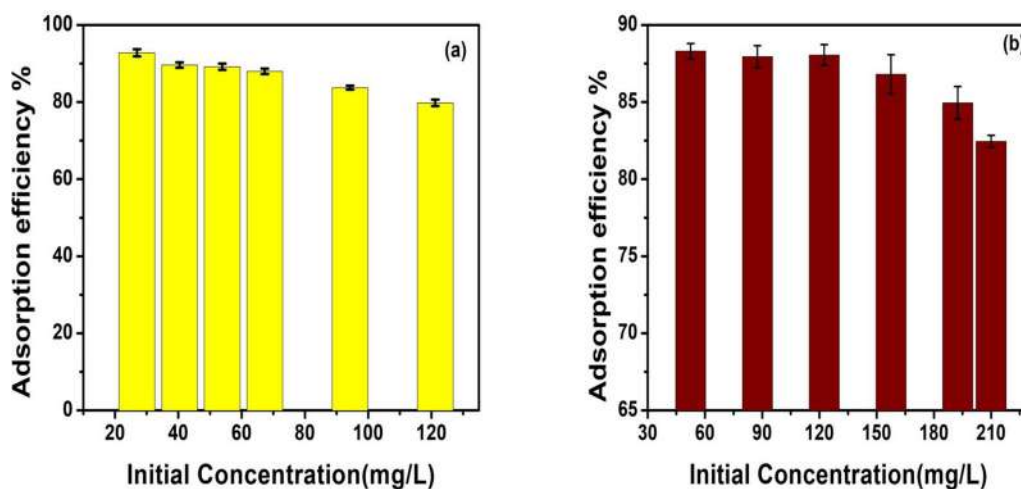


Figure 11. Effect of initial dye concentration on adsorption efficiency of methyl red over (a) CuAl-LDH and (b) CuAl/SDS-LDH (adsorbent dosages = 22 mg, volume = 20 mL, contact time = 6 h).

initial concentration. Nevertheless, in some cases, the higher dye concentration can increase the adsorption percentage due to the creation of the pressure gradient by large number of dye molecules on the adsorption site.^[49] For the initial dye concentration of methyl red (25–120 mg/L) for CuAl-LDH and (52–210 mg/L) for CuAl/SDS-LDH, the sorption percentage lies in the range (79.81–92.79%) and (82.45–88.30%), respectively.

Effect of adsorbent dosages

It is very crucial to determine the suitable adsorbent dosages for the maintenance of cost-effective system. Subsequently, the variation in adsorbent dosages having a significant effect on the decontamination of methyl red dye from its aqueous solution was analyzed. From Figure 12(a, b), the adsorption performance of SDS-modified CuAl-LDH at different dosages from 0.010 to 0.030 g are clearly distinguishable in comparison to the pristine CuAl-LDH. However, with increasing adsorbent amount the percentage of dye removal also increases in both materials but the surfactants modified LDH showed a relatively higher adsorption behavior. As observed, the result implies that CuAl/SDS-LDH provides stronger electrostatic attraction and holds the target dye molecule more tightly. In contrast, the low positive charge on CuAl-LDH and lesser anion exchange capacity can be accounted for the poor removal efficiency of methyl red. The amount of adsorbed dye increases sharply until 0.025 g, after this dose the percentage of adsorption almost remains the same. This could be attributed to the well-dispersed particle of the adsorbent material on the dye solutions where the active adsorption and interchangeable sites present over the surface of the adsorbent are more exposed.^[20,50] Besides, the continuous and excessive increase in the amount of adsorbent can possibly cause the accumulation of LDH particle which reduces the easily accessible adsorption site by lowering specific surface area and providing higher diffusion path length value.^[51] Moreover, under the studied catalyst dosages the maximum percentage of dye removal was achieved up to 92% and 42.24% on CuAl/SDS-LDH and

CuAl-LDH, respectively, for the initial dye concentration of 95 mg/L and a contact time of 1 hr at room temperature. The large number of available adsorption sites by increasing the catalyst amount and high surface area can be responsible for the higher removal of dye.

Effect of contact time

With an emphasis to the rate of decontamination of dye from its aqueous solution, the contact time between the adsorbent and adsorbate molecule is an important factor. In general, most of the previously utilized LDH-based adsorbents, it has been observed that at the initial stage of contact time the rate of dye removal is fast which then gradually declines to minimum and reached the equilibrium stage. It is due to the sufficient and excess number of free available adsorption site and highest concentration gradient of adsorbate molecule at the initial stage.^[52] The effect of contact time on the adsorbate-adsorbent system are represented in Figure 13. It is evident that the rate of adsorption starts increasing rapidly after a contact time of 15 minutes. The rapid intake of dye molecules can be ascribed to the presence of large number of available vacant sites. However, during the adsorption process, the external surface and intergallery space of LDH are occupied by the dye molecules with the association of different possible interactions including electrostatic and H-bonding.^[53] In CuAl-LDH, the curve displays inflexion at a contact time of 50–75 minutes, which can be ascertained due to the transportation of adsorbed methyl red molecule present on the external surface to the internal pores of LDH via slow diffusion. Consequently, the rate of adsorption started to decline.^[54] The complete saturation of free vacant site was attained at a contact time of 120 min and 150 min for CuAl/SDS-LDH and CuAl-LDH, respectively. Furthermore, it is also clear that for similar initial concentration of methyl red dye the removal capacity of SDS-modified LDH is found to be comparatively higher than CuAl-LDH. After complete saturation, there exist a steric repulsion between incoming dye molecules and adsorbed dye molecules which is forming clusters with SDS-loaded LDH. As a result

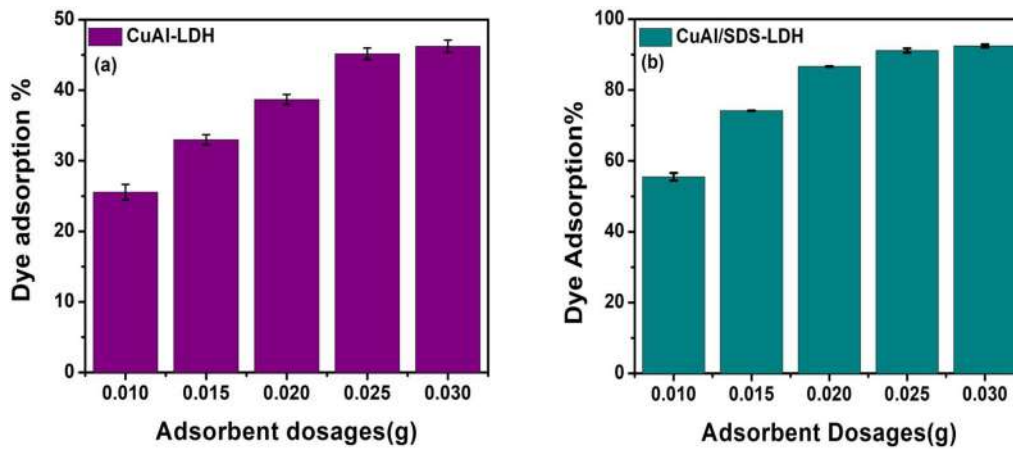


Figure 12. Influence of adsorbent dosages on the removal efficiency of methyl red dye by CuAl-LDH (a) and CuAl/SDS-LDH (b) (Initial dye concentration = 95 mg/L, pH = neutral, contact time = 1 h, volume = 20 mL).

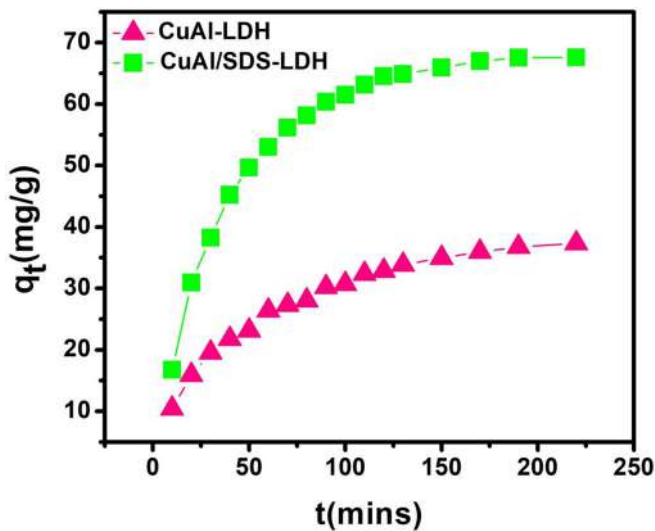


Figure 13. Effect of contact time on the adsorption capacities of CuAl-LDH and CuAl/SDS-LDH (Initial dye concentration = 60 mg/L, pH = neutral, adsorbent dosages = 44 mg, volume = 50 mL).

after reaching equilibrium contact time the amount of dye adsorbed remains constant throughout the time.

Effect of solution pH

Another essential parameter that influences the adsorption process is the solution pH, and it can also affect the liquid phase chemistry and binding sites of LDH surface. The effect of pH during the adsorption process was observed in the range of 4–10, which is shown in Figure 14. It is seen that for CuAl-LDH and CuAl/SDS-LDH under acidic pH-4, the highest adsorption up to 86% and 96.93%, respectively, was achieved while on moving toward the basic pH 10 it denotes a lower amount of dye retained on the surface of adsorbent. Under alkaline conditions, the increase in the concentration of OH⁻ ions competes with anionic methyl red dyes for the positively charged vacant sites and simultaneously the positively charged surface of the adsorbent also gets reduced, as a result at high pH value adsorption capacity is low. On the contrary, at low acidic solution pH the existence of additional H⁺ ion which get accumulated

over LDH surface imparts a large number of positively charged that can easily interact with anionic dyes and favors greater intake.^[28] From the result displayed in Figure 14, it can be analyzed that within the examined pH range (4–10) the surfactant-modified LDH can enhance greater removal of dye compared to unmodified LDH. At pH below 4 generally the structure of LDH gets destroyed which can decrease the adsorption capacity for Methyl red. However, the main factor contributing to the adsorption of methyl red dye on pristine LDH and CuAl/SDS-LDH may be explained by the electrostatic forces of attraction between positively charged LDH surfaces and negatively charged anionic dye.^[20] The chemical structure of methyl red possesses carboxy (-COO⁻) group can be easily attracted in the positively charged adsorption site. From the theoretical consideration, the point of zero charge value (PZC) can provide an optimum pH value for better adsorption of dyes, in general if the solution pH is less than PZC then the adsorbent will prefer anionic dyes whereas for pH > PZC the adsorbent shows greater adsorption for cationic dyes.^[55]

Mechanism of adsorption

The schematic illustration of methyl red uptake mechanism by CuAl-LDH and CuAl/SDS-LDH is demonstrated in Figure 15. The adsorption behavior of the methyl red dye on both CuAl-LDH and CuAl/SDS-LDH follows pseudo-second-order kinetics. Considering the adsorption capacity, this kinetic model envisages the nature of adsorption throughout the entire concentration of dye solution and favors chemisorption as the rate-determining mechanism. Generally, most of the LDH material exhibits important characteristics like high surface area, high porosity and exchangeable interlayer ions that may be accounted for the extraction of different anionic dye species from its aqueous solution. Moreover, the main factor responsible for the adsorption process can be owed to highly positive charged density on LDH layers and the stronger interactions between incoming anionic dyes and LDH.^[56] Besides, modification with the surfactants molecules creates a partitioning medium on both the internal and external surface of CuAl/SDS-LDH which can improve the hydrophobic nature of LDH

particles. This organic medium is essential and preferably increases the interaction among organic dyes and organo-modified LDH and it also acts as a partitioning medium for contaminants. However, the adsorption process involves an intricate mechanism, and it may be due to a combination of several possible interactions such as vander waals force,

H-bonding, electrostatic attraction and partitioning effect.^[20,53] To further investigate the adsorption process analysis of FT-IR spectrum displayed in Figure 2 clearly confirms adsorption of dye.

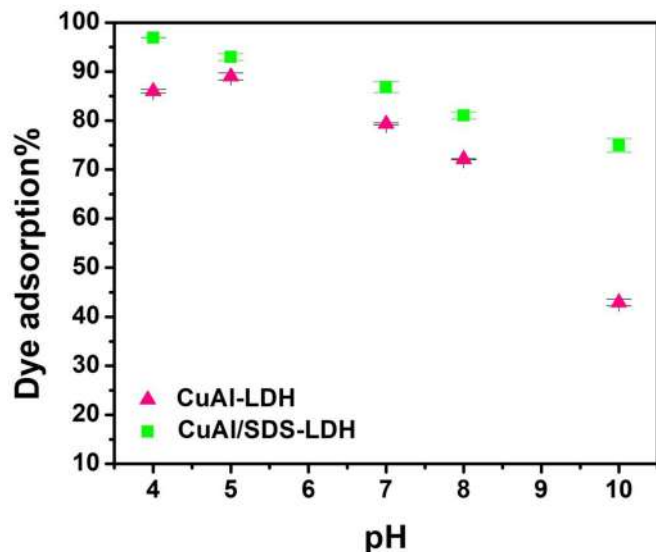


Figure 14. Effect of solution pH on the adsorption efficiency of methyl red dye by two adsorbents (Initial concentration = 95 mg/L, volume = 20 mL, contact time = 2 h, catalyst dosages = 22 mg).

Reusability

Reusability performances can reveal the efficacy of the material by using the same adsorbent repeatedly for industrial applications therefore, it is important to determine the economic feasibility of the adsorbents. The reusability experiment displayed in Figure 16 for the pristine LDH and surfactant-modified CuAl/SDS-LDH was examined up to the fourth cycle on 60 mg/L methyl red dye at neutral pH and 22 mg of adsorbent dosages. The initially adsorbed methyl red dye on the surface of the adsorbent was removed after each cycle by washing in a solvent acetone which is then dried at room temperature. For CuAl/SDS-LDH, the percentage of dye removal efficiency declines after every consecutive cycle and in the first cycle the removal efficiency reached up to 98% which then continuously decrease to 28.86% in the last cycle. In case of CuAl-LDH, the removal percentage is comparatively lower and lies between 72.36% and 28.86%. The gradual decreases in dye adsorption capacity can be ascribed to the loss of active adsorption sites due to the destruction in the structure of surfactant-loaded LDH.

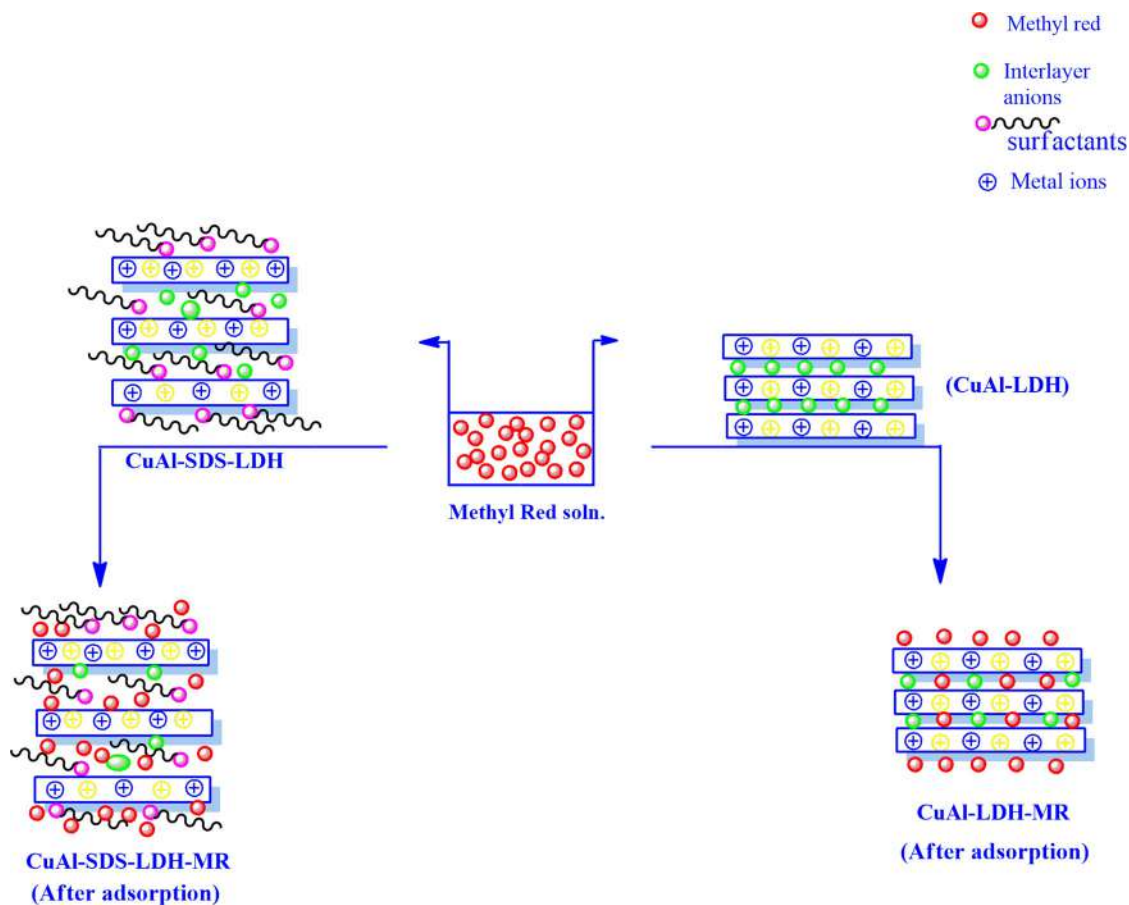


Figure 15. Schematic illustration for the methyl red uptake mechanism by CuAl-LDH and CuAl/SDS-LDH.

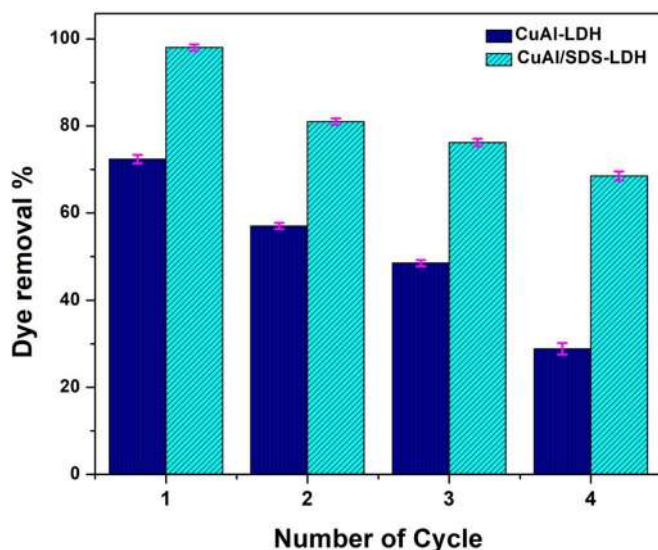


Figure 16. Reusability studies for the removal efficiency of methyl red dye over two adsorbents (Initial dye concentration = 60 mg/L, adsorbent dosages = 22 mg, pH = neutral, contact time = 12 h).

Conclusions

The study suggests that both adsorbents CuAl-LDH and surfactants modified CuAl/SDS-LDH can be easily synthesized and showed excellent efficiency for the removal of targeted anionic dyes. The results obtained from the physicochemical characterization infers the mesoporous nature, crystallinity and the expected elemental compositions of the materials without impurity. However, the adsorption isotherm and kinetics data are well fitted according to Langmuir and pseudo-second-order kinetic model. The CuAl/SDS-LDH indicates higher intake of organic dye pollutants with the maximum monolayer adsorption capacity $q_{\max} = 411$ mg/g compared to CuAl-LDH ($q_{\max} = 209$ mg/g). The influence of temperature toward the adsorption activity exhibits a spontaneous and endothermic process. The adsorbents can be reused up to the fourth cycle. Therefore, modification with the surfactants in the present materials has shed light on the emerging researchers for further investigation of the surfactants fabricated LDH-based adsorbents.

Acknowledgements

We are thankful to several institutes for providing instrumental facility for characterization of material with SEM-EDX, BET and Powder X-ray from CIF, IIT Guwahati, FT-Infrared from Cotton University and NEHU university, and Thermogravimetric analysis from IIT-Kanpur. We are also thankful to our institute Bodoland University for providing UV-spectrophotometer instruments and all the necessary materials and equipment required for our research works.

Disclosure statement

No potential conflict of interest was reported by the authors.

References

- Lu, F.; Astruc, D. Nanomaterials for Removal of Toxic Elements from Water. *Coord. Chem. Rev.* **2018**, *356*, 147–164. DOI: 10.1016/j.ccr.2017.11.003.
- Peláez-Cid, A. A.; Herrera-González, A. M.; Salazar-Villanueva, M.; Bautista-Hernández, A. Elimination of Textile Dyes Using Activated Carbons Prepared from Vegetable Residues and Their Characterization. *J. Environ. Manage.* **2016**, *181*, 269–278. DOI: 10.1016/j.jenvman.2016.06.026.
- Wang, L.; Wang, A. Adsorption Characteristics of Congo Red onto the Chitosan/Montmorillonite Nanocomposite. *J. Hazard. Mater.* **2007**, *147*, 979–985. DOI: 10.1016/j.jhazmat.2007.01.145.
- Özcan, A. S.; Erdem, B.; Özcan, A. Adsorption of Acid Blue 193 from Aqueous Solutions onto BTMA-Bentonite. *Colloids Surf. A Physicochem. Eng.* **2005**, *266*, 73–81. DOI: 10.1016/j.jcis.2004.07.035.
- Badr, Y.; Abd El-Wahed, M. G.; Mahmoud, M. A. Photocatalytic Degradation of Methyl Red Dye by Silica Nanoparticles. *J. Hazard. Mater.* **2008**, *154*, 245–253. DOI: 10.1016/j.jhazmat.2007.10.020.
- Lellis, B.; Fávoro-Polonio, C. Z.; Pamphile, J. A.; Polonio, J. C. Effects of Textile Dyes on Health and the Environment and Bioremediation Potential of Living Organisms. *Biotechnology. Res. Innov.* **2019**, *3*, 275–290. DOI: 10.1016/j.biori.2019.09.001.
- Yang, Z.; Wang, F.; Zhang, C.; Zeng, G.; Tan, X.; Yu, Z.; Zhong, Y.; Wang, H.; Cui, F. Utilization of LDH-Based Materials as Potential Adsorbents and Photocatalyst for the Decontamination of Dyes Wastewater: A Review. *RSC Adv.* **2016**, *6*, 79415–79436. DOI: 10.1039/C6RA12727D.
- Zahrim, A. Y.; Hilal, N. Treatment of Highly Concentrated Dye Solution by Coagulation/Flocculation-Sand Filtration and Nanofiltration. *Water Resour. Ind.* **2013**, *3*, 23–34. [Mismatch] DOI: 10.1016/j.wri.2013.06.001.
- Sahoo, C.; Gupta, A. K.; Pal, A. Photocatalytic Degradation of Methyl Red Dye in Aqueous Solutions under UV Irradiations Using Ag⁺ Doped TiO₂. *Desalination.* **2005**, *181*, 91–100. DOI: 10.1016/j.desal.2005.02.014.
- Wang, Q.; Tang, A.; Zhong, L.; Wen, X.; Yan, P.; Wang, J. Amino-Modified γ -Fe₂O₃/Sepiolite Composite with Rod-like Morphology for Magnetic Separation Removal of Congo Red Dye from Aqueous Solution. *Powder Technol.* **2018**, *339*, 872–881. DOI: 10.1016/j.powtec.2018.08.055.
- Al-Bastaki, N. Removal of Methyl Orange Dye and Na₂SO₄ Salt from Synthetic Waste Water Using Reverse Osmosis. *Chem. Eng. Process.* **2004**, *43*, 1561–1567. DOI: 10.1016/j.ccep.2004.03.001.
- Zahrim, A. Y.; Tizaoui, C.; Hilal, N. Removal of Highly Concentrated Industrial Grade Leather Dye: Study on Several Flocculation and Sand Filtration Parameters. *Sep. Sci. Technol.* **2011**, *46*, 883–892. DOI: 10.1080/01496395.2010.550596.
- Ahmed, I. M.; Gasser, M. S. Adsorption Study of Anionic Reactive Dye from Aqueous Solution to Mg-Fe-CO₃ Layered Double Hydroxide (LDH). *Appl. Surf. Sci.* **2012**, *259*, 650–656. DOI: 10.1016/j.apsusc.2012.07.092.
- Zaheer, Z.; Aisha, A. A.; Aazam, E. S. Adsorption of Methyl Red on Biogenic Ag@Fe Nanocomposite Adsorbent: Isotherms, Kinetics and Mechanisms. *J. Mol. Liq.* **2019**, *283*, 287–298. DOI: 10.1016/j.molliq.2019.03.030.
- Eltaweil, A. S.; Abd El-Monaem, E. M.; El-Subruiti, G. M.; Abd El-Latif, M. M.; Omer, A. M. Fabrication of UiO-66/MIL-101(Fe) Binary MOF/Carboxylated-GO Composite for Adsorptive Removal of Methylene Blue Dye from Aqueous Solutions. *RSC Adv.* **2020**, *10*, 19008–19019. DOI: 10.1039/d0ra02424d.
- Mishra, G.; Dash, B.; Pandey, S. Layered Double Hydroxides: A Brief Review from Fundamentals to Applications as Evolving Biomaterials. *Appl. Clay Sci.* **2018**, *153*, 172–186. DOI: 10.1016/j.clay.2017.12.021.
- Chen, Y. X.; Zhu, R.; Xu, Z. L.; Ke, Q. F.; Zhang, Q.; Guo, Y. P. Self-Assembly of Pifithrin- α -Loaded Layered Double

- Hydride/Chitosan Nanohybrid Composites as a Drug Delivery System for Bone Repair Materials. *J. Mater. Chem. B* **2017**, *5*, 2245–2253. DOI: [10.1039/c6tb02730j](https://doi.org/10.1039/c6tb02730j).
18. Jiang, Y.; Hao, Z.; Luo, H.; Shao, Z.; Yu, Q.; Sun, M.; Ke, Y.; Chen, Y. Synergistic Effects of Boron-Doped Silicone Resin and a Layered Double Hydroxide Modified with Sodium Dodecyl Benzenesulfonate for Enhancing the Flame Retardancy of Polycarbonate. *RSC Adv.* **2018**, *8*, 11078–11086. DOI: [10.1039/c8ra01086b](https://doi.org/10.1039/c8ra01086b).
 19. Wu, P.; Wu, T.; He, W.; Sun, L.; Li, Y.; Sun, D. Adsorption Properties of Dodecylsulfate-Intercalated Layered Double Hydroxide for Various Dyes in Water. *Colloids Surf. A Physicochem. Eng. Asp.* **2013**, *436*, 726–731. DOI: [10.1016/j.col-surf.2013.08.015](https://doi.org/10.1016/j.col-surf.2013.08.015).
 20. Zhang, B.; Dong, Z.; Sun, D.; Wu, T.; Li, Y. J. Enhanced Adsorption Capacity of Dyes by Surfactant-Modified Layered Double Hydroxides from Aqueous Solution. *J. Ind. Eng. Chem.* **2017**, *49*, 208–218. DOI: [10.1016/j.jiec.2017.01.029](https://doi.org/10.1016/j.jiec.2017.01.029).
 21. Li, J.; Zhang, S.; Chen, Y.; Liu, T.; Liu, C.; Zhang, X.; Yi, M.; Chu, Z.; Han, X. A Novel Three-Dimensional Hierarchical CuAl Layered Double Hydroxide with Excellent Catalytic Activity for Degradation of Methyl Orange. *RSC Adv.* **2017**, *7*, 29051–29057. DOI: [10.1039/C7RA03848H](https://doi.org/10.1039/C7RA03848H).
 22. Qu, J.; He, X.; Lei, Z.; Zhang, Q.; Liu, X. Mechanochemical Synthesis of Dodecyl Sulfate Anion (DS⁻) Intercalated Cu-Al Layered Double Hydroxide. *Solid State Sci.* **2017**, *74*, 125–130. DOI: [10.1016/j.solidstatesciences.2017.10.015](https://doi.org/10.1016/j.solidstatesciences.2017.10.015).
 23. Meyn, M.; Beneke, K.; Lagaly, G. Anionic-Exchange Reactions of Layered Double Hydroxides. *Inorg. Chem.* **1990**, *29*, 5201–5207. DOI: [10.1021/ie9004332](https://doi.org/10.1021/ie9004332).
 24. Iyi, N.; Tamura, K.; Yamada, H. One-Pot Synthesis of Organophilic Layered Double Hydroxides (LDHs) Containing Aliphatic Carboxylates: Extended “Homogeneous Precipitation” Method. *J. Colloid Interface Sci.* **2009**, *340*, 67–73. DOI: [10.1016/j.jcis.2009.08.026](https://doi.org/10.1016/j.jcis.2009.08.026).
 25. Berner, S.; Araya, P.; Govan, J.; Palza, H. Cu/Al and Cu/Cr Based Layered Double Hydroxide Nanoparticles as Adsorption Materials for Water Treatment. *J. Ind. Eng. Chem.* **2018**, *59*, 134–140. DOI: [10.1016/j.jiec.2017.10.016](https://doi.org/10.1016/j.jiec.2017.10.016).
 26. El-Mansy, M. A. M.; Yahia, I. S. Spectroscopic Notes of Methyl Red (MR) Dye. *Spectrochim. Acta A Mol. Biomol. Spectrosc.* **2014**, *130*, 59–63. DOI: [10.1016/j.saa.2014.03.113](https://doi.org/10.1016/j.saa.2014.03.113).
 27. Rathee, G.; Singh, N.; Chandra, R. Simultaneous Elimination of Dyes and Antibiotic with a Hydrothermally Generated NiAlTi Layered Double Hydroxide Adsorbent. *ACS Omega.* **2020**, *5*, 2368–2377. DOI: [10.1021/acsomega.9b03785](https://doi.org/10.1021/acsomega.9b03785).
 28. Chen, Y.; Jing, C.; Zhang, X.; Jiang, D.; Liu, X.; Dong, B.; Feng, L.; Li, S.; Zhang, Y. Acid-Salt Treated CoAl Layered Double Hydroxide Nanosheets with Enhanced Adsorption Capacity of Methyl Orange Dye. *J. Colloid Interface Sci.* **2019**, *548*, 100–109. DOI: [10.1016/j.jcis.2019.03.107](https://doi.org/10.1016/j.jcis.2019.03.107).
 29. Natarajan, S.; Naresh, R.; Thiagarajan, V. Removal of Anionic Dyes from Water Using Polyethylene Glycol Modified Ni-Al Layered Double Hydroxide Nanocomposites. *Chemistry Select.* **2020**, *5*, 4165–4174. DOI: [10.1002/slct.202000051](https://doi.org/10.1002/slct.202000051).
 30. Mindru, I.; Gingasu, D.; Patron, L.; Marinescu, G.; Calderon-Moreno, J. M.; Preda, S.; Oprea, O.; Sultana, N. Copper Aluminate Spinel by Soft Chemical Routes. *Ceram. Int.* **2016**, *42*, 154–164. doi.org/10.1016%2Fj.ceramint.2015.08.058 DOI: [10.1016/j.ceramint.2015.08.058](https://doi.org/10.1016/j.ceramint.2015.08.058).
 31. Lei, S.; Wang, S.; Gao, B.; Zhan, Y.; Zhao, Q.; Jin, S.; Song, G.; Lyu, X.; Zhang, Y.; Tang, Y. Ultrathin Dodecyl-Sulfate-Intercalated Mg-Al Layered Double Hydroxide Nanosheets with High Adsorption Capability for Dye Pollution. *J. Colloid Interface Sci.* **2020**, *577*, 181–190. DOI: [10.1016/j.jcis.2020.05.050](https://doi.org/10.1016/j.jcis.2020.05.050).
 32. González-Olvera, R.; Urquiza-Castro, C. I.; Negrón-Silva, G. E.; Ángeles-Beltrán, D.; Lomas-Romero, L.; Gutiérrez-Carrillo, A.; Lara, V. H.; Santillan, R.; Morales-Serna, J. A. Cu-Al Mixed Oxide Catalysts for Azide-Alkyne 1,3-Cycloaddition in Ethanol-Water. *RSC Adv.* **2016**, *6*, 63660–63666. DOI: [10.1039/C6RA10097J](https://doi.org/10.1039/C6RA10097J).
 33. Dutta, R.; Nagarjuna, T. V.; Mandavgane, S. A.; Ekhe, J. D. Ultrafast Removal of Cationic Dye Using Agrowaste-Derived Mesoporous Adsorbent. *Ind. Eng. Chem. Res.* **2014**, *53*, 18558–18567. DOI: [10.1021/ie5030003](https://doi.org/10.1021/ie5030003).
 34. Langmuir, I. The Adsorption of Gases on Plane Surfaces of Glass, Mica and Platinum. *J. Am. Chem. Soc.* **1918**, *40*, 1361–1403. DOI: [10.1021/ja02242a004](https://doi.org/10.1021/ja02242a004).
 35. Rathee, G.; Awasthi, A.; Sood, D.; Tomar, R.; Tomar, V.; Chandra, C. A New Biocompatible Ternary Layered Double Hydroxide Adsorbent for Ultrafast Removal of Anionic Organic Dyes. *Sci. Rep.* **2019**, *9*, 16225. doi.org/s41598-019-52849-4.
 36. Freundlich, H. Over the Adsorption in Solution. *J. Phys. Chem.* **1906**, *57*, 385–471.
 37. Temkin, M. I.; Pyzhev, V. Kinetic of Ammonia Synthesis on Promoted Iron Catalyst. *Acta Physicochim. URSS.* **1940**, *12*, 327–356.
 38. Romdhane, D. F.; Satlaoui, Y.; Nasraoui, R.; Charef, A.; Azouzi, R. Adsorption, Modeling, Thermodynamic, and Kinetic Studies of Methyl Red Removal from Textile-Polluted Water Using Natural and Purified Organic Matter Rich Clays as Low-Cost Adsorbent. *J. Chem.* **2020**, *2020*, 1–17. pages article id-4376173. DOI: [10.1155/2020/4376173](https://doi.org/10.1155/2020/4376173).
 39. Ghaedi, M.; Hassani, R.; Dashtian, K.; Shafie, G.; Purkait, M. K.; Dehghan, H. Adsorption of Methyl Red on to Palladium Nanoparticles Loaded on Activated Carbon: experimental Design Optimization. *Desalin. Water Treat.* **2016**, *57*, 22646–22654. DOI: [10.1080/19443994.2015.1136963](https://doi.org/10.1080/19443994.2015.1136963).
 40. Dadfarnia, S.; Shabani, A. M.; Moradi, S. E.; Emami, S. Methyl Red Removal from Water by Iron Based Metal-Organic Frameworks Loaded on to Iron Oxide Nanoparticle Adsorbents. *Appl. Surf. Sci.* **2015**, *330*, 85–93. doi.org/10.1016%2Fj.apsusc.2014.12.196. DOI: [10.1016/j.apsusc.2014.12.196](https://doi.org/10.1016/j.apsusc.2014.12.196).
 41. Khan, E. A.; Khan, T. A.; Shahjahan. Adsorption of Methyl Red on Activated Carbon Derived from Custard Apple (*Annona squamosa*) Fruit Shell: Equilibrium Isotherm and Kinetic Studies. *J. Mol. Liq.* **2018**, *249*, 1195–1211. DOI: [10.1016/j.molliq.2017.11.125](https://doi.org/10.1016/j.molliq.2017.11.125).
 42. Ahmad, M. A.; Ahmad, N.; Bello, O. S. Modified Durian Seed as Adsorbent for the Removal of Methyl Red Dye from Aqueous Solutions. *Appl. Water Sci.* **2015**, *5*, 407–423. DOI: [10.1007/s13201-014-0208-4](https://doi.org/10.1007/s13201-014-0208-4).
 43. Yilmaz, E.; Sert, E.; Atalay, F. S. Synthesis, Characterization of a Metal Organic Framework: MIL-53(Fe) and Adsorption Mechanisms of Methyl Red onto MIL-53 (Fe). *J. Taiwan Inst. Chem. Eng.* **2016**, *65*, 323–330. DOI: [10.1016/j.jtice.2016.05.028](https://doi.org/10.1016/j.jtice.2016.05.028).
 44. Lagergren, S. About the Theory of so-Called Adsorption of Soluble Substances. *Kungl. Svenska Vetenskapsakad. Handl.* **1898**, *24*, 1–39.
 45. Ho, Y. S.; McKay, G. Sorption of Dye from Aqueous Solution by Peat. *Chem. Eng. J.* **1998**, *70*, 115–124. DOI: [10.1016/S0923-0467%2898%2900076-1](https://doi.org/10.1016/S0923-0467%2898%2900076-1).
 46. Weber, W. J.; Morris, J. C. Kinetics of Adsorption on Carbon from Solutions. *J. Sanit. Engrg. Div.* **1963**, *89*, 31–59. DOI: [10.1061/JSEDA1.0000430](https://doi.org/10.1061/JSEDA1.0000430).
 47. Patanjali, P.; Mandal, A.; Chopra, I.; Singh, R. Adsorption of Cationic Dyes on to Biopolymer-Bentonite Composites: Kinetics and Isotherm Studies. *Int. J. Environ. Anal. Chem.* **2020**, *100*, 1–23. DOI: [10.1080/03067319.2020.1849660](https://doi.org/10.1080/03067319.2020.1849660).
 48. Zaghouane-Boudiaf, H.; Boutahala, M.; Arab, L. Removal of Methyl Orange from Aqueous Solution by Uncalcined and Calcined MgNiAl Layered Double Hydroxides (LDHs). *Chem. Eng. J.* **2012**, *187*, 142–149. DOI: [10.1016/j.cej.2012.01.112](https://doi.org/10.1016/j.cej.2012.01.112).
 49. Kameda, T.; Kondo, E.; Yoshioka, T. Preparation of Mg-Al Layered Double Hydroxide Doped with Fe²⁺ and Its Application to Cr(VI) Removal. *Sep. Purif. Technol.* **2014**, *122*, 12–16. DOI: [10.1016/j.seppur.2013.10.033](https://doi.org/10.1016/j.seppur.2013.10.033).

50. Huang, J.; Liu, Y.; Wang, X. Selective Adsorption of Tannin from Flavonoids by Organically Modified Attapulgite Clay. *J. Hazard. Mater.* **2008**, *160*, 382–387. DOI: [10.1016/j.jhazmat.2008.03.008](https://doi.org/10.1016/j.jhazmat.2008.03.008).
51. Zhao, D.; Sheng, G.; Hu, J.; Chen, C.; Wang, X. The Adsorption of pb(II) on Mg₂Al Layered Double Hydroxide. *Chem. Eng. J.* **2011**, *171*, 167–174. DOI: [10.1016/j.cej.2011.03.082](https://doi.org/10.1016/j.cej.2011.03.082).
52. Inbaraj, B. S.; Chiu, C. P.; Ho, G. H.; Yang, J.; Chen, B. H. Removal of Cationic Dyes from Aqueous Solution Using an Anionic Poly- γ -Glutamic Acid-Based Adsorbent. *J. Hazard. Mater.* **2006**, *137*, 226–234. DOI: [10.1016/j.jhazmat.2006.01.057](https://doi.org/10.1016/j.jhazmat.2006.01.057).
53. Chun, Y.; Sheng, G.; Boyd, S. A. Sorptive Characteristics of Tetraalkylammonium-Exchanged Smectite Clays. *Clays Clay Miner.* **2003**, *51*, 415–420. DOI: [10.1346/CCMN.2003.0510407](https://doi.org/10.1346/CCMN.2003.0510407).
54. Enache, D. F.; Vasile, E.; Simonescu, C. M.; Răzvan, A.; Nicolescu, A.; Nechifor, A. C.; Oprea, O.; Pătescu, R. E.; Onose, C.; Dumitru, F. Cysteine-Functionalized Silica-Coated Magnetite Nanoparticles as Potential Nanoadsorbents. *J. Solid State Chem.* **2017**, *253*, 318–328. DOI: [10.1016/j.jssc.2017.06.013](https://doi.org/10.1016/j.jssc.2017.06.013).
55. Jun, H.; Zhiliang, Z.; Hongtao, L.; Yanling, Q. Effect of Metal Composition in Lanthanum-Doped Ferric-Based Layered Double Hydroxides and Their Calcined Products on Adsorption of Arsenate. *RSC Adv.* **2014**, *4*, 5156–5164. DOI: [10.1039/c3ra46680a](https://doi.org/10.1039/c3ra46680a).
56. Shan, R. R.; Yan, L. G.; Yang, Y. M.; Yang, K.; Yu, S. J.; Yu, H. Q.; Zhu, B. C.; Du, B. Highly Efficient Removal of Three Red Dyes by Adsorption on to Mg-Al-Layered Double Hydroxide. *J. Ind. Eng. Chem.* **2015**, *21*, 561–568. DOI: [10.1016/j.jiec.2014.03.019](https://doi.org/10.1016/j.jiec.2014.03.019).



Synthesis of ZrO₂/MgAl-LDH composites and evaluation of its isotherm, kinetics and thermodynamic properties in the adsorption of congo red dye

Deepmoni Brahma^{1,2}, Hemaprobha Saikia^{1,*}

¹ Department of Chemistry, Bodoland University, Kokrajhar 783370, Assam, India

² Department of Chemistry, Bodoland University, Kokrajhar, BTR, Assam, Pin-783370

ARTICLE INFO

Keywords:

Congo red
Dye removal
Urea hydrolysis
ZrO₂/MgAl-LDH composite
Adsorption

ABSTRACT

Recently, the treatment of waste water by Zr-based adsorbents had significantly attracted wide interest among researchers owing to its distinct features. The unique properties of Zr such as thermal stability, large size, high positive charge, greater mechanical rigidity and acid-base nature are mainly responsible for its diverse application. In this work, designing of the new adsorbent material containing tetravalent Zr metal oxide layered double hydroxide (LDH) composite for the removal of anionic dye was studied. The modification of LDH was conducted via the urea hydrolysis method by using zirconium salts as a precursor material. The adsorption efficiency of the as-synthesized material represented as ZrO₂/MgAl-LDH was investigated for the decontamination of congo red (CR) dye from an aqueous medium. The adsorbent ZrO₂/MgAl-LDH composite was characterized by several instrumental techniques including powder X-ray diffraction (P-XRD), Brunauer-Emmett-Teller (BET), X-ray photoelectron spectroscopy (XPS), Fourier transform infrared spectroscopy (FT-IR), scanning emission microscopy (SEM), energy dispersive X-ray (EDX), transmission emission microscopy (TEM) and thermogravimetric analysis (TGA). The influence of several experimental factors on the adsorption equilibrium studies such as pH, temperature, initial dye concentration, contact time, adsorbent dosages, and interfering ions are examined under optimized conditions. The thermodynamic study manifests the spontaneous and endothermic nature of the sorption process. Additionally, based on fitting the experimental data with different models the isotherm and kinetics mechanism are found to be more appropriate with Langmuir isotherm, Redlich-Peterson isotherm, and pseudo-second-order kinetics. The spectral analysis further indicates the oxidizing nature of the material, therefore favoring the adsorption of anionic dye. The maximum dye removal efficiency of ZrO₂/MgAl-LDH reached up to 97.19% under the optimum reaction condition (initial dye concentration = 50 mg/L, contact dosages = 0.02 g, temperature = 303 K). In addition, the maximum monolayer adsorption capacity ($q_{\max} = 169.42$ mg) for CR adsorption also reveals its superiority in adsorption test. Moreover, the adsorbent can be easily retrieved and reused up to fifth cycle. Therefore, the characterization and experimental results of ZrO₂/MgAl-LDH affirms its potential application for effective decontamination of waste water.

1. Introduction

With the rapid expansion of modern industries, the increasing emissions of potentially toxic synthetic dyes had caused a severe global threats to the environment affecting aquatic systems and other habitats living in the ecosystem. Despite, its high toxic effect synthetic dyes are also widely used in various industries such as textile, paper, paint, food, pharmaceuticals, cosmetics, and plastics for dyeing purposes [1,2]. Currently, synthetic azo dyes are the major water pollutants that are discharged from several manufacturing industries and carried directly to natural water bodies, including rivers, oceans, canals, lakes and other geographical regions [3,4]. Accounting for its stable chemical structure, non-biodegradable and toxic nature, the azo dye

can change the biochemical characteristics of the fresh water system which in turn leads to adverse effects on aquatic life. In addition, the presence of such organic pollutants can also decrease the biological oxygen demand and increases chemical oxygen demand [5–7]. Nearly, 7×10^5 tons of varieties of dye are manufactured yearly all over the world. In particular, congo red (CR) dye is one of the most extensively used dyes which decompose to benzidine compound, and it is known for its potential effect to cause carcinogenic activities in living creatures [8–10]. Concerning the public health and environmental protection regulation, the development of environmental remediation material for the elimination of CR dye from the effluent before releasing it into the environment is very crucial and could be an interesting research field.

* Corresponding author: Dr. Hemaprobha Saikia, Assistant Professor, Department of Chemistry, Bodoland University, Kokrajhar, BTR, Assam, Pin-783370
E-mail addresses: brahmadeepmoni@gmail.com (D. Brahma), saikiahemaprobha@gmail.com (H. Saikia).

Over the past two decades, numerous wastewater remediation techniques including photocatalytic degradation, reverse osmosis, membrane filtration, flocculation, magnetic separation, and electro dialysis are employed. Nevertheless, most of these methods involve high expensive, low removal capacity, critical process, high energy consumption, and generation of secondary waste products. Consequently, these methods are not appropriate for large scale treatment of dye contaminated waste water [11–16]. Alternatively, the adsorption method has proven to be an excellent process for separation of dye stuff contaminants. Owing to its reversible nature, robust, universal approach, low cost, high efficiency, easy separation and simple operation, this technique have a great potential to be utilized for a large scale industrial application in developing nations. Several adsorbent materials for decontamination of waste water are available which include agricultural waste-derived activated carbon [17], metal organic frameworks [18], zeolite [19], polymer-based gel [20], grapheme oxide nanomaterials [21] and clay minerals [22]. Moreover, in search of outstanding adsorption performances and to make sustainable adsorbents fabrication of these materials to enhance its adsorption characteristics are gaining considerable attraction among researchers. For instance, Hu et al. have reported a polyacrylic super adsorbent hydrogel, synthesized via free radical polymerization by using nano spherulites (CNS) crosslinker which display a large adsorption capacity (2100 mg/g) for methylene dye [20]. Mosavi et al. prepared MOF-5 through solvothermal method and modified with CuCl_2 under ambient temperature, which is further adapted for a CR adsorption [18]. Mao et al. fabricated pristine graphene oxide and synthesized interconnected reduced graphene oxide and fluorinated graphene oxide, and its adsorptive performance in aqueous medium were examined by implementing water pollutant dyes such as Rhodamine B and methylene blue, where the maximum adsorption capacity obtained was 686.6 mg/g and 403.3 mg/g, respectively [21].

Layered double hydroxide (LDH) also known as anionic clays are the hierarchically structured materials containing brucite sheets composed of divalent M^{2+} and M^{3+} cations with interlayer anions A^{2-} such as OH^- , CO_3^{2-} , Cl^- . The electro neutrality in the structure is ensured by the colombic force of attraction between intergallery anions and positive charge metals on LDH layer [23]. Due to its wide range of application, including flame retardant, drug delivery, adsorbents, and catalysis, layered double hydroxide can be regarded as an exceptionally promising material. Consequently, researchers find interesting to further explore the ability of LDH to evaluate the issues emerging due to azo-dye contaminants. Among the clay materials, LDHs are the most versatile material which displays excellent dye removal characteristics during the water purification process. The structure of LDH is flexible and possesses important structural features such as porosity, high surface area, anion exchangeability, isomorphous substitution of metal ions on brucite sheets, surface modification, and transformation to mixed metal oxides upon calcinations at 500° C. Nevertheless, low cost and less toxic nature of LDH are also other advantages making it more viable and environmentally benign material for removal of hazardous organic contaminants from effluents [24,25].

Based on the literature, most of the LDH employed for wastewater treatment are generally containing monovalent to trivalent cation in their structure. However, modification with tetravalent cation can alter the charge of LDH sheets which may enhance its sorption characteristics. Since, Zr based sorbents are known for its effective removal of various inorganic and organic contaminants, which can be attributed due to the high positive charge of Zr ions possessing a strong tendency for electronegative ions. Besides, zirconium has also been manifested as a non-toxic, ecofriendly and cost effective metal precursors [26]. Thus, the synthesis of the composite material $\text{ZrO}_2/\text{MgAl-LDH}$ by fabricating LDH with Zr salts may benefit the resulting adsorbent by making it more sustainable and also due to integration of characteristic features of both LDH and Zr(IV) metal oxide. Additionally, it might widened its sorption properties which is not only limited to anionic dyes, but the removal of several other harmful inorganic ions such as F^- , PO_4^{2-} , AsO_2^- could be

feasible. On that account, grabbing the advantage of both Zr(IV) metal oxide and LDH, the present work mainly focuses on the development of novel composite material viz; $\text{ZrO}_2/\text{MgAl-LDH}$ by adopting urea hydrolysis method and evaluated its adsorption efficiency by taking CR dye as a model pollutant. The synthesized adsorbent $\text{ZrO}_2/\text{MgAl-LDH}$ is well characterized and the influence of various experimental factors such as adsorbent dosages, contact time, ionic strength, co-existing anions, pH, and temperature are investigated. The adsorption isotherm and kinetics model are used for fitting experimental data. In order to analyze the adsorption mechanism powder XRD and FT-IR spectra after adsorption is recorded.

2. Experimental

2.1. Materials and Methods

Zirconium oxychloride ($\text{ZrOCl}_2 \cdot 8\text{H}_2\text{O}$), Aluminium chloride (AlCl_3), Magnesium chloridehexahydrate ($\text{MgCl}_2 \cdot 6\text{H}_2\text{O}$) were purchased from Merck. Urea (NH_2CONH_2) and CR ($\text{C}_{32}\text{H}_{22}\text{N}_6\text{Na}_2\text{O}_6\text{S}_2$) (purity = 98%) were obtained from Qualigens India Pvt. Limited. All the chemicals are of analytical grade and used without any further purification. The required solution for adsorption experiments is prepared by using distilled water.

2.1.1. Synthesis of the $\text{ZrO}_2/\text{MgAl-LDH}$ composite

The synthesis of $\text{ZrO}_2/\text{MgAl-LDH}$ was prepared by the urea hydrolysis method. Initially, a mixture of 3 mmol $\text{MgCl}_2 \cdot 6\text{H}_2\text{O}$, 1 mmol ZrOCl_2 , and 2 mmol AlCl_3 was dissolved in a 100 mL distilled water taken in a beaker. The resulting solution containing metal precursors was vigorously stirred in a magnetic stirrer. 2.1 g of urea is added further to the solution, followed by continuous stirring for 15 minutes until the clear homogeneous solution was obtained. This liquid suspension is then transferred in an autoclave and heated in the oven at 150°C for 6 hours. The resulting white precipitate was then centrifuged at 800 rpm and washed with distilled water up to five times. The obtained slurry was dried in the oven at 50°C for 12 hours. Finally, the white product is ground with mortar to get powder form which is denoted as $\text{ZrO}_2/\text{MgAl-LDH}$.

2.1.2. Characterization

The synthesized sample $\text{ZrO}_2/\text{MgAl-LDH}$ was characterized by different spectroscopic techniques in order to get detailed information about Physico-chemical properties. The X-ray diffraction pattern was recorded by Rigaku Ultima-IV powder x-ray diffractometer by using CuK_α radiation. The FT-IR spectrum of the sample was recorded on Shimadzu IR Affinity-1 by using a KBr background. The thermal decomposition of the adsorbent was studied in TGA (Mettler Toledo) under N_2 atmosphere at the heating rate of 20°C/min and the operating temperature was 30–1100°C. The external microstructure was examined by scanning emission microscopy (Gemini Carl Zeiss Sigma 300). The internal morphology was investigated by using transmission emission microscopy (JEOL JEM-2100). The specific surface area, and porosity of the sample were determined at 77K by using the surface area analyser (Quantachrome Novawin version 11.05) by conducting adsorption-desorption of N_2 gas. The atomic composition and valence state of the constituent elements in the sample was estimated by X-ray photoelectron spectroscopy (XPS) (PHI 5000 Versa Probe II). The residual dye concentration was measured by using UV-Spectrophotometer -3375 (Electronics India). The point of zero charge (PZC) of $\text{ZrO}_2/\text{MgAl-LDH}$ was determined by pH drift method. Initially, a series of solutions at different pH values (3–9) containing 20 mL each of 0.1M NaCl was prepared, meanwhile the pH of the solution was adjusted by using 0.1M HCl and 0.1M NaOH. Subsequently, 0.3 g of the adsorbent was added to each of the prepared solutions which is further stirred for 24 hours. After completion of stirring the final pH of the solution was measured by a digital

pH meter MK VI and the point of zero charge (PZC) value was evaluated from the plot of pH initial vs pH final.

2.1.3. Adsorption experiment

The various adsorption experiments are conducted in batch mode. In isotherm studies, an aqueous CR dye solution at a varying initial concentration (30 mg/L-180 mg/L) containing 20 mL each were taken in a 150 mL conical flask. Thereafter, 0.02 g of the adsorbent ZrO₂/MgAl-LDH was mixed with a CR dye solution which was followed by agitation in a water bath shaker for a time period of 4hours to attain equilibrium. The experiment was carried out at an operating temperatures of 30°C, 40°C, and 50°C. Furthermore, after reaching equilibrium the adsorbent was separated from the solution by filtration and the residual dye concentration remaining in the filtrate was calculated spectrophotometrically by UV-Spectrophotometer (EI-3315) which was set at the maximum wavelength of 498 nm. The quantity of the CR adsorbed on ZrO₂/MgAl-LDH was estimated by the equation (1).

$$q_e = \frac{(C_0 - C_e) V}{W} \quad (1)$$

The percentage of dye removal was calculated by the equation (2)

$$\% \text{ of dye removal} = \frac{(C_0 - C_e) \times 100}{C_0} \quad (2)$$

where C₀ and C_e indicates initial and the equilibrium concentration of CR dye solution in mg/L. q_e (mg/g) signifies the equilibrium adsorption capacity, V is the total volume of solution in litres (L) and W denotes amount of adsorbent in gram (g).

For kinetic studies the experiment was performed under a constant temperature of 30°C. Initially, 0.02 g of adsorbent was dispersed in 40 mL of CR solution at different initial concentration 30, 60 and 90 mg/L. The resulting solution is then agitated in a thermostatic shaker similar to the isotherm experiment for a time period of 180 minutes. However, 2 mL of the solution is withdrawn after a definite time interval which is separated from the adsorbent by centrifugation at 1000 rpm/min. After separation the concentration of residual dye is analyzed to determine the rate of dye adsorption with time. The CR dye uptake by the adsorbent with time was evaluated by the equation (3).

$$q_t = \frac{(C_0 - C_t) V}{W} \quad (3)$$

where q_t (mg/g) is the amount of dye uptake at time t(min), V is the total volume of the solution(L), W is the quantity of adsorbent (g), C₀ and C_t are the concentration of dye at initial and at time t respectively.

2.1.4. Desorption Studies

The desorption experiment was investigated by using eluents of different nature such as acetone, ethanol, methanol, 0.1 M NaOH, and 0.1 M Na₂CO₃. Initially, 20 mL of CR dye solution at 40 mg/L concentration was allowed to treat with 0.015 g of ZrO₂/MgAl-LDH for a contact time of 3hours. After complete adsorption, the adsorbent was separated from the suspension and dried. Subsequently, the dye-loaded adsorbent was further agitated in 20 mL eluent solution to desorb the initially adsorbed dye molecule under the same reaction time. The percentage of desorption was calculated by the equation (4):

$$\text{Desorption}\% = \frac{C_{\text{desorbed}}}{C_{\text{sorbed}}} \times 100 \quad (4)$$

where C_{desorbed} and C_{sorbed} are the quantity of dye desorbed and adsorbed respectively.

2.1.5. Error Analysis

To test the best fitting of isotherm data with different adsorption isotherm models, χ² value was computed which is represented by the following equation [27]

$$\chi^2 = \sum \frac{(q_{e,\text{exp}} - q_{e,\text{cal}})^2}{q_{e,\text{exp}}} \quad (5)$$

where q_{e,exp} is the equilibrium sorption capacity calculated from the experiment, and q_{e,cal} is the equilibrium sorption capacity predicted by the isotherm model.

However, for determining the most appropriate kinetic model that can describe the sorption process, the sum of the squares error was evaluated by the equation [28]

$$\text{Sum of square error}(SSE) = \frac{\sqrt{\sum (q_{e,\text{cal}} - q_{e,\text{exp}})^2}}{N} \quad (6)$$

where q_{e,cal} is the equilibrium sorption capacity evaluated from pseudo-first order and pseudo-second order kinetic model, q_{e,exp} is the experimental amount of adsorbate adsorbed at equilibrium, N is the number of data points.

2.2. Adsorption Isotherm

To investigate the affinity of CR dye towards the adsorbent ZrO₂/MgAl-LDH, the adsorption isotherm experiment was conducted. From the isotherm studies the qualitative nature of the adsorbate-adsorbent system can be well understood. The experimental equilibrium data were fitted based on the four different isotherm models, especially Langmuir, Freundlich, Temkin and Redlich-Peterson isotherm. According to Langmuir model it assumes that the heat of adsorption is equal for all the adsorption site of the material and the solute molecules are homogeneously adsorbed throughout the surface of the adsorbent [29].

The non linear equation for Langmuir model is formulated as:

$$q_e = \frac{q_{\text{max}} C_e K_1}{1 + K_1 C_e} \quad (7)$$

where q_{max} and q_e indicates the maximum monolayer adsorption capacity and the amount of dye adsorbed at equilibrium respectively. K₁ signifies Langmuir constant which is related to the free energy of adsorption and C_e (mg/L) denotes the concentration of dye at equilibrium.

In order to interpret feasibility of the adsorption process, the dimensionless separation factor R_L was computed by the equation given as [30]:

$$R_L = \frac{1}{1 + K_1 C_0} \quad (8)$$

where K₁ and C₀ (mg/L) are Langmuir constant and initial concentration of dye, respectively.

2.2.1. Freundlich Isotherm

Freundlich isotherm is an empirical equation which describes adsorption in the heterogeneous system and relates the amount of adsorbate intake per unit mass of the adsorbent. The model is generally more appropriate for the adsorption on heterogeneous surfaces. The non linear Freundlich isotherm equation is given as [31]:

$$q_e = K_f C_e^{1/n} \quad (9)$$

where n and K_f are Freundlich constants related to intensity and adsorption capacity in the sorption process.

2.2.2. Temkin Isotherm

Accounting for the interaction with the adsorbate-adsorbent system, the Temkin model considers that linear reduction in the heat of adsorption arises for the solute molecules by increasing coverage of the sites. The non-linear Temkin isotherm is formulated as [32]:

$$q_e = B_T \ln(K_T C_e) \quad (10)$$

Where B_T and K_T indicates Temkin constant which implies heat of adsorption (KJ/mol) and equilibrium binding constant (L/mg).

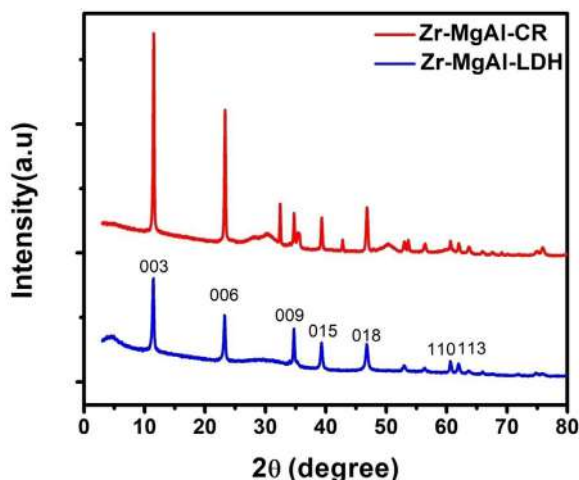


Figure 1. XRD pattern of ZrO₂/MgAl-LDH and CR adsorbed ZrO₂/ MgAl-LDH-CR.

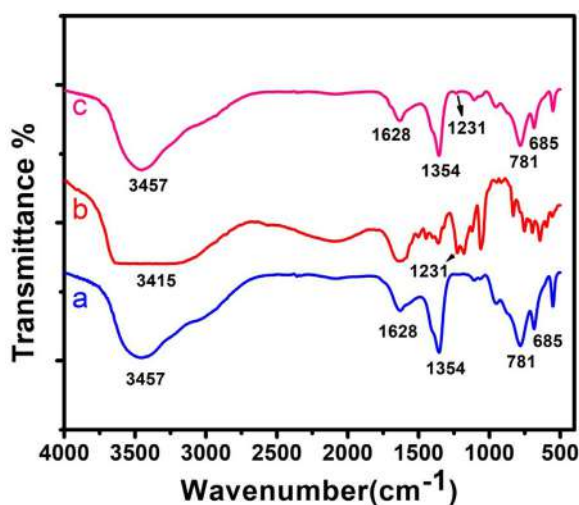


Figure 2. FT-IR spectra (a) ZrO₂/MgAl-LDH (b) Congo red (c) ZrO₂/MgAl-LDH-CR.

2.2.3. Redlich-Peterson Isotherm

Redlich-Peterson isotherm is a three parameter isotherm model that includes the elements present in both Langmuir and Freundlich equation for better fitting with experimental data. Unlike ideal monolayer adsorption the mechanism of adsorption is unique and shows the combined characteristic mechanism. The nonlinear equation of Redlich-Peterson is given as [33]:

$$q_e = \frac{A C_e}{1 + B C_e^\beta} \quad (11)$$

It is a hybrid model which describes both homogeneous and heterogeneous adsorption by combining both Langmuir and Freundlich equation. Several studies shows that Redlich-Peterson model is more accurate compare to both model. A and B is Redlich-Peterson constant and β is the exponential factor lying between 0-1. If $\beta=1$ then Redlich-Peterson equation reduces to Langmuir whereas for $\beta=0$ it is transformed to Freundlich equation.

2.2.4. Adsorption Kinetics

To further analyze the rate of dye adsorption and the mechanism involved kinetics studies were executed and further examined by using the five most widely used models such as pseudo first order, pseudo second order, intraparticle diffusion, Bangham and Boyd. Based on the pseudo

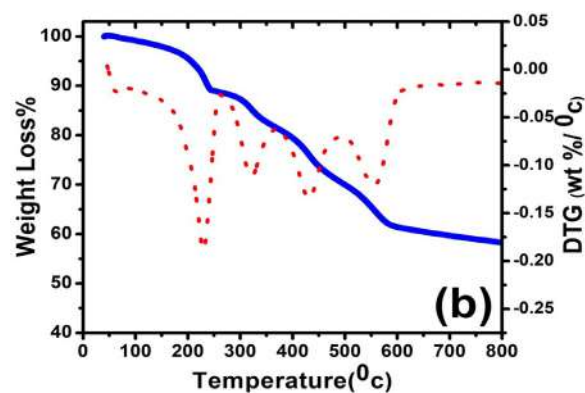
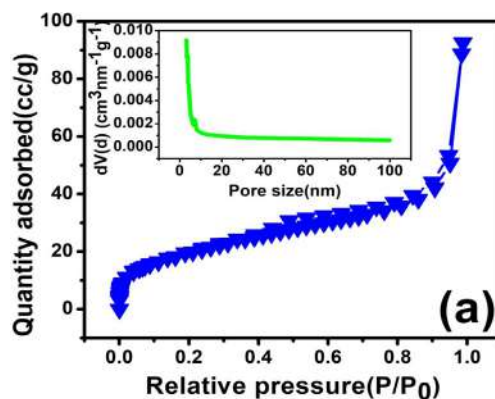


Figure 3. (a) N₂ adsorption-desorption isotherm and pore sized distribution of ZrO₂/MgAl-LDH (b) Thermogravimetric analysis of ZrO₂/MgAl-LDH.

first order kinetic model, it is assumed that the adsorption process is physical in nature and the rate of solute intake is proportional to the ratio of the concentration of the solute and the quantity of adsorbent. The pseudo first order equation is represented as [34]:

$$\log(q_e - q_t) = \log q_e - \frac{K_1 t}{2.303} \quad (12)$$

where q_e and q_t signifies the amount of dye adsorbed at equilibrium and at time t , respectively. K_1 is the first order rate constant which is obtained from the slope of linear plot $\log(q_e - q_t)$ vs t . In contrast, the pseudo second order model postulates that the adsorption process involves chemisorption where there is an interchange of electron between the solute molecules and adsorbent used. The pseudo second order kinetic equation is given as [35]:

$$\frac{t}{q_t} = \frac{1}{K_2 q_e^2} + \frac{t}{q_e} \quad (13)$$

where q_t , q_e , t have their usual meaning and K_2 is the second order rate constant which is evaluated from the intercept of the linear plot of t/q_t vs t . Besides, the intraparticle diffusion model proposed by Weber-Morris assumes that there is a possibility for the diffusion of solute molecules on the pores present on the surface of the adsorbents which may affect the rate limiting step during the adsorption process. The equation for the intraparticle diffusion model is presented as [36]:

$$q_t = K_i t^{0.5} + C \quad (14)$$

where K_i and C are the intraparticle diffusion constant and boundary layer thickness respectively, which is determined from the slope and intercept of the linear plot q_t vs $t^{0.5}$.

To further elucidate the actual process that controls the overall rate of sorption, a complex mathematical expression proposed by Boyd was applied to the kinetics data. This model helps in distinguishing between

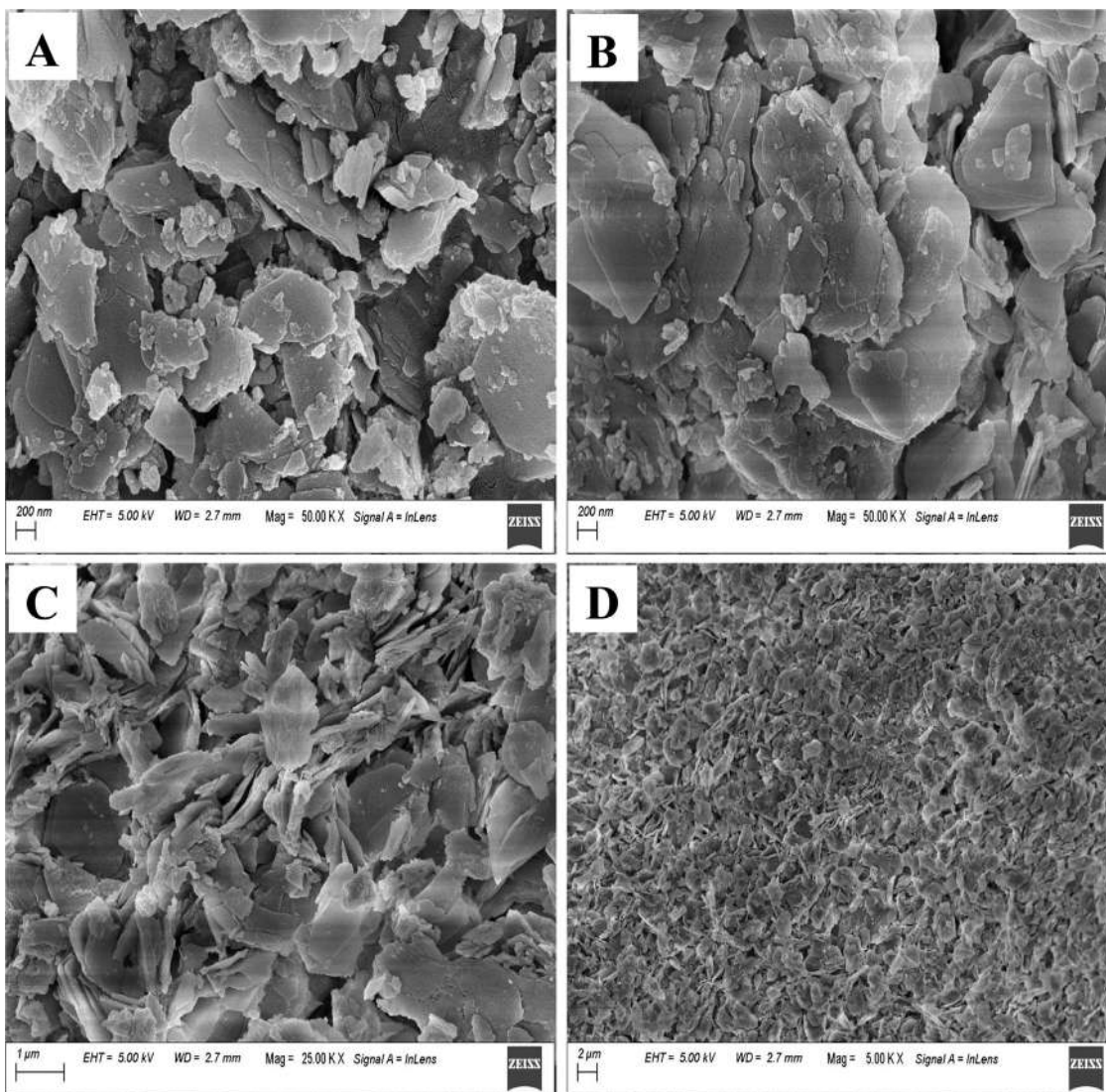


Figure 4. SEM micrograph (A-D) of ZrO₂/MgAl-LDH at different resolution.

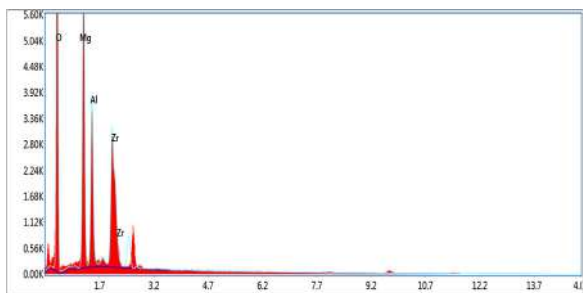


Figure 5. EDX spectra of ZrO₂/MgAl-LDH composite.

boundary layer diffusion and pore diffusion. The Boyd equation is formulated as [37]:

$$F = \left(1 - \frac{6}{\pi^2}\right) \exp(-Bt) \tag{15}$$

$$B_t = -0.4977 \cdot \ln(1-F) \tag{16}$$

$$F = \frac{q_t}{q_e} \tag{17}$$

$$B = \frac{\pi D_i}{r^2} \tag{18}$$

where q_t (mg/g), q_e (mg/g) are the quantity of dye adsorbed at time t and at equilibrium, B_t is the mathematical function of F , D_i is the diffusion coefficient and r denotes radius of the adsorbent particle (m). The value of B was determined from the slope of B_t vs t plot.

In general, the rate limiting step during the sorption process in several adsorbate-adsorbent systems could be only due to pore diffusion. As a result, to confirm the possibility of pore diffusion in the ZrO₂/MgAl-LDH-CR system, it is further interpreted by fitting the kinetics data based on Bangham equation. The Bangham equation is represented by the following equation [38]:

$$\log \left[\log \left(\frac{C_o}{C_o - m q_t} \right) \right] = \log \left(\frac{K_o m}{2.303 V} \right) + \alpha \log t \tag{19}$$

where K_o and α are Bangham constant, C_o indicates initial dye concentration (mg/L), q_t represents amount of dye adsorbed at any time t , V is the volume of solution (mL) and m denotes the weight of the adsorbent (g).

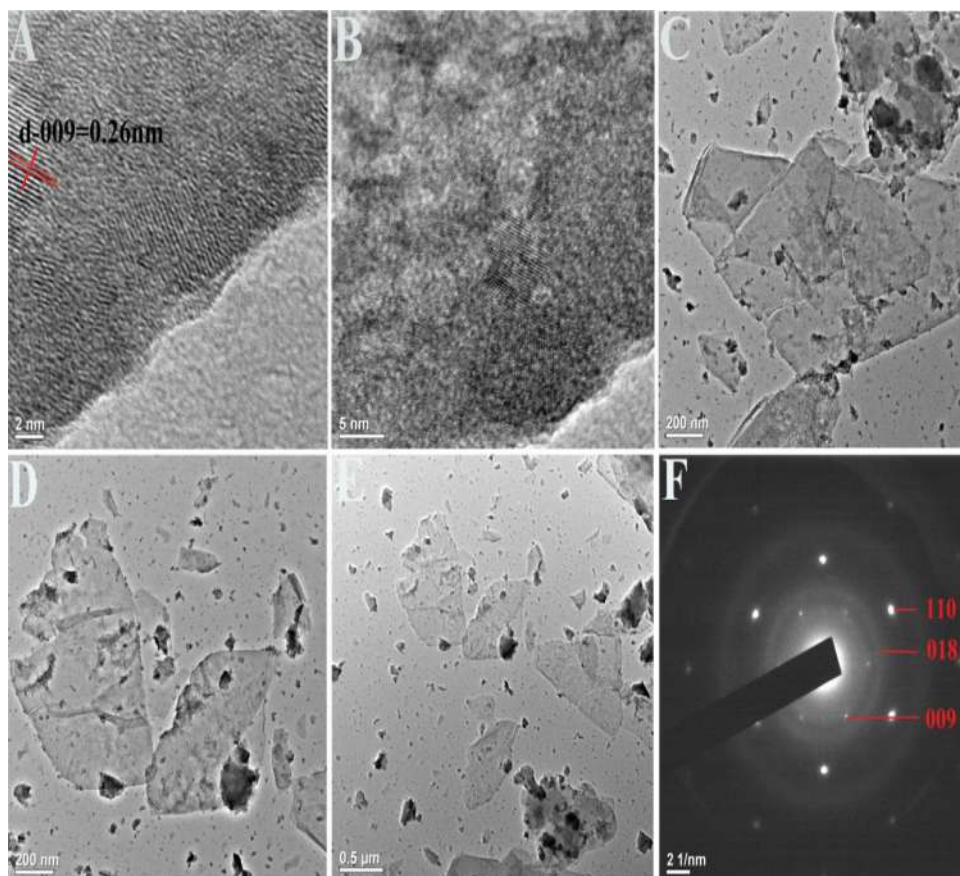


Figure 6. TEM images (A-E) and SAED pattern (F) of ZrO₂/MgAl-LDH composite.

Table 1

The characteristics cell parameters of ZrO₂/MgAl-LDH before and after the adsorption of CR dye.

Adsorbent	d ₀₀₃ (Å)	d ₀₀₉ (Å)	d ₁₁₀ (Å)	Unit cell a (Å)	Unit cell c (Å)
ZrO ₂ /MgAl-LDH	7.8	2.60	1.5	3	23.4
ZrO ₂ /MgAl-LDH-CR	7.7	2.61	1.5	3	23.1

3. Results and Discussions

3.1. Characterization of ZrO₂/MgAl-LDH

The powder X-ray diffraction (P-XRD) spectrum of ZrO₂/MgAl-LDH is presented in Fig. 1. The diffraction pattern reveals sharp and intense peaks which are corresponding to indexed planes 003, 006, 009, 015, 018, 110, 113. The observed characteristic peaks are consistent with a typical LDH diffraction pattern reported in previous work [39]. The diffractograms of the synthesized sample reveal the formation of pure sample ZrO₂/MgAl-LDH. Moreover, the highly intense and sharp peaks occur at lower 2θ values while with increasing 2θ value at a higher angle the intensity of peak decreases. The absence of broad peaks infers a crystalline phase in the sample. The lattice parameters a and c of ZrO₂/MgAl-LDH was evaluated theoretically by the expression $a=2d_{110}$ and $c=3d_{003}$. The parameter a represents an intermetallic distance in LDH and c is related to the thickness of the interlayer which relies on the positively charged density of LDH sheets and intergallery anions. The calculated values are summarized in Table 1. It is obvious from the obtained results that the calculated cell parameter $a=3\text{Å}$ and $c=23.4\text{Å}$ of ZrO₂/MgAl-LDH is found almost similar to the MgAl-LDH synthesized in the previous literature. However, the incorporation of Zr ions having a large ionic radius in brucite sheets should increase intermetallic distance a, meanwhile in our study it is seen that lattice parameter a value

does not increase, which reveals that Zr ions are not introduced inside LDH sheets rather it exist as ZrO₂ phase. In addition, Fig. 1 does not reveal the diffraction pattern of crystalline ZrO₂ which can be due to its existence as an amorphous phase. Nevertheless, it can be suggested that sample is a composite material containing MgAl-LDH and amorphous ZrO₂ phase [40]. After adsorption of CR dye molecules new peak arises at diffraction angle (2θ) of 32.40, 35.57, 42.81, 53.72, 50.37 which can be ascribed to surface adsorbed congo red molecule. Besides, there are no significant changes observed in cell parameters a and c before and after adsorption. From Fig. 1 shifting of peaks corresponding to 003 and 110 was not noticed in ZrO₂/MgAl-CR. The basal spacing d_{003} value was almost identical for both ZrO₂/MgAl-LDH (0.78nm) and CR adsorbed Zr-MgAl-CR (0.77nm). Consequently, it can be envisaged that the adsorption of CR dye takes place on external surfaces via weak interactions such as H-bonding, electrostatic forces and surface complexation rather than intercalation between the interlamellar regions [41].

The FT-IR spectroscopy technique has been used to analyze the stretching vibration of existing functional groups present on adsorbents. Fig. 2(a-c) demonstrates the FT-IR spectrum of ZrO₂/MgAl-LDH, congo red and ZrO₂/MgAl-CR after adsorption of CR dye molecules. In pristine ZrO₂/MgAl-LDH (Fig. 2a) the broad band at 3457cm^{-1} arises due to stretching vibration of ν -OH functional group present on metal hydroxide brucite layers. Another band observed at 1628cm^{-1} may be attributed to the -OH bending vibration of interlayer water molecule.

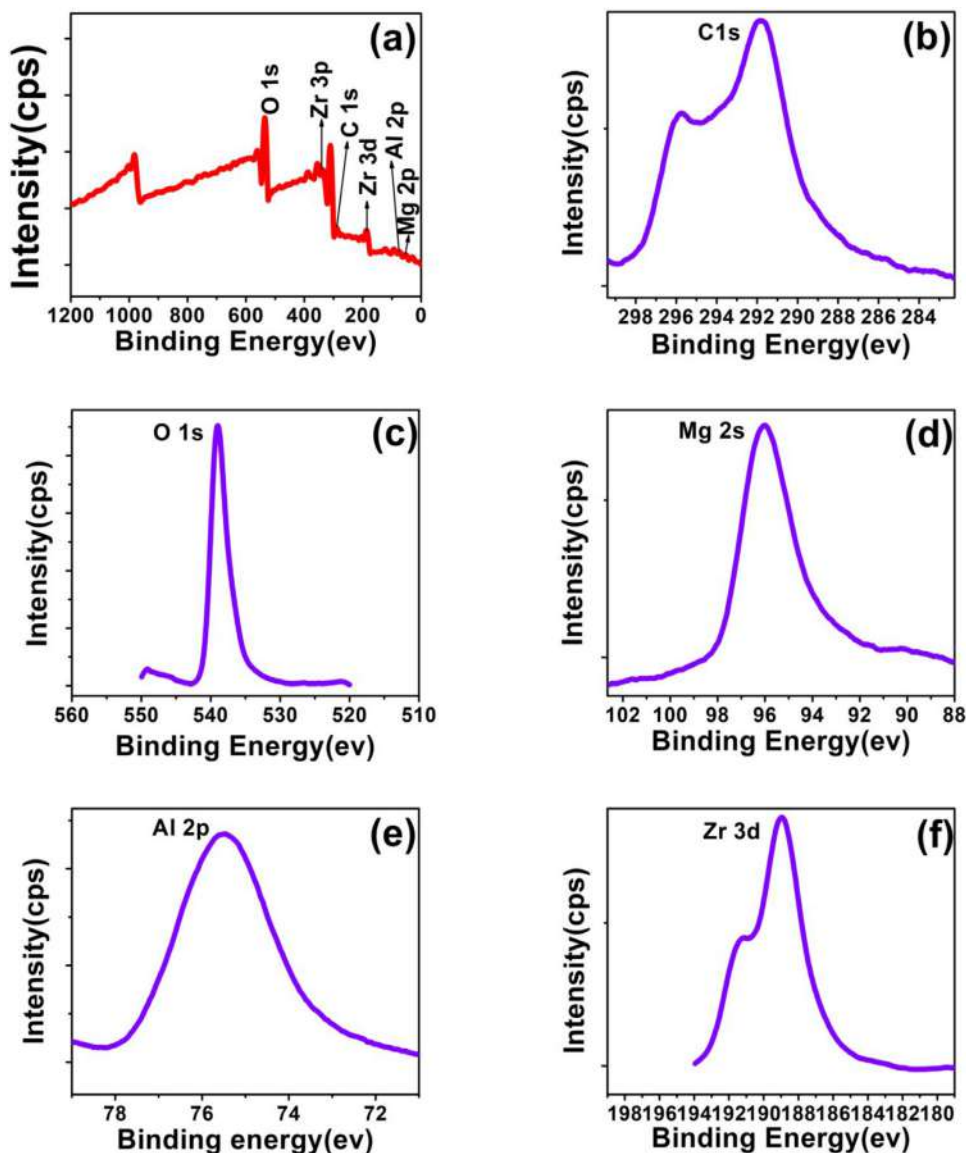


Figure 7. XPS spectra of ZrO₂/MgAl-LDH (a- wide scan, b- C1s, c- O1s, d- Mg2s, e- Al 2p, f- Zr3d).

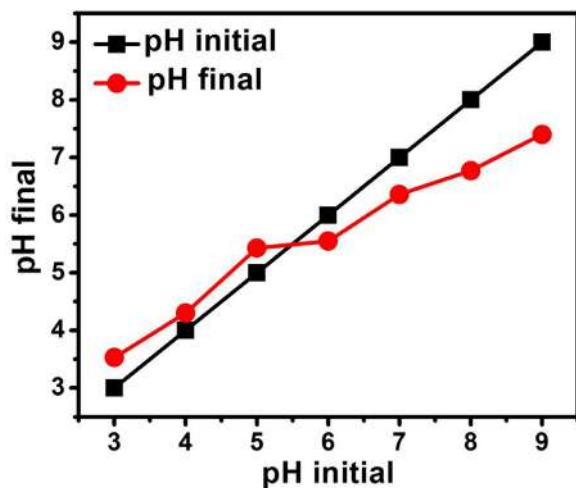


Figure 8. Determination of the point of zero charge (PZC) value of ZrO₂/MgAl-LDH from pH initial vs pH final plot.

A weak band at 1354cm^{-1} may be due to the presence of asymmetric stretching vibration of CO_3^{2-} ions. Since, LDH has a strong affinity for CO_2 , a small amount of atmospheric CO_2 gets adsorbed. The broad absorption band at 781cm^{-1} can be assigned to Mg-Al-O vibration and the less intense weak band at 685cm^{-1} can be accounted for M-O stretching vibrations. Moreover, after adsorption of CR dye molecule in Fig. 2c, the appearance of a new small peak at 1231cm^{-1} could be due to S=O stretching vibration of dye adsorbed on the LDH surfaces. The obtained result confirms the successful intake of CR dye over the proposed adsorbent ZrO₂/MgAl-LDH [42,43].

In general, the adsorption property of the adsorbent is greatly influenced by their specific surface area and porosity which can provide imperative information about sorption characteristics. Consequently, it is essential to measure the structural properties such as surface area and porosity which is conducted by the BET adsorption method. The N₂-adsorption-desorption isotherm and pore size distribution of ZrO₂/MgAl-LDH is presented in Fig. 3(a). The estimated BET specific surface area, pore volume and pore diameter are $71.55\text{m}^2/\text{g}$, 0.119cc/g and 3.04nm , respectively. The inset of Fig. 3(a) indicates that the pore size distribution lies in the range between 3.22nm to 8.15nm . However, it is seen that the area of the pore size distribution is narrow which reveals that the distribution of pores is uniform throughout the structure. The

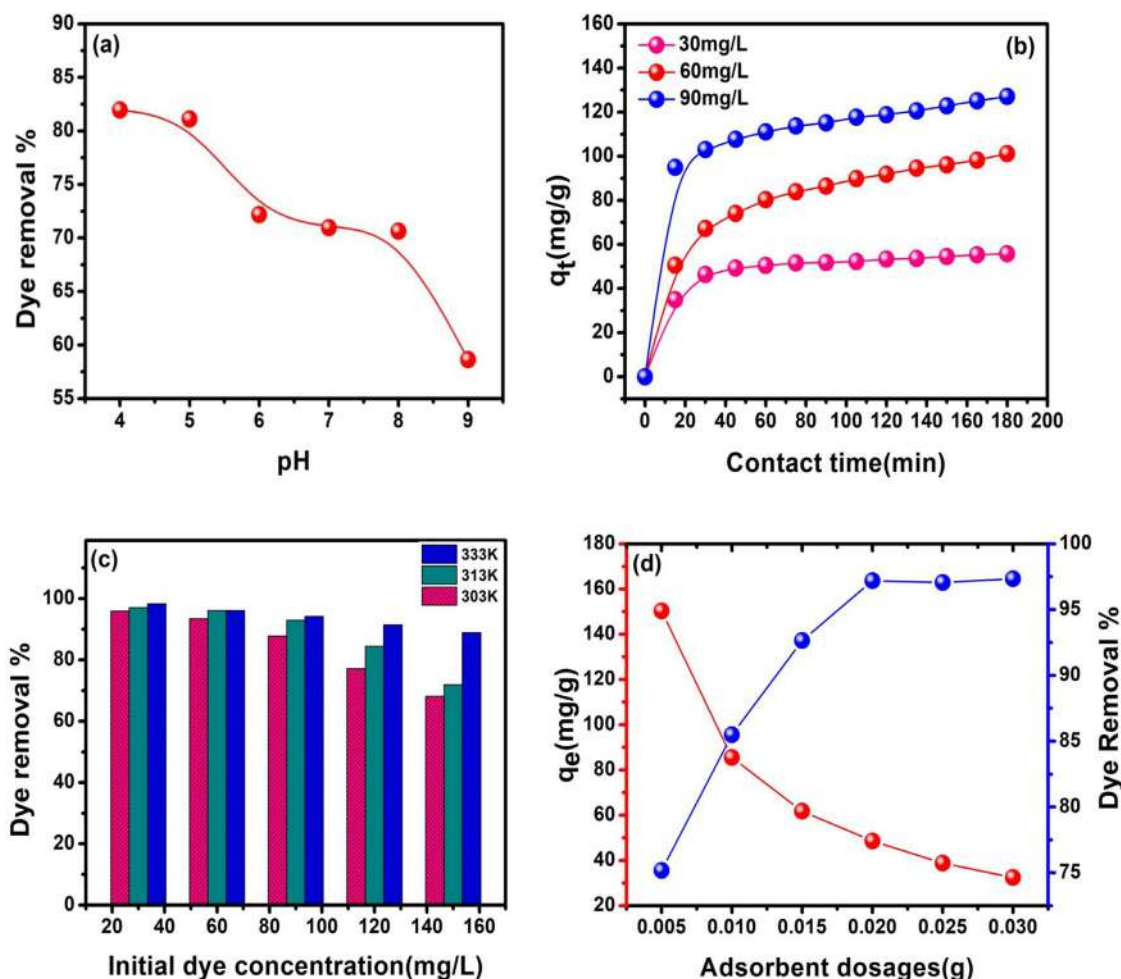


Figure 9. Effect of various parameters for adsorption of CR dye over ZrO₂/MgAl-LDH (a) pH (C₀=50mg/L, adsorbent dosages=0.02g, time=90min, volume=20mL). (b) Contact time (C₀= 30, 60, 90mg/L, adsorbent dosages=0.02g, time=90 min, volume=40mL) (c) Initial dye concentration (C₀=30-150mg/L, adsorbent dosages=0.02g, time=240min, volume=20mL, temperature= 303-333K) (d) Adsorbent dosages (C₀=50mg/L, time= 240min, volume=20mL).

sample ZrO₂/MgAl-LDH exhibits type IV isotherm with H-4 hysteresis loop which infers the mesoporous nature of the materials based on IUPAC classification [44].

The thermal stability of ZrO₂/MgAl-LDH was investigated by TGA which is depicted in Fig. 3b. The TGA profile reveals that weight loss takes place in four steps which is noted by exothermic peaks in DTG curves. The initial weight loss of 11.26% in the first step lying below 262°C may be attributed to evaporation of physically adsorbed water molecules. In the second and third step the small amount of weight loss 5.83% and 8.95% identified between 263-446.28°C were observed due to the removal of interlayer ions such as Cl⁻, CO₃²⁻ and OH⁻. The mass loss of 12.97% in the last stage indicates the complete breakdown of LDH structure into mixed metal oxide due to complete dehydroxylation of brucite layers. After 610°C there is no further weight loss observed leading to a constant straight line curve [45,46].

SEM images of ZrO₂/MgAl-LDH depict the detailed surface morphology at different resolution, which is shown in Fig. 4(A-D). The image confirms aggregation of plate like particles at a resolution below 1 μm which is typical for LDH morphology. The hexagonal shape LDH platelets are found stacked upon one another at an average size greater than 1 μm. From the analysis of SEM micrograph, it is also evident that the surface feature of LDH is not uniform and reveals existences of pores between LDH platelets [47]. Fig. 5 revealed the elemental composition of ZrO₂/MgAl-LDH composite obtained by energy dispersive x-ray (EDX) analysis. It is obvious that the main constituent elements

present in the adsorbents in terms of weight percentage are Zr(13.92%), Mg(19.38%), Al(11.50%) and O(55.20%), respectively.

The high resolution TEM micrograph of ZrO₂/MgAl-LDH was presented in Fig. 6(A-F). It is seen that in Fig. 6(A) the evaluated lattice fringes d_{009} (0.26nm) corresponding to 009 plane of ZrO₂/MgAl-LDH was manifested, which is consistent with powder XRD results. Fig. 6(C-E) depicts the structure of LDH platelets. The pattern observed in the selected area electron diffraction shown in Fig. 6(F) conforms to the polycrystalline nature of the materials. In addition, the d-spacing value of 0.26 nm, 0.2 nm and 0.14 nm was measured from SAED pattern which can be related corresponding to 009, 018 and 110 planes [48].

Fig. 7(a) depicts the full XPS spectrum of ZrO₂/MgAl-LDH which shows the presences of constituting elements such as Zr, Mg, Al, O and C. The XPS spectra of C 1s presented in Fig. 7(b) reveals three peaks at 291.82 eV, 293.57 eV and 295.76 eV, which can be accounted due to the small quantity of atmospheric CO₂ adsorbed on LDH. The peak for O 1s was visible at 539.09 eV, which may be ascribed to the CO₃²⁻ and OH⁻ ion present in the LDH structure [49]. In Fig. 7(f) the doublet peak corresponds to Zr-O-Zr bonds, meanwhile Zr (3d) have a binding energy of 186.94 eV and 191.16 eV with energy separation (4.22 eV), which are mainly contributed from Zr 3d_{5/2} and Zr 3d_{3/2} respectively. Besides, the peak noted at a binding energy of 337 eV corresponds to Zr 3p_{3/2} as shown in Fig. 6(a). The existence of Zr metal in 3p_{3/2} and 3d_{5/2} states affirms its oxidizing nature. Additionally, the Zr metal in ZrO₂ form having +4 valency state in the composite material can also

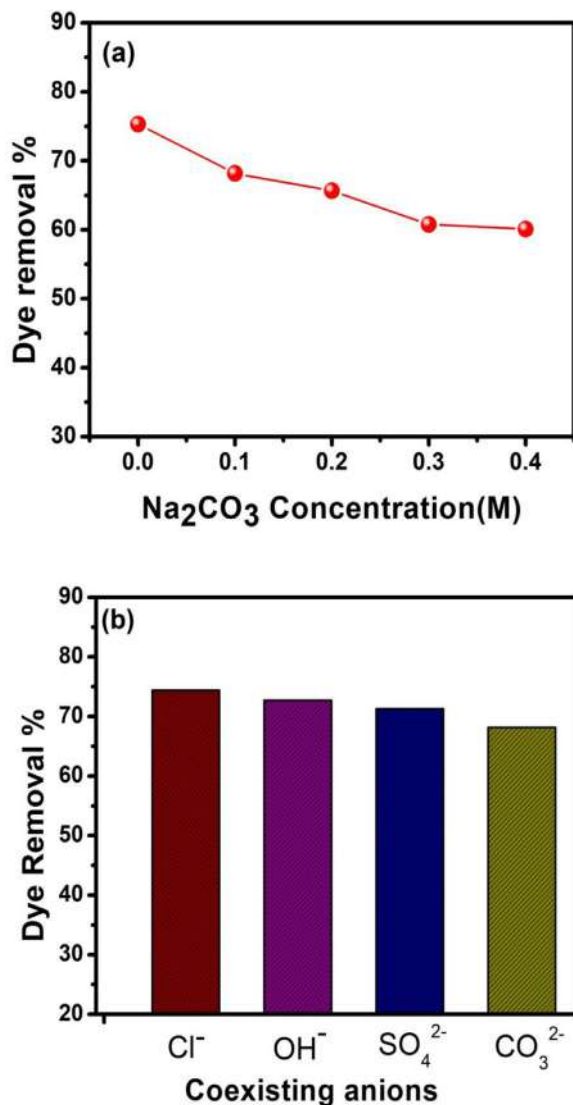


Figure 10. (a) Effect of ionic strength ($C_0 = 50 \text{ mg/L}$, adsorbent dosages = 0.02 g , time = 120 min , volume = 20 mL) (b) Influence of coexisting ions ($C_0 = 50 \text{ mg/L}$, adsorbent dosages = 0.02 g , time = 120 min , volume = 20 mL).

be anticipated. In general, the binding energy of Zr for valency state (0, +1, +2, +3) lies in between the range (178 to 184 eV) as per the results reported by Lackner et al. The peak corresponding to Mg 2s and Al 2p was obtained at 75.49 eV and 96 eV respectively [50, 51].

3.1.1. Effect of adsorption parameters

3.1.1.1. Effect of pH. During the adsorption process, the pH of the solution plays a significant role which can have an impact on the structure and charge of the sorbents. It can influence the dissociation of functional group presents on the binding sites of adsorbents, and it also affects the solubility of solutes in an aqueous solution. Fig. 9(a) demonstrates the removal efficiency of CR by $\text{ZrO}_2/\text{MgAl-LDH}$ over a pH ranging between 4-9. The pH of the dye solution is varied from 4-9, while other parameters in the reaction conditions such as adsorbent dosages, temperature, contact time, initial dye concentration, and volume of solution were fixed at 0.02 g , room temperature, 90 minutes, 50 mg/L and 20 mL respectively. The observed results shown in Fig. 9(a), it implies that the effects of pH change is remarkable and possess characteristic information regarding the interaction between adsorbate and adsorbent molecules. The maximum removal of CR dye (81.96%) was achieved at pH 4 while on increasing pH from 4 to 9 there is a continuous decrease in the dye

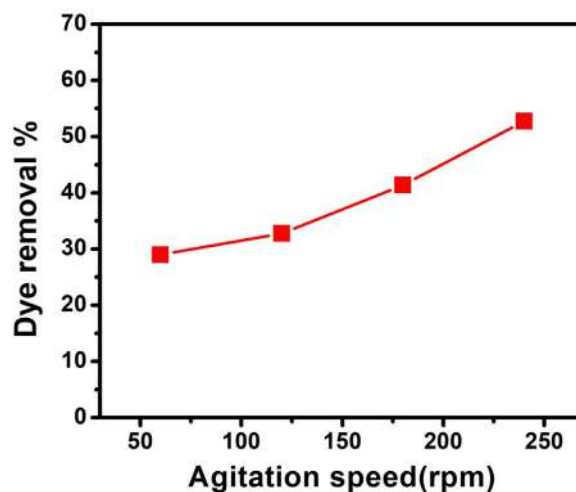


Fig. 11. Effect of agitation speed on the adsorption of CR dye ($C_0 = 40 \text{ mg/L}$, dosages = 0.015 g , contact time = 1 hour).

removal percentages which declines up to 58.64%. In general, below pH 4 the structure of LDH breaks down and loses its adsorption property. However, the characteristic variation displayed in removal efficiency of $\text{ZrO}_2/\text{MgAl-LDH}$ can be well understood from the ionic chemistry of the solution and the charge of the sorbents [24,52]. Consequently, the point of zero charge (PZC) described in terms of pH value where the net charge on the adsorbent surface is zero was estimated by pH drift method. From Fig. 8 the point of intersection in the pH initial vs pH final plot lies at 5.49, which refers to the point of zero charge value (PZC). At pH values less than PZC, around 4 to 5.49 the presences of a greater number of protonated ions H^+ which accumulates on the LDH surfaces provides additional positive charges on the $\text{ZrO}_2/\text{MgAl-LDH}$. These positive charges on the $\text{ZrO}_2/\text{MgAl-LDH}$ surface attracts the negatively charged anionic dyes more strongly and bound with the help of electrostatic forces. In contrast, at $\text{pH} > \text{PZC}$ (5.49), the surface of the particle acquires negatively charged and the existing hydroxyl ion competes with the incoming negative charged anionic dyes for the adsorption sites. Hence, the adsorption capacities of $\text{ZrO}_2/\text{MgAl-LDH}$ get reduced with increasing pH. Nevertheless, the main factor on which adsorption of CR over $\text{ZrO}_2/\text{MgAl-LDH}$ strongly depends on the electrostatic forces between functional groups of dyes and positive charge LDH sheets [34,53].

3.1.2. Effect of contact time

The contact time between adsorbate and adsorbent is another important parameter to be investigated during the sorption process. The effect of contact time on the adsorption of CR dye by $\text{ZrO}_2/\text{MgAl-LDH}$ at different initial dye concentration 30, 60, 90 mg/L is depicted in Fig. 9(b). The result obtained manifests that at the initial stage of contact time up to 20 minutes, the rate of dye adsorption is fast for all the concentration of CR dye. It can be attributed to the large number of adsorption site and high concentration gradient of dye at the initial stage, which can promote the rapid intake of solute dye molecules [22, 54]. Subsequently, the inflexion of the curve observed in the region between 20-50 minutes can be ascribed to the slow diffusion of dye molecules inside the pores of LDH, therefore the rate of adsorption becomes slow. However, the equilibrium state of CR adsorption was achieved near the contact time of 180 minutes. In addition, with the progress of adsorption process the access to the remaining vacant site are less available for sorption because of the steric repulsion between the incoming solute molecules and the adsorbed molecules [55]. After complete saturation at 180 minutes the maximum q_e value obtained corresponding to initial concentration 30 mg/L, 60 mg/L, 90 mg/L are 55.74, 101.19 and 127.14 mg/g, respectively.

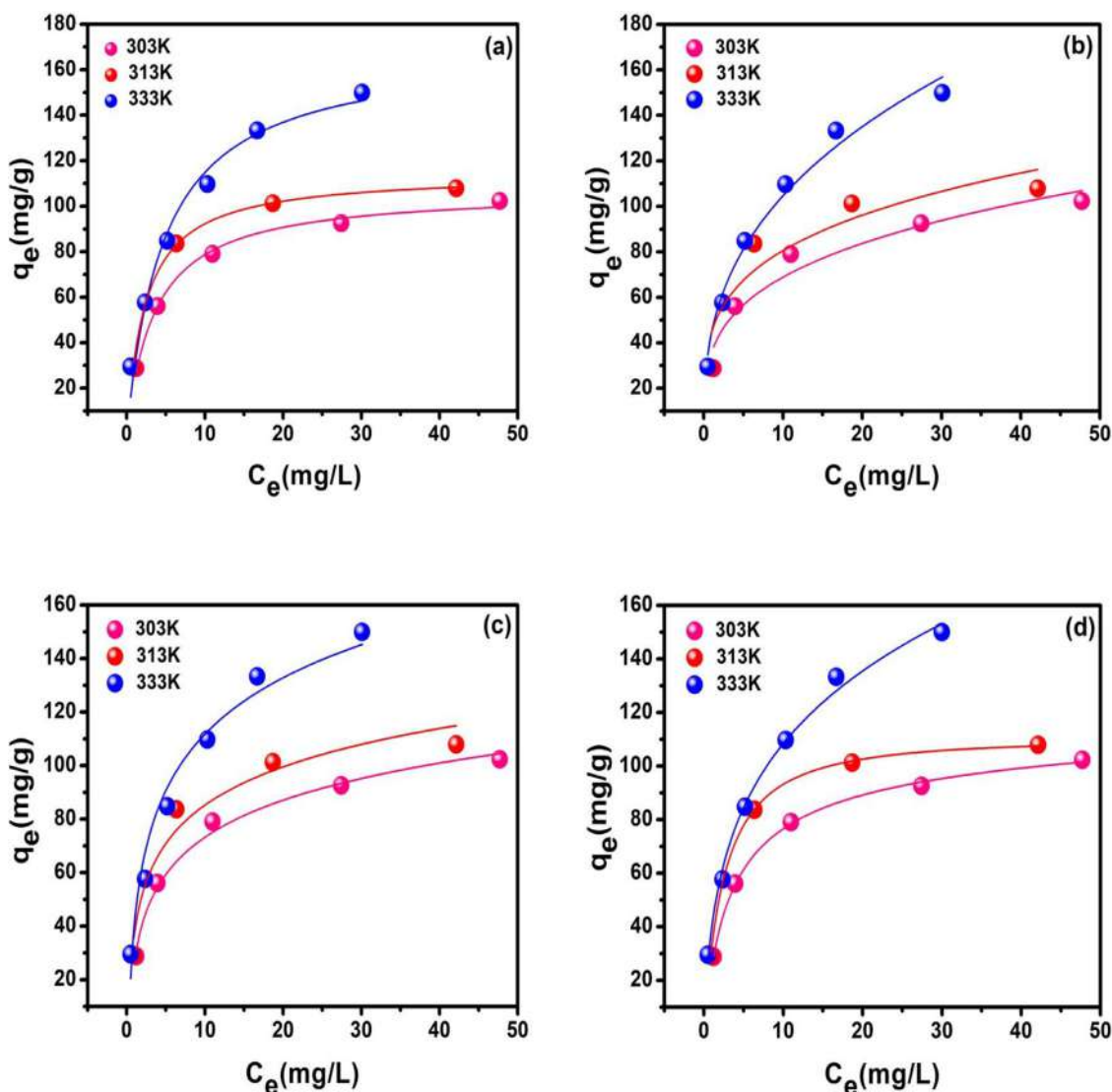


Figure. 12. Non-Linear fitting of various adsorption isotherm model (a) Langmuir (b) Freundlich (c) Temkin (d) Redlich-Peterson for adsorption of CR over ZrO₂/MgAl-LDH.

3.1.3. Effect of initial dye concentration

The effect of initial dye concentration on adsorption over ZrO₂/MgAl-LDH was investigated by varying the concentration from 30-150 mg/L under the reaction temperature of 303 K, 313 K and 333 K which is shown in Fig. 9(c). The results clearly indicate that there is a gradual decrease in dye removal percentage with the increase in the initial concentration of solute at all temperatures. This can be ascribed to the limited number of active sites in adsorbent due to increasing solute concentration. In general, at a low initial dye concentration the adsorption process is mainly monolayer, which is further extended to multilayer until the equilibrium stage is reached at high solute concentrations. Moreover, the driving force required is more to overcome the mass transfer resistance of solute molecules between solid and liquid phase at high dye concentrations [43,56]. The dye removal efficiency decreases from 95.90-68.18%, 97-71.91% and 98.33-88.87% at 303 K, 313 K and 323 K, respectively. In addition dye removal efficiency is found to be higher at 323K.

3.1.4. Effect of dosages

Accounting for the cost effective system, it is important to evaluate the optimum dosages of adsorbent. The influence of dosages on the removal efficiency of CR dye was examined by changing the quantity of

adsorbent from 0.005 g to 0.030 g which is presented in Fig. 9(d). It is obvious that the percentage removal of dye increases initially with an increase in adsorbent amount until 0.02 g, beyond this dosages the removal percentage remains almost similar. This can be attributed to the presences of a greater number of available adsorption sites with increasing adsorbent dosages. However, it was noted that there is no remarkable changes observed in adsorption performances after 0.02 g. Moreover, the excessive use of adsorbent beyond optimum ranges can lead to aggregation of LDH particle due to collision which can restrict the accessible adsorption site for the incoming dye molecules by declining specific surface area and increasing diffusion path length value [43,57]. On the other hand, it is observed that the equilibrium adsorption capacity q_e decreases from 150.34 mg/L to 32.44 mg/L with increasing dosages of 0.005 g to 0.030 g. Moreover, the maximum removal efficiency up to 97.19 was achieved at 0.02 g dosages which can be considered as an optimum dosages for the reaction condition fixed at 50 mg/L initial dye concentration and a contact time of 4 hours.

3.1.5. Effect of ionic strength and coexisting ions

The effluent discharges from various textile industries have adequate amounts of salts which can affect the adsorption performances. Consequently, it is important to investigate the effect of ionic strength during

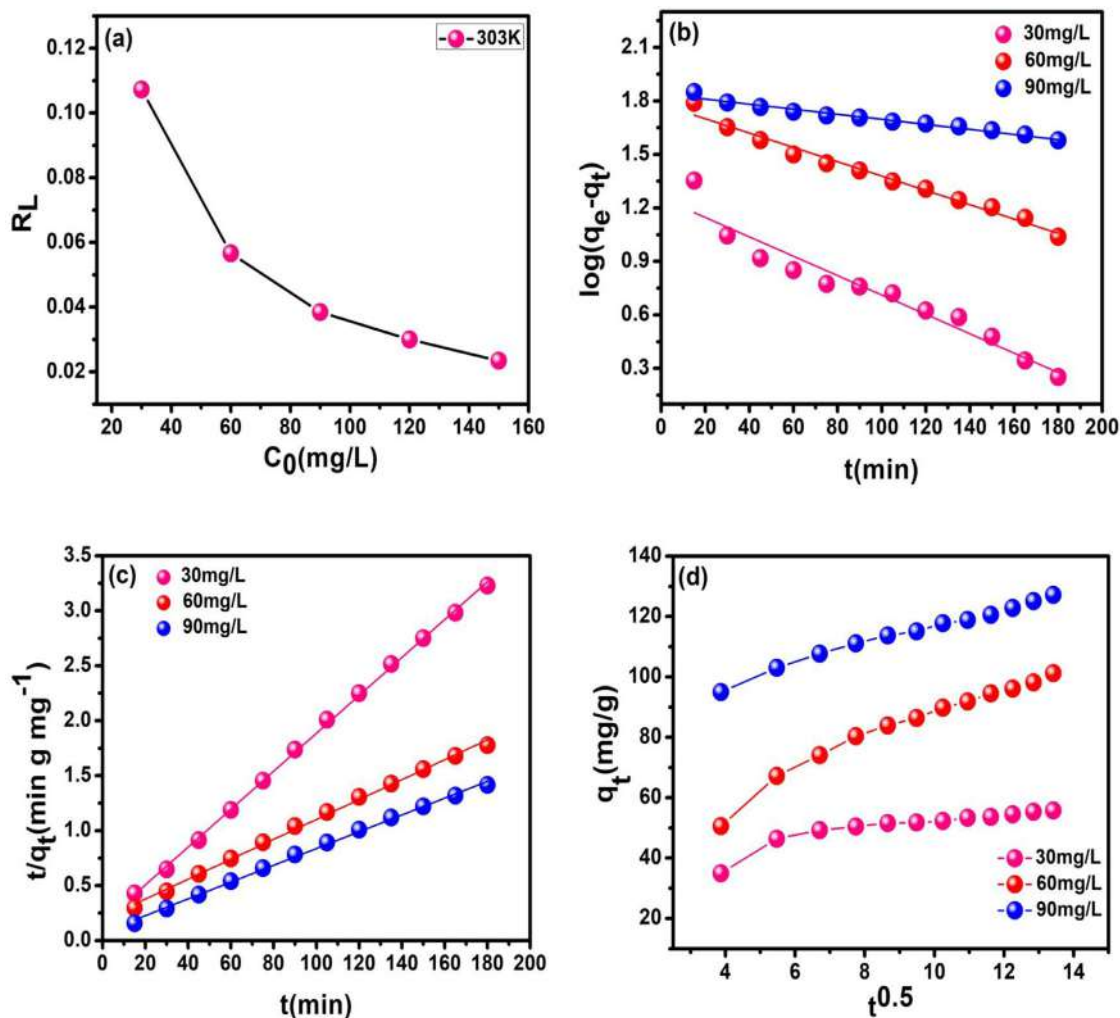


Figure 13. (a) RL vs C₀ plot at 303K (b) Pseudo first order kinetics plot (c) Pseudo second order kinetics plot (d) Intraparticle diffusion plot.

adsorption process. The increasing ionic strength of the solution can either enhance or retards the adsorption of organic dyes or it may not be effective in some adsorbate-adsorbent system which is clearly not known due to less report. However, the ionic strength is controlled by the nature of the salt, dyes and adsorbent used during the reaction [58]. In this work, the ionic strength is adjusted by adding 0.5 mL each of Na₂CO₃ solution at different strengths from 0.1 M to 0.4 M to the congo red dye solution fixed at an initial concentration 50 mg/L and adsorbent dosages 0.02 g. From the result shown in Fig. 10(a) it was obvious that the removal efficiency of CR dye decreases with an increase in the ionic strength of Na₂CO₃ which may be due to the competition existing between CO₃²⁻ ion and CR dye ions for surface adsorption on ZrO₂/MgAl-LDH. It is noticed that the dye removal % gets reduced from 73.03% to 60.11 by increasing the concentration of Na₂CO₃.

The influence of coexisting ions such as OH⁻, Cl⁻, SO₄²⁻, CO₃²⁻ on the removal efficiency of congo red dye was examined under the operating conditions: 50 mg/L congo red solution, 0.02 g adsorbent, contact time = 2 hours, 0.5 mL from each of the 0.1 M salt solutions (NaOH, NaCl, Na₂SO₄, Na₂CO₃) was added. The observed result in Fig. 9(b) indicates that the competitive effects of coexisting ions are in the order: CO₃²⁻ > SO₄²⁻ > OH⁻ > Cl⁻. Moreover, the dye removal % increases from 68% to 74.38% where the lowest efficiency is found in the case of CO₃²⁻ ions which infers that CO₃²⁻ is more competitive compared to other anions. Nevertheless, it is believed that the divalent ions have more competitive effects than monovalent anions, since the ionic potentials of divalent ions are greater than monovalent ions [59,60].

3.1.6. Effect of agitation speed

Graphical representation of CR adsorption over ZrO₂/MgAl-LDH as a function of agitation speed is shown in Fig. 11. The influence in CR adsorption was conducted by varying the agitation speed from 60rpm to 240 rpm at a contact time of 60minutes with 0.015 g adsorbent dosages. The degree of agitation can influence the distribution of solute in bulk solution as well as the creation of boundary film. Usually, the increase in agitation speed can lead to a better interaction between adsorbate and adsorbent molecules by exposing all the vacant sites more effectively to the incoming CR molecules. As a result, the adsorption efficiency was found to increase from 28.97 to 52.73% by increasing agitation speed. At low agitation speed the contact between the adsorbent and solute molecules was found less which could be responsible for the low sorption percentage. Thus, it also suggests that rate of dye removal is also depended on agitation speed and is relatively faster at greater speed [61].

3.2. Isotherm Studies

Adsorption isotherm studies can provide qualitative information concerning the adsorption capacity of the adsorbent, and the distribution of solute molecules between solid-liquid phases at equilibrium. The isotherms data obtained at 303 K, 313 K, and 333 K were fitted based on Langmuir, Freundlich, Temkin and Redlich-Peterson model which is shown in Fig. 12(a-d). The isotherm parameters of all models are summarized in Table 2. It is evident that after non linear fitting of the

Table 2
Adsorption isotherm parameters for adsorption of CR dye on to ZrO₂/MgAl-LDH obtained from the non linear fitting of Langmuir, Freundlich, Temkin and Redlich-Peterson model.

Isotherm model	Parameters	Temperature		
		303K	313K	333K
Langmuir	q_{\max} (mg/g)	107.05±2.28	114.48±1.34	169.42±11
	K_L (L/mg)	0.27±0.02	0.41±0.01	0.21±0.04
	R^2	0.993	0.998	0.970
	χ^2	5.520	2.102	62.249
Freundlich	K_F (mg/g)(L/mg) ^{1/n}	36.06±5.29	44.85±7.90	44.91±3.63
	n	3.55±0.58	3.93±0.92	2.72±0.21
	R^2	0.927	0.851	0.980
	χ^2	63.42	157.34	40.37
Temkin	B_T	20±1.06	20.66±2.41	30.42±2.57
	K_T	3.88±0.79	6.17±2.84	3.93±1.12
	R^2	0.988	0.947	0.965
	χ^2	9.93	55.762	73
Redlich-Peterson	A (L/g)	36.42±3.60	44.90±3.10	99.31±47.23
	B (L/g) ^{β}	0.43±0.08	0.36±0.05	1.47±0.99
	β	0.932±0.02	1.02±0.02	0.742±0.05
	R^2	0.997	0.998	0.990
	χ^2	1.779	2.117	20.95

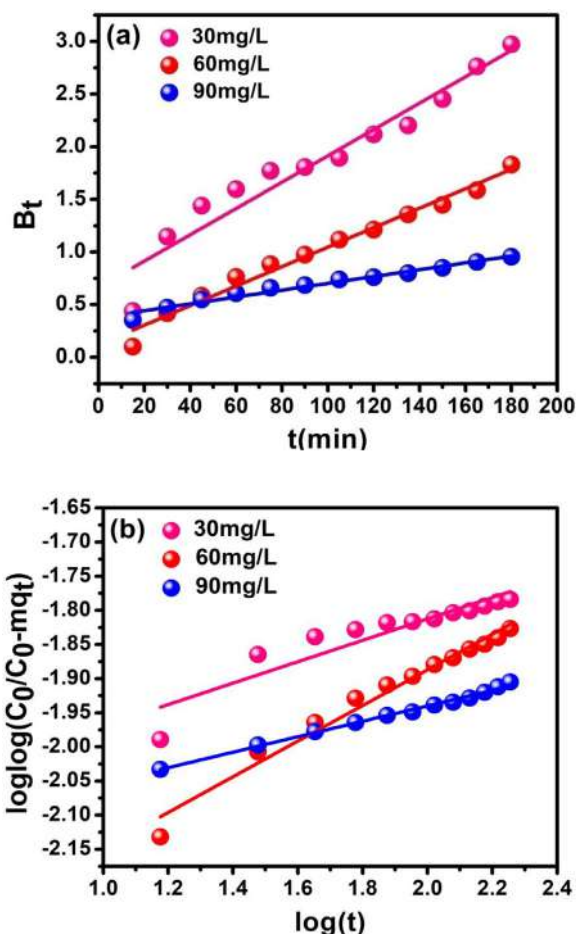


Figure 14. (a) Boyd kinetic plot and (b) Bangham kinetic plot.

experimental data the greater coefficient of determination R^2 value is in the order: Redlich-Peterson > Langmuir > Temkin > Freundlich. However, the acceptability of the isotherm model that best fit the experimental data is determined based on the lowest value of χ^2 and closer value of coefficient of determination (R^2) to unity. Comparing the χ^2 and R^2 value shown in Table 2, it implies that the two isotherm model,

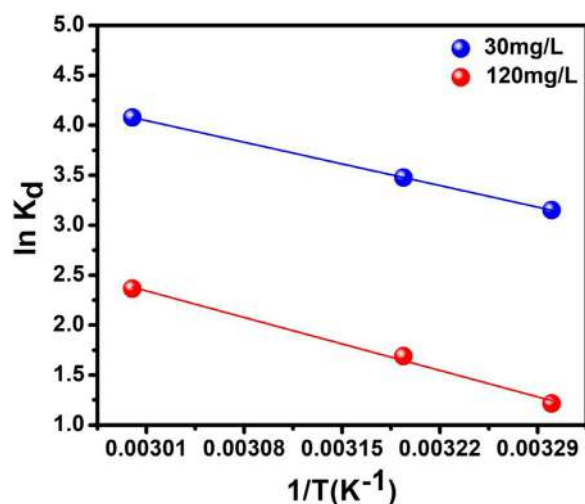


Figure 15. Vant Hoff plot for the adsorption behavior of the CR by the adsorbent ZrO₂/MgAl-LDH. ($C_0=30,120$ mg/L, temperature=303K, 313K, 333K, adsorbent dosages=0.02g, volume=20mL, contact time=240min).

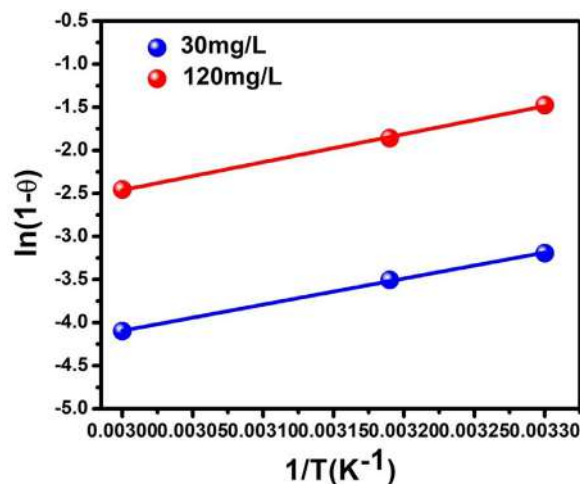


Figure 16. Modified Arrhenius plot for the adsorption behavior of the CR by the adsorbent ZrO₂/MgAl-LDH. ($C_0=30,120$ mg/L, temperature=303K, 313K, 333K, adsorbent dosages=0.02g, volume=20mL, contact time=240min).

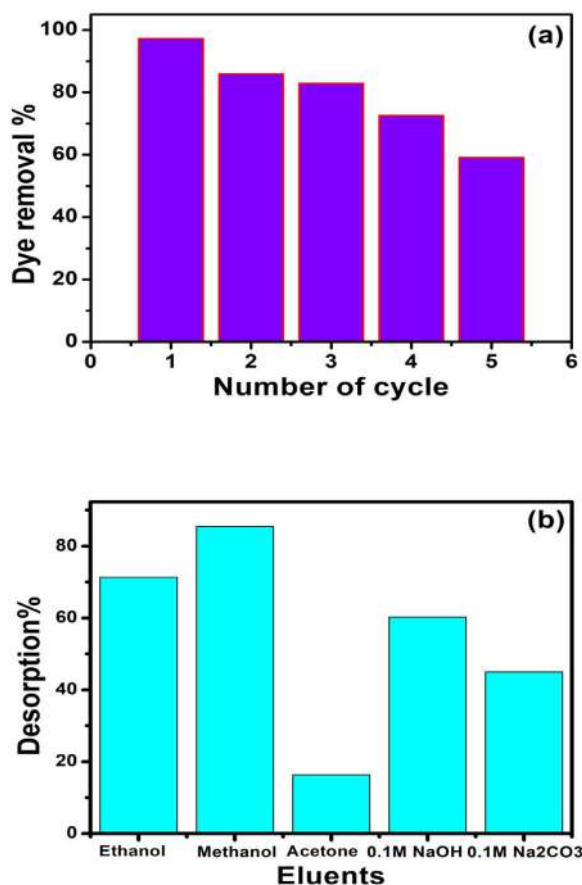


Figure 17. (a) Reusability studies for the adsorption of CR dye by ZrO₂/MgAl-LDH (C₀=50mg/L, adsorbent dosages=0.02g, volume=20mL, contact time=6hours). (b) Desorption percentage of CR dye from ZrO₂/MgAl-LDH at different eluents.

especially Redlich-Peterson and Langmuir can better explain the studied adsorption process contrary to other models. In addition, it also suggests that the surface of the adsorbent is a combination of both homogeneous and heterogeneous nature [52,62]. Fig. 13(a) represent the plot of R_L vs C_0 . It is believed that for R_L value lying between 0-1, the adsorption process is feasible while for $R_L > 1$, it indicates unfavorable process. For irreversible process R_L is equal to zero. Table 2 clearly shows that values of the Langmuir constant lie between 0-1 which further represents that the sorption process is highly favored. Moreover, it is obvious that Freundlich constant n values are greater than 1 at all temperatures, which also implies that the adsorbate molecules are suitably adsorbed on ZrO₂/MgAl-LDH under the operated experimental conditions. The maximum monolayer adsorption capacity by ZrO₂/MgAl-LDH for CR dye at 303K, 313K and 333K are 107.05, 114.48 and 169.42 mg/g, respectively.

3.3. Kinetics studies

The kinetic parameters of pseudo first order, pseudo second order, intraparticle diffusion, Boyd, and Bangham model for the adsorption of CR dye by ZrO₂/MgAl-LDH, at different initial concentrations (30, 60, 90 mg/L) is shown in Table 3. The linear fitting of employed kinetic models are demonstrated in Fig. 13(b-d). The suitability of kinetic model was determined by comparing sum of square error (SSE) function and of determination (R^2). The lower values of SSE and higher values of R^2 are expected to give better fitting in a kinetic model as shown in Table 3. Concomitantly, for all initial dye concentrations (30-90 mg/L), it implies that the obtained kinetics data fit well, according to pseudo

second order model which can be considered as a predominant mechanism [30, 63]. Moreover, the pseudo second order rate constant (K_2) constant value decreases with the increase in dye concentration and is in the magnitude of 10^{-4} , the lower values further indicate the longer time taken to attain equilibrium. Besides, the q_{e2} value calculated by the pseudo second order model resembles the experimental q_e value more closely compare to pseudo first order which further envisages that the associated rate controlling mechanism during the adsorption process can be best described by the pseudo second kinetic model. The second order rate constant K_2 corresponding to initial concentrations 30 mg/L, 60 mg/L and 90 mg/L is $(18.55, 4.18, 1.82) \times 10^{-4} \text{ g.mg}^{-1}\text{min}^{-1}$ respectively.

Furthermore, the plot of q_t vs $t^{0.5}$ displayed in Fig. 13(d) clearly reveals the existences of multiple steps during the adsorption process. The initial step represents adsorption on the freely available external adsorption site, while in the middle region, it indicates diffusion of dye molecules inside the pores, and the last step represents the equilibrium stage where complete adsorption on vacant sites was achieved. According to this model if the linear plot passed through the origin, then intraparticle diffusion controls the rate of adsorption kinetics. But from Fig. 13(d) it is clearly seen that the plot did not pass through the origin, which manifests that although the adsorption process involves intraparticle diffusion, it is not the sole rate limiting step. In addition, the thickness of boundary layer C increases (35.15–85.63 mg/g) with the increase in CR dye concentration (30-90 mg/L) which can be explained on the basis of the increasing boundary layer effect due to instantaneous occupation of readily available adsorption sites [52,64].

The dual nature of the adsorbent particle, especially film and pore diffusion during the sorption process can be easily identified by analyzing Boyd plot. The graph of B_t vs t at different initial dye concentration (30, 60, 90 mg/L) was illustrated in Fig. 14(a). The plot was found to be almost linear for all concentration and did not pass through the origin, thus film diffusion seems to be governing the sorption rate of CR dye on to ZrO₂/MgAl-LDH composite, but it is not the only rate controlling step. The values of effective diffusion coefficient D_i (cm^2/min) were evaluated according to equation (18) and summarized in Table 3. In this study, the D_i value was found to be increased with the increase in concentration of CR dye, which can be attributed due to the greater concentration gradient at high CR content [65].

The graph of $\log[\log C_0/C_0 - q_t]$ vs $\log t$ based on Bangham equation was presented in Fig. 14(b) The values of the parameter K_0 and α were evaluated from the intercept and slope of the graph as shown in Table 3. The experimental data modeled by the equation (19) corresponding to the initial dye concentration (60, 90 mg/L) showed linear plot, while for lower concentration (30 mg/L) it did not yield desired linear fit. The higher coefficient of determination (R^2) value obtained from this model also suggests good fitting with the experimental data. This observation further conveys the applicability of this model which can perfectly explains adsorption kinetics data as a pore diffusion controlled adsorption. Thus, from the overall results obtained in kinetic studies, it can be concluded that both film and pore diffusion plays a key role at different stages of the sorption process [38].

3.4. Thermodynamic studies

Temperature is an essential parameter that can affect the adsorption process by influencing mobility, solubility of adsorbate and also by changing the equilibrium adsorption capacity. The thermodynamic studies of adsorption process were executed by subjecting at various reaction temperature (303 K, 313 K, 333 K) corresponding to the initial dye concentration (30 mg/L, 120 mg/L), whereas other parameters in reaction conditions usually adsorbent dosages, contact time are fixed at 0.02 g, 4 hours respectively. The essential thermodynamic parameters such as ΔG , ΔH , ΔS were evaluated. For thermodynamic studies the equation for the determination of related parameters are formulated as [55,66]:

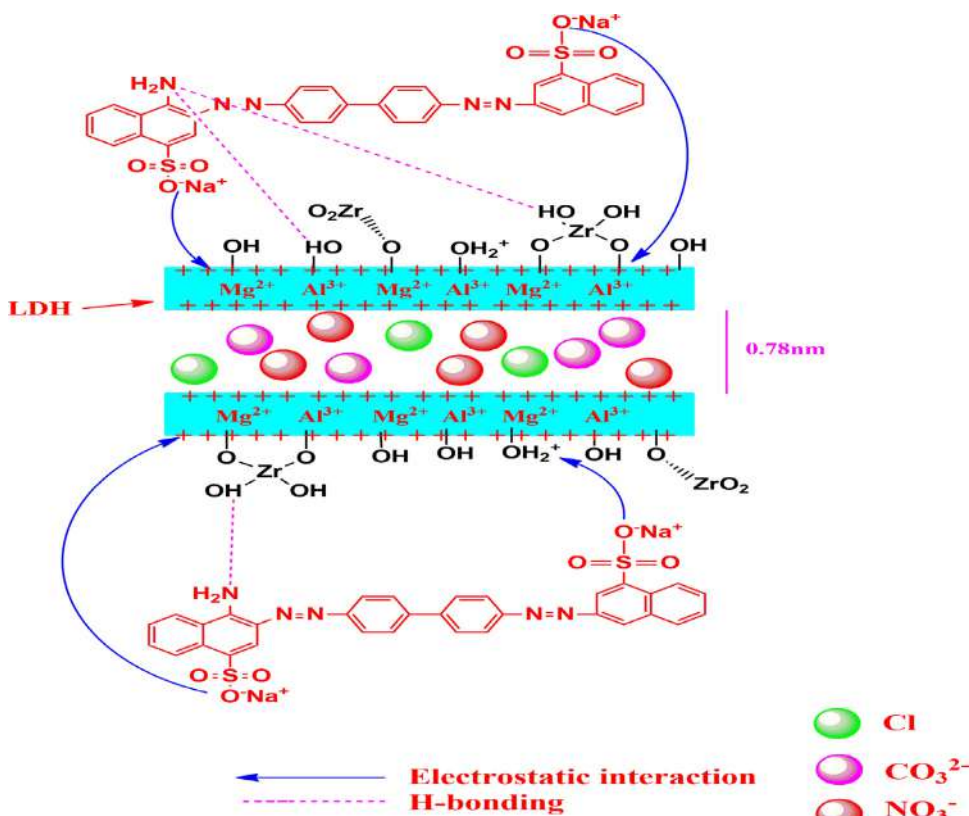


Figure 18. Schematic representation of the plausible adsorption mechanism in CR adsorption on to ZrO₂/MgAl-LDH.

Table 3

Parameters of pseudo first order, pseudo second order and intraparticle diffusion model for the adsorptive removal of CR by ZrO₂/MgAl-LDH.

Kinetics model	Parameters	Initial concentration (mg/L)			
		30	60	90	
Pseudo-first order	$q_e(\text{exp})$	57.53	112.12	166	
	$q_{e1}(\text{mg/g})$	17.98	60.39	68.94	
	$K_1 \times 10^{-2} \text{ min}^{-1}$	1.25	0.92	0.32	
	R^2	0.931	0.979	0.967	
	SSE	3.29	4.30	8.08	
Pseudo-second order	$q_{e2}(\text{mg/g})$	57.97	110.37	130.89	
	$K_2 \times 10^{-4} (\text{g.mg}^{-1} \text{ min}^{-1})$	18.55	4.18	1.82	
	R^2	0.999	0.997	0.997	
	SSE	0.036	0.145	2.925	
	Intraparticle diffusion	$K_i(\text{mg/g.min}^{-1})$	1.654	4.735	3.092
$C(\text{mg/g})$		35.15	39.81	85.63	
R^2		0.768	0.949	0.983	
Boyd		$D_1 \times 10^{-15} (\text{m}^2/\text{min})$	0.319	0.236	0.083
	B	0.012	0.009	0.003	
	R^2	0.931	0.980	0.967	
	Bangham	K_0	34.44	17.93	31.38
		α	0.156	0.261	0.113
R^2		0.925	0.988	0.997	

$$\Delta G = -RT \ln K_d \quad (20)$$

$$\ln K_d = \frac{\Delta S}{R} - \frac{\Delta H}{RT} \quad (21)$$

where K_d (C_e/q_e) signifies adsorption distribution coefficient, ΔG indicates standard free energy (KJ/mol), R denotes universal gas constant, T is the temperature in Kelvin, ΔH is the standard enthalpy (KJ/mol) and ΔS represents standard entropy (J/mol).

The Vant Hoff plot shown in Fig. 15 is obtained from the linear plot of $\ln K_d$ vs $1/T$. The standard entropy ΔS and enthalpy ΔH can be de-

termined from the intercept and slope of the plot. The thermodynamic parameters are demonstrated in Table 4. It was noted that for both initial dye concentration (30,120mg/L) with the increasing temperature from 303K to 333K the negative value of ΔG is observed which infers that the adsorption of CR dye by ZrO₂/MgAl-LDH is spontaneous in nature. The standard free energy ΔG decreases from -7.94 to -11.29 KJ/mol and -3.06 to -6.54 KJ/mol for initial dye concentration 30 mg/L and 120 mg/L respectively. Nevertheless, the obtained ΔH values are positive (+25.70 KJ/mol, +31.51 KJ/mol) which refers to endothermic nature during the adsorption process. The positive ΔS value also signifies the

Table 4
Thermodynamic parameters for the CR uptake on to ZrO₂/MgAl-LDH.

C ₀ (mg/L)	T(K)	K _d	ΔG(KJ/mol)	ΔH(KJ/mol)	ΔS(J/molK)	E _a (KJ/mol)	S*
30	303	23.390	-7.940	25.708	111.032	25.15	0.1913 × 10 ⁻⁵
	313	32.333	-9.045				
	333	59.118	-11.292				
120	303	3.373	-3.062	31.513	114.332	27.04	0.4943 × 10 ⁻⁵
	313	5.416	-4.395				
	333	10.650	-6.549				

Table 5
The comparison of optimum experimental conditions for the removal of CR dye by several reported adsorbents.

Adsorbent	q _{max} (mg/g)	pH	Time(min)	Dosages(g)	Isotherm	References
NiFeTi-LDH	29.97	7	10	0.02	L	[52]
ZnAl-LDH	591.80	3	2-200	0.7	F	[53]
Cornulca monacantha Stem	43.42	2	135	0.05	L	[55]
MgAl-mixed metal oxide	96.99	9	120	0.03	L	[56]
NiAl-LDH	120.5	6	30	0.01	L	[63]
Nanocrystalline Hydroxyapatite	139	5.5	20	2	F	[71]
MgAl-LDH/CF	271	3	4320	0.05	L	[72]
Al(OH) ₃ /CuMnAl-LDH	172	7	-	0.02	L	[73]
GO-NiFe-LDH	489	6-7	350	-	Liu	[74]
ZrO ₂ /MgAl-LDH	169.42	7	240	0.02	L	This work

increase in randomness of adsorbate molecules on solid liquid phase. Furthermore, it has been found that the adsorption of CR increases at higher temperature which indicates more feasibility at 333 K.

To further discern whether the adsorption process is governed by chemisorption or physisorption, the activation energy (E_a) and sticking probability (S*) value during the thermodynamic studies was estimated from the modified Arrhenius equation which is expressed by the following equation [67]:

$$S^* = (1 - \theta) e^{-E_a/RT} \quad (22)$$

$$\theta = \left(1 - \frac{C_e}{C_0}\right) \quad (23)$$

$$\ln S^* = \ln(1 - \theta) - \frac{E_a}{RT} \quad (24)$$

$$\ln(1 - \theta) = \ln S^* + \frac{E_a}{RT} \quad (25)$$

where C₀ and C_e are the initial and equilibrium concentration of dye solution (mg/L), θ denotes surface coverage, E_a (KJ/mol) signifies activation energy, T is the temperature in Kelvin, S* indicates sticking probability which is dependent on the adsorbate- adsorbent system.

The plot of ln(1-θ) vs 1/T was depicted in Fig. 16 and the values of thermodynamic parameters E_a and S* are presented in Table 5. It is evident that the activation energy (E_a) values obtained corresponding to the initial CR dye concentration 30 mg/L and 120 mg/L are 25.15 KJ/mol and 27.04 KJ/mol respectively, while the sticking probability was found between (0 < S* < 1). Usually the chemisorption mechanism has activation energy (E_a) ranging between (40-800 KJ/mol), while in case of physisorption the relatively lower E_a (5-40 KJ/mol) is associated during the process. Since, the activation energy of CR adsorption lies between 5-40 KJ/mol, it further implies the existences of low potential energy barrier. Thus, it can be suggested that adsorption of CR dye over ZrO₂/MgAl-LDH composite involved physisorption as a dominant process [68].

3.5. Mechanism of Congo red adsorption on ZrO₂/MgAl-LDH

The plausible adsorption mechanism of CR dye onto ZrO₂/MgAl-LDH composite is depicted in Fig. 18. To further analyze the adsorption mechanism, FT-IR and powder XRD spectra are recorded after adsorption experiment which is presented in Fig. 1 and Fig. 2 respectively. As

it is confirmed from powder XRD spectra of ZrO₂/MgAl-CR displayed in Fig. 1 it does not reveal any significant changes in the peak position corresponding to 003 and 110 planes, which further suggests that insertion of adsorbate molecules between interlayer space of LDH sheets does not occur, rather it is held on the adsorbent surfaces through a combination of several weak and strong bond interactions. Since, adsorption mechanism is dependent on solution pH, it occurs differently at varying pH. At lower pH values, the -OH group of LDH surface gets partially protonated thereby making it relatively suitable for the strong interaction with -SO₃⁻ anion. In contrast, at higher pH values, the repulsion between -OH⁻ and SO₃⁻ counteracted the electrostatic interaction where only anion exchangeability may be possible for adsorption. Additionally, the FT-IR spectra after adsorption showed the existences of stretching vibration corresponding to SO₃⁻ group of CR dye. Therefore, the electrostatic attraction between the SO₃⁻ groups of CR and positive charge (OH₂⁺) on the LDH sheets are predominantly responsible for decontamination of aqueous solution from azo dye. Besides, the presences of other weak interactions such as Vander waals, H-bonding, surface complexation may also be prevalent [41,43].

3.6. Reusability and Desorption studies

Reusability performance of a material is an important aspect to evaluate the efficacy of adsorbent for its industrial application. The reusability studies of ZrO₂/MgAl-LDH shown in Fig. 17(a) was investigated up to fifth cycle at an operating conditions fixed at initial concentration 50 mg/L, adsorbent dosages 0.02 g, contact time 6 hours. The initially adsorbed CR dye on the material surface was desorbed by dispersing in a 0.1M NaOH solution after each cycle. The alkalinity of the solution can decrease the strong electrostatic interaction between adsorbent and adsorbate, thereby leading to an ease desorption of CR dye. Subsequently, the regenerated adsorbent is dried and reuse up to fifth cycle. From Fig. 17(a) it is obvious that the adsorbent showed reduction in its performance after each cycle. The maximum dye removal percentage in the first cycle showed up to 97.19%, which slowly decreases to 59.04% in the fifth cycle. The dye removal efficiency reduces to 38.15% between initial and last cycle. However, the decrease in adsorption capacity can be attributed to the loss of adsorption sites during the repeated regeneration process [69].

The graphical representation of the desorption studies conducted in various solvents were displayed in Fig. 17(b). In aqueous solution the desorption activity of CR dye from the adsorbent ZrO₂/MgAl-LDH sur-

face was not observed, thus indicating that adsorption process is completely opposite to the desorption process in aqueous medium. However, the maximum desorption percentage of CR dye was obtained in methanol solvent with 85.47% desorption efficiency, which is comparatively higher than other desorbing eluents such as ethanol (71.37%), acetone (16.28%), 0.1M NaOH (60.27%) and 0.1M Na₂CO₃ (45%). The tendency to desorb CR dye in different solvents can be explained on the basis of their relative ability to weaken the strongly bound adsorbate-adsorbent interaction especially electrostatic attraction and H-bonding. In solvent such as methanol and ethanol the higher affinity towards the CR dye molecule may be accounted to the greater desorption percentage. In alkaline medium the desorption takes place due to hydrophobic interaction and greater anionic exchangeability between existing OH⁻ and CR ions over the positively charged adsorbent [70].

3.7. Comparison with reported adsorbents

With an emphasis to the maximum monolayer adsorption capacity shown by previously reported adsorbent for CR, the currently proposed adsorbent ZrO₂/MgAl-LDH displays greater q_{\max} value of 169.42 mg/g. In Table 5 several adsorbents such as nanocrystalline hydroxyapatite, NiAl-LDH, MgAl-mixed metal oxide and NiFeTi-LDH have relatively lower adsorption capacity than currently studied material. Only a few of the materials such as ZnAl-LDH and GO-NiFe-LDH showed better performances than ZrO₂/MgAl-LDH. Besides, due to its facile synthetic procedure and comparatively remarkable higher sorption activity than most of the presented adsorbents, ZrO₂/MgAl-LDH can be regarded as the potential candidate for the efficient removal of CR dye from aqueous solution [71–74].

4. Conclusions

In this work, we have reported the synthesis of novel tetravalent metal-containing as-synthesized ZrO₂/MgAl-LDH and its potential adsorption performance toward CR dye. The as synthesized ZrO₂/MgAl-LDH prepared by urea hydrolysis method offers high crystallinity, porosity within the mesopore range and intermediate specific surface area of 71.55 m²/g. The maximum removal of congo red was observed at the optimum pH-4 for a contact time of 90 minutes. However, isotherm and kinetics analysis showed that the mechanism can be best described by Redlich-Peterson, Langmuir and pseudo second order kinetic model. In addition, the proposed adsorbent ZrO₂/MgAl-LDH revealed higher uptake of CR (q_{\max} =169.42 mg/g) compare to pristine MgAl-LDH previously reported. The thermodynamic parameter ΔG decreases with the increase in temperature from 301 to 333K indicating the spontaneous and endothermic process. The reusability test up to fifth cycle infers the superiority of the adsorbent materials. Moreover, this study has made a new approach to modify MgAl-LDH with tetravalent Zr⁴⁺ metal to enhance its sorption characteristics. The obtained results may encourage new emerging researchers and shed light to further explore designing of multivalent metal containing LDH for dye adsorption.

5. Funding Agencies

Nil.

Declaration of Competing Interest

The authors do not have any conflict of interest.

The authors do not have any conflict of interest to disclose.

CRediT authorship contribution statement

Deepmoni Brahma: Data curation, Investigation, Formal analysis, Writing – original draft, Visualization. **Hemaprobra Saikia:** Supervision, Methodology, Conceptualization, Project administration, Writing – review & editing, Resources, Validation.

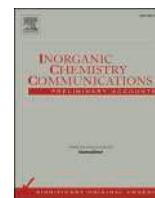
Acknowledgement

We are thankful to several institutes for providing instrumental facility for characterization of material with SEM-EDX, BET and Powder X-ray from CIF, IIT Guwahati, FT-Infrared from Gauhati University, TEM from NEHU SAIF, TGA and XPES from IIT-Kanpur. We are also thankful to our institute Bodoland University for providing UV-spectrophotometer instruments and all the necessary chemicals and equipments required for our research works. We would like to acknowledge Prof. Hilloljyoti Singha Department of Zoology, Bodoland University for his valuable advice.

References

- [1] S. Benhaya, S. M' rabet, A.E. Harfi, A review on classifications, recent synthesis and applications of textile dyes, *Inorganic Chemistry Communications* 115 (2020) 107891.
- [2] K. Abdellaoui, I. Pavlovic, C. Barriga, Nanohybrid Layered Double Hydroxides Used to Remove Several Dyes from Water, *ChemEngineering* 3 (2019) 41.
- [3] R. Krishnamoorthy, A. Roy Choudhury, P. Arul Jose, K. Suganya, M. Senthikumar, J. Prabhakaran, N. Olagathan Gopal, J. Choi, K. Kim, R. Anandham, T. Sa, Long-Term Exposure to Azo Dyes from Textile Wastewater Causes the Abundance of Saccharibacteria Population, *Applied Science* 11 (2021) 379.
- [4] T. Shindhal, P. Rakholiya, S. Varjani, A. Pandey, H.H. Ngo, W. Guo, H.Y. Ng, M.J. Taherzadeh, Acritical review on advances in the practices and perspectives for the treatment of dye industry wastewater, *Bioengineered* 12 (2020) 70–87.
- [5] W. Konicki, D. Sibera, U. Narkiewicz, Adsorptive removal of cationic dye from aqueous solutions by ZnO/ZnMn₂O₄ nanocomposite, *Separation Science and Technology* 53 (2018) 1295–1306.
- [6] S.K. Sela, A.K.K. Nayab-Ul-Hossain, S.Z. Hussain, N. Hasan, Utilization of prawn to reduce the value of BOD and COD of textile wastewater, *Cleaner Engineering and Technology* 1 (2020) 100021.
- [7] B. Lellis, C.Z. Favaro-Polonio, J.A. Pamphile, J.C. Polonio, Effects of textile dyes on health and the environment and bioremediation potential of living organisms, *Biotechnology Research and Innovation* 3 (2019) 275–290.
- [8] J.N. Wekoye, W.C. Wanyonyi, P.T. Wangila, M.K. Tonui, Kinetic and equilibrium studies of Congo red dye adsorption on cabbage waste powder, *Environmental Chemistry and Ecotoxicology* 2 (2020) 24–31.
- [9] S. Farhadi, F. Manteghi, R. Tondfekr, Removal of Congo red by two new zirconium metal-organic frameworks: Kinetics and isotherm study, *Monatshfte für Chemie-Chemical Monthly* 150 (2019) 193–205.
- [10] B. Sherino, S.N.A. Halim, S. Shahabuddin, S. Mohamad, Simultaneous removal of carcinogenic anionic and cationic dyes from environmental water using a new Zn-based metal-organic framework, *Separation Science and Technology* 56 (2021) 330–343.
- [11] Nisar, Ali, A. Said, F. Ali, F. Raziq, Z. Ali, M. Bilal, L. Reinert, T. Begum, H.M.N. Iqbal, Photocatalytic Degradation of Congo Red Dye from Aqueous Environment Using Cobalt Ferrite Nanostructures: Development, Characterization, and Photocatalytic Performance, *Water, Air, & Soil Pollution* 231 (2020) 1–16.
- [12] M.R. Gadekar, M.M. Ahammed, Use of water treatment residuals for colour removal from real textile dye wastewater, *Applied Science* 10 (2020) 1–8.
- [13] S. Natarajan, V. Anitha, G.P. Gajula, V. Thiagarajan, Synthesis and Characterization of Magnetic Superadsorbent Fe₃O₄-PEG-Mg-Al-LDH Nanocomposites for Ultrahigh Removal of Organic Dyes, *ACS Omega* 5 (2020) 3181–3193.
- [14] K. Ikehata, Y. Zhao, H.V. Kulkarni, Y. Li, S.A. Snyder, K.P. Ishida, M.A. Anderson, Water Recovery from Advanced Water Purification Facility Reverse Osmosis Concentrate by Photobiological Treatment Followed by Secondary Reverse Osmosis, *Environmental Science & Technology* 52 (2018) 8588–8595.
- [15] Q. Wang, A. Tang, L. Zhong, X. Wen, P. Yan, J. Wang, Amino-modified γ -Fe₂O₃/sepiolite composite with rod-like morphology for magnetic separation removal of congo red dye from aqueous solution, *Powder Technology* 339 (2018) 872–881.
- [16] R. Lafi, L. Zgara, R.H. Lajimi, A. Hafiane, Treatment of textile wastewater by a hybrid ultrafiltration/electrodialysis process, *Chemical Engineering and Processing-Process Intensification* 132 (2018) 105–113.
- [17] N. Elhadiri, M. Benchanaa, R. Chikri, Activated carbon for dyes removal: modeling and understanding the adsorption process, *Journal of Chemistry* 2020 (2020) 2096834.
- [18] G. Moussavi, M. Mahmoudi, Removal of azo and anthraquinone reactive dyes from industrial wastewaters using MgO nanoparticles, *Journal of Hazardous Materials* 168 (2019) 806–812.
- [19] M.R. Abukhadra, A.S. Mohamed, Adsorption removal of safranin dye contaminants from water using various types of natural zeolite, *Silicon* 11 (2019) 1635–1647.
- [20] X.S. Hu, R. Liang, G. Sun, Super-adsorbent hydrogel for removal of methylene blue dye from aqueous solution, *Journal of Materials Chemistry A* 6 (2018) 17612–17624.
- [21] B. Mao, B. Sidhureddy, A.R. Thiruppathi, P.C. Wood, A. Chen, Efficient dye removal and separation based on graphene oxide nanomaterials, *New Journal of Chemistry* 44 (2020) 4519–4528.
- [22] M. Munir, M.F. Nazar, M.N. Zafar, M. Zubair, M. Asfaq, A. Hosseini-Bandegharai, S.U. Khan, A. Ahmad, Effective Adsorptive Removal of Methylene Blue from Water by Didodecyltrimethylammonium Bromide-Modified Brown Clay, *ACS Omega* 5 (2020) 16711–16721.

- [23] M. Mohapi, J.S. Sefadi, M.J. Mochane, S.I. Magagula, K. Lebelo, Effect of LDHs and Others Clays on Polymer Composite in adsorptive Removal of Contaminants: A Review, *Crystals* 10 (2020) 957.
- [24] M. Daud, A. Hai, F. Banat, M.B. Wazir, M. Habib, G. Bharath, M.A. Al-Harathi, A review on the recent advances, challenges and future aspect of layered double hydroxide(LDH)- Containing hybrids as promising adsorbents for dyes removal, *Journal of Molecular Liquids* 288 (2019) 110989.
- [25] R.K. Mahmoud, M. Taha, A. Zaher, R.M. Amin, Understanding the physicochemical properties of Zn-Fe LDH nanostructure as sorbent material for removing of anionic and cationic dyes mixture, *Scientific report* 11 (2021) 1–19.
- [26] S. Sonal, B.K. Mishra, A comprehensive review on the synthesis and performance of different zirconium-based adsorbents for the removal of various water contaminants, *Chemical Engineering Journal* 424 (2021) 130509.
- [27] R. Torres-Caban, C.A. Vega-Olivencia, N. Mina-Camilde, Adsorption of Ni²⁺ and Cd²⁺ from Water by Calcium Alginate/Spent Coffee Grounds Composite Beads, *Applied Science* 9 (2019) 4531.
- [28] J.M. Jabbar, Y.A. Odusote, K.A. Alabi, I.B. Ahmed, Kinetics and mechanisms of congo-red dye removal from aqueous solution using activated Moringa oleifera seed coat as adsorbent, *Applied Water Science* 10 (2020) 1–11.
- [29] I. Langmuir, THE ADSORPTION OF GASES ON PLANE SURFACES OF GLASS, MICA AND PLATINUM, *Journal of American Chemical Society* 40 (1918) 1361–1403.
- [30] S. Das, S.K. Dash, K.M. Parida, Kinetics, isotherm, and thermodynamic study for ultrafast adsorption of azo dye by an efficient sorbent: ternary Mg/(Al+Fe) layered double hydroxides, *ACS Omega* 3 (2018) 2532–2545.
- [31] H.M.F. Freundlich, Over the Adsorption in Solution, *Journal of Physical Chemistry* 57 (1906) 385–471.
- [32] M.I. Temkin, The Kinetics of Some Industrial Heterogeneous Catalytic Reactions, *Advances in Catalysis* 28 (1979) 173–291.
- [33] O. Redlich, D.L. Peterson, A useful adsorption isotherm, *Journal of Physical Chemistry* 63 (1959) 1024–1024.
- [34] S. Sonal, P. Prakash, B.K. Mishra, G.C. Nayak, Synthesis, characterization and sorption studies of a zirconium (IV) impregnated highly functionalized mesoporous activated carbons, *RSC Advance* 10 (2020) 13783–13798.
- [35] Y.S. Ho, G. McKay, Pseudo-second order model for sorption processes, *Process biochemistry* 34 (1999) 451–465.
- [36] W.J. Weber, J.C. Morris, Kinetics of adsorption on carbon from solution, *Journal of the sanitary engineering division* 89 (1963) 31–59.
- [37] M. Benjelloun, Y. Miyah, G.A. Evrendilek, F. Zerrouq, S. Lairini, Recent Advances in Adsorption Kinetic Models: Their Application to Dye Types, *Arabian Journal of Chemistry* 14 (2021) 103031.
- [38] S. Vahidhabanu, A.I. Adeogun, B.R. Babu, Biopolymer-Grafted, Magnetically Tuned Halloysite Nanotubes as Efficient and Recyclable Spongelike Adsorbents for Anionic Azo Dye Removal, *ACS Omega* 4 (2019) 2425–2436.
- [39] R. Benhiti, A.A. Ichou, A. Zaghloul, R. Aziam, G. Carja, M. Zerbet, F. Sinan, M. Chiban, Synthesis, characterization, and comparative study of MgAl-LDHs prepared by standard coprecipitation and urea hydrolysis methods for phosphate removal, *Environmental Science and Pollution Research* 27 (2020) 45767–45774.
- [40] A. Nuryadin, T. Imai, Application of amorphous zirconium (hydr) oxide/MgFe layered double hydroxides composite in fixed-bed column for phosphate removal from water, *Global Journal of Environmental Science* 7 (2021) 485–502.
- [41] J. Poonosamy, F. Brandt, M. Stekiel, P. Kegler, M. Klinkenberg, B. Winkler, V. Vinograd, Zr-containing layered double hydroxides: Synthesis, characterization and evaluation of thermodynamic properties, *Applied Clay Science* 151 (2018) 54–65.
- [42] A.K. Avila-Martinez, J.H. Roque-Ruiz, J. Torres-Perez, N.A. Medellin-Castillo, S.Y. Reyes-Lopez, Allura Red dye sorption on to electrospun zirconia nanofibers, *Environmental Technology & Innovation* 18 (2020) 100760.
- [43] R. Shabbir, A. Gu, J. Chen, M.M. Khan, P. Wang, Y. Jiao, Z. Zhang, Y. Liu, Y. Yang, Highly efficient removal of congo red and methyl orange by using petal-like Fe-Mg layered double hydroxide, *International Journal of Environmental Analytical Chemistry* (2020) 1–18.
- [44] O.S. Travkina, M.R. Agliullin, R.Z. Kuvatova, I.N. Pavlova, N. Narender, B.I. Kutepov, New method of synthesis of hierarchical mordenite of high crystallinity and its application in hydrozomerization of benzene-n-heptane mixture, *Journal of Porous Material* 26 (2018) 995–1004.
- [45] B. Priyadarshini, T. Patra, T.R. Sahoo, An efficient and comparative adsorption of Congo red and Trypan blue dyes on MgO nanoparticles: Kinetics, thermodynamics and isotherm studies, *Journal of Magnesium and Alloys* 9 (2021) 478–488.
- [46] V.R. Magri, A. Duarte, G.F. Perotti, V.R.L. Constantino, Investigation of Thermal Behaviour of Layered Double Hydroxides Intercalated with Carboxymethylcellulose Aiming Bio-Carbon Based Nanocomposite, *Chemengineering* 3 (2019) 55.
- [47] S. Naseem, B. Gevers, R. Boldt, F.J.W.J. Labuschagne, A. Leuteritz, Comparison of transition metal (Fe, Co, Ni, Cu, Zn) containing tri-metal layered double hydroxides (LDHs) prepared by urea hydrolysis, *RSC Advances* 9 (2019) 3030–3040.
- [48] Hobbs, C.; Jaskaniec, S.; McCarthy, E.K.; Downing, C.; Opelt, K.; Guth, K.; Shmeliiov, A.; Mourad, M.C.D.; Mandel, K.; Nicolosi, V. Structural transformation of layered double hydroxides: an in situ TEM analysis. *Njp 2D Materials and Applications*, 2: 1-10.
- [49] J. Zhu, Z. Zhu, H. Zhang, H. Lu, Y. Qiu, Efficient degradation of organic pollutants by peroxymonosulfate activated with MgCuFe-layered double hydroxide, *RSC Advances* 9 (2019) 2284–2291.
- [50] P. Lackner, Z. Zou, S. Mayr, U. Diebold, M. Schmid, Using photoelectron spectroscopy to observe oxygen spillover to zirconia, *Physical Chemistry Chemical Physics* 21 (2019) 17613–17620.
- [51] Z. Azzad, L. Marot, L. Moser, R. Steiner, E. Meyer, Valence band behavior of zirconium oxide, *Photoelectron and Auger spectroscopy study*, *Scientific Reports* 8 (2018) 1–6.
- [52] G. Rathee, A. Awasthi, D. Sood, R. Tomar, V. Tomar, R. Chandra, A new biocompatible ternary Layered Double Hydroxide Adsorbent for ultrafast removal of anionic organic dyes, *Scientific Reports* 9 (2019) 1–14.
- [53] A.E. Khanchaoui, M. Sajjeddine, M. Mansori, A. Essoumi, Anionic dye adsorption on ZnAl hydrotalcite-type and regeneration studies based on “memory effect”, *International Journal of Environmental Analytical Chemistry* (2020) 1–19.
- [54] S. Popa, M.E. Radulescu-Grad, A. Perdivara, G. Mosoarca, Aspects regarding colour fastness and adsorption studies of a new azo-stilbene dye for acrylic resins, *Scientific Reports* 11 (2021) 1–9.
- [55] A. Sharma, Z.M. Siddiqui, S. Dhar, P. Mehta, D. Pathania, Adsorptive removal of congo red dye (CR) from aqueous solution by *Cornulaca monacantha* stem and biomass-based activated carbon: isotherm, kinetics and thermodynamics, *Separation Science and Technology* 54 (2019) 916–929.
- [56] Y. Lv, L. Gao, S. Feng, S. Wang, Y. Qiao, Q. Li, Hierarchically structured Mg-Al mixed metal oxides template from pine sawdust: fabrication, Congo red adsorption and antibacterial properties, *Separation Science and Technology* 54 (2019) 2625–2637.
- [57] Ihsanullah N.I. Blaisi, M. Zubair, S. Ali, T.S. Kazeem, M.S. Manzar, W. Al-Kutti, M.A. Al Harthi, Date palm ash-MgAl-layered double hydroxide composite: sustainable adsorbent for effective removal of methyl orange and eriochrome black-T from aqueous phase, *Environmental Science and Pollution Research* 25 (2018) 34319–34331.
- [58] N.K. Gupta, M. Saifuddin, S. Kim, K.S. Kim, Microscopic, spectroscopic, and experimental approach towards understanding the phosphate adsorption on to Zn-Fe layered double hydroxide, *Journal of Molecular Liquids* 297 (2020) 111935.
- [59] Y. Chen, C. Jing, X. Zhang, D. Jiang, X. Liu, B. Dong, Li. Feng, S. Li, Y. Zhang, Acid-salt treated CoAl layered double hydroxide nanosheets with enhanced adsorption capacity of methyl orange dye, *Journal of Colloids and Interface Science* 548 (2019) 100–109.
- [60] G.Y. Abo El-Reesh, A.A. Farghali, M. Taha, R.K. Mahmoud, Novel synthesis of Ni/Fe layered double hydroxides using urea and glycerol and their enhanced adsorption behavior for Cr(VI) removal, *Scientific Reports* 10 (2020) 1–20.
- [61] S. Dutta, B. Gupta, S.K. Srivastava, A.K. Gupta, Recent advances on the removal of dyes from wastewater using various adsorbents: a critical review, *Materials Advances* 2 (2021) 4497–4531.
- [62] R. Gopinathan, A. Bhowal, C. Garlapati, Adsorption Studies of Some Anionic Dyes Adsorbed by Chitosan and New Four-Parameter Adsorption Isotherm Model, *Journal of Chemical and Engineering Data* 64 (2019) 2320–2328.
- [63] D. Bharali, R.C. Deka, Adsorptive removal of congo red from aqueous solution by sonochemically synthesized NiAl layered double hydroxide, *Journal of Environmental Chemical Engineering* 5 (2017) 2056–2067.
- [64] L. Jiang, Y. Liu, S. Liu, X. Hu, G. Zeng, X. Hu, S. Liu, S. Liu, B. Huang, M. Li, Fabrication of β -cyclodextrin/poly(L-glutamic acid) supported magnetic graphene oxide and its adsorption behavior for 17 β -estradiol, *Chemical Engineering Journal* 308 (2017) 597–605.
- [65] P.K. Singh, S. Banerjee, A.L. Srivastava, Y.C. Sharma, Kinetic and equilibrium modeling for removal of nitrate from aqueous solutions and drinking water by a potential adsorbent, hydrous bismuth oxide, *RSC Advance* 5 (2015) 35365–35376.
- [66] X. Zheng, X. Li, J. Li, L. Wang, W. Jin, J. Liu, Y. Pei, K. Tang, Efficient removal of anionic dye (Congo red) by dialdehyde microfibrillated cellulose/chitosan composite film with significantly improved stability in dye solution, *International Journal of Biological Macromolecule* 107 (2018) 283–289.
- [67] V.O. Shikuku, R. Zanella, C.O. Kowenje, F.F. Donato, N.M.G. Bandeira, O.D. Prestes, Single and binary adsorption of sulfonamide antibiotics on to iron-modified clay: linear and non linear isotherms, kinetics, thermodynamics, and mechanistic studies, *Applied Water Science* 8 (2018) 1–12.
- [68] Y. Li, H.Y. Bi, Y.S. Jin, X.Q. Shi, Removal of disperse violet 28 from water using self-assembled organo-layered double hydroxides through a one-step process, *RSC Advance* 4 (2014) 58307–58314.
- [69] D.N. Ahmed, L.A. Naji, A.A.H. Faisal, N. Al-Ansari, Mu. Naushad, Waste foundry sand /MgFe-layered double hydroxides composite material for efficient removal of Congo red dye from aqueous solution, *Scientific Reports* 10 (2020) 1–12.
- [70] E. Rapo, S. Tonk, Factors Affecting Synthetic Dye Adsorption; Desorption Studies: A Review of Results from the Last Five Years (2017–2021), *Molecules* 26 (2021) 5419.
- [71] H. Bensalah, S.A. Younsi, M. Ouammou, A. Gurlo, M.F. Bekheet, Azo dye adsorption on an industrial waste-transformed hydroxyapatite adsorbent: Kinetics, isotherms, mechanism and regeneration studies, *Journal of Environmental Chemical Engineering* 8 (2020) 103807.
- [72] Q. Sun, Bo. Chen, Biotemplated Fabrication of 3D Hierarchically Porous MgAl-LDH/CF Composites with Effective Adsorption of Organic Dyes from Wastewater, *Industrial & Engineering Chemistry Research* 59 (2020) 16838–16850.
- [73] J.O. Eniola, R. Kumar, A.A. Al-Rashdi, M.O. Ansari, M.A. Barakat, Fabrication of Novel Al(OH)₃/CuMnAl-Layered Double Hydroxide for Detoxification of Organic Contaminants from Aqueous Solution, *ACS Omega* 4 (2019) 18268–18278.
- [74] Y. Zheng, B. Cheng, W. You, J. Yu, W. Ho, 3D hierarchical graphene oxide-NiFe LDH composite with enhanced adsorption affinity to Congo red, methyl orange and Cr(VI) ions, *Journal of Hazardous Materials* 369 (2019) 214–225.



Coconut Husk Ash Fabricated CoAl-Layered Double Hydroxide Composite for the Enhanced Sorption of Malachite Green Dye: Isotherm, kinetics and thermodynamic studies

Deepmoni Brahma, Harshajit Nath, Debasis Borah, Mandira Debnath, Hemaprobha Saikia *

Department of Chemistry, Bodoland University, Kokrajhar-783370, Assam, India

ARTICLE INFO

Keywords:

Coconut Husk Ash
CoAl-LDH
Malachite Green
Adsorption
Composite

ABSTRACT

In this work, the new composite material has been designed by using coconut husk ash (CHA) as the supporting material for CoAl layered double hydroxide (LDH), and investigated the adsorptive removal of organic dye malachite green (MG) from the aqueous media. The as-synthesized sorbent was prepared via simple co-precipitation method by loading 3 g of coconut husk derived carbon on to the structure of CoAl-LDH. The physicochemical properties and the formation of the composite material was confirmed by various characterization techniques such as powder X-ray diffraction (PXRD), Fourier transform infrared spectroscopy (FTIR), Scanning emission microscopy (SEM), Energy dispersive X-ray (EDX), Transmission emission microscopy (TEM) and Brunauer-Emmett-Teller (BET). The experimental results envisages that the proposed adsorbent CHA/CoAl-LDH composite showed the significant removal efficiency up to 98.16 % at 0.015 g dosages under initial dye concentration of 100 mg/L and pH 10. In addition, the maximum monolayer adsorption capacity exhibited by CHA/CoAl-LDH from the isotherm studies was 666.4 mg/g. The isotherm and kinetics data was fitted well according to Langmuir and pseudo second order model. The thermodynamic studies obtained positive value of ΔH (CHA = 72.49 KJ/mol, CHA/CoAl-LDH = 110 KJ/mol) and negative ΔG values (CHA = -9.36 KJ/mol, CHA/CoAl-LDH = -6.62KJ/mol) at 303 K, which further confirmed the spontaneous and endothermic nature of adsorption process. Furthermore, the estimated value of activation energy (E_a) determined from the modified Arrhenius equation was 101.35 KJ/mol and 69.50 KJ/mol for CHA and CHA/CoAl-LDH, respectively. Besides, the proposed adsorbent also reveals excellent reusability up to third cycle, as well as effective for the removal of other cationic and anionic dyes. Therefore, the overall result advocated that the adsorbent CHA/CoAl-LDH can be chosen as an alternative for dye treatment in aqueous media.

1. Introduction

The availability of fresh and quality water has decline across the world due to the rapid advancement in manufacturing industry. Since, water is a universal solvent, most of the water soluble pollutants either organic or inorganic molecules get readily dissolved into it. Consequently, the chemical properties of the safe and quality drinking water get altered due to the contaminants from various industrial discharged [1]. Among several water pollutants the problem emerging from organic dyes are regarded as a serious issue. The ubiquitous presence of dye in the effluents discharged from various industries such as textiles, cosmetics, food, pharmaceuticals, paints, plastics and leather are toxic, and

causes severe health hazard to the residential communities. These harmful effects include carcinogenic, mutagenic, heart diseases, skin irritation and allergies [2,3]. In addition, the toxicity of these organic dyes had also posed detrimental effect in the aquatic ecosystem and is of great concern. Among different cationic dyes, Malachite green (MG) a triphenylmethane dye has been extensively used for coloring wool, silk, paper, cotton, leather and several printed products. As a result, these toxic dyes present in the form of untreated industrial wastes when discharged freely into natural environment could enter into the food chain that can further lead to severe diseases for all living organism [4,5]. Thus, effective removal of this pollutant is very crucial in order to prevent potential hazards. Although, the treatment of waste water

* Corresponding author.

E-mail addresses: brahmadeepmoni@gmail.com (D. Brahma), harshanath1@yahoo.in (H. Nath), debasishborah@gmail.com (D. Borah), mandiradebnath.54321@gmail.com (M. Debnath), saikiahemaprobha@gmail.com (H. Saikia).

<https://doi.org/10.1016/j.inoche.2022.109878>

Received 27 May 2022; Received in revised form 4 August 2022; Accepted 12 August 2022

Available online 19 August 2022

1387-7003/© 2022 Elsevier B.V. All rights reserved.

contaminants is a major challenge, therefore investigation on the science of interface between water pollutants and adsorbent, and the development of smart material is highly urgent.

Several approaches such as filtration [6], photocatalytic degradation [7], ozonation [8], oxidation [9], reverse osmosis [10], microbiological process [11], flocculation [12] and adsorption [13] techniques were addressed for the efficient removal of organic and inorganic contaminants from the effluents. Despite numerous methods for water remediation are available, most of these techniques encounter major drawbacks. However, adsorption process is one of the most widely used superior treatment alternatives due to its low cost, high efficiency, eco-friendly and simplicity [14].

In previous works, various types of adsorbents viz; MOF [15,16], inorganic polymer [17], metal oxide nanocomposite [18–20], biochar [21,22] and MXenes [23] were investigated and found capable of purifying dyes contaminated waste water. Nevertheless, LDH was also used in water detoxification process which are the ionic lamellar solids constituted by brucite sheets containing divalent and trivalent metal cations along with interlayer anions like NO_3^- , Cl^- , CO_3^{2-} , SO_4^{2-} . These hierarchically structured materials display attractive features such as low toxicity, high surface area, anion exchangeability, tunable structure with various transition metal cations, and facile synthesis method [24]. Due to its diverse application such as adsorption related process, polymer chemistry, photocatalysis, biomedicine and electrochemistry, these materials have been extensively used as a component of hybrid materials. Despite, its numerous advantages the main drawbacks of pristine LDH were its inadequate surface functional groups and limited for only anionic dyes [25,26].

Recently, the synthesis of hybrid materials between LDH and biomass derived carbon had received wide attention among researchers due to its promising sorption potentiality towards hazardous organic and inorganic toxins from the effluents. For instance, Zubair et al. studied the adsorption performance of date palm biochar/CuFe-LDH composite for the removal of eriochrome black T and suggested that the strong electrostatic attraction between protonated hydroxyl group of the adsorbent and SO_3^{2-} anion of eriochrome black T was mainly responsible for exhibiting maximum adsorption of 565.32 mg/g [27]. Zhang et al. have reported the effective and simultaneous adsorption of inorganic nitrogen and heavy metal by MgFe/biochar composite, which is prepared by in situ loading of LDH particles over the surface of activated biochar [28]. Qu et al. investigated the removal of malachite green dye by four types of commercial activated carbon where they have advocated that the presence of strong acidic group over adsorbent surface had negative effects on adsorption performance [29]. Meili et al. successfully synthesized a series of bovine based biochar/LDH composite as an adsorbent via simple co-precipitation method and observed the removal of methylene blue dye from aqueous solution with high adsorption capacity (406.47 mg/g) [30].

During the fiscal year 2021, India is the second largest producer of coconut in the world accounting to over 14 million metric tons. It is a permanent crop, easily available and largely supplied across different nations throughout the year. However, this massive production generates agricultural waste which can be transformed into carbon material like charcoal and ash, otherwise left unused. Due to the great sorption capacity, high surface area, renewable and high availability of these resources, further research on development of adsorbents based on this material could be significant in the progress of water treatment technologies. Consequently, the utilization of cheap coconut husk biomass in synthesizing composite material with layered double hydroxide (LDH) can be considered as a sustainable approach in the field of water remediation. Since, a large quantity of locally available feedstock such as coconut husk has been used only for the purposes of burning fuel and fibers, while its application in waste water treatment was not explored. The availability of such low cost feedstock could be utilized in preparing carbonaceous material which can act as an ideal supporting material for LDH [31,32]. Accordingly, we have adopted a suitable strategy of

coupling the coconut husk derived ash with LDH to enhance their properties. The synergistic effects of LDH and coconut husk ash might widen its adsorption affinity for various water pollutants including both cationic and anionic.

Based on the detailed literature, adsorption studies of MG dye by CHA/CoAl-LDH composite was not reported. Herein, in this work we have fabricated CoAl-LDH by introducing coconut husk derived ash as a supporting material. The hybrid material CHA/CoAl-LDH was prepared via facile co-precipitation method and its dye remediation efficiency was tested for cationic dye (MG) from the aqueous solution. The as-synthesized adsorbent was characterized by various spectroscopic techniques and the effect of several experimental parameters such as temperature; pH, dosages, initial dye concentration and contact time were studied. In addition, the isotherm and kinetic modeling of the experimental data were analyzed and the possible adsorption mechanism was also demonstrated after recording the FTIR spectra of MG loaded adsorbents.

2. Experimental

2.1. Materials and methods

The coconut husk was collected from the local place Dotma Bazar part-II, Assam, India. Cobalt(II) nitrate hexahydrate ($\text{Co}(\text{NO}_3)_2 \cdot 6\text{H}_2\text{O}$) (98 %), Aluminium nitrate nonahydrate ($\text{Al}(\text{NO}_3)_3 \cdot 9\text{H}_2\text{O}$) (98 %), NaOH (97 %) and Malachite green ($\text{C}_{23}\text{H}_{25}\text{ClN}_2$) (98 %) was procured from Merck. The obtained chemicals are of analytical grade and used without any further purification. The required solution in the experiment was prepared by deionised water.

2.1.1. Synthesis of CHA/CoAl-LDH Composite

The synthesis of CHA/CoAl-LDH composite was conducted via co-precipitation method. Initially, the collected coconut husk was heated in a muffle furnace at 300 °C until it was completely carbonized and transformed into ash which is denoted by CHA. Subsequently, 2 g of coconut husk ash (CHA) was added in 100 mL aqueous solution containing mixture of 0.1 M AlNO_3 and 0.2 M CoNO_3 metal precursors salts. The resulting mixture was allowed to agitate in a magnetic stirrer for 30 min. Subsequently, the alkalinity of the solution was maintained at pH 10 by adding 50 mL of 0.1 M NaOH solution in a drop wise manner which was followed by continuous stirring the liquid suspension for 3 h. The precipitate obtained was centrifuged and washed several times with deionised water. The resulting black slurry was then dried in an oven at 50 °C for 6 hour. The final product obtained was denoted as CHA/CoAl-LDH composite.

2.1.2. Characterisation

Several instrumental techniques were adopted to characterize the synthesized composites. X-ray diffraction pattern of the adsorbents were obtained from Rigaku Ultima-IV powder X-ray diffractometer. The $\text{Cu-K}\alpha$ radiation ($\lambda = 0.154 \text{ \AA}$, 40 KV, 30 mA) was employed as an X-ray source. The PXRD spectrum was recorded in the 2θ range from 0 to 80°. The external microstructure of the sample was observed by SEM (Gemini Carl Zeiss Sigma 300). The internal morphology was discerned by using TEM (JEOL JEM-2100) under the accelerating potential of 200 KV. The FTIR spectra of the sample were recorded by Shimadzu IRAffinity-1 by taking KBr as a reference background under the frequency range of 0–4000 cm^{-1} . The thermal stability of the composite was investigated with TGA (Mettlab Toledo). The specific surface area and pore volume was measured by conducting N_2 -adsorption-desorption with BET and BJH method by employing an instrument Quantachrome Novawin version 11.05. For the determination of the residual dye concentration UV-Spectrophotometer-3375 (Electronics India) was utilized. The percentage composition of the constituent elements was examined by EDX. The point of zero charge (PZC) of the adsorbents CHA and CHA/CoAl-LDH was evaluated by using pH drift method. During the experiment

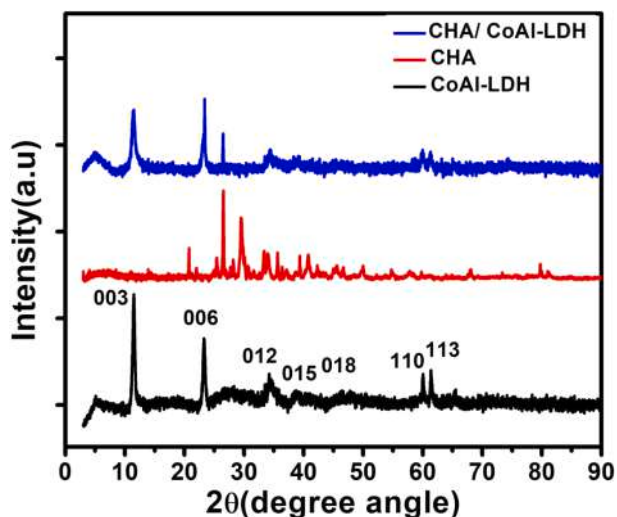


Fig. 1. Powder XRD pattern of CoAl-LDH, coconut husk ash (CHA) and CHA/CoAl-LDH composite.

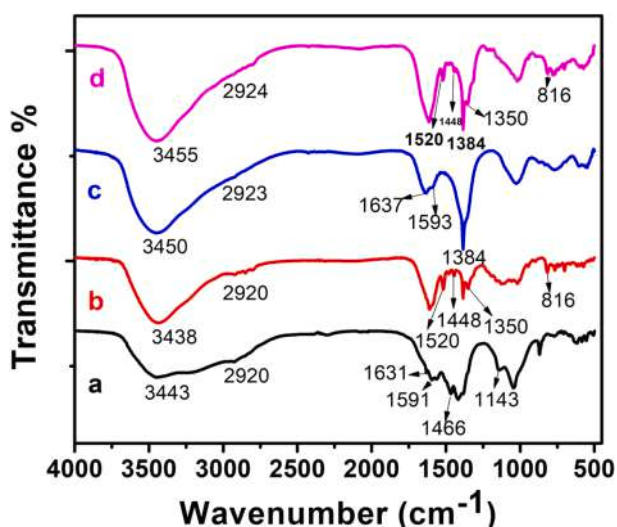


Fig. 2. FTIR spectra of (a) CHA (b) CHA-MG (c) CHA/CoAl-LDH (d) CHA/CoAl-LDH-MG.

a series of 20 mL NaCl (0.1 M) solution was poured in a conical flask, and the pH value of the solution was varied from 2 to 12. Eventually, 0.15 g of the adsorbents were dispersed in the solution and shaken at room temperature for a time period of 24 h. Afterwards, the suspension was filtered to separate the adsorbent and the final pH of the supernatant liquid was measured by digital pH meter (EI). The PZC value can be estimated from the point of intersection of line which is obtained from the graph of pH initial vs pH final.

2.2. Adsorption Experiment

The adsorption activity of the two proposed adsorbents was investigated by applying batch equilibrium method at the room temperature of 30 °C. For isotherm studies, a series of malachite green dye solution having initial concentration (25 mg/L to 150 mg/L) was prepared in a conical flask bottle containing 20 mL each. 0.015 g of the adsorbent was dispersed in the dye solution which is followed by agitation in a thermostatic shaker. The batches were shaken for a time period of 6 hour to achieve adsorption equilibrium. Furthermore, the resulting dye solution was filtered to separate the adsorbent and the filtrate was analyzed with

UV-vis spectrophotometer to evaluate malachite green concentration.

The amount of malachite green dye adsorbed on to the adsorbents is determined by the equation:

$$q_e = \frac{(C_0 - C_e)V}{W} \quad (1)$$

The percentage of malachite green dye removal efficiency.

$$\% \text{ of dye removal} = \frac{(C_0 - C_e) \times 100}{C_0} \quad (2)$$

where C_e and C_0 represents the equilibrium and initial concentration of malachite green dye solution in mg/L. q_e (mg/g) denotes the equilibrium adsorption capacity, W and V indicates quantity of adsorbent (g) and volume of the dye solution (L), respectively.

For conducting the kinetics experiments, 0.015 g of the adsorbents was mixed with 40 mL of malachite green dye solution having initial concentrations (50,100 mg/L). The dye solution is then subjected to agitation in a thermostatic shaker which is followed by withdrawal of 2 mL liquid suspension after a specific time interval. Subsequently, the amount of dye adsorbed over the adsorbent was analyzed for the reaction time period of 0 to 180 min. Again, the adsorbent was separated from the dye solution by filtration and its absorbance value was measured at the λ -max value (655 nm) of the pollutant. The adsorption capacity at time t is evaluated by the equation:

$$q_t = \frac{(C_0 - C_t)V}{W} \quad (3)$$

where C_0 and C_t are the concentrations of dye at initial and at time t .

However, for determining the most appropriate kinetic model that can describe the sorption process, the normalized standard deviation was evaluated by the equation [33]:

$$\Delta q = \sqrt{\frac{\sum [(q_{e, \text{exp}} - q_{e, \text{cal}})/q_{e, \text{exp}}]^2}{N - 1}} \quad (4)$$

where $q_{e, \text{cal}}$ is the equilibrium sorption capacity evaluated from pseudo-first order and pseudo-second order kinetic model, $q_{e, \text{exp}}$ is the experimental amount of adsorbate adsorbed at equilibrium, N is the number of data points.

2.2.1. Adsorption Isotherm

The adsorption isotherm is an important parameter for describing the adsorbate-adsorbent interaction. It interprets the distribution of solute molecules between solid-liquid interfaces, and it is also essential for the experimental designing of the adsorption application in industries. Several empirical models for adsorption isotherm were utilized to analyze the experimental data, and for identifying the most appropriate isotherm model. The most widely used adsorption isotherm models are especially Langmuir, Freundlich and Temkin. Based on the Langmuir model, it assumed a uniform and single layer adsorption of the molecules over the surface of the adsorbents [34]. The linear equation for the Langmuir model is represented as:

$$\frac{1}{q_e} = \frac{1}{K_1 q_m C_e} + \frac{1}{q_m}$$

where C_e denotes the equilibrium concentration of malachite green dye, q_m represents maximum monolayer adsorption capacity, K_1 signifies the Langmuir constant which indicates the affinity between adsorbate and adsorbent, q_e indicates quantity of dye adsorbed at equilibrium (mg/L).

The dimensionless separation factor for determining the feasibility of adsorption is given by the equation [35]:

$$R_L = \frac{1}{1 + K_1 C_0} \quad (6)$$

where C_0 and K_1 signifies initial concentration of malachite green dye

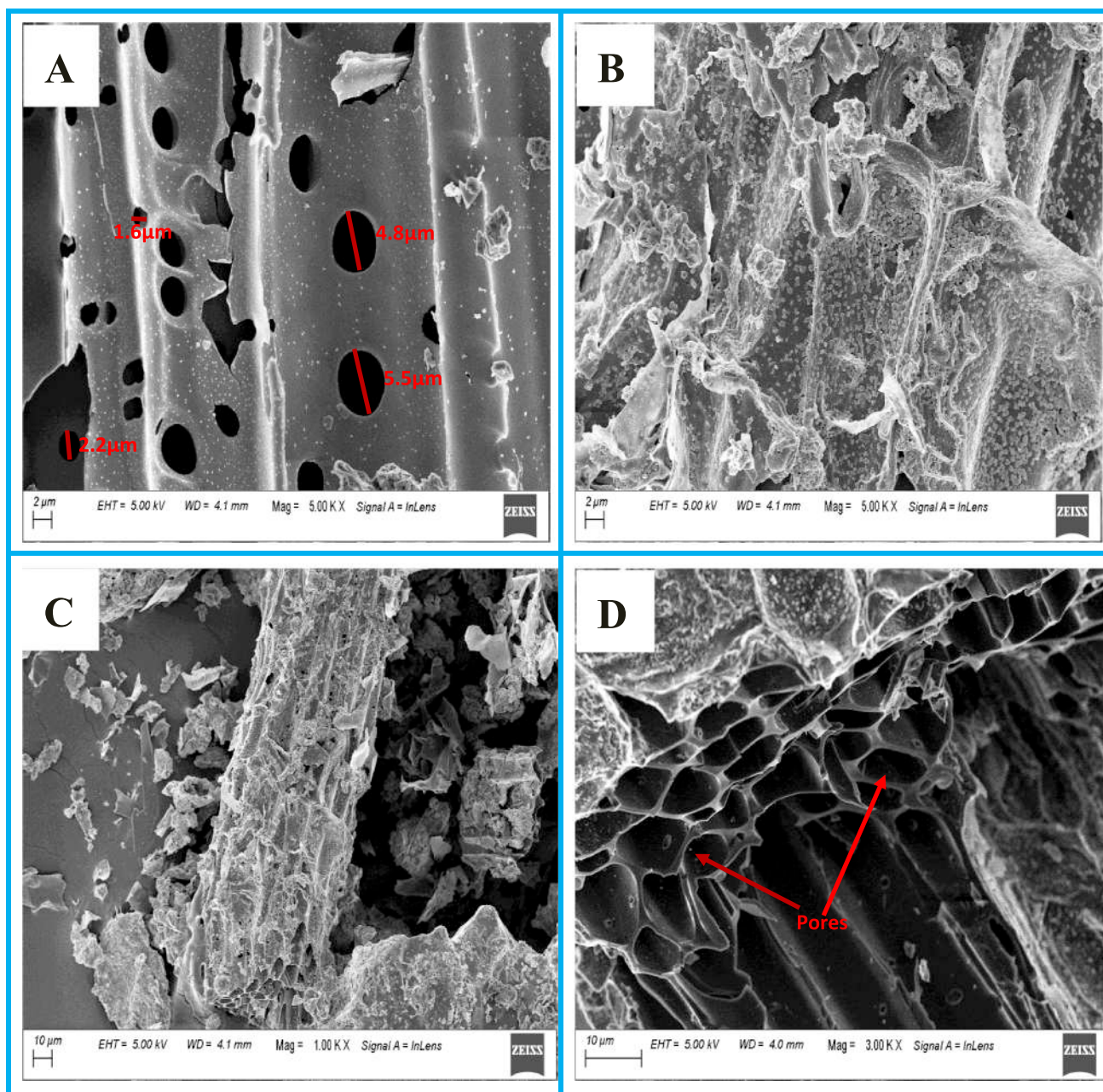


Fig. 3. SEM images of coconut husk ash (CHA).

and Langmuir constant, respectively.

2.2.2. Freundlich

The Freundlich model is a multilayer non uniform adsorption model which is found to be more appropriate with the heterogeneous surface of the adsorbents [36]. The linearized equation is denoted by:

$$\log q_e = \log K_f + 1/n \log C_e \quad (7)$$

where C_e and q_e have their usual meanings, n and K_f are Freundlich exponent and constant, respectively. The exponent n indicates the favorability or the intensity of the adsorption process while K_f reveals the adsorption capacity.

2.2.3. Temkin

According to Temkin model, it considers that the adsorption heat of all the incoming adsorbate molecules decreases linearly with the in-

crease in the coverage of the adsorption site on to adsorbent surfaces. The nature of adsorption system is characterized by the uniform arrangement of binding energy until certain maximum value [37]. The linear form of Temkin equation is described by:

$$q_e = B_T \ln A_T + B_T \ln C_e \quad (8)$$

where $B_T = \frac{RT}{b_T}$, B_T is related to the heat of adsorption (KJ/mol) and A_T is the binding constant with respect to the maximum binding energy (L/mg), T is the temperature in Kelvin, R is the universal gas constant (8.314 J/mol.K).

2.2.4. Adsorption Kinetics

The time dependent adsorption rate and the transfer characteristic of adsorbate molecules in the adsorption system can be well understood from the kinetics studies. As a result, the kinetic parameters are very important for the evaluating the adsorbent performances, and also the

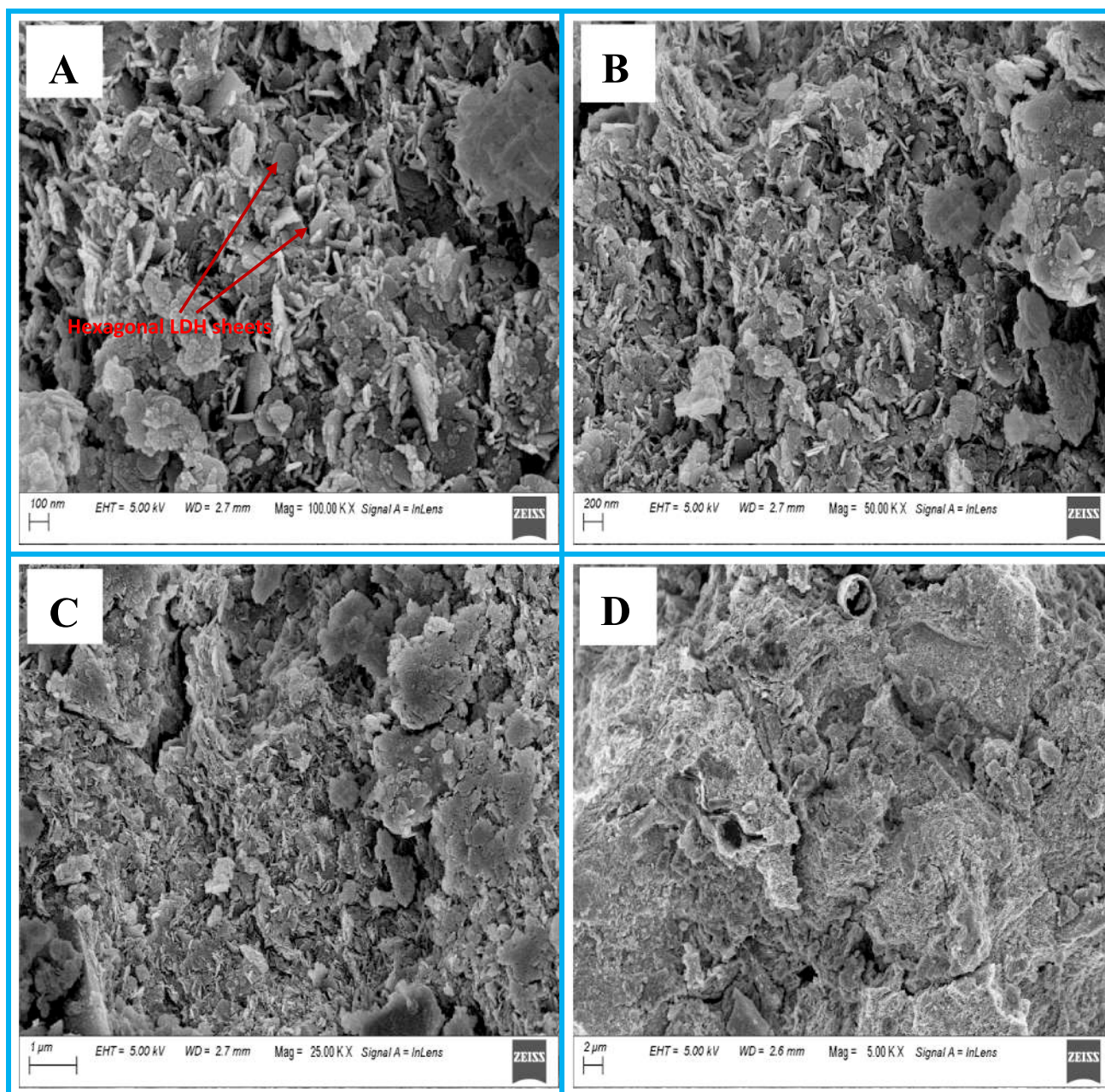


Fig. 4. SEM images of CHA/CoAl-LDH composite.

mechanism associated during the reaction process. The different kinetics model employed for evaluating the kinetic parameters are pseudo first order, pseudo second order, intraparticle diffusion, Bangham and Elovich model. According to pseudo first order model, the rate of adsorption is directly proportional to the ratio of the concentration of solutes and the amount of adsorbent [38]. The linear form of pseudo first order equation is formulated as:

$$\log(q_e - q_t) = \log q_e - \frac{K_1 t}{2.303} \quad (9)$$

where q_t and q_e are the quantity of dye adsorbed at time t and at equilibrium stage respectively. The values of the rate constant K_1 can be evaluated from the slope of the $\log(q_e - q_t)$ vs t plot. On the contrary, pseudo second model is based on chemisorption where exchange of electrons between adsorbate and adsorbent molecules occurs [39]. The linearised equation for pseudo second order is given as:

$$\frac{t}{q_t} = \frac{1}{K_2 q_e^2} + \frac{t}{q_e} \quad (10)$$

where K_2 is the pseudo second order rate constant and its value is calculated from the intercept of the plot (t/q_t vs t).

Another model proposed by Weber-Morris is the intraparticle diffusion model, which assumes that the diffusion of adsorbed molecules inside the pores of the adsorbent can also contribute in the rate determining step of the adsorption process [40]. The equation for the intraparticle diffusion model is given by:

$$q_t = K_i t^{0.5} + I \quad (11)$$

where K_i and I are the intraparticle diffusion constant and boundary layer thickness, respectively. The values of K_i and I can be determined from the slope and intercept of q_t against $t^{0.5}$ plot.

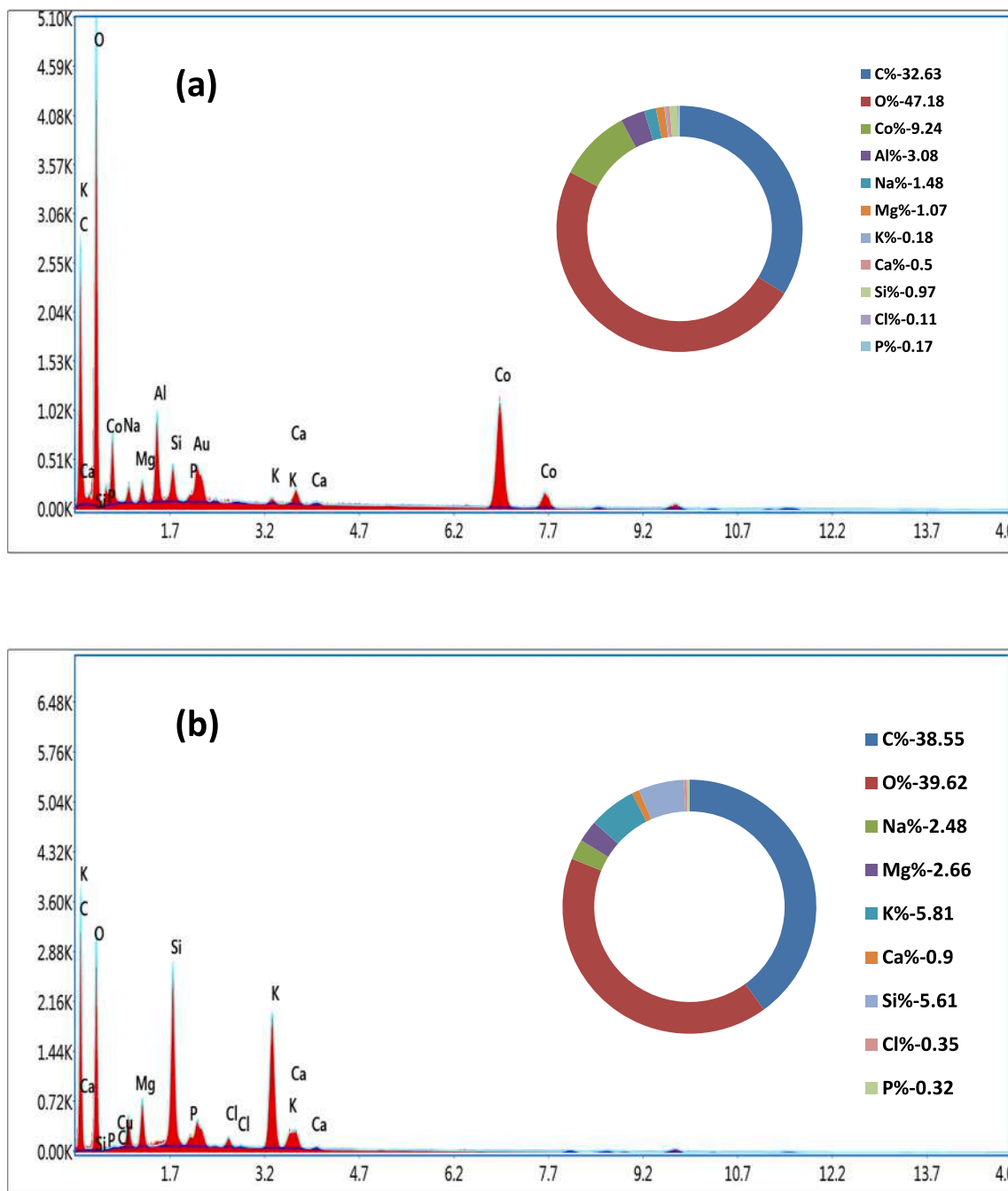


Fig. 5. EDX spectra of (a) CHA/CoAl-LDH composite and (b) CHA.

Table 1

The elemental composition of the proposed adsorbents CHA and CHA/CoAl-LDH.

Adsorbent	Elemental Composition										
	C%	O%	Co%	Al%	Na%	Mg%	K%	Ca%	Si%	Cl%	P%
CHA	38.55	39.62	–	–	2.48	2.66	5.81	0.90	5.61	0.35	0.32
CHA/CoAl-LDH	32.63	47.18	9.24	3.08	1.48	1.07	0.18	0.50	0.97	0.11	0.17

2.2.5. Elovich model

To elaborate the chemisorption nature of the adsorption system, Elovich model was applied to the experimental kinetics data, and with the help of this model the activation and deactivation energy of the system can be estimated. Initially, it was utilized only in gaseous system, later on its application in the solid–liquid system was also considered

valid [41]. The linearised form of Elovich equation is represented as:

$$q_t = \frac{1}{\beta} \ln(\alpha\beta) + \frac{1}{\beta} \ln(t) \quad (12)$$

where q_t is the amount of malachite green dye adsorbed on CHA and

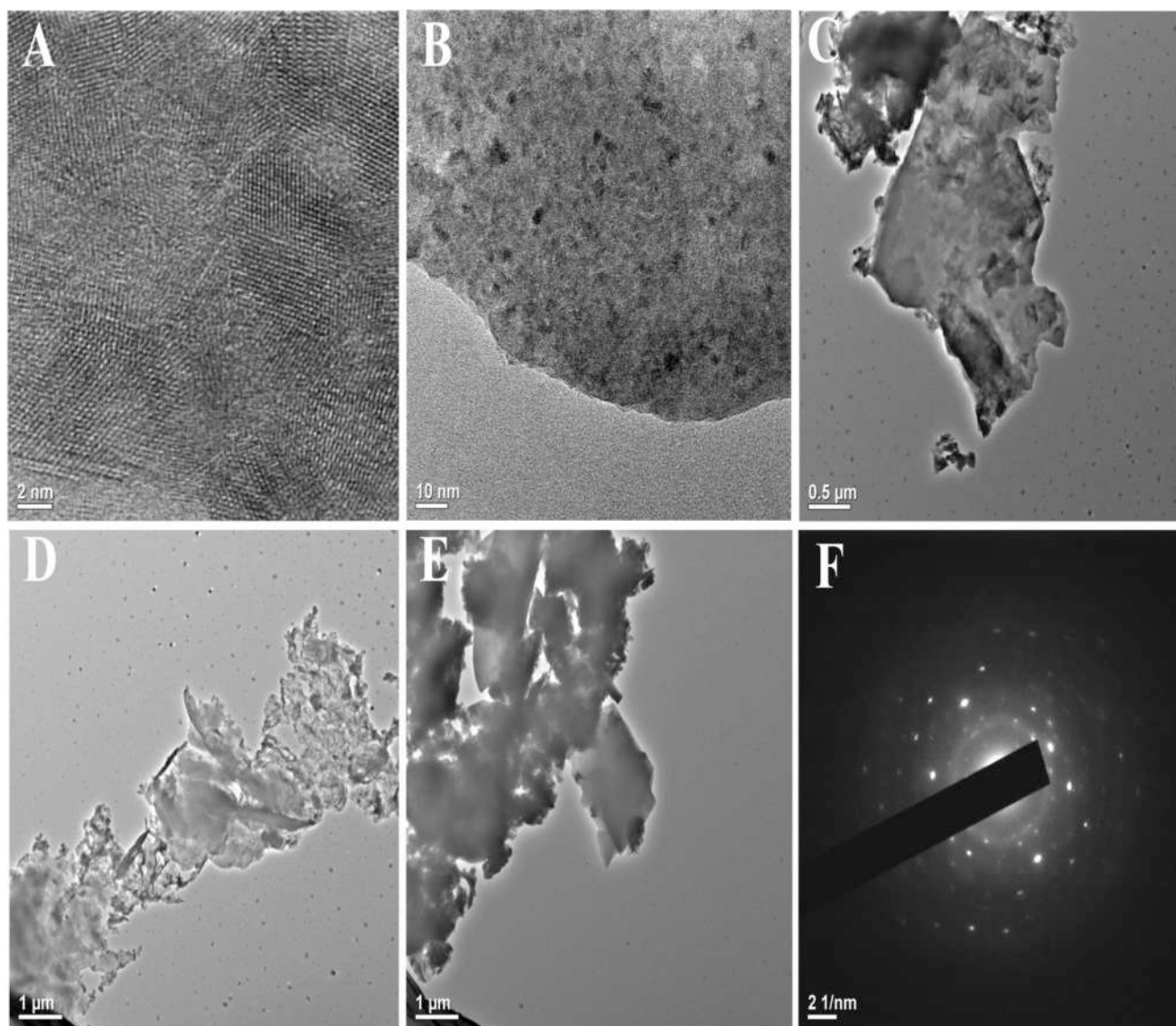


Fig. 6. TEM images of coconut husk ash (CHA) at different magnifications (A-E) and SAED pattern (F).

CHA/LDH nanocomposite at time t , β indicates the extent of surface coverage (g/mg), α denotes the initial sorption rate (mg/g.min). The magnitude of slope and intercepts obtained from the q_t vs $\ln(t)$ plot was used for the determination of α and β values.

2.2.6. Bangham model

The Bangham kinetic model also known as pore diffusion model explores the influence of pore diffusions in adsorption kinetic system. To corroborate the existence of pore diffusion, the obtained kinetics data was further analyzed by Bangham model [42]. The mathematical expression of Bangham equation is given as:

$$\log\left[\log\left(\frac{C_0}{C_0 - m q_t}\right)\right] = \log\left(\frac{K_B m}{2.303 V}\right) + \Delta B \log t \quad (13)$$

where m is the mass of the adsorbent (g), q_t is the quantity of dye adsorbed at time t , V indicates volume of the solution (mL), C_0 represents initial dye concentration, K_B and ΔB are Bangham constants.

3. Results and Discussion

3.1. Characterisation of CHA and CHA/CoAl-LDH composite

The XRD pattern of the CHA and CHA/CoAl-LDH composite was illustrated in Fig. 1. The diffraction spectrum of CHA/CoAl-LDH composite displayed characteristic peaks of pristine LDH, which is observed at the 2θ values of 11.35, 23.32, 34.28, 38.88, 46.33, 60.04 and 61.38. Moreover, the indexed plane corresponding to each observed peaks were 003, 006, 012, 015, 018, 110 and 113, respectively. The obtained result is consistent with the formation of typical LDH structure, which is based on the previous report [43]. In addition, the peak observed in CHA at corresponding 2θ values (26.51, 38.29, 39.14, 41.29 and 58.58) was also manifested in CHA/CoAl-LDH composite, which further implies the association of carbonaceous material derived from coconut husk on to LDH structure. The appearance of sharp and intense peaks corroborates with the well defined crystalline nature of the synthesized sample. However, the peak intensity in CHA/CoAl-LDH composite was decreased slightly in comparison to pristine CoAl-LDH, which might be due to the accumulation of coconut husk carbon over the crystallographic structure of LDH [44]. The lattice parameter a and c of the LDH present in composite material was evaluated by the expression $a = 2d_{110}$

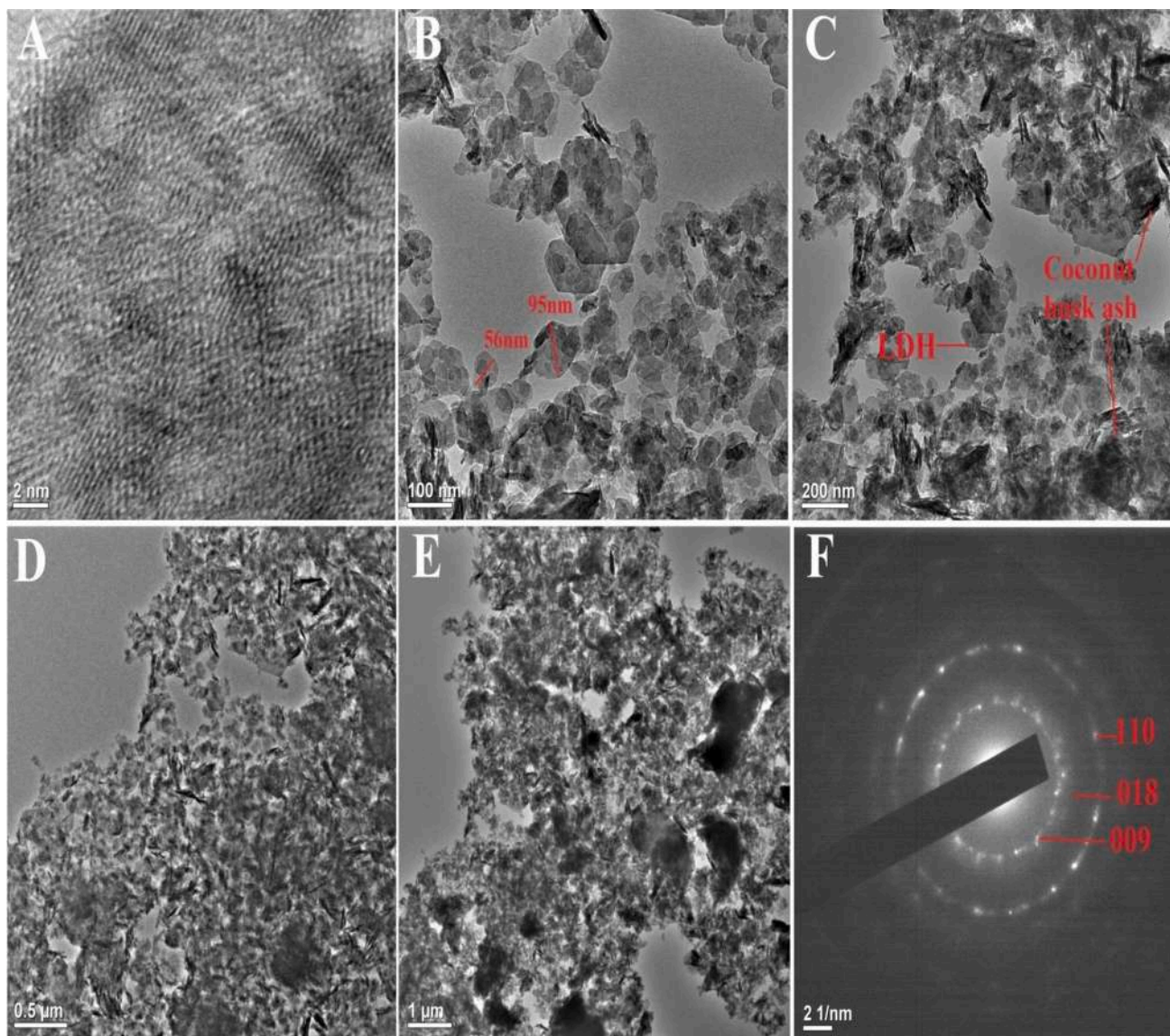


Fig. 7. TEM images of CHA/CoAl-LDH composites (A-E) and SAED pattern (F).

and $c = 3d_{003}$, respectively. However, the determined value ($a = 3 \text{ \AA}$, $c = 23.4 \text{ \AA}$) was found almost similar to the pristine LDH. Moreover, the d-spacing value of 0.28 nm , obtained from the 003 plane indicates the interlayer distance of LDH sheet which is not disrupted after modification with CHA material [45].

The surface functionalities of the two adsorbents viz; CHA and CHA/CoAl-LDH composites were elucidated by recording the FTIR spectra, as shown in Fig. 2. The respective functional groups present in CHA adsorbent (Fig. 2a) were observed at the stretching frequency of 3443 cm^{-1} (–OH), 1631 cm^{-1} (C=C stretch in aromatic ring), 1591 cm^{-1} (conjugated C–O group of aromatic skeletal), 1466.73 cm^{-1} (C–H bond), 1143 cm^{-1} (C–O stretching vibration of ether, phenol, ester) and 2920 cm^{-1} (C–H bond stretch) [46]. After modification, in CHA/CoAl-LDH composite (Fig. 2c), the absorption peak observed at 3450 cm^{-1} can be attributed to –OH group, while the weak band at 2923 and 2848 cm^{-1} were related to the C–H stretching vibration. Another band detected at 1637 cm^{-1} is also assigned due to –OH bending vibration. The stretching vibration of C–O bond and $-\text{NO}_3^-$ ion was also visible around 1593 and 1404.81 cm^{-1} , respectively. Moreover, the presence of M–O stretching vibration was displayed between 500 and 800 cm^{-1} . After analysis of FTIR spectrum the overall results confirmed the presences of C=C, C–O,

C–H, OH and other chemical groups over the surface of CHA adsorbents. However, few functional groups were not observed in CHA/CoAl-LDH composite, which indicates the destruction in surface functional groups during the synthesis of composite material [47,48].

The external surface morphology and the particle size of the sample CHA and CHA/CoAl-LDH composite were examined by SEM analysis. Fig. 3 and Fig. 4 illustrates the SEM images of CHA and fabricated CHA/CoAl-LDH composite. The micrograph of CHA depicted presences of porous structure with pore diameter lying in the range of $1 \text{ }\mu\text{m}$ to $10 \text{ }\mu\text{m}$. This porous nature facilitates in trapping the incoming malachite green dye molecules during the adsorption process. However, existences of micropore and mesopore were not visible which lie covered within the macropores. Furthermore, after fabrication of CHA with LDH, it is evident that the hexagonal platelets of LDH sheets get highly distributed over the surface of coconut husk carbon particles. Nevertheless, the relative number of macropores was also found to decrease in the composite material which may be due to the deposition of nanosized hexagonal shape LDH particles over the outer surface of coconut husk ash. The surface of CHA/CoAl-LDH composite (Fig. 4) also revealed irregular shape and the typical crystalline hexagonal CoAl nanoparticles was successfully assembled on the carbon matrix [30].

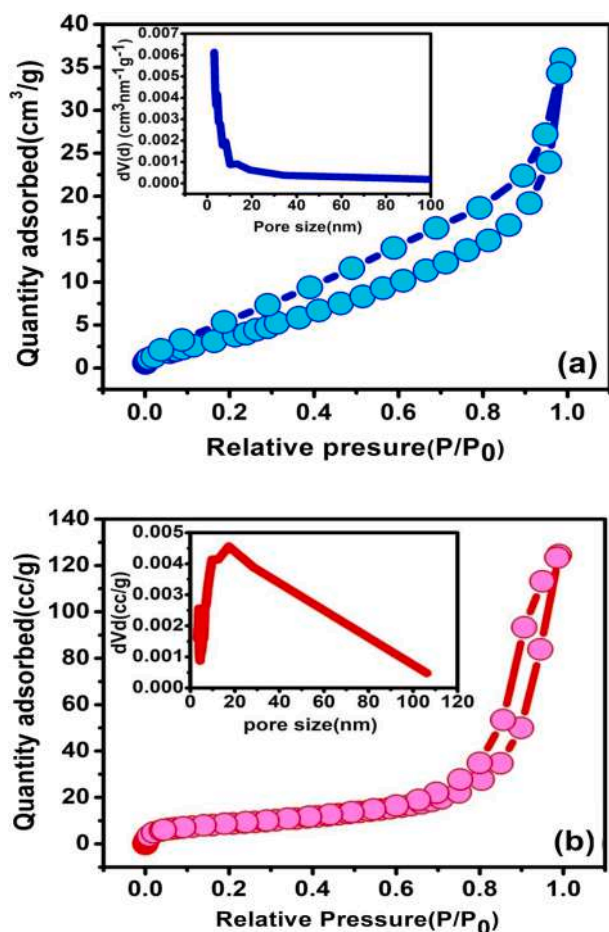


Fig. 8. N_2 adsorption-desorption isotherm and pore sized distribution of (a) CHA and (b) CHA/CoAl-LDH composite.

The EDX analysis of the two adsorbents CHA and CHA/CoAl-LDH composite was executed to determine the chemical composition, and to confirm the successful formation of composite materials between CoAl-LDH and CHA. Fig. 5(a) shows the EDX spectra of CHA, indicating the presences of high intense peak corresponding to C(38.55 %) and O (39.62 %) having greater weight % value compare to other existing elements such as Si, K, Na, Mg, P, Ca and Cl (Table 1). After fabrication of coconut husk ash with LDH, the EDX spectra (Fig. 5b) of the composite material CHA/CoAl-LDH also revealed detection of all the constituent elements present in the sample CHA in addition to Co and Al. Therefore, it confirmed the formation of composite material containing both LDH phase and carbon material derived from CHA. However, the weight percentage of all the elements including C slightly decreased in CHA/CoAl-LDH composite material, due to the incorporation of LDH phase. In addition, the high C and O content in both CHA and CHA/CoAl-LDH composite infers the presences of acidic O containing functional groups such as -R-OH, -OH, -C-OR and C=C. Overall, the EDX results affirmed the greater quantity of carbonaceous material exists in the composite material compare to LDH phase [49].

The size, shape and internal morphology of the as-synthesized sample were visualized by TEM analysis. TEM micrographs of the adsorbent at different resolution were depicted in Fig. 6 and Fig. 7, respectively. From Fig. 7 the structure of CHA/CoAl-LDH composite also displayed aggregation of LDH particles with an average size below 100 nm, as already confirmed from SEM analysis. The heterogeneous structure of CHA/CoAl-LDH observed in Fig. 7-(B,C) shows that CoAl platelets was not suppressed, which further infers that the layered structure remains unaltered. However, the increasing content of coconut husk ash could

lead to the significant reduction in crystallinity of the sample. The relatively darker region spotted in Fig. 7-(C, E) can be attributed to the carbon material derived from CHA. In addition, the TEM images in Fig. 6-(C, D, E) also manifests the development of porous nature of CHA adsorbents. The selected area electron diffraction (SAED) pattern observed in Fig. 6 (F) and Fig. 7(F), further corroborates with the polycrystallinity of the as-synthesized sorbents [50].

The surface properties including specific surface area, pore volume and pore size of the adsorbents CHA and CHA/CoAl-LDH composite were investigated by BET method. The porosity and specific surface area of the material is an important structural feature that can delineate characteristic information about the sorption capacity. In several cases, it was reported that an adsorbent with high specific surface area is highly preferable over low surface area due to its ability for a greater sorption capacity for organic and inorganic pollutants [51]. The N_2 adsorption-desorption isotherm curve of CHA and CHA/CoAl-LDH composite is depicted in Fig. 8(a,b). The insets of Fig. 8(a,b) represents the pore size distribution based on the BJH method analysis. The specific surface area and pore volume of CHA (20.71 m^2/g , 0.051 cc/g) was relatively lower than CHA/CoAl-LDH composite (49.52 m^2/g , 0.202 cc/g). Despite its lower value of specific surface area and pore volume, the sorption capacity of CHA was better and showed greater q_{max} value than CHA/CoAl-LDH composite. Thus, in the present studies the specific surface area of the adsorbents cannot be directly correlated in terms of adsorption capacity. Furthermore, in case of CHA (Fig. 8(a)) the hysteresis loop is generated quickly at low relative pressure (0.127) while for CHA/CoAl-LDH composite it initiates from higher relative pressure value (0.8). Again, from the pore size distribution curve, it is evident that porosity inside CHA adsorbent is mainly composed of mesopores which is mainly distributed between 4.01 nm and 10.17 nm. Similarly, in CHA/CoAl-LDH composite, the mesopores dominate over micropores and the pore size lies in the range (3.88 nm to 18.32 nm). Thus, the existences of mesopores can be advantageous for adsorption of small molecules. However, the adsorption-desorption isotherm curves of both adsorbents can be categorized under type-IV isotherm and hysteresis loop exhibits type-III based on IUPAC classification [52,53].

3.2. Effect of adsorption parameters

3.2.1. Effect of contact time

Fig. 9(a) demonstrates the effect of contact time in the adsorption of malachite green dye on to CHA and CHA/CoAl-LDH composite. The influence of contact time on the adsorption capacity of the proposed adsorbent was studied under the initial dye concentration (50, 100 mg/L) and adsorbent dosages (0.015 g). Several noteworthy results can be seen in Fig. 9(a) in which q_t value increases with the extension of adsorption time. At the initial stage of contact time up to 15 min the rapid adsorption rate was noticed for both adsorbent which can be ascribed to the large number of freely available adsorption sites [54]. The bending of curve between (15–60 min) could be ascertained due to the diffusion of solute molecules inside the internal pores of the adsorbent. Subsequently, the adsorption rate slowed down due to decrease in active site and attained equilibrium stage after 165 min, where the complete coverage of the adsorption site was achieved [55]. Notably, for the studied initial adsorbate concentration (50, 100 mg/L), the maximum quantity of dye adsorbed (q_t) at 180 min for CHA and CHA/CoAl-LDH composite were 131.38, 258.21, 115.34 and 235.09 mg/g , respectively. Since, adsorption occurred over the surface, during the process when the complete saturation of the adsorption site was attained, the steric hindrance between the incoming dye molecules and the initially adsorbed dye arises which leads to the restriction of further dye intake. In addition, it was observed that at the fixed adsorbent dosages the adsorption capacity of adsorbent decreased with the increase in the molar mass of the solute molecules [56].

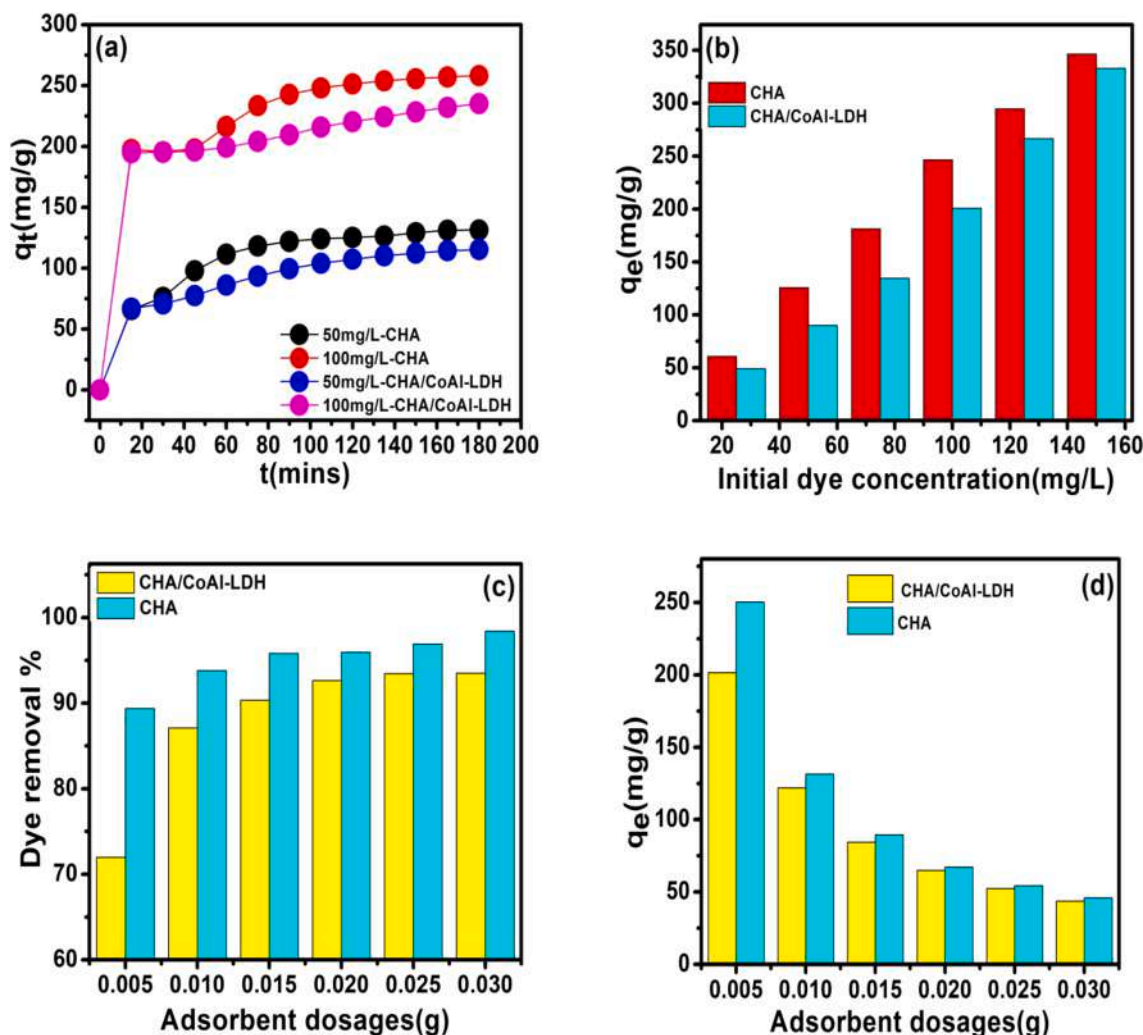


Fig. 9. Effect of various parameters for adsorption of MG dye over CHA and CHA/CoAl-LDH composite (a) Contact time ($C_0 = 50, 100$ mg/L, adsorbent dosages = 0.015 g, time = 180 min, volume = 40 mL) (b) Initial dye concentration ($C_0 = 25\text{--}150$ mg/L, adsorbent dosages = 0.015 g, time = 120 min, volume = 40 mL) (c) and (d) Adsorbent dosages ($C_0 = 70$ mg/L, time = 180 min, volume = 20 mL).

3.2.2. Effect of initial dye concentration

The effect of initial dye concentration on the adsorption capacity of CHA and CHA/CoAl-LDH composites was plotted and presented in Fig. 9 (b). The experiment was performed under the given operating condition: ($C_0 = 25\text{--}150$ mg/L, dosages = 0.015 g, time = 120 min, volume = 40 mL). It is obvious that the equilibrium adsorption capacity increased linearly for both CHA ($q_e = 60.77$ to 346.36 mg/L) and CHA/CoAl-LDH composite ($q_e = 49.12$ to 332.89 mg/L) with the increase in the initial dye concentration. In general, at constant adsorbent dosages with the increase in dye concentration, the diffusion of solute molecules in the solution also increases. Consequently, the physical contact of dye molecule with the adsorbent surface occurs significantly which can make the adsorption process more favorable. Moreover, the creation of a large concentration gradient in the adsorption site could help to overcome the mass transfer resistance of the dye molecules in the solid liquid interfaces. As a result, the adsorbent reveals greater capacity to capture dye molecules at high concentrations [57].

3.2.3. Effect of adsorbent dosages

The quantity of adsorbent dosages added in the dye solution can affect the adsorption process. To evaluate the effect of adsorbent dosages for the removal of malachite green dye, the amount of adsorbent was varied from 0.005 to 0.03 g for both CHA and CHA/CoAl-LDH composite sorbents. The experimental condition was fixed at initial dye

concentration (C_0) = 70 mg/L, volume = 20 mL and contact time = 180 min. In Fig. 9(c) it is noteworthy that the percentage of dye removal increases rapidly at the adsorbent dosages of 0.005 g to 0.015 g for both adsorbent which then slowly elevates further from 0.02 to 0.03 g. The greater percentage of dye adsorption with the increase in quantity of adsorbent can be attributed to the larger adsorption sites and also due to the stronger driving force [58]. However, in Fig. 9(c) it is apparent that there is no significant change observed in the dye removal percentage beyond 0.025 g dosages. Moreover, the equilibrium adsorption capacity q_e (mg/g) in Fig. 9(d) decreases from 250.32 to 45.92 mg/g for coconut husk ash (CHA), whereas in CHA/CoAl-LDH composite q_e (mg/g) value get reduced from 201.56 to 43.64 mg/g with the rise in adsorbent dosages. Nevertheless, the excessive use of adsorbent beyond the optimum dosages can cause accumulation of adsorbent particles due to the collision which can further hinder the adsorption of incoming dye molecule. In addition, the maximum dye percentage for CHA (98.39 %) and CHA/CoAl-LDH (93.52 %) was achieved at 0.03 g dosages [59].

3.2.4. Effect of pH

The pH value of the aqueous solution is an essential factor to be accounted that can influence the adsorption of malachite green dye. The dye removal % of malachite green was investigated in the pH range of 3–10 at 100 mg/L MG concentration and 0.015 g adsorbent dosages. The pH of the solution can change the binding site of the adsorbent as well as

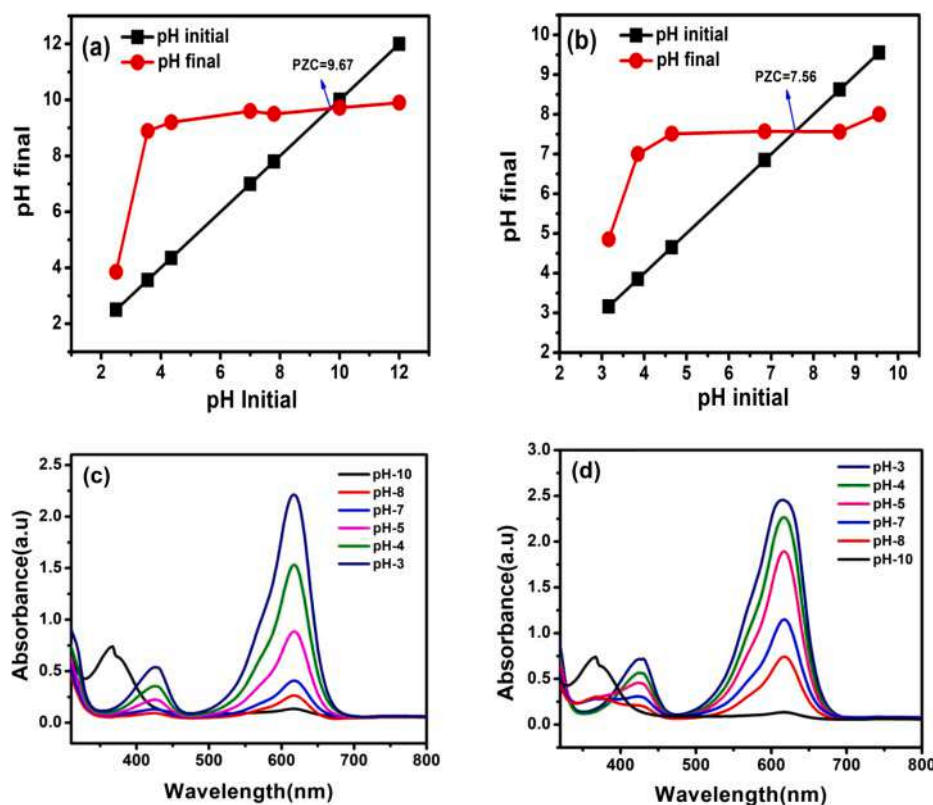


Fig. 10. Determination of the point of zero charge (PZC) value of CHA (a) and CHA/CoAl-LDH composite (b) from pH initial vs pH final plot. Uv-Visible Spectra for the adsorption of MG dye on to CHA (c) and CHA/CoAl-LDH (d) adsorbents at different solution pH.

the degree of ionization of the adsorbate molecule [60]. The point of zero charge value (PZC) of CHA and CHA/CoAl-LDH was determined by pH drift method and their respective values were obtained at 9.67 and 7.56, as displayed in Fig. 10 (a,b). In general, it is believed that at $\text{pH} > \text{PZC}$, the surface charge of the adsorbent becomes negative while for $\text{pH} < \text{PZC}$, it acquires +ve charge. Under acidic medium at low pH, the H^+ ion get accumulated over the surface and impart additional positive charge on the adsorbent which causes repulsion to the cationic MG dye. Therefore, it leads to the decreased % in dye uptake. However, at higher pH under alkaline medium, dye removal % increases due to deprotonation of the surface group [61]. Fig. 10 (c,d) depicted the decrease in absorbance intensity after the adsorption of MG dye on to CHA and CHA/CoAl-LDH when the pH value increases from 3 to 10. In CHA, the sorption efficiency increased rapidly from 77.94 to 90.83 % up to pH 5, while above pH7 the sorption % elevates slowly from 95.38 % to 98.39 % as shown in Fig. 11(a). Similarly, the uptake of MG dye by CHA/LDH composite also rises with the pH value ranging from (3–10) and attained maximum adsorption of 98.16 % at pH 10, towards the end of the experiment. Thus, the obtained results indicates that the variation in the pH values significantly affects the adsorption of MG dye due to altered charged from +ve to -ve over surface.

3.2.5. Adsorption efficiency for various organic dyes

The removal efficiency of various organic dyes on to CHA and CHA/CoAl-LDH composite was examined. Fig. 11(b). clearly shows that the cationic dyes methylene blue (MB) (91.4 %) and malachite green (MG) (99.39 %) were more effectively adsorbed over CHA adsorbent than anionic dye congo red (CR) (35.45). However, in CHA/CoAl-LDH composite, both cationic (MG, MB) and anionic (CR) dyes are retained with the respective adsorption percentage of 91.4, 66.15 and 92 %. The lower affinity for anionic (CR) in CHA adsorbent is due to the resistance offered by negatively charged functional groups ($-\text{COO}^-$, COOR , OH^-) present in the adsorbent surface. On the contrary, despite having

negatively charged functional sites, the existing positively charge LDH sheets and surface hydroxyl OH^- in CHA/CoAl-LDH composites makes it a suitable candidate for adsorption of both cationic and anionic dyes. Anionic dyes (CR) can be easily retained in CHA/CoAl-LDH composite due to the electrostatic forces and H-bonding, whereas the adsorption of cationic dyes is also attributed due to the presences of oppositely charged attraction between CHA/CoAl-LDH and dye molecules [62]. Although CHA reveal high adsorption capacity for cationic dyes while its affinity for anionic dyes was found relatively lower than CHA/CoAl-LDH composites.

3.3. Effect of Temperature

Thermodynamic studies were relevant to elucidate the spontaneity, adsorption mechanism, nature of adsorption and heterogeneity of the adsorbent surface. For the in depth information about the effect of temperature in adsorption process, the adsorption reaction was carried out at three different temperature (303 K, 313 K, 323 K) for the initial dye concentration of 50 mg/L, with 0.015 g dosages and a contact time of 120 min. The thermodynamic nature in the present adsorbate-adsorbent system was interpreted by evaluating various thermodynamic parameters such as Gibbs free energy (ΔG), enthalpy (ΔH) and entropy (ΔS) with the following equations [63,64]:

$$\Delta G = -RT \ln K_d \quad (14)$$

$$\ln K_d = \frac{\Delta S}{R} - \frac{\Delta H}{RT} \quad (15)$$

where ΔG refers to Gibbs free energy, $K_d = (q_e/C_e)$ indicates adsorption distribution coefficient, T is the temperature in Kelvin and R denotes universal gas constant. Based on the malachite green adsorption data which is obtained from the thermodynamic studies, the Vant-Hoff plot i. e. the linear plot of $\ln K_d$ vs $1/T$ was obtained. The values of the enthalpy

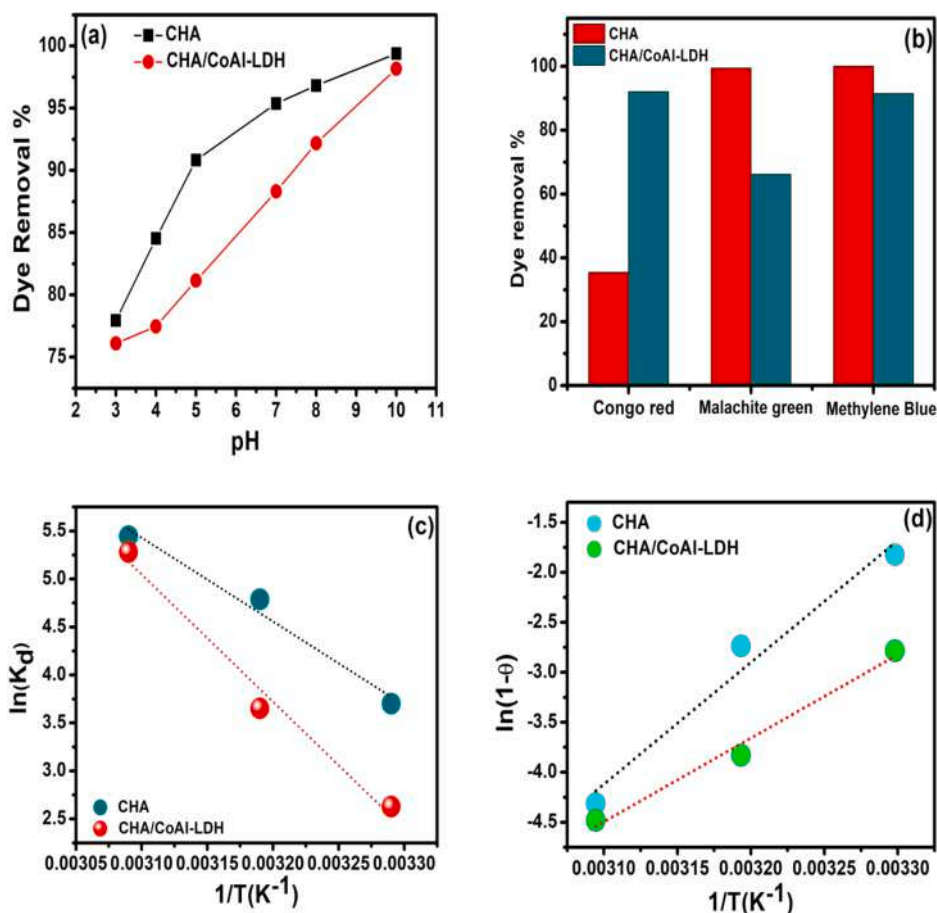


Fig. 11. (a) Effect of pH on the removal percentage of MG dye ($C_0 = 100$ mg/L, contact time = 120 min, dosages = 0.015 g). (b) Adsorption efficiency over various organic dyes ($C_0 = 20$ mg/L, dosages = 0.02 g, contact time = 24 hrs). (c) Vant-Hoff plot and (d) Modified Arrhenius plot for the adsorption of MG dye on to CHA and CHA/CoAl-LDH.

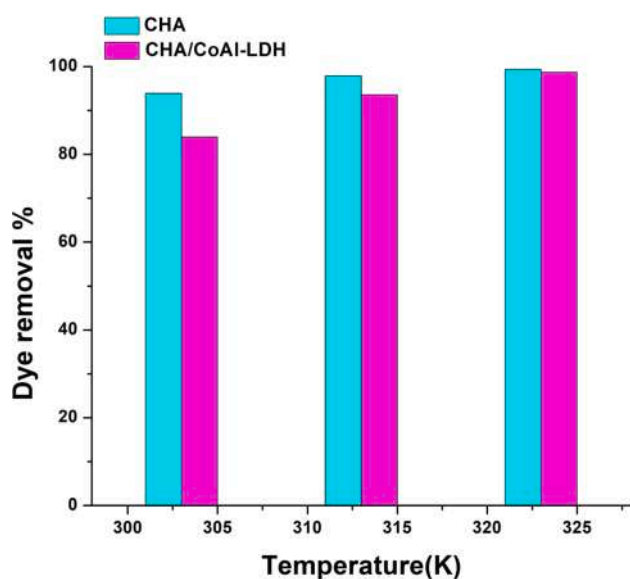


Fig. 12. Effect of temperature on the removal percentage of MG dye on to CHA and CHA/CoAl-LDH. ($C_0 = 150$ mg/L, contact time = 90 min, dosages = 0.015 g, volume = 40 mL).

ΔH and entropy ΔS were calculated from the slope and intercept of the plot as shown in Fig. 11 (c). Table 4 summarizes the determined values of various thermodynamic parameters during sorption experiment. It is apparent that ΔG values decrease as the temperature increases from 303 K to 323 K in both cases which further implies the feasibility and spontaneity of adsorption process. The positive values of enthalpy change ΔH for malachite green adsorption over CHA (72.49 KJ/mol) and CHA/CoAl-LDH composite (110.24 KJ/mol) indicates the endothermic nature of adsorption. Again, the entropy change ΔS indicates the randomness of solute molecules in the solid-liquid interface. It is obvious that the greater +ve value of ΔH in case of CHA/CoAl-LDH composite revealed increased randomness in CHA/CoAl-LDH-MG interface thereby reflecting its affinity for the dye molecules. Moreover, the obtained result shows that the adsorbent CHA has relatively higher adsorption capacity than CHA/CoAl-LDH composite. In addition, the adsorption has been found to be favored at higher temperature which confirms more feasibility at 323 K.

To further elucidate the dominance of either chemisorption or physisorption as the most appropriate adsorption mechanism, thermodynamic parameters such as activation energy (E_a) and sticking probability (S^*) were evaluated by applying the experimental data in the modified Arrhenius equation related to surface coverage (θ). The modified Arrhenius equation is presented by the following equations [65]:

$$S^* = (1 - \theta)e^{-E_a/RT} \quad (16)$$

$$\theta = \left(1 - \frac{C_e}{C_0}\right) \quad (17)$$

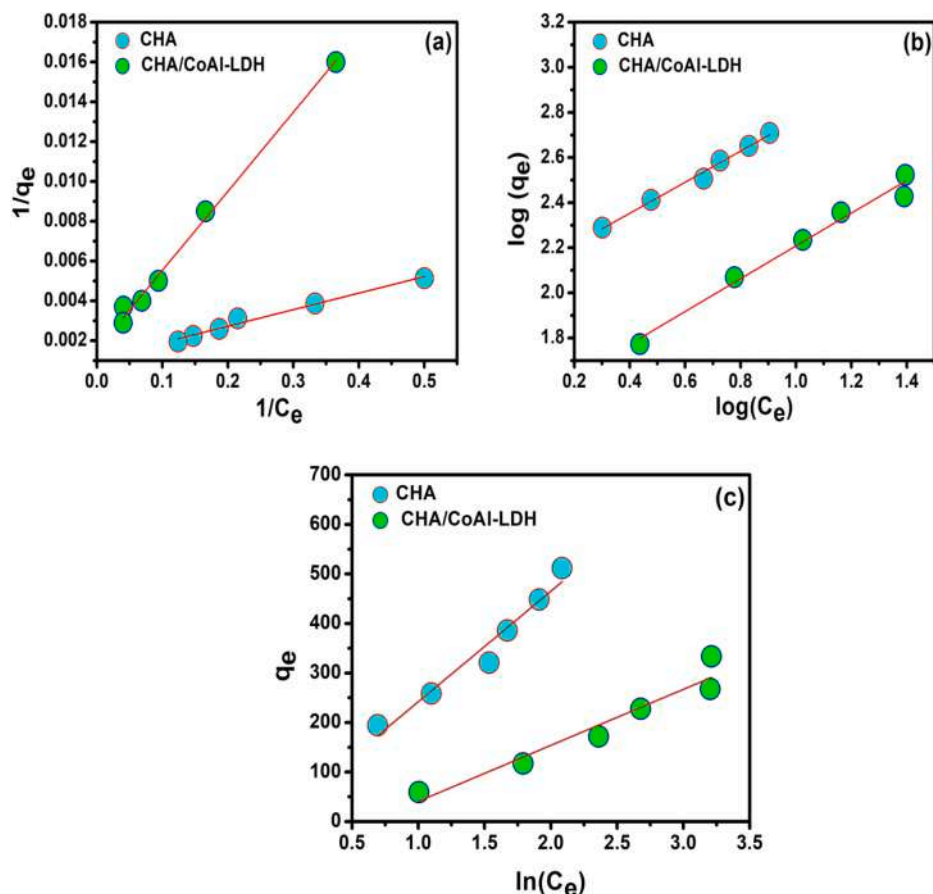


Fig. 13. The linear plot of different isotherm models namely Langmuir (a) Freundlich (b) Temkin (c) for the adsorption of MG dye on to CHA and CHA/CoAl-LDH composite.

Table 2

Langmuir, Freundlich and Temkin isotherm parameters for the adsorption of MG dye on to CHA and CHA/CoAl-LDH composite.

Adsorbent	Langmuir			Freundlich			Temkin		
	q_{max} mg/g	K_l L/mg	R^2	K_f (mg/g) (L/mg) ^{1/n}	n	R^2	B_T	A_T	R^2
CHA	943.39	0.12755	0.981	119.53	1.452	0.966	223.30	1.087	0.947
CHA/CoAl-LDH	666.65	0.03772	0.993	30.25	1.374	0.976	113.12	0.527	0.917

$$\ln S^* = \ln(1 - \theta) - \frac{E_a}{RT} \quad (18)$$

$$\ln(1 - \theta) = \ln S^* + \frac{E_a}{RT} \quad (19)$$

where θ indicates surface coverage, E_a (KJ/mol) denotes activation energy, S^* represents the sticking probability, which is a temperature dependent parameter and its magnitude lies between (0–1) for a preferable process. C_0 and C_e are the concentration of adsorbate at initial and at equilibrium, respectively.

The graphical representation of $\ln(1-\theta)$ vs $1/T$ is displayed in Fig. 11 (d). The activation energy E_a and sticking probability (S^*) were calculated from the slope and intercept of the plot (Fig. 11 d). In Table 4, it is clearly seen that the activation energy (E_a) of CHA and CHA/CoAl-LDH composite in malachite green adsorption were 101.35 and 69.50 KJ/mol, respectively. In general, the chemisorption process requires more energy, as a result it is associated with high activation energy (E_a)

(40–800 KJ/mol). On the contrary, the relatively lower activation energy (E_a) below 40 KJ/mol is involved in physisorption process. Since, the magnitude of E_a ranges between 40–800 KJ/mol for both adsorbents, therefore, it further corroborates chemisorption, possessing higher potential energy barrier as the most suitable mechanism during the sorption process [66].

The influence of temperature on the removal efficiency of MG onto CHA and CHA/CoAl-LDH was illustrated in Fig. 12. It was observed that as the temperature elevates from 303 K to 323 K, both CHA and CHA/CoAl-LDH showed increased in dye removal %. This ensures with the endothermic properties of the adsorption process. Moreover, the obtained results in thermodynamic studies also validate the suitability of the present adsorbents to be applied at high temperature reaction conditions.

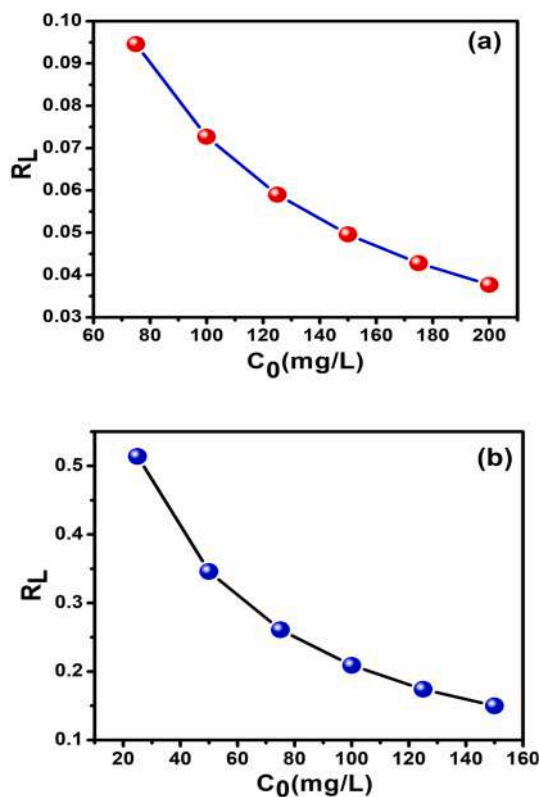


Fig. 14. R_L vs C_0 plot of (a) CHA and (b) CHA/CoAl-LDH composite.

Table 3

Parameters of pseudo first order, pseudo second order, intraparticle diffusion, Elovich model and Bangham model for the adsorptive removal of MG dye by CHA and CHA/CoAl-LDH adsorbent.

Kinetics model	Parameters	CHA/CoAl-LDH			
		CHA	CoAl-LDH	CHA/CoAl-LDH	CHA/CoAl-LDH
Pseudo-first order	q_e (exp)	50 mg/L	100 mg/L	50 mg/L	100 mg/L
		133.33	266.65	128	253.32
	q_{e1} (mg/g)	90.03	102.72	75.04	77.76
	$K_1 \times 10^{-2}$ min ⁻¹	2.12	1.47	1.03	0.74
	R^2	0.978	0.964	0.991	0.951
Pseudo-second order	Δq	0.097	0.185	0.124	0.208
	q_{e2} (mg/g)	148.14	276.24	130.71	242.71
	$K_2 \times 10^{-4}$ (g. mg ⁻¹ min ⁻¹)	3.13	2.88	2.95	4.05
Intraparticle diffusion	R^2	0.996	0.996	0.992	0.995
	Δq	0.033	0.010	0.006	0.012
	K_f (mg/g. min ⁻¹)	5.68	7.96	6.81	4.78
Elovich	C (mg/g)	42.80	158.89	48.94	167.86
	R^2	0.976	0.905	0.869	0.919
	β	0.035	0.031	0.044	0.034
Bangham	α	19.40	693.58	20.74	953.89
	R^2	0.947	0.872	0.949	0.793
	K_B	24.92	51.46	25.31	59.46
	ΔB	0.294	0.141	0.254	0.085
	R^2	0.924	0.870	0.962	0.805

3.4. Adsorption Isotherm

The adsorption isotherm behavior of malachite green over CHA and CHA/CoAl-LDH composite was evaluated to discern the quantitative information regarding adsorption capacity of the adsorbent and the distribution of dye molecules between solid-liquid interfaces on reaching equilibrium. The experimental isotherm data was analyzed based on the widely used three isotherm models namely Langmuir, Freundlich and Temkin which is presented in Fig. 13. However, the linear regression R^2 value for CHA and CHA/CoAl-LDH composite in Langmuir model are 0.981 and 0.993, respectively which is relatively greater in comparison to Freundlich and Temkin model as shown in Table 2. Consequently, Langmuir model is found to be more appropriate and can best describe the experimental isotherm data. Nevertheless, it suggests that the adsorption of solute molecules takes place in a homogeneous surface through the formation of monolayer [67]. The calculated q_m value obtained from the linear plot of $1/C_e$ vs $1/q_e$ for CHA (943.39 mg/g) and CHA/CoAl-LDH composite (666.65 mg/g) were significantly higher compare to the other adsorbents for malachite green removal.

The plot of R_L vs C_0 is displayed in Fig. 14(a, b). The dimensionless separation R_L which is an important parameter for elucidation of Langmuir isotherm is determined and lies in the range of 0–1 for both adsorbents. In general, the values of R_L indicates the type of isotherm such as irreversible ($R_L = 0$), favorable ($0 < R_L < 1$) and unfavorable (R_L greater than 1). Since, the R_L value is less than unity for both CHA and CHA/CoAl-LDH composite. Therefore, it implies favorable intake of malachite green dye during sorption process [68].

3.5. Kinetics studies

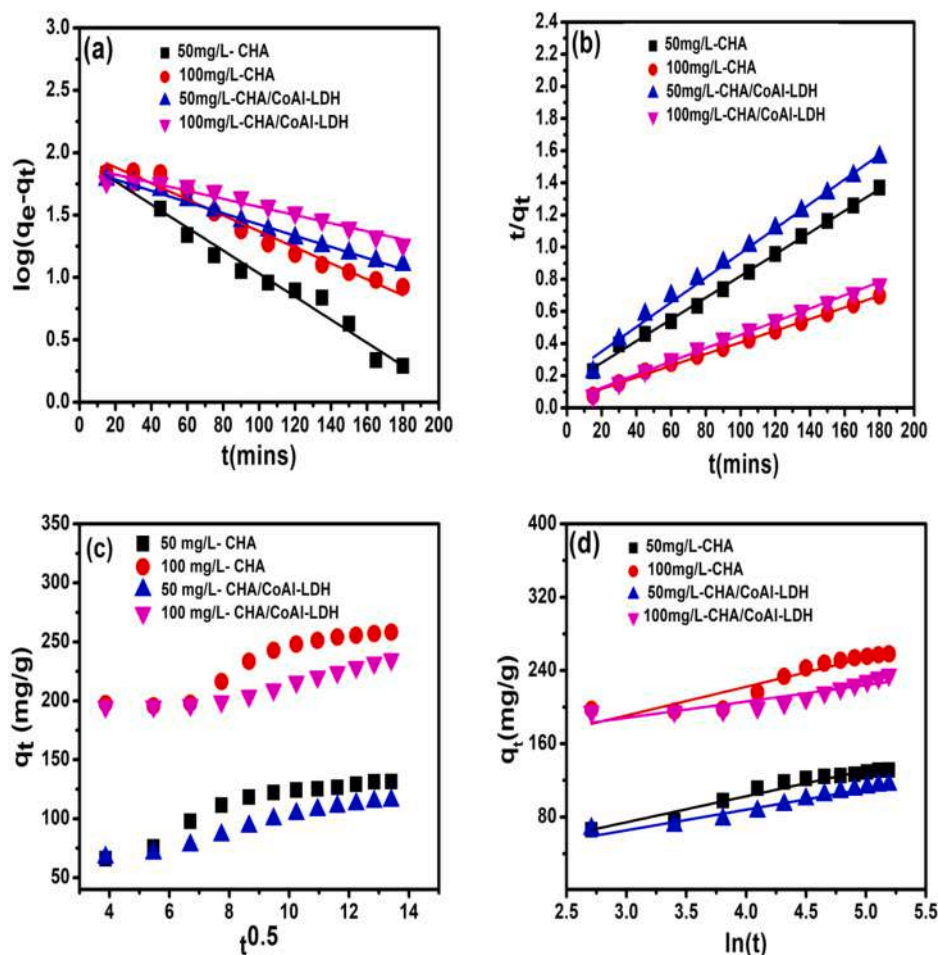
The experimental data obtained from the kinetics studies was interpreted by pseudo first order, pseudo second order, Elovich, intraparticle diffusion and Bangham model. The determined values of kinetics parameters for the adsorption of malachite green dye by two adsorbents were presented in Table 3. The linear fitting of the kinetics data based on these four models are shown in Fig. 15. The coefficient correlation R^2 value listed in Table 3 corresponding to pseudo second order model is closer to unity, and also lower normalized standard deviation Δq value was obtained compare to the first order kinetic model. Thus, it is apparent that pseudo second order model is more appropriate model for elucidation of adsorption kinetics while adsorption of malachite green dye over CHA and CHA/CoAl-LDH composites. Furthermore, the rate limiting step during the sorption process is predominantly controlled due to chemisorption. In addition the q_e (mg/g) values calculated from pseudo second order model for CHA and CHA/CoAl-LDH composite at the initial dye concentration (50 mg/L) were 148.14 and 130.71 mg/L, respectively. The obtained values are relatively consistent with experimental q_e values which are higher than the q_{e1} value evaluated from pseudo first order model [69].

The Weber Morris plot of q_t vs $t^{0.5}$ illustrated in Fig. 15 (c) was not a straight line passing through the origin which confirmed that intraparticle diffusion is not the rate limiting step in the adsorption of malachite green from aqueous solution. The coefficient of determination R^2 lies between (0.86–0.97) for the entire range of contact time while fitting the kinetics data based on this model. However, it is evident that sorption of dye takes place in three stages, initially most of the malachite green molecules quickly occupy the vacant adsorption site present on the external surface. In the second stage, the rate of adsorption retards due to the slow diffusion of adsorbed dye molecules inside the pore of adsorbent. Subsequently, the equilibrium adsorption was achieved at the last stage. The thickness of boundary layer C corresponding to CHA and CHA/CoAl-LDH was listed in Table 3 which displayed higher value at greater initial dye concentration. The obtained results can be described based on the increasing boundary layer effect which is due to the rapid adsorption of vacant site by adsorbate molecules at high concentration [70].

Table 4

Thermodynamic parameters for the adsorption of MG dye on to CHA and CHA/CoAl-LDH composite.

Adsorbent	T(K)	K_d	ΔG (KJ/mol)	ΔH (KJ/mol)	ΔS (J/ mol. K)	E_a (KJ/mol)	S^*
CHA	303	3.701	-9.367	72.498	269.872	101.35	6.45×10^{-19}
	313	4.789	-12.468				
	323	5.445	-14.059				
CHA/CoAl-LDH	303	2.629	-6.628	110.24	383.716	69.50	6.23×10^{-14}
	313	3.652	-9.508				
	323	5.281	-13.751				

**Fig. 15.** Linear plot of different kinetic models (a) Pseudo-first order (b) Pseudo-second order (c) Intraparticle diffusion and (d) Elovich model.

The plot of q_t vs $\ln t$ was demonstrated in Fig. 15 (d). Based on fitting the experimental kinetics data by Elovich model, the obtained values of α were greater than β , which is summarized in Table 3 for all initial dye concentration (50, 100 mg/L). Thus, it suggests that the adsorption rate of malachite green dye on to CHA and CHA/CoAl-LDH composite were comparatively higher than desorption rate. Moreover, the coefficient of determination R^2 values of the linear fit were greater than 0.90 at low dye concentration which also further validate the applicability of this model [71].

Kinetics data were further investigated by Bangham model to identify if pore diffusion is the slowest step occurring in adsorption kinetics experiment. The results obtained from Bangham model was displayed in Fig. 16(a) and Table 3. The non linear graph was obtained from the kinetics data which reveals that pore diffusion is not the rate limiting step during the sorption process [72]. However, the value of linear regression coefficient (R^2) for MG (50 mg/L) adsorption over CHA and

CHA/CoAl-LDH composite adsorbent was in the range between (0.92–0.96). Although, it is not significantly high enough but it also indicates the applicability of this model to interpret the diffusion of MG dyes molecules over adsorbent surface. The determined values of K_B and ΔB were CHA(0.294, 24.92) and CHA/ CoAl-LDH (0.254, 25.31), respectively.

3.6. Adsorption Mechanism

The adsorption of MG onto CHA and CHA/CoAL-LDH composite involves a complicated mechanism. However, the various plausible interaction associated during dye sorption are electrostatic attraction, H-bonding, π - π , n - π , ion exchange and pore filling, which is illustrated in Fig. 17. The effect of pH studies had already confirmed the influence of solution pH in the electrostatic attraction between adsorbate and adsorbent molecules. Besides, electrostatic attractions the aromatic

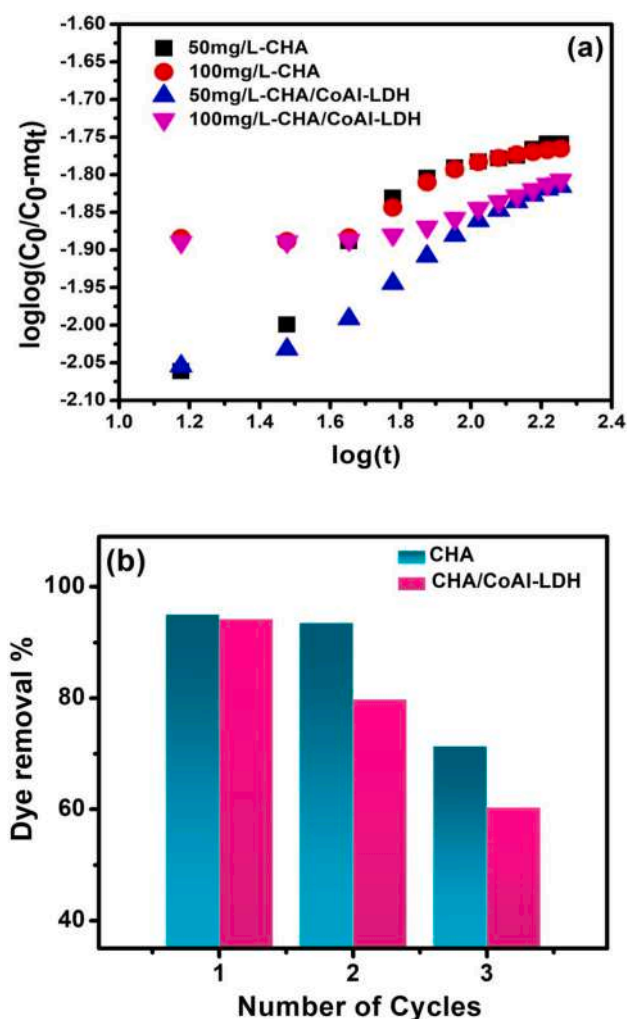


Fig. 16. (a) Bangham kinetic plot and (b) Reusability studies.

structure of MG dye could also be adsorbed through weak π - π and n - π interactions. The n - π and π - π interaction was initially proposed by Mattson et al. [73] and Coughlin et al. [74]. As depicted in Fig. 16 the π - π interaction takes place between π electrons of the negatively charged CHA or CHA/CoAl-LDH surface, and the π electrons of the aromatic ring of MG. Moreover, the oxygen containing functional group such as OH, C=O can also act as an electron donor, in which the aromatic ring of MG can accept this electron, thereby making the n - π interaction feasible. Thus, the existence of π - π and n - π interaction can be speculated in the present studies [75,76]. However, H-bonding is another possible mechanism that can occur between OH group of the adsorbent and the electronegative elements O and N of the MG dye. The shifting of the -OH peaks in CHA (3453 to 3438 cm^{-1}) and CHA/CoAl-LDH composite (3447 to 3455 cm^{-1}) can be observed from the IR spectrum after MG adsorption which further clarify the existences of H-bonding. Furthermore, the contribution of ion exchange and pore filling mechanism are also reported in the adsorption of cationic dye by several activated carbon and LDH/biochar composites [77]. Although, the contribution of ion exchange in the current system is not clearly known, a small quantity of cations such as K^+ , Na^+ and Ca^{2+} present in the adsorbents CHA and CHA/CoAl-LDH may be substituted with the positively charged MG dye. Since, CHA and CHA/CoAl-LDH are porous material as evidenced from the aforementioned BET and SEM analysis, so it can also be predicted that adsorption of MG dye into its non micropore might take place via pore filling mechanism. Additionally, after adsorption of MG dye several new peaks were detected in between (300–1700 cm^{-1}) in both CHA and

CHA/CoAl-LDH composite. The peak observed at stretching frequency ranging between (1162–1225 cm^{-1}) can be attributed to the C–N stretching vibrations of the aromatic ring. In addition, the peak corresponding to C=C stretch, CH_2 scissoring, CH_3 asymmetric and NH_2 wag were displayed at 1520 cm^{-1} , 1444 cm^{-1} , 1350 cm^{-1} and 816 cm^{-1} respectively [35]. Thus, the obtained result further supports the successful adsorption of MG dye over the proposed adsorbents.

3.7. Comparative analysis with other adsorbents

The maximum monolayer adsorption capacity (q_{max}) value of CHA and CHA/CoAl-LDH composite was compared with previously explored LDH and activated carbon, to determine the potentiality of the currently studied adsorbent. From Table 5 it was observed that the adsorption capacity of CHA and CHA/CoAl-LDH composite for MG adsorption was significantly high compare to most of the listed adsorbents. However, along with high q_{max} value another advantage of CHA/CoAl-LDH composite was its feasibility for removing both cationic and anionic dye [78–85].

3.8. Reusability

The reusability test of the adsorbent is an important aspect to understand the stability and economic feasibility for commercial and industrial application. The reusability performance of CHA and CHA/CoAl-LDH composite was executed up to third cycle under the experimental condition fixed at $C_0 = 60$ mg/L, dosages = 0.015 g and contact time = 6 h. After each consecutive cycle the initially adsorbed MG dye was desorbed from the adsorbent by washing thoroughly with ethanol and distilled water. The graph of reusability test is depicted in Fig. 15(b), it is evident that both the adsorbent showed decrease in dye removal % after each cycle. At first run, the removal capacity of MG dye by the adsorbent CHA (95 %) and CHA/CoAl-LDH composite (94.2 %) was achieved, which then slowly declines to 71.35 % and 60.3 %, respectively. However, this reduction in adsorption performance can occur due to the loss of the active sites during the regeneration of the adsorbents.

4. Conclusion

In summary, the composite material CHA/CoAl-LDH was successfully prepared by a facile co-precipitation method and employed for investigating its adsorptive removal of malachite green dye from the aqueous medium. SEM and TEM results indicate that CHA/CoAl-LDH as a composite exhibited porous carbon and nano sized hexagonal LDH platelets. The modification of CoAl-LDH with coconut husk ash (CHA) had significantly improved the surface characteristics by enriching with several functionalities and promoted better adsorption performance towards the targeted organic pollutant. Nevertheless, the pristine CoAl-LDH does not show its adsorption affinity to cationic dye (MG), due to its inherent positively charge brucite sheets which caused repulsion to the adsorbate molecule, while after fabrication with CHA the maximum monolayer adsorption capacity was exceeded up to 666.4 mg/g. The effect of pH studies showed better feasibility of CHA/CoAl-LDH in dye removal under basic pH conditions. The reusability test of the composite material indicates that after third cycle the removal capacity drops to 60.3 %. The utilization of such low cost and environmentally benign carbonaceous material had produced a suitable candidate which can be exploited in multi dye removal system. The adsorption data has been validated well according to Langmuir and pseudo second order model, which mainly supports that the uptake of MG dye occurs through the formation of monolayer over the surface of CHA/CoAl-LDH, and also hinted the existence of chemisorption process. The probable sorption mechanism associated in CHA-MG and CHA/CoAl-LDH-MG system resulted from several interactions including electrostatic, H-bonding, π - π , n - π , pore filling and ion exchange. Therefore, the present study would intrigued the new researchers for designing LDH composite by

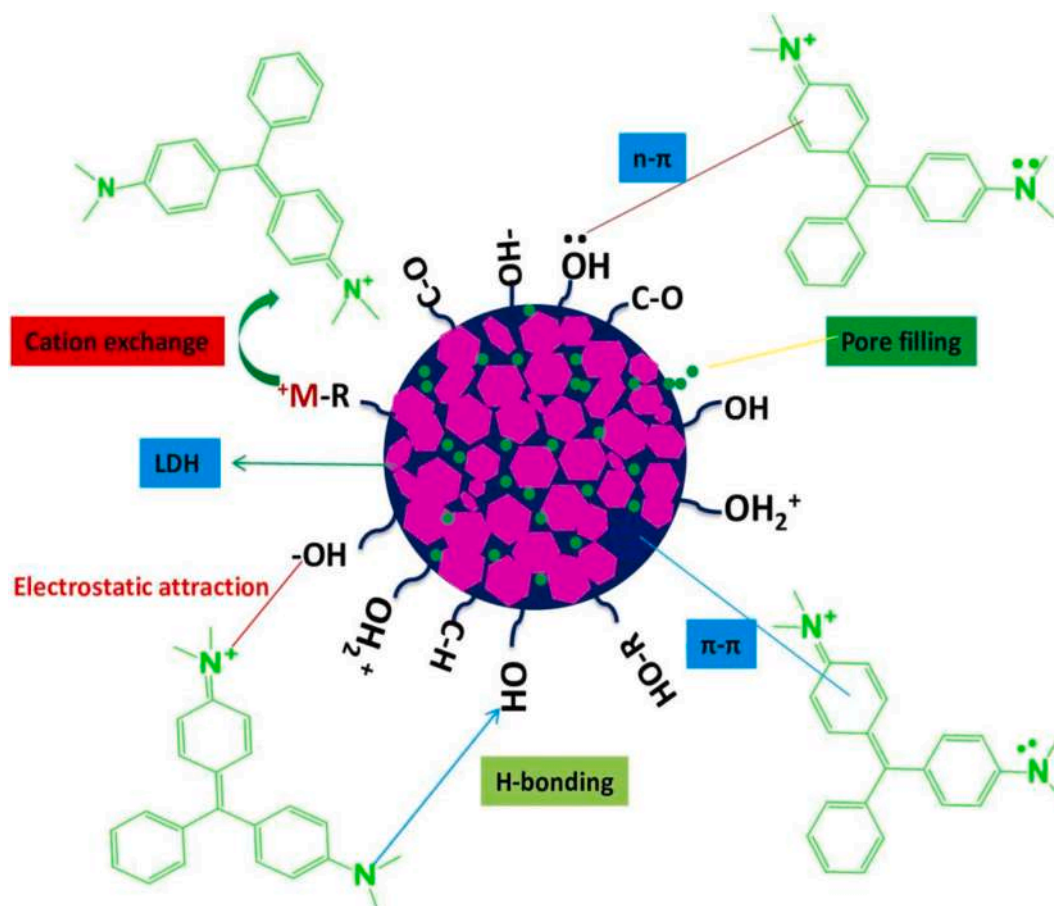


Fig. 17. Plausible adsorption mechanism for adsorption of MG dye on to CHA/CoAl-LDH composite.

Table 5

Comparison of the optimum experimental condition for the adsorption of MG dye by previously reported adsorbents.

Adsorbent	pH	Dosages	Isotherm	Kinetics	q_{max} (mg/g)	Reference
Mn-Fe LDH/PES composite membrane	7	0.02 g	Langmuir	Pseudo-second	13.49	[78]
Amygdalus Scoparia AC	7	0.01 g	Langmuir	Pseudo-second	144.30	[79]
Zn Fe-LDH Nanostructure	6	0.05 g	Langmuir-Freundlich	-	71.74	[80]
CuAl-SiW ₁₂ O ₄₀	-	-	Langmuir	Pseudo-second	149.25	[81]
ZIF@ZnAl-LDH	10	0.01 g	Langmuir	-	155.27	[82]
NiCoAl-LDH	10	-	Langmuir	-	110.13	[83]
MgAl/Biochar	-	-	Freundlich	Pseudo-second	70.92	[84]
Heveabrsiliensis root AC	4-10	0.2 g	n-BET	Avrami model	259.49	[85]
CHA	10	0.03g	Langmuir	Pseudo-second	943.39	This Work
CHA/CoAl-LDH nanocomposite	10	0.03g	Langmuir	Pseudo-second	666.40	This Work

using various agricultural waste derived carbon for decontamination of various organic and inorganic water pollutants.

Declaration of Competing Interest

The authors declare that they have no known competing financial interests or personal relationships that could have appeared to influence the work reported in this paper.

Data availability

Data will be made available on request.

Acknowledgement

We are thankful to several institutes for providing instrumental facility for characterization of material with SEM-EDX, BET and Powder X-ray from CIF, IIT Guwahati, FT-Infrared from Cotton University, TEM from NEHU SAIF. We are also thankful to our institute Bodoland University for providing UV-spectrophotometer instruments and all the

necessary chemicals and equipments required for our research works.

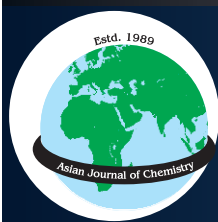
References

- [1] B.A. Fil, Isotherm, kinetic, and thermodynamic studies on the adsorption behavior of malachite green dye onto montmorillonite clay, *Part. Sci. Technol.* 34 (1) (2016) 118–126.
- [2] J. Khatri, P.V. Nidheesh, T.S.A. Singh, M.S. Kumar, Advanced oxidation processes based on zero-valent aluminium for treating textile wastewater, *Chem. Eng. J.* 348 (2018) 67–73.
- [3] L.D. Ardila-Leal, R.A. Poutou-Pinales, A.M. Pedroza-Rodríguez, B.E. Quevedo-Hidalgo, A Brief History of Colour, the Environmental Impact of Synthetic Dyes and Removal by Using Laccases, *Molecules*. 26 (2021) 3813.
- [4] S. Srivastava, R. Sinha, D. Roy, Toxicological effects of malachite green, *Aquat. Toxicol.* 66 (3) (2004) 319–329.
- [5] N. Hidayah, F.A. Bakar, N.A. Mahyudin, S. Faridah, M.S. Nur-Azura, M.Z. Zaman, Detection of malachite green and leuco-malachite green in fishery industry, *Int. Food Res. J.* 20 (2013) 1511.
- [6] P.S. David, A. Karunanithi, N.N. Fathima, Improved filtration for dye removal using keratin-polyamide blend nanofibrous membranes, *Environ. Sci. Pollut. Res.* 27 (36) (2020) 45629–45638.
- [7] A.M. Saad, M.R. Abukhadra, A.K. Ahmed, A.M. Elzanaty, A.H. Mady, M.A. Betiha, J.J. Shim, A.M. Rabie, Photocatalytic degradation of malachite green dye using chitosan supported ZnO nano-flowers under visible light, *J. Environ. Manage.* 258 (2020), 110043.
- [8] M.G. Abrile, M.L. Fiasconaro, M.E. Lovato, Optimization of Reactive Blue 19 dye removal using ozone and ozone/UV employing response surface methodology, *SN Appl. Sci.* 2 (2020) 995.
- [9] V.S. Watwe, S.D. Kulkarni, P.S. Kulkarni, Cr(VI)- Mediated Homogeneous Fenton Oxidation for Decolorization of Methylene Blue Dye: Sludge Free and Pertinent to a Wide pH Range, *ACS Omega*. 6 (2021) 27288–27296.
- [10] K. Ikehata, Y. Zhao, H.V. Kulkarni, Y. Li, S.A. Snyder, K.P. Ishida, M.A. Anderson, Water Recovery from Advanced Water Purification Facility Reverse Osmosis Concentrate by Photobiological Treatment Followed by Secondary Reverse Osmosis, *Environ. Sci. Technol.* 52 (15) (2018) 8588–8595.
- [11] S.S. Mohanty, A. Kumar, Enhanced degradation of anthraquinone dyes by microbiological monoculture and developed consortium through the production of specific enzymes, *Sci. Rep.* 11 (2021) 1–5.
- [12] M.R. Gadekar, M.M. Ahammed, Use of water treatment residuals for colour removal from real textile dye wastewater, *Appl. Water Sci.* 10 (2020) 1–8.
- [13] L.J. Martis, N. Parushuram, Y. Sangappa, Preparation, characterization, and methylene blue dye adsorption study of silk fibroin-graphene oxide nanocomposites, *Environ. Sci.: Adv.* 1 (3) (2022) 285–296.
- [14] S. Moosavi, C.W. Lai, S. Gan, G. Zamiri, O. Akbarzadeh Pivehzhani, M.R. Johan, Application of Efficient Magnetic Particles and Activated Carbon for Dye Removal from Wastewater, *ACS Omega*. 5 (33) (2020) 20684–20697.
- [15] S. Yu, H. Pang, S. Huang, H. Tang, S. Wang, M. Qiu, Z. Chen, H. Yang, G. Song, D. Fu, B. Hu, X. Wang, Recent advances in metal-organic framework membranes for water treatment: A review, *Sci. Total Environ.* 800 (2021) 149662.
- [16] S. Zhang, J. Wang, Y. Zhang, J. Ma, L. Huang, S. Yu, L. Chen, G. Song, M. Qiu, X. Wang, Applications of water-stable metal-organic frameworks in the removal of water pollutants: A review, *Environ. Pollut.* 291 (2021) 118076.
- [17] M.E. Alouani, S. Alehyen, H.E. Hadki, H. Saufi, A. Elhalil, O.K. Kabbaj, M. Taibi, Synergistic influence between adsorption and photodegradation of Rhodamine B using synthesized fly ash based inorganic polymer, *Surf. Interfaces*. 24 (2021), 101136.
- [18] M.M. Sabzehmeidani, H. Karimi, M. Ghaedi, Enhanced visible light-active CeO₂/CuO/Ag₂CrO₄ ternary heterostructures based on CeO₂/CuO nanofibre heterojunctions for the simultaneous degradation of a binary mixture of dyes, *New J. Chem.* 44 (2020) 5033–5048.
- [19] H. Abbasi-Asl, M.M. Sabzehmeidani, M. Ghaedi, Efficient degradation of metronidazole antibiotic by TiO₂/Ag₃PO₄/g-C₃N₄ ternary composite photocatalyst in a continuous flow-loop photoreactor, *J. Environ. Chem. Eng.* 9 (2021), 105963.
- [20] M.M. Sabzehmeidani, H. Karimi, M. Ghaedi, CeO₂ nanofibres-CdS nanostructures n-n junction with enhanced visible-light photocatalytic activity, *Arab. J. Chem.* 13 (2020) 7583–7597.
- [21] L. Liang, F. Xi, W. Tan, X.u. Meng, B. Hu, X. Wang, Review of organic and inorganic pollutants removal by biochar and biochar-based composites, *Biochar*. 3 (3) (2021) 255–281.
- [22] A. Machrouhi, M. Farnane, A. Elhalil, R. Elmoubarki, M. Abdennouri, S. Qourzal, H. Tounsadi, N. Barka, Effectiveness of beetroot seeds and H₃PO₄ activated beetroot seeds for the removal of dyes from aqueous solutions, *J. Water Reuse Desalination*. 8 (2018) 522–531.
- [23] S. Yu, H. Tang, D. Zhang, S. Wang, M. Qiu, G. Song, D. Fu, B. Hu, X. Wang, MXenes as emerging nanomaterials in water purification and environmental remediation, *Sci. Total Environ.* 811 (2022), 152280.
- [24] R. Elmoubarki, W. Boumya, F.Z. Mahjoubi, A. Elhalil, M. Sadiq, N. Barka, NiFe-SDS and Ni-Fe-SO₄ layered double hydroxides: Preparation, characterization and application in dyes removal, *Mater. Today: Proc.* 37 (2021) 3871–3875.
- [25] J. Yu, Q. Wang, D. O'Hare, L. Sun, Preparation of two dimensional layered double hydroxide nanosheets and their applications, *Chem. Soc. Rev.* 46 (19) (2017) 5950–5974.
- [26] L.i. Yan, S. Gonca, G. Zhu, W. Zhang, X. Chen, Layered double hydroxide nanostructures and nanocomposites for biomedical applications, *J. Mater. Chem. B*. 7 (37) (2019) 5583–5601.
- [27] M. Zubair, H.A. Aziz, I. Ihsanullah, M.A. Ahmad, M.A. Al-Harathi, Biochar supported CuFe layered double hydroxide composite as a sustainable adsorbent for efficient removal of anionic azo dye from water, *Environ. Technol. Innov.* 23 (2021), 101614.
- [28] L. Zhang, S. Tang, C. Jiang, X. Jiang, Y. Guan, Simultaneous and Efficient Capture of Inorganic Nitrogen and Heavy Metals by Porous Layered Double Hydroxide and Biochar Composite for Agricultural Nonpoint Pollution Control, *ACS Appl. Mater. Interfaces*. 10 (49) (2018) 43013–43030.
- [29] W. Qu, T. Yuan, G. Yin, S. Xu, Q. Zhang, H. Su, Effect of properties of activated carbon on malachite green adsorption, *Fuel*. 249 (2019) 45–53.
- [30] L. Meili, P.V. Lins, C.L.P.S. Zanta, J.I. Soletti, L.M.O. Ribeiro, C.B. Dornelas, T.L. Silva, M.G.A. Vieira, MgAl-LDH/Biochar composites for methylene blue removal by adsorption, *Appl. Clay Sci.* 168 (2019) 11–20.
- [31] L. Mishra, G. Basu, Coconut fibre: its structure, properties and applications, *Wood head, Handbook of Natural Fibres*, 2020, pp. 231–255.
- [32] R.K. Ahmad, S.A. Sulaiman, S. Yusup, S.S. Dol, M. Inayat, H.A. Umar, Exploring the potential of coconut shell biomass for charcoal production, *Ain Shams Eng. J.* 13 (2022), 101499.
- [33] A. Kundu, B.S. Gupta, M.A. Hashim, G. Redzwan, Taguchi optimization approach for production of activated carbon from phosphoric acid impregnated palm kernel shell by microwave heating, *J. Clean. Prod.* 105 (2015) 420–427.
- [34] I. Langmuir, The adsorption of gases on plane surfaces of glass, mica and platinum, *J. Am. Chem. Soc.* 40 (9) (1918) 1361–1403.
- [35] S. Das, S.K. Dash, K.M.P. Kinetics, Isotherm, and Thermodynamic Study for Ultrafast Adsorption of Azo Dye by an Efficient Sorbent: Ternary Mg/(Al+Fe) Layered Double Hydroxides, *ACS, Omega*. 3 (2018) 2532–2545.
- [36] H.M.F. Freundlich, Over the Adsorption in Solution, *J. Phys. Chem.* 57 (1906) 385–471.
- [37] M.I. Temkin, The Kinetics of Some Industrial Heterogeneous Catalytic Reactions, *Adv. Catal.* 28 (1979) 173–291.
- [38] C.-R. Lee, H.-S. Kim, I.-H. Jang, J.-H. Im, N.-G. Park, Pseudo First-Order Adsorption Kinetics of N719 Dye on TiO₂ Surface, *ACS Appl. Mater. Interfaces*. 3 (6) (2011) 1953–1957.
- [39] Y.S. Ho, G. McKay, Pseudo-second order model for sorption processes, *Process Biochem.* 34 (5) (1999) 451–465.
- [40] W.J. Weber, J.C. Morris, Kinetics of adsorption on carbon from solution, *Journal of the sanitary engineering division* 89 (1963) 31–59.
- [41] F.C. Wu, R.L. Tseng, R.s. j., Characteristics of Elovich equation used for the analysis of adsorption kinetics in dye-chitosan systems, *Chem. Eng. J.* 150 (2009) 366–373.
- [42] Sumanjit, S. Rani, R.K. Mahajan, Equilibrium, kinetics and thermodynamic parameters for adsorptive removal of dye Basic Blue 9 by ground nut shells and Eichhornia, *Arab. J. Chem.* 9 (2016) S1464–S1477.
- [43] Z. Lu, W. Zhu, X. Lei, G.R. Williams, D. O'Hare, Z. Chang, X. Sun, X. Duan, D. High pseudocapacitive cobalt carbonate hydroxide films derived from CoAl layered double hydroxides, *Nanoscale*. 4 (12) (2012) 3640.
- [44] M.F. Anuar, Y.W. Fen, M.H.M. Zaid, K.A. Matori, R.E.M. Khaidir, Synthesis and structural properties of coconut husk as potential silica source, *Results Phys.* 11 (2018) 1–4.
- [45] Z.P. Diao, Y.X. Zhang, X.D. Hao, Z.Q. Wen, Facile synthesis of CoAl-LDH/MnO₂ hierarchical nanocomposites for high-performance supercapacitors, *Ceram. Int.* 40 (1) (2014) 2115–2120.
- [46] L. Zhang, L.-y. Tu, Y. Liang, Q.i. Chen, Z.-S. Li, C.-H. Li, Z.-H. Wang, W. Li, Coconut-based activated carbon fibers for efficient adsorption of various organic dyes, *RSC Adv.* 8 (74) (2018) 42280–42291.
- [47] Y. Chen, C. Jing, X. Zhang, D. Jiang, X. Liu, B. Dong, L.i. Feng, S. Li, Y. Zhang, Acid-salt treated CoAl layered double hydroxide nanosheets with enhanced adsorption capacity of methyl orange dye, *J. Colloid Interface Sci.* 548 (2019) 100–109.
- [48] O.S. Bello, K.A. Adegoka, S.O. Fagbenro, O.S. Lameed, Functionalized coconut husks for rhodamine-B dye sequestration, *Appl. Water Sci.* 9 (2019) 1–15.
- [49] M.F. Anuar, Y.W. Fen, M.H.M. Zaid, K.A. Matori, R.E.M. Khaidir, The Physical and Optical Studies of Crystalline Silica Derived from the Green Synthesis of Coconut Husk Ash, *Appl. Sci.* 10 (2020) 2128.
- [50] R.S. Piriya, R.M. Jayabalakrishnan, M. Maheshwari, K. Boomiraj, S. Qumabady, Coconut shell derived ZnCl₂ activated carbon for malachite green dye removal, *Water Sci. Technol.* 83 (2021) 1167–1182.
- [51] Z. Hu, M.P. Srinivasan, Preparation of high-surface-area activated carbons from coconut shell, *Microporous Mesoporous Mater.* 27 (1) (1999) 11–18.
- [52] S. Kundu, M.K. Naskar, Carbon-layered double hydroxide nanocomposite for efficient removal of inorganic and organic based water contaminants-unravelling the adsorption mechanism, *Materials Advances*. 2 (2021) 3600–3612.
- [53] H. Ma, Z. Xu, W. Wang, X. Gao, H. Ma, Adsorption and regeneration of leaf-based biochar for p-nitrophenol adsorption from aqueous solution, *RSC Adv.* 9 (67) (2019) 39282–39293.
- [54] G.Y. Abate, A.N. Alene, A.T. Habte, D.M. Getahun, Adsorptive removal of malachite green dye from aqueous solution onto activated carbon of Cathaedulis stem as a low cost bio-adsorbent, *Environ. Syst. Res.* 9 (2020) 1–13.
- [55] N.A. Rahmat, A.A. Ali, N. Hussain, M.S. Muhammad, R.A. Kristanti, T. Hadibarata, Removal of Remazol Brilliant Blue R from Aqueous Solution by Adsorption Using Pineapple Leaf Powder and Lime Peel Powder, *Water Air Soil Pollut.* 227 (2016) 1–11.
- [56] N.K. Mondal, S. k., Potentiality of banana peel for removal of Congo red dye from aqueous solution: isotherm, kinetics and thermodynamics studies, *Appl. Water Sci.* 8 (2018) 1–12.
- [57] L. Ai, C. Zhang, F. Liao, Y. Wang, M. Li, L. Meng, J. Jiang, Removal of methylene blue from aqueous solution with magnetite loaded multi-wall carbon nanotube: Kinetic, isotherm and mechanism analysis, *J. Hazard. Mater.* 198 (2011) 282–290.

- [58] K.G. Akpomie, F.A. Dawodu, K.O. Adebowale, Mechanism on the sorption of heavy metals from binary-solution by a low cost montmorillonite and its desorption potential, *Alex. Eng. J.* 54 (3) (2015) 757–767.
- [59] F. Ali, S. Bibi, N. Ali, Z. Ali, A. Said, Z.U. Wahab, M. Bilal, H.M.N. Iqbal, Sorptive removal of malachite green dye by activated charcoal: Process optimization, kinetic, and thermodynamic evaluation, *Case Studies in Chemical and Environmental Engineering*. 2 (2020) 100025.
- [60] V.P. Dinh, T.D.T. Huynh, H.M. Le, V.D. Nguyen, V.A. Dao, N.Q. Hung, L.A. Tuyen, S. Lee, J. Yi, T.D. Nguyen, L.V. Tan, Insight into the adsorption mechanisms of methylene blue and chromium (III) from aqueous solution onto pomelo fruit peel, *RSC Adv.* 9 (2019) 25847–25860.
- [61] I. Savva, O. Marinica, C.A. Papatryfonos, L. Vekas, T. Krasia-Christoforou, Evaluation of electrospun polymer-Fe₃O₄ nanocomposite mats in malachite green adsorption, *RSC Adv.* 5 (21) (2015) 16484–16496.
- [62] G. Rathee, A. Awasthi, D. Sood, R. Tomar, R. Chandra, A new biocompatible ternary Layered Double Hydroxide Adsorbent for ultrafast removal of anionic organic dyes, *Sci. Rep.* 9 (2019) 1–14.
- [63] Y.T. Gebreslassie, Equilibrium, kinetics, and thermodynamic studies of malachite green adsorption onto Fig (*Ficus cartia*) leaves, *J. Anal. Methods Chem.* 2020 (2020) 7384675.
- [64] M.A. Ahmad, R. Alrozi, Removal of malachite green dye from aqueous solution using rambutan peel-based activated carbon: Equilibrium, kinetic and thermodynamic studies, *Chem. Eng. J.* 171 (2011) 510–516.
- [65] V.O. Shikuku, R. Zanella, C.O. Kowenje, F.F. Donato, N.M.G. Bandeira, O. D. Prestes, Single and binary adsorption of sulfonamide antibiotics onto iron-modified clay: linear and nonlinear isotherms, kinetics, thermodynamics and mechanistic studies, *Appl. Water Sci.* 8 (2018) 1–12.
- [66] J.H. Potgieter, C. Paredes, S. Pearson, A kinetic and thermodynamic investigation into the removal of methyl orange from wastewater utilizing fly ash in different process configurations, *Environ. Geochem. Health.* 43 (7) (2021) 2539–2550.
- [67] M. Maruthapandi, V.B. Kumar, J.H.T. Luong, A. Gedanken, Kinetics, Isotherm, and Thermodynamic Studies of Methylene Blue Adsorption on Polyaniline And Polypyrrole Macro-Nanoparticles Synthesized by C-Dot-Initiated Polymerization, *ACS, Omega.* 3 (7) (2018) 7196–7203.
- [68] K. Sharma, H.K. Sadhanala, Y. Mastai, Ze'ev Porat, A. Gedanken, Sonochemically Prepared BSA Microspheres as Adsorbents for the Removal of Organic Pollutants From Water, *Langmuir.* 37 (32) (2021) 9927–9938.
- [69] E. Sterenzon, V.K. Vadivel, Y. Gerchman, T. Luxbacher, R. Narayanan, H. Mamane, Effective Removal OF Acid Dye in Synthetic and Silk Dyeing Effluents: Isotherm and Kinetic Studies, *ACS Omega.* 7 (2022) 118–128.
- [70] F.C. Wu, R.L. Tseng, R.S. Juang, Initial behavior of intraparticle diffusion model used in the description of adsorption kinetics, *Chem. Eng. J.* 153 (153) (2009) 1–8.
- [71] I. Ali, C. Peng, T. Ye, I. Naz, Sorption of cationic malachite green dye on phytogetic magnetite nanoparticles functionalized by 3-mercaptopropanic acid, *RSC Adv.* 8 (2018) 8878–8897.
- [72] A.E. Ofomaja, E.B. Naidoo, A. Pholosi, Intraparticle diffusion of Cr(VI) through biomass: A comparative kinetic and diffusion study, *S, Afr. J. Chem. Eng.* 32 (2020) 39–55.
- [73] J.A. Mattson, H.B. Mark, M.D. Malbin, W.J. Weber, J.C. Crittenden, Surface chemistry of active carbon: Specific adsorption of phenols, *J. Colloid Interface Sci.* 31 (1) (1969) 116–130.
- [74] R.W. Coughlin, F.S. Ezra, Role of surface acidity in the adsorption of organic pollutants on the surface of carbon, *Environ. Sci. Technol.* 2 (1968) 291–297.
- [75] T.G. Ambaye, M. Vaccari, E.D. van Hullebusch, A. Amrane, S. Rtimi, Mechanisms and adsorption capacities of biochar for the removal of organic and inorganic pollutants from industrial wastewater, *Int J Environ Sci Technol.* 18 (10) (2021) 3273–3294.
- [76] H.N. Tran, Y.F. Wang, S.J. You, H.P. Chao, Insights into the mechanism of cationic dye adsorption on activated charcoal: The importance of π - π interactions, *Process Saf. Environ. Prot.* 107 (2017) 168–180.
- [77] S. Fan, J. Tang, Y. Wang, H. Li, H. Zhang, J. Tang, Z. Wang, X. Li, Biochar prepared from co-pyrolysis of municipal sewage sludge and tea waste for the adsorption of methylene blue from aqueous solutions: kinetics, isotherm, thermodynamic and mechanism, *J. Mol. Liq.* 220 (2016) 432–441.
- [78] M. Abbasi, M.M. Sabzehmeidani, M. Ghaedi, R. Jannesar, A. Shokrollahi, Synthesis of grass-like structured Mn-Fe layered double hydroxides/PES composite adsorptive membrane for removal of malachite green, *Appl. Clay Sci.* 203 (2021), 105946.
- [79] R. Bagheri, M. Ghaedi, A. Asfaram, E.A. Dil, H. Javadian, RSM-CCD design of malachite green adsorption onto activated carbon with multimodal pore size distribution prepared from *Amygdalus scoparia*: Kinetic and isotherm studies, *Polyhedron.* 171 (2019) 464–472.
- [80] R.K. Mahmoud, M. Taha, A. Zaher, R.M. Amin, Understanding the physicochemical properties of Zn-Fe LDH nanostructure as sorbent material for removing of anionic and cationic dyes mixture, *Sci. Rep.* 11 (2021) 1–19.
- [81] N.R. Palapa, N. Juleanti, N. Normah, T. Taher, A. Lesbani, Unique Adsorption Properties of Malachite Green on Interlayer Space of Cu-Al and Cu-Al-SiW₁₂O₄₀ Layered Double Hydroxides, *Bull. Chem. React. Eng. Catal.* 15 (3) (2020) 653–661.
- [82] M.A. Nazir, M.A. Bashir, T. Najam, M.S. Javed, S. Suleman, S. Hussain, O.P. Kumar, S.S.A. Shah, Combining structurally ordered intermetallic nodes: Kinetic and isothermal studies for removal of malachite green and methyl orange with mechanistic aspects, *Microchem. J.* 164 (2021), 105973.
- [83] M.A. Nazir, T. Najam, M.S. Bashir, M.S. Javed, M.A. Bashir, M. Imran, U. Azhar, S. S.A. Shah, A.U. Rehman, Kinetics, isothermal and mechanistic insight into the adsorption of eosin yellow and malachite green from water via tri-metallic layered double hydroxide nanosheets, *Korean J Chem Eng.* 39 (1) (2022) 216–226.
- [84] A.F. Badri, P.M.S.B.N. Siregar, N.R. Palapa, R. Mohadi, M. Mardiyanto, A. Lesbani, Mg-Al/biochar composite with stable structure for malachite green adsorption from aqueous solutions, *Bull. Chem. React. Eng. Catal.* 16 (1) (2021) 149–160.
- [85] A.A. Ahmad, M.A. Ahmad, N.K.E. Yahaya, J. Karim, Adsorption of malachite green by activated carbon derived from gasified *Hevea brasiliensis* root, *Arab. J. Chem.* 14 (2021).



Dr. Hemaprobha Saikia received her M.Sc. in Chemistry from Assam University Silchar in 2006. She has completed B.Ed. in 2009 from Gossaigaon B.Ed. College and Ph.D from Gauhati University, Guwahati in 2013. She is currently working at Bodoland University, Kokrajhar, Assam, India, as a Assistant Professor (II stage) in Department of Chemistry from 2015. Her research interest includes Inorganic Synthesis, Nanomaterial, Adsorption, Catalysis, Material Science. She has published 8 Research articles in a Peer Reviewed Journals and presented more than 10 conferences



Synthesis of Ternary CaNiAl-Layered Double Hydroxide as Potential Adsorbent for Congo Red Dye Removal in Aqueous Solution

DEEPMONI BRAHMA¹, KASTURI PRIYOM NATH¹, MADHUSMITA PATGIRI¹ and HEMAPROBHA SAIKIA^{1*}

Department of Chemistry, Bodoland University, Kokrajhar-783370, India

*Corresponding author: E-mail: saikiahemaprobha@gmail.com

Received: 21 June 2022;

Accepted: 30 September 2022;

Published online: 25 November 2022;

AJC-21047

A hierarchically porous ternary CaNiAl-LDH material was synthesized *via* a facile urea hydrolysis method and characterized by PXRD, FT-IR, BET, SEM and TGA techniques. The adsorption efficiency of synthesized ternary CaNiAl-layered double hydroxide was also examined using Congo red dye as a model pollutant. Material characteristics affirmed with the formation of circular and flower-like LDH particles with accessible mesopores of 3.85 nm and intermediate surface area of 58.45 m²/g. The synthesized ternary CaNiAl-LDH material exhibited the maximum adsorption capacity of 135.21 mg/g towards the targeted organic pollutant from an aqueous medium. The obtained results in isotherm and kinetic studies demonstrated that sorption of Congo red dye onto CaNiAl-LDH followed Langmuir isotherm and pseudo-second order model, respectively. In addition, the thermodynamic studies also suggested the endothermic and spontaneity of the sorption process. The reusability studies confirmed that CaNiAl-LDH can be reused up to fourth cycle. Therefore, the proposed material CaNiAl-LDH can be advocated as a highly effective low cost adsorbent for the treatment of water contaminants.

Keywords: Layered double hydroxide, Congo red dye, Adsorption, Intercalation.

INTRODUCTION

With the fast growth of urbanization, the discharge of effluents from various manufacturing industries had created environmental hazard for all living species due to its diverse effect. Among several water pollutants, the use of synthetic azo dyes had emerged rapidly due to its wide applications in industries such as textile, plastic, leather, foods, cosmetics, medicine and paper [1]. Dyes disperse in water bodies leads to coloured water, which can block the radiation from sunlight and can affect aquatic life forms. In addition, azo dyes have complex and stable chemical structure that makes it very difficult to separate or degrade from the water bodies *via* conventional methods [2]. Due to its recognized carcinogenic and mutagenic effects, it is also extremely poisonous and causes variations in parameters like BOD and COD levels, which can be harmful for all types of habitat. In particular, Congo red (CR) dye a type of azo dye is highlighted toxic and causes adverse effects such as irritation, cancer, photosynthesis inhibition, reduction in oxygen level and suffocating flora and fauna [3]. Therefore, it is imperative to treat azo dye-polluted waste-

waters in order to reduce the pollutants present in the industrial effluents.

For wastewater treatment, a number of techniques and methods are developed in order to reduce the adverse affects of poisonous dyes. Some widely used efficient techniques that can achieve dye separation from an aqueous medium are filtration [4], coagulation/flocculation [5], ozonation [6], photo-degradation [7] and adsorption [8]. However, adsorption method is deemed as one of the most preferred approach in remediation of various toxins from liquid phase. Due to ease of operation, low cost, high efficiency, non-toxic and mild reaction condition, it can be easily afforded. This technique can be applied to separate, purify, detoxify and deodorize the toxic product in both liquid and gaseous medium. A large number of adsorbents were reported for the removal of Congo red dye, for instances Metal-organic frameworks (MOFs) [9], activated carbon [10], polymer composite [11], zeolite [12] and LDH [13]. Moreover, due to its multiple advantages, such as flexible structure, high surface area, thermal stability, ease of regeneration and non-toxicity, layered double hydroxide (LDH) can be considered one of the most promising candidates in water pollution treatment.

Layered double hydroxides (LDHs) are the broad class of anionic clays, which is generally represented by the chemical formula $[M_{1-x}^{2+}M_x^{3+}(\text{OH})_2]^{x+}(\text{A}^{n-})_{x/n}\cdot\text{H}_2\text{O}$ where M^{2+} (Ca^{2+} , Mg^{2+} , Fe^{2+} , Ni^{2+}), M^{3+} (Fe^{3+} , Al^{3+} , Cr^{3+}) and A^{n-} (CO_3^{2-} , Cl^- , NO_3^-) are divalent metal cation, trivalent metal cations and interlayer ions, respectively. Designing of LDH can be achieved through various synthetic routes such as hydrothermal, urea hydrolysis, co-precipitation, rehydration/construction, ion exchange. In addition, anion exchange in the structure can be tuned by intercalating with various organic and inorganic ions, which plays a key role in the adsorption process [14,15]. Consequently, to improve the sorption characteristics of binary LDH, the variation in the structure can be made by introducing third metal ions.

In this work, an attempt is made to synthesize ternary CaNiAl-LDH *via* urea hydrolysis method. The as-synthesized sorbents were implemented for the removal of targeted azo-dye (Congo red dye) from the aqueous solution. The influence of the adsorption parameters such as pH, temperature, dosages, contact time, initial dye concentration on the adsorption performances was investigated. The reusability studies are also conducted. The isotherm and kinetic studies were also reported and the plausible mechanism of dye sorption were also analyzed by recording P-XRD and FT-IR spectra of the sample after adsorption of Congo red dye.

EXPERIMENTAL

Nickel chloride hexahydrate ($\text{NiCl}_2\cdot 6\text{H}_2\text{O}$), calcium chloride dihydrate ($\text{CaCl}_2\cdot 2\text{H}_2\text{O}$), aluminium chloride, sodium hydroxide were procured from Merck, while urea and Congo red dye ($\text{C}_{32}\text{H}_{22}\text{N}_6\text{O}_6\text{S}_2\text{Na}_2$) were purchased from Qualigens India Pvt. Ltd. All the obtained chemicals were of analytical grade and utilized directly without any further purifications.

Preparation of adsorbents: Layered double hydroxide (LDH) sample was prepared *via* a facile urea hydrolysis method. Initially, a mixture of metal precursor's solutions containing 8 mmol $\text{NiCl}_2\cdot 6\text{H}_2\text{O}$, 8 mmol $\text{CaCl}_2\cdot \text{H}_2\text{O}$ and 4 mmol AlCl_3 in a 100 mL aqueous solution was stirred. Subsequently, 2.1 g of urea was further added to the above solution mixture and continuously stirred until the precursors were completely dissolved. The resulting suspension was then transferred in autoclave and heated at 150 °C in an oven for 6 h. The obtained green precipitate was collected and washed several times with deionized water. Finally, the resulting product was dried in a vacuum at 50 °C and crushed with mortar to obtain the powder form, which is denoted as CaNiAl-LDH.

Adsorption experiments: To investigate the adsorption efficiency of ternary CaNiAl-LDH, the adsorption isotherm experiment was conducted in a batch mode. In isotherm studies, a stock solution of Congo red dye having initial concentration from 30 to 270 mg/L was prepared in distilled water. A Congo red dye solution (20 mL) at varying initial concentration was taken in a conical flask and 0.025 g of adsorbent was mixed. The resulting solution was then allowed to stir at 28 °C (room temperature) in a water bath shaker for time period of 6 h to attain equilibrium. The adsorbent was separated from the liquid

suspension by filtration and the concentration of Congo red dye in filtrate was measured by using UV-Spectrophotometer at the absorption maximum wavelength of 498 nm. The percentage removal and quantity of Congo red dye adsorbed on to CaNiAl-LDH was calculated by the given equation:

$$\text{Dye removal (\%)} = \frac{C_o - C_e}{C_o} \times 100 \quad (1)$$

$$q_e = \frac{(C_o - C_e)V}{W} \quad (2)$$

where C_o and C_e denotes initial and equilibrium dye concentration, respectively; q_e indicates amount of dye adsorbed at equilibrium, V represents volume of the adsorbate solution (mL) and W signifies the quantity of adsorbent (g).

In kinetic studies, 0.025 g of adsorbent CaNiAl-LDH was mixed with 40 mL of Congo red dye solution at the initial dye concentration (50 mg/L). The liquid suspension is then allowed to agitate in a shaker for a time period of 3 h. After a definite time interval, 2 mL of the solution was withdrawn and separated from the adsorbent by centrifugation at 1000 rpm. Similarly, the residual dye concentration was estimated at the maximum absorption wavelength of 498 nm. The quantity of dye uptake at time 't' was evaluated by the equation:

$$q_t = \frac{(C_o - C_t)V}{W} \quad (3)$$

where q_t represents amount of dye adsorbed at time 't', C_t indicates the concentration of dye at time 't'.

RESULTS AND DISCUSSION

XRD studies: The PXRD spectra of the synthesized hierarchically porous ternary CaNiAl-LDH before and after sorption of Congo red dye are shown in Fig. 1. The characteristics pattern of the typical layered double hydroxide structure was exhibited in pristine CaNiAl-LDH. The peaks observed at 2θ values 11.34°, 22.94°, 34.88°, 39.17°, 46.48°, 60.75°, 62.17° were attributed to corresponding indexed plane 003, 006, 009, 015, 018, 110, 113, respectively [16]. A well-crystalline character of the as-synthesised sample is further supported by a strong reflection in the XRD spectrum. However, the evaluated values of $a = 0.3$ nm and $c = 2.34$ nm based on expressions ($a = 2d_{110}$, $c = 3d_{003}$) were found almost constant for CaNiAl-LDH and CaNiAl-LDH-Congo red. Since, the shifting of peaks was not observed after the adsorption of Congo red dye, thus it can be anticipated that sorption takes place on the external surface rather than intercalation on the interlamellar spaces [17].

FT-IR studies: The identification of surface functionalities was performed by FT-IR analysis as shown in Fig. 2. The broad band at 3489 cm^{-1} arises due to -OH stretching vibration of water molecule. Another band detected at 1641 cm^{-1} is attributed to the bending vibration of -OH group. A sharp absorption peak at 1370 is assigned to the interlayer NO_3^- ion and the low intensity band between 800-600 cm^{-1} was noticed due to M-O stretching vibration (Ca-O, Al-O, Ni-O). After adsorption of Congo red molecule, the spectrum of CaNiAl-LDH-Congo red manifested two small new peaks at 1043 cm^{-1} and

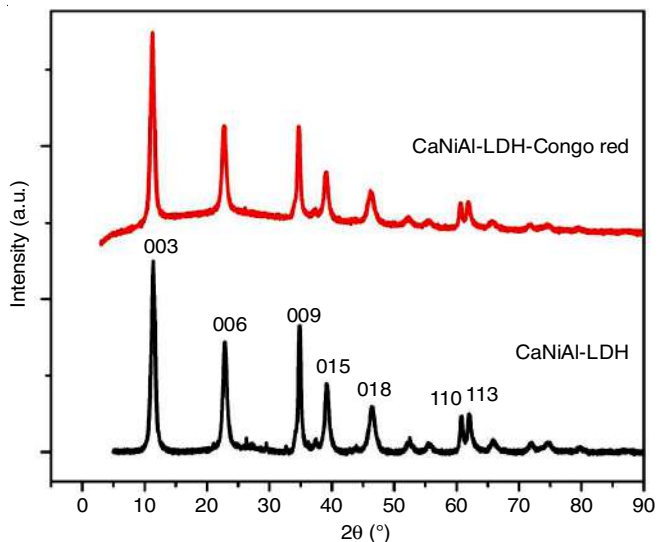


Fig. 1. P-XRD spectra of CaNiAl-LDH before and after adsorption of Congo red dye

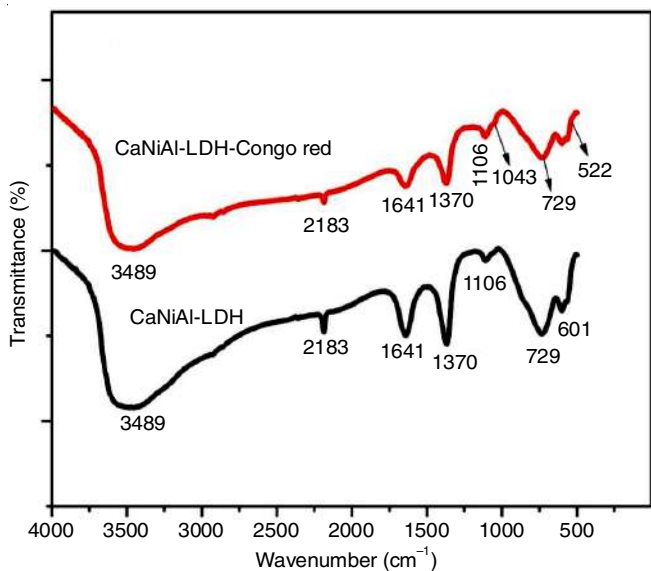


Fig. 2. FT-IR spectra of CaNiAl-LDH before and after adsorption of Congo red dye

522 cm^{-1} , which confirms that sorption of Congo red dye molecules over the surface of adsorbent occurred. In addition, the intensity of the peaks also reduced after adsorption in comparison to pristine CaNiAl-LDH. Thus, the result was consistent and strongly suggests the active role of surface functional groups during the adsorption of targeted pollutants [18,19].

Adsorption-desorption isotherms: Fig. 3 illustrates the N_2 -adsorption-desorption isotherms of ternary CaNiAl-LDH; while the insets of Fig. 3 showed the pore size distribution curve determined based on BJH method of the sample. The isotherm curve is consistent with type-IV isotherm and H_3 -hysteresis loop, which signifies the presences of mesopores on the material. In Fig. 3, it is observed that the isotherm curve generates slowly at higher relative pressure ($P/P_0 < 0.8$), which depicts the inter particle mesoporosity of CaNiAl-LDH. The specific surface area, pore size and pore volume of the as synthesized sample were 58.45 m^2/g , 3.85 nm and 0.106 cc/g , respectively [20].

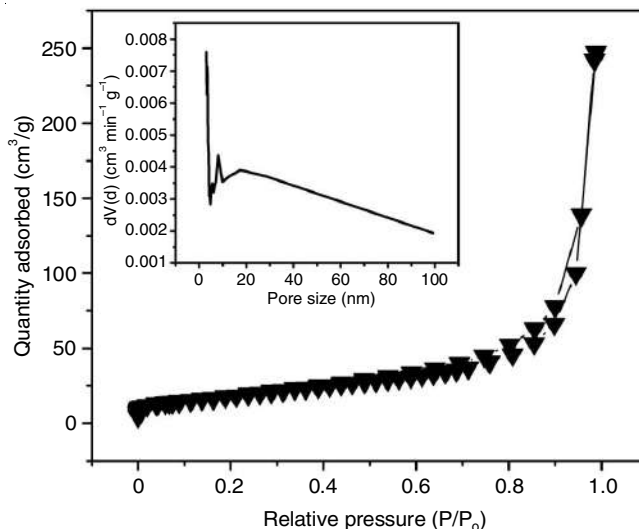


Fig. 3. N_2 -adsorption-desorption isotherm curve of CaNiAl-LDH

Thermal studies: The mass decomposition of the synthesized CaNiAl-LDH sample was studied by thermogravimetric analysis. The TGA curve (Fig. 4) shows that mass losses takes place at three different stages. The initial mass loss of 11.62% in the region between 30-220 $^\circ\text{C}$ was observed due to the elimination of physio adsorbed water molecule. The highest mass loss of 19.07% takes place in the second step around (220-574 $^\circ\text{C}$), which can be ascribed to the removal of interlayer ions such as NO_3^- , CO_3^{2-} , Cl^- . Moreover, the final stage of mass loss (4.4%) arises between 574-721 $^\circ\text{C}$, where the layered structure of CaNiAl-LDH gets completely destroyed and beyond 720 $^\circ\text{C}$, the curve appears to be a constant straight line without further mass loss [21].

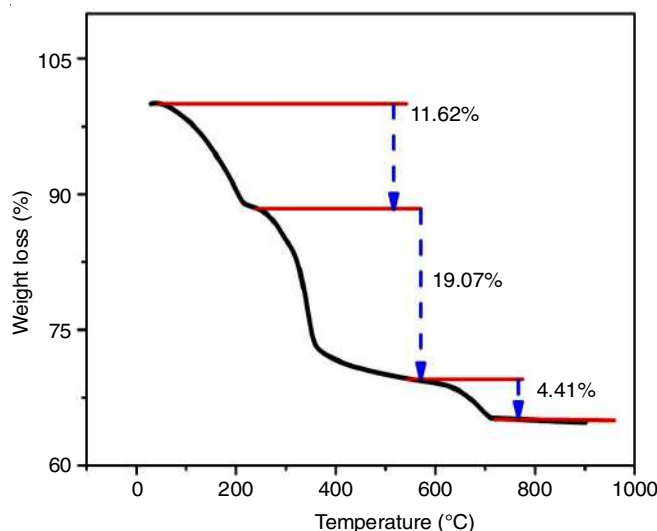


Fig. 4. TGA profile of the adsorbent CaNiAl-LDH

Morphology studies: The SEM images of pristine CaNiAl-LDH at different resolution (100 nm, 200 nm, 1 μm) are shown in Fig. 5. The synthesized hierarchically porous ternary LDH showed smooth structure with circular and flower petals like shape with an average size below 300 nm. The uniform distribution of the LDH particle over the adsorbent

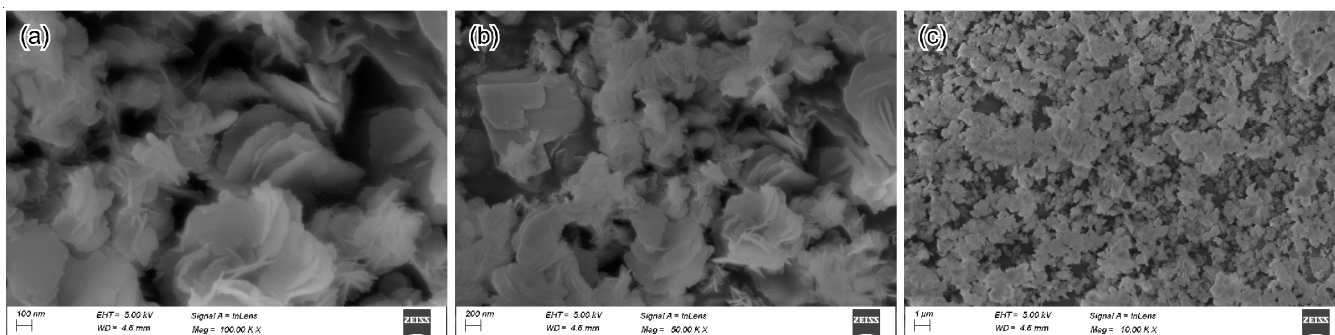


Fig. 5. SEM images of the adsorbent at different magnifications (10 K \times , 50 K \times and 100 K \times)

surface can be ruled out (Fig. 5c), which also reflect the formation of characteristics LDH platelets with many pores existing in it, which could be responsible and contributes in the good adsorption performance of the material [22,23].

Adsorption isotherm: In isotherm studies the three most widely used models namely Langmuir [24], Freundlich [25] and Temkin [26] were employed for investigating the sorption behaviour of Congo red dye on to ternary CaNiAl-LDH. Based on Langmuir model, it assumes that adsorption of the solute molecules over the homogeneous surface takes place through the formation of monolayer, while the Freundlich model explains the adsorption process where development of multiple layer occurs in the heterogeneous surface. The non-linear expression for Langmuir, Freundlich and Temkin model are given as:

$$q_e = \frac{q_{\max} C_e K_L}{1 + K_L C_e} \quad (4)$$

$$q_e = K_f C_e^{1/n} \quad (5)$$

$$q_e = B_T \ln(K_T C_e) \quad (6)$$

where C_e (mg/g) is the equilibrium concentration of dye solution; q_m is the maximum monolayer adsorption capacity, K_L and K_f are the Langmuir constant and Freundlich constant, respectively. The index 'n' indicates the intensity of adsorption; B_T and K_T are the Temkin constant, which signifies heat of adsorption and equilibrium binding constant.

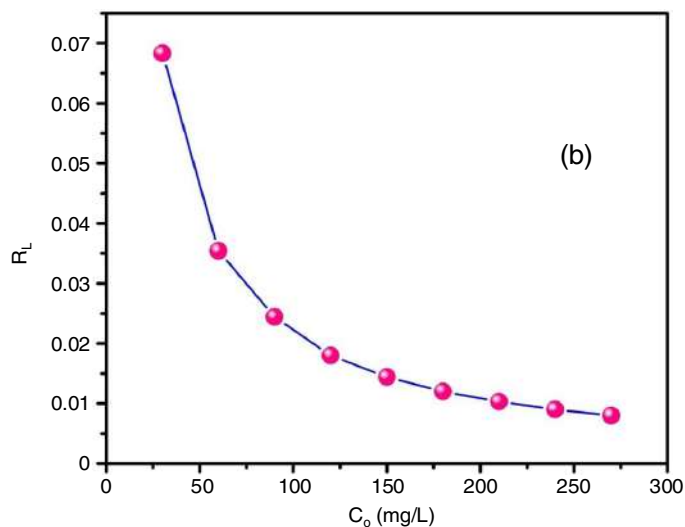
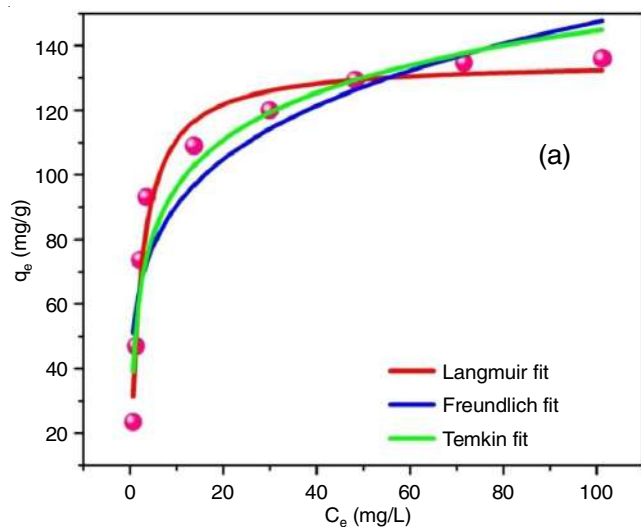


Fig. 6. (a) Non-linear adsorption isotherm curves based on Langmuir, Freundlich and Temkin models, (b) Graph of R_L vs. C_0 plot

Fig. 6 demonstrates the non-linear fitting of adsorption isotherms data for the sorption of Congo red dye molecules on to CaNiAl-LDH. The isotherm parameters are listed in Table-1. It is observed that the coefficient of determination for Langmuir ($R^2 = 0.972$) was found higher than other isotherm models such as Freundlich ($R^2 = 0.850$) and Temkin ($R^2 = 0.926$). The maximum monolayer adsorption capacity ($q_{\max} = 135.21$ mg/g) value was evaluated from Langmuir model. The adsorption of Congo red dye on to CaNiAl-LDH was more suitable and can be best described according to Langmuir model, which shown

TABLE-1 ADSORPTION ISOTHERM PARAMETERS DETERMINED BY LANGMUIR, FREUNDLICH AND TEMKIN MODELS		
Isotherm model	Isotherm constant	Values
Langmuir	q_{\max} (mg/g)	135.21
	K_L (L/mg)	0.4543
	R^2	0.972
	χ^2	44.62
Freundlich	K_f (mg/g)(L/mg) $^{1/n}$	55.59
	n	4.72
	R^2	0.850
	χ^2	245.09
Temkin	B_T	21.07
	K_T	9.581
	R^2	0.926
	χ^2	120.43

that adsorption was more likely to occur through single layer development.

The feasibility of the adsorption process was predicted by a separation factor (R_L), which can be estimated by the following equation:

$$R_L = \frac{1}{1 + K_L C_0} \quad (7)$$

The evaluated value of R_L lies in the range of 0-1 for all initial dye concentration (30-270 mg/L). Thus, the obtained results indicated that adsorption was favourable [27].

Adsorption kinetics: To understand the adsorption rate of Congo red dye and the dynamics associated during the process, the kinetics studies was executed. The kinetic models applied for investigating Congo red dye adsorption on to the synthesized CaNiAl-LDH were pseudo-first order [28], pseudo-second order [29], intraparticle diffusion [30] and Elovich model [31]. The linearized equation for the respective models are given by:

$$\log(q_e - q_t) = \log q_e - \frac{K_1 t}{2.303} \quad (8)$$

$$\frac{1}{q_t} = \frac{1}{K_2 q_e^2} + \frac{t}{q_e} \quad (9)$$

$$q_t = K_1 t^{0.5} + C \quad (10)$$

$$q_t = \frac{1}{\beta} \ln(\alpha\beta) + \frac{1}{\beta} \ln(t) \quad (11)$$

where q_e is the quantity of dye adsorbed at equilibrium (mg g^{-1}); q_t indicates the quantity of dye adsorbed at time t (mg g^{-1}); K_1 represents intraparticle diffusion constant and C is the boundary layer thickness.

The kinetics parameters for Congo red dye adsorption are summarized in Table-2. The best fitting of the kinetic model was determined by comparing the coefficient of determination (R^2) value. It is obvious that R^2 value (0.919) for pseudo-first order was lower than pseudo-second order (0.998), which indicates the more suitability of experimental data based on pseudo-second order model. The experimental q_e (mg/g) value was

also close to q_{e2} (mg/g) than q_{e1} (mg/g). Thus, the adsorption kinetics can be well explained with pseudo-second order model and thereby indicating the presences of chemisorptions [32].

Fig. 7c displayed the intraparticle diffusion plot (q_t vs. $t^{0.5}$), which showed the presences of multiple stages during the sorption of Congo red dye molecules. The q_t value between ($t_{0.5} = 0.385-0.833$) increased quickly, while in the middle region bending of curves occurs due to diffusion into external pores. At the last stage, it tends to a constant straight line due to the achievement of equilibrium. Since, the plot of q_t vs. $t^{0.5}$ did not pass through the origin, therefore the intraparticle diffusion is not the rate limiting step [33].

Similarly, based on Elovich model, the determined value of adsorption rate (α) and desorption rate (β) were found to be 0.128 and 0.321, respectively. The coefficient of determination value ($R^2 = 0.923$) also further suggests the applicability of this model [34].

Effect of contact time: The effect of contact time plays a key role in dye uptake. The removal efficiency of the adsorbate species as a function of contact time was investigated by fixing the experimental conditions with 50 mg/L initial concentration, 0.025 g dosages and contact time of 260 min, respectively. As shown in Fig. 8a, it is apparent that the adsorption rate occurs rapidly at the first 70 min where adsorption capacity (q_t) reaches up to 31.62 mg/g. This can be explained due to the easily available active site at the initial stage of contact time, which is followed by the steric repulsion of incoming Congo red dye molecules on the sorption site, thereby leading to the equilibrium stage after 175 min [35].

Effect of adsorbent dosages: Estimating the optimal dosages is critical for maintaining a cost-effective system. To investigate the effect of doses, the amount of adsorbent was varied from 0.005 g to 0.03 g at an initial dye concentration of 50 mg/L. The quantity of dye adsorbed (q_e) decreases from 170.16 to 32.44 mg/g and the removal percentage elevates from 85.08 to 97.34%. After 0.02 g dosages the removal efficiency does not increase significantly and remains constant (Fig. 8b). It is due to the fact that further increase in the applied adsorbent quantity may results in the accumulation of LDH particles which will not promote sorption of Congo red dye [36].

Effect of initial dye concentration: The effect of initial dye concentration is an important parameter and provides the essential driving force for adsorbing Congo red dye ions over the surface of adsorbents. Fig. 9a displayed the influence of initial dye concentration (30 to 270 mg/L) with 0.025 g dosages on the adsorption of Congo red dye molecules on to CaNiAl-LDH. Initially, high adsorption efficiency (97.77%) was observed at low adsorbate concentration due to the freely accessible sorption site, when the concentration of Congo red dye solution increases, the saturation on the adsorbent surfaces steadily decreases the removal efficiency [37].

Effect of pH: In present study, Congo red dye dye was selected as adsorbate and considering the effect of pH, the adsorption % were analyzed under pH 4, 7 and 10. The maximum removal % at pH 4, 7, 10 corresponding to the initial dye concentration (30 mg/L) were 97, 95.7 and 80%, respectively. Under acidic pH 4, the surface of CaNiAl-LDH bears the

TABLE-2
KINETIC PARAMETERS FOR THE ADSORPTION
OF CONGO RED DYE ON To CaNiAl-LDH

Kinetic model	Parameters	Values
Pseudo-first order	q_{exp}	38.396
	q_{e1} (mg/g)	18.927
	$K_1 \times 10^{-2}$ (min^{-1})	1.156106
	R^2	0.919
Pseudo-second order	q_{e2}	41.152
	$K_2 \times 10^{-3}$ ($\text{g mg}^{-1} \text{min}^{-1}$)	1.072451
	R^2	0.998
Intraparticle diffusion	K_1 (mg/g min^{-1})	1.620
	C (mg/g)	15.245
	R^2	0.774
Elovich	β	0.3215
	α	0.1284
	R^2	0.923

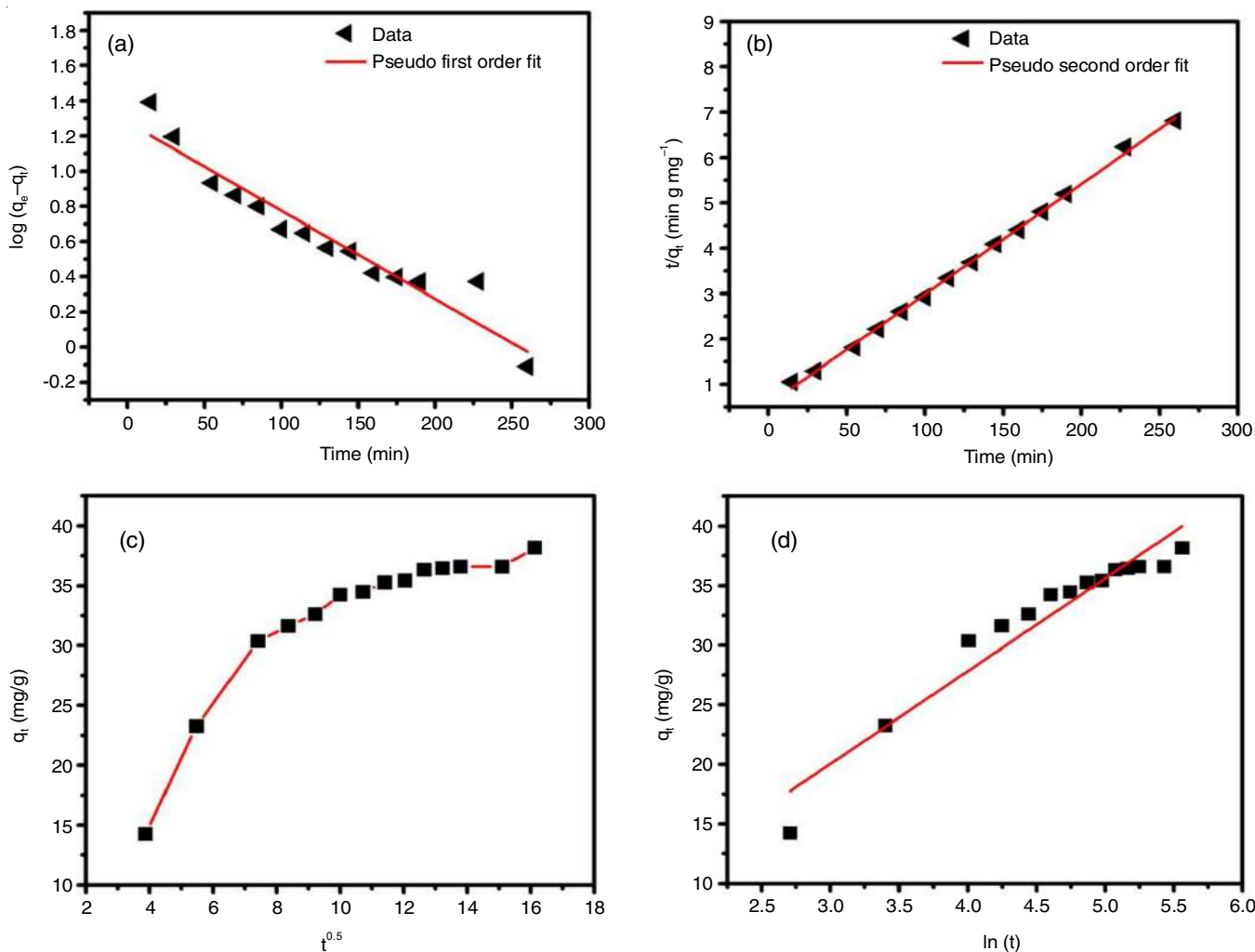


Fig. 7. Adsorption kinetic plots of Congo red sorption on to CaNiAl-LDH: (a) pseudo-first order, (b) pseudo-second order, (c) intraparticle diffusion and (d) Elovich plot

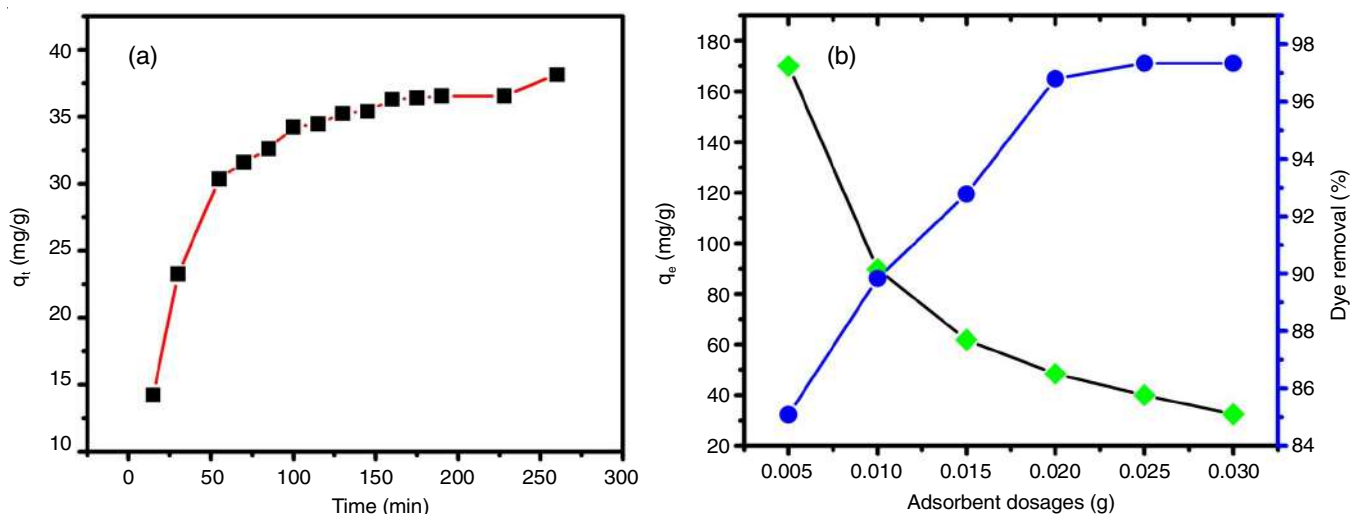


Fig. 8. Effect of contact time (a) and adsorbent dosages (b) on Congo red dye uptake by the adsorbent CaNiAl-LDH

additional positive charge due to protonation (H_3O^+) from the solution (Fig. 9b). As a result, the electrostatic attraction between anionic Congo red dye ions and the positive charge LDH surfaces increases the sorption efficiency. On the contrary, at

basic pH due to the presence of competing negatively charged OH^- ions, the adsorption of excess Congo red dye ions on the active site declines. Thus, the pH of the solution during the studies had shown notable effect [38].

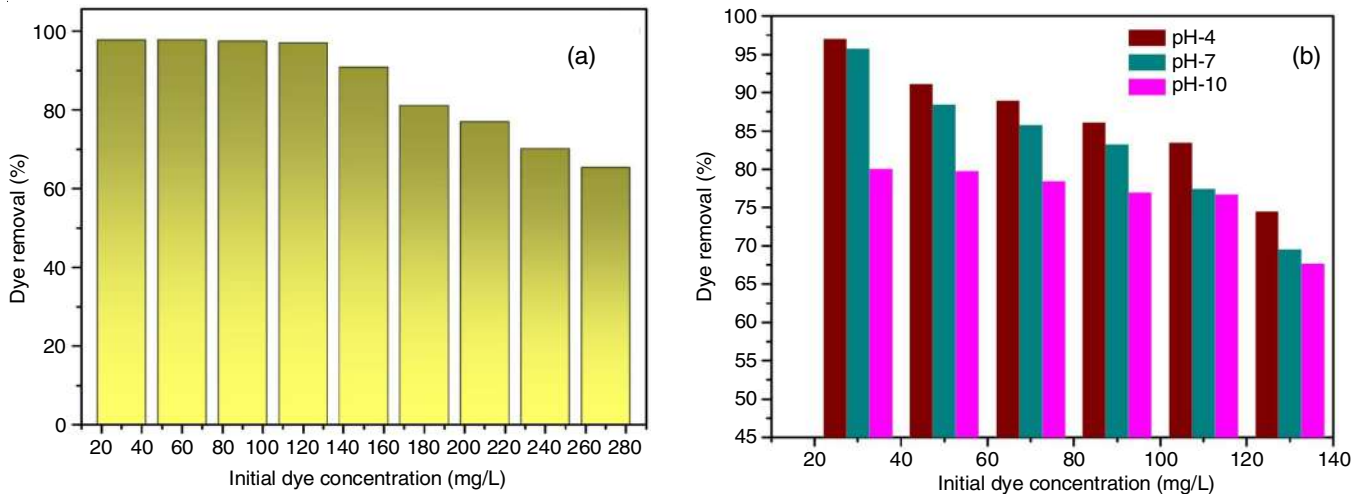


Fig. 9. Effect of initial concentration (a) and pH (b) on the percentage removal of Congo red dye

Thermodynamic studies: The thermodynamic studies were carried out for the adsorptive removal of Congo red dye ions at various temperature (30, 40, 50 °C) using ternary CaNiAl-LDH adsorbents. The thermodynamic parameters such as Gibbs free energy (ΔG), enthalpy (ΔH) and entropy (ΔS) provide essential information regarding the feasibility of adsorption process. As a result, the estimation of these parameters was executed by using the following equations [39]:

$$\ln K_d = \frac{\Delta S}{R} - \frac{\Delta H}{RT} \quad (12)$$

$$\Delta G = -RT \ln K_d \quad (13)$$

where K_d indicates adsorption distribution coefficient and R denotes the universal gas constant. The values of enthalpy change (ΔH) and entropy change (ΔS) was measured from the slope and intercept of the graph $\ln K_d$ vs. $1/T$ (K^{-1}), respectively. The vant Hoff's plot was displayed in Fig. 10a and the obtained thermodynamic parameters are listed in Table-3. The negative value of ΔG implies that Congo red dye adsorption onto the CaNiAl-LDH was spontaneous and feasible process. As the temperature increased from 313 K to 333 K, ΔG value was found to decrease from -2.14 KJ/mol to -6.31 KJ/mol, thereby indicating the favourable adsorption process at higher temperature. However, the positive value of ΔH and ΔS , both demonstrated the endothermic nature of adsorption and increase in the randomness of the solid-liquid interfaces, respectively. The calculated ΔH value (63.10 KJ/mol) in the current research falls within the range for chemisorption processes, which typically have ΔH values between 80 and 200 KJ/mol. Therefore, it is hypothesized that the process of Congo red dye adsorption on CaNiAl-LDH will occur through physisorption [40].

Comparison with reported adsorbents: In previous report, various modified LDH listed in Table-4 showed the removal of Congo red dye from an aqueous solution. However, in recent studies, it is notable that the use of ternary CaNiAl-LDH exhibits greater adsorption capacity (135.21 mg/g) when compared to other adsorbents such as Mg-Fe-Al-LDH, MgAl-LDH, MNPs@NiFe-LDH and DS-Zn-Y hydroxide [41-48]. Therefore, the comparative result shows the feasibility of

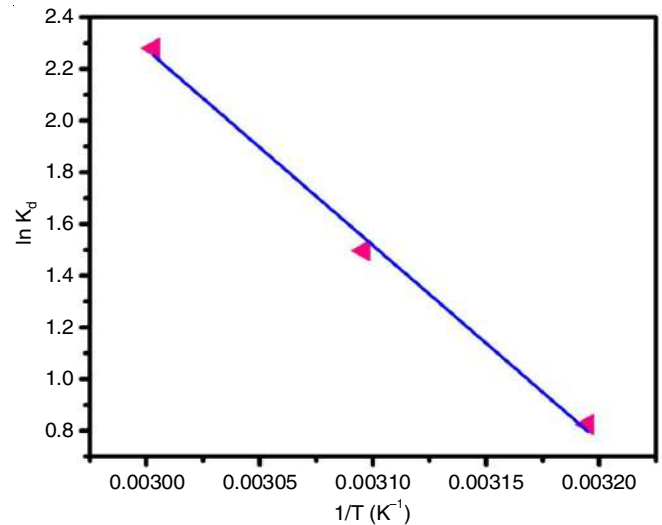


Fig. 10. vant-Hoff plot for estimation of various thermodynamic parameters in the sorption of Congo red dye

TABLE-3
CALCULATED THERMODYNAMIC PARAMETERS
FOR THE CaNiAl-LDH-CR SYSTEM

Adsorbent	+ ΔH (KJ/mol)	+ ΔS (J/mol)	- ΔG (KJ/mol)		
			313 K	323 K	333 K
CaNiAl-LDH	63.038	208.032	2.14	4.02	6.31

TABLE-4
LIST OF REPORTED LDH BASED SORBENTS WITH
THEIR q_{max} VALUE FOR CONGO RED REMOVAL

Adsorbents	q_{max} (mg/g)	Ref.
MgAl-LDH	111.11	[40]
LDH-EDTA-AM	632.9	[41]
Mg-Fe-Al-LDH	11	[42]
ZnAl-LDH	571.43	[43]
Mg-Fe-CO ₃ -LDH	104.6	[44]
MNPs@NiFe-LDH	79.6	[45]
β -Ni(OH) ₂ / γ -Fe ₂ O ₃ /NiFe-LDH	98.6-142.4	[46]
DS-Zn-Y hydroxide	96.24	[47]
MgAl-LDH/ γ -AlO(OH)/C	447	[48]
CaNiAl-LDH	135.21	This work

CaNiAl-LDH as an effective adsorbent in Congo red dye removal.

Reusability: To determine the potentiality of the proposed adsorbents on industrial applications, the reusability test in the adsorption process was examined. For good adsorbents, the repeated use does not significantly decline its affinity towards targeted contaminants. In present studies, the reusability test was investigated up to fifth cycle. Fig. 11 revealed that the removal efficiency decreases from 95.73% to 75.99% as the recycle proceeds from first to last cycle. However, it is observed that the high sorption % of adsorbate molecules up to 75.99% was maintained even after fifth cycle, which shows its excellent performance for Congo red dye sorption. The slight decrease in removal percentage after successive use might be attributed to the loss of active site during regeneration.

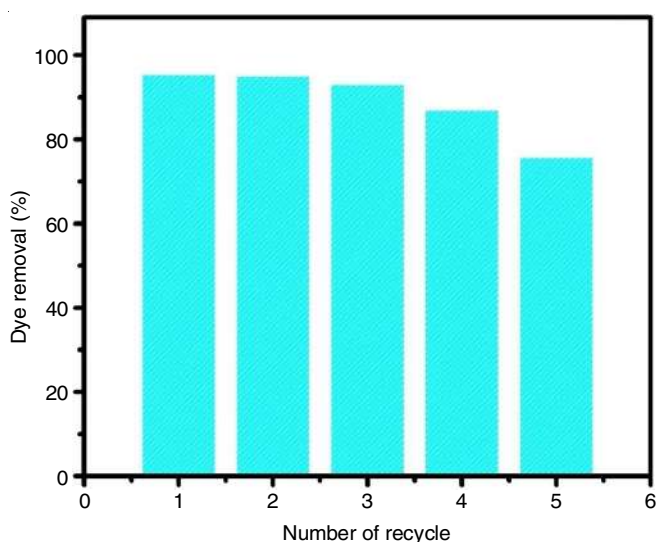


Fig. 11. Reusability efficiency of ternary CaNiAl-LDH in the removal of Congo red dye from an aqueous solution

Conclusion

In summary, a ternary CaNiAl-LDH was synthesized by urea hydrolysis method and applied for the treatment of aqueous solution by selecting Congo red dye as a targeted pollutant. The unique physico-chemical properties of the proposed adsorbent CaNiAl-LDH such as porosity, high surface area and flower shaped LDH particles have contributed for the enhance sorption of Congo red dye. Moreover, the isotherm and kinetics data fitted well according to the Langmuir and pseudo-second order kinetic models. In addition, the main factor responsible for the adsorption of Congo red dye is due to the electrostatic attraction between the positively charged brucite sheets of LDH and negatively charged Congo red dye molecules. Thus, the present study sheds light in exploring ternary LDH and suggest that CaNiAl-LDH can be use as an alternative adsorbent for the treatment of dye contaminated wastewater.

ACKNOWLEDGEMENTS

The authors are thankful to several institutes for providing instrumental facility for characterization of material with SEM, BET and powder X-ray from CIF, IIT Guwahati, FT-IR from

Cotton University and thermogravimetric analysis from North East Hill University, Shillong, India

CONFLICT OF INTEREST

The authors declare that there is no conflict of interests regarding the publication of this article.

REFERENCES

- W.-W. Li, H.-Q. Yu and B.E. Rittmann, *Nature*, **528**, 29 (2015); <https://doi.org/10.1038/528029a>
- D. Iark, A.J.R. Buzzo, J.A.A. Garcia, V.G. Côrrea, C.V. Helm, R.C.G. Corrêa, R.A. Peralta, R.F. Peralta Muniz Moreira, A. Bracht and R.M. Peralta, *Bioresour. Technol.*, **289**, 121655 (2019); <https://doi.org/10.1016/j.biortech.2019.121655>
- S.S. Yang, J.H. Kang, T.R. Xie, D.F. Xing, N.Q. Ren, S.H. Ho and W.M. Wu, *J. Clean. Prod.*, **227**, 33 (2019); <https://doi.org/10.1016/j.jclepro.2019.04.005>
- A.B. Fradj, A. Boubakri, A. Hafiane and S.B. Hamouda, *Results in Chemistry*, **2**, 100017 (2020); <https://doi.org/10.1016/j.rechem.2019.100017>
- C.Y. Teh, P.M. Budiman, K.P.Y. Shak and T.Y. Wu, *Ind. Eng. Chem. Res.*, **55**, 4363 (2016); <https://doi.org/10.1021/acs.iecr.5b04703>
- S. Venkatesh, K. Venkatesh and A.R. Quaff, *J. Appl. Res. Technol.*, **15**, 340 (2017); <https://doi.org/10.1016/j.jart.2017.02.006>
- S.Y. Lee, D. Kang, S. Jeong, H.T. Do and J.H. Kim, *ACS Omega*, **5**, 4233 (2020); <https://doi.org/10.1021/acsomega.9b04127>
- A.K. Badawi, M. Abd Elkodous and G.A.M. Ali, *RSC Adv.*, **11**, 36528 (2021); <https://doi.org/10.1039/D1RA06892J>
- Y. Tanimoto and S.I. Noro, *RSC Adv.*, **11**, 23707 (2021); <https://doi.org/10.1039/D1RA03348D>
- R.A. El-Ghany Mansour, M.G. Smeda and A.A. Zaatout, *RSC Adv.*, **11**, 7851 (2021); <https://doi.org/10.1039/D0RA08488C>
- G.Ö. Kayan and A. Kayan, *J. Polym. Environ.*, **29**, 3477 (2021); <https://doi.org/10.1007/s10924-021-02154-x>
- S. Radoor, J. Karayil, A. Jayakumar, D. Nandi, J. Parameswaranpillai, J. Lee, J.M. Shivanna, R. Nithya and S. Siengchin, *J. Polym. Environ.*, **30**, 3279 (2022); <https://doi.org/10.1007/s10924-022-02421-5>
- P. Huang, J. Liu, F. Wei, Y. Zhu, X. Wang, C. Cao and W. Song, *Mater. Chem. Front.*, **1**, 1550 (2017); <https://doi.org/10.1039/C7QM00079K>
- M. Khorshidi, S. Asadpour, N. Sarmast and M. Dinari, *J. Mol. Liq.*, **348**, 118399 (2022); <https://doi.org/10.1016/j.molliq.2021.118399>
- M. Daud, A. Hai, F. Banat, M.B. Wazir, M. Habib, G. Bharath and M.A. Al-Harhi, *J. Mol. Liq.*, **288**, 110989 (2019); <https://doi.org/10.1016/j.molliq.2019.110989>
- L. Jafari Foruzin, Z. Rezvani and B. Habibi, *Appl. Clay Sci.*, **188**, 105511 (2020); <https://doi.org/10.1016/j.clay.2020.105511>
- G. Rathee, N. Singh and R. Chandra, *ACS Omega*, **5**, 2368 (2020); <https://doi.org/10.1021/acsomega.9b03785>
- T.R.R. Timóteo, C.G. Melo, L.J.A. Danda, L.C.P.B.B. Silva, D.A.F. Fontes, P.C.D. Silva, C.S.B. Aguilera, L.P. Siqueira, L.A. Rolim and P.J. Rolim Neto, *Appl. Clay Sci.*, **180**, 105197 (2019); <https://doi.org/10.1016/j.jclay.2019.105197>
- D. Bharali and R.C. Deka, *J. Environ. Chem. Eng.*, **5**, 2056 (2017); <https://doi.org/10.1016/j.jece.2017.04.012>
- S.S. Ravuru, A. Jana and S. De, *J. Hazard. Mater.*, **373**, 791 (2019); <https://doi.org/10.1016/j.jhazmat.2019.03.122>
- M.A. Iqbal, L. Sun and M. Fedel, *SN Appl. Sci.*, **1**, 1415 (2019); <https://doi.org/10.1007/s42452-019-1474-4>

22. Z. Wang, L. Zhang, P. Fang, L. Wang and W. Wang, *ACS Omega*, **5**, 21805 (2020); <https://doi.org/10.1021/acsomega.0c02875>
23. H. Lv, H. Rao, Z. Liu, Z. Zhou, Y. Zhao, H. Wei and Z. Chen, *J. Energy Storage*, **52B**, 104940 (2022); <https://doi.org/10.1016/j.est.2022.104940>
24. I. Langmuir, *J. Am. Chem. Soc.*, **40**, 1361 (1918); <https://doi.org/10.1021/ja02242a004>
25. H. Freundlich, *J. Phys. Chem.*, **57**, 385 (1906).
26. M.I. Temkin and V. Pyzhev, *Acta Physicochimica URSS*, **12**, 327 (1940).
27. M.K. Raman and G. Muthuraman, *Asian J. Chem.*, **31**, 1255 (2019); <https://doi.org/10.14233/ajchem.2019.21772>
28. S. Lagergren, *K. Sven. Vetensk. Akad. Handl.*, **24**, 1 (1898).
29. Y.S. Ho and G. McKay, *Chem. Eng. J.*, **70**, 115 (1998); [https://doi.org/10.1016/S0923-0467\(98\)00076-1](https://doi.org/10.1016/S0923-0467(98)00076-1)
30. W.J. Weber and J.C. Morris, *J. Sanit. Eng. Div.*, **89**, 31 (1963).
31. J.R. Guarin, J.C. Moreno-Pirajan and L. Giraldo, *J. Chem.*, **2018**, 2124845 (2018); <https://doi.org/10.1155/2018/2124845>
32. J.M. Jabar, Y.A. Odusote, K.A. Alabi and I.B. Ahmed, *Appl. Water Sci.*, **10**, 136 (2020); <https://doi.org/10.1007/s13201-020-01221-3>
33. F.C. Wu, R.L. Tseng and R.S. Juang, *Chem. Eng. J.*, **153**, 1 (2009); <https://doi.org/10.1016/j.cej.2009.04.042>
34. F.C. Wu, R.L. Tseng and R.S. Juang, *Chem. Eng. J.*, **150**, 366 (2009); <https://doi.org/10.1016/j.cej.2009.01.014>
35. H.T.N. Thi, D.C. Nguyen, T.T. Nguyen, V.T. Tran, H.V. Nguyen, L.G. Bach, D.V.N. Vo, D.H. Nguyen, D.V. Thuan, S.T. Do and T.D. Nguyen, *Key Eng. Mater.*, **814**, 463 (2019); <https://doi.org/10.4028/www.scientific.net/KEM.814.463>
36. D. Maiti, S. Mukhopadhyay and P.S. Devi, *ACS Sustain. Chem. Eng.*, **5**, 11255 (2017); <https://doi.org/10.1021/acssuschemeng.7b01684>
37. K.L. Muedi, V. Masindi, J.P. Maree, N. Haneklaus and H.G. Brink, *Nanomaterials*, **12**, 776 (2022); <https://doi.org/10.3390/nano12050776>
38. A. Li, H. Deng, C. Ye and Y. Jiang, *ACS Omega*, **5**, 15152 (2020); <https://doi.org/10.1021/acsomega.0c01092>
39. B. Priyadarshini, T. Patra and T.R. Sahoo, *J. Magnes. Alloys*, **9**, 478 (2021); <https://doi.org/10.1016/j.jma.2020.09.004>
40. R. Lafi, K. Charradi, M.A. Djebbi, A.B. Haj Amara and A. Hafiane, *Adv. Powder Technol.*, **27**, 232 (2016); <https://doi.org/10.1016/j.apt.2015.12.004>
41. J. Li, H. Yu, X. Zhang, R. Zhu and L. Yan, *Front. Environ. Sci. Eng.*, **14**, 52 (2020); <https://doi.org/10.1007/s11783-020-1229-x>
42. H.A. Tabti, B. Medjahed, M. Boudinar, A. Kadeche, N. Bouchikhi, A. Ramdani, S. Taleb and M. Adjdir, *Res. Chem. Intermed.*, **48**, 2683 (2022); <https://doi.org/10.1007/s11164-022-04722-9>
43. S. Chilukoti and T. Thangavel, *Inorg. Chem. Commun.*, **100**, 107 (2019); <https://doi.org/10.1016/j.inoche.2018.12.027>
44. I.M. Ahmed and M.S. Gasser, *Appl. Surf. Sci.*, **259**, 650 (2012); <https://doi.org/10.1016/j.apsusc.2012.07.092>
45. T. Taher, R. Putra, N. Rahayu Palapa and A. Lesbani, *Chem. Phys. Lett.*, **777**, 138712 (2021); <https://doi.org/10.1016/j.cplett.2021.138712>
46. C. Suppasso, N. Pongkan, S. Intachai, M. Ogawa and N. Khaorapapong, *Appl. Surf. Sci.*, **213**, 106115 (2021); <https://doi.org/10.1016/j.clay.2021.106115>
47. P. Chakraborty and R. Nagarajan, *Appl. Surf. Sci.*, **118**, 308 (2015); <https://doi.org/10.1016/j.clay.2015.10.011>
48. J. Li, N. Zhang and D.H.L. Ng, *J. Mater. Chem. A.*, **3**, 21106 (2015); <https://doi.org/10.1039/C5TA04497A>



NATIONAL CONFERENCE
ON

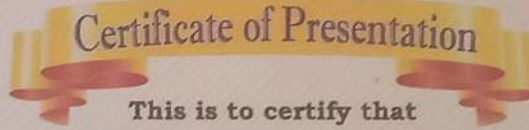
SCIENCE & TECHNOLOGY FOR SUSTAINABLE DEVELOPMENT
(STSD-2022)

Organized jointly by

SCIENCE COLLEGE, KOKRAJHAR & VIJNANA BHARATI, NESM

In collaboration with

IASST, Guwahati, India & NECTAR, Shillong, India



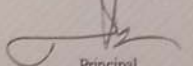
This is to certify that

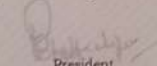
Mr. Deepmoni Brahma

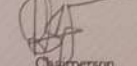
of

Bodoland University, Kokrajhar

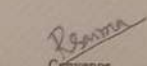
has presented a paper entitled "*Synthesis of ZrO₂/MgAl-LDH composites and evaluation of its isotherm, kinetics and thermodynamic properties in the adsorption of congo red dye*" in the National Conference on "Science & Technology for Sustainable Development (STSD-2022)" held on 9th-10th September, 2022 at Science College, Kokrajhar, Assam, India.

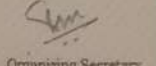

Principal
Science College, Kokrajhar


President
Vijnana Bharati, NESM


Chairperson
National Conference
STSD-2022


Convener
National Conference
STSD-2022


Convener
National Conference
STSD-2022


Organizing Secretary
National Conference
STSD-2022



National Conference on
Advances in Sustainable Chemistry and Material Science
(ASCMS-2022)



Paper Presentation Certificate

This is to certify that

Prof./Dr./Mr./Ms. Deepmoni Brahma of
Bodoland University, Kokrajhar has made oral
presentation on the topic entitled "Surfactants assisted synthesis of CuAl/SDS-LDH
and its adsorptive removal of Methyl Red dye from aqueous solution" in the National
Conference on Advances in Sustainable Chemistry and Material Science-2022 held on 29th & 30th
April 2022 in the Department of Chemistry, Bodoland University, Kokrajhar, Assam, India.

Prof. Laishram Ladu Singh
(Vice Chancellor)

Dr. Manil Basumatary
(Chairperson)

Dr. Sanjay Basumatary
(Convenor)

Dr. Dhruvajyoti Haloi
(Convenor)

Dr. Hemabhabha Saikia
(Convenor)



INTERNATIONAL CONFERENCE

on



EMERGING TRENDS IN NANOMATERIALS SCIENCE AND TECHNOLOGY
(ICETNMST-2022)

January 27 – 29, 2022

Organized by

DEPARTMENT OF SCIENCE AND HUMANITIES, NATIONAL INSTITUTE OF TECHNOLOGY NAGALAND

(An Institute of National Importance)

Certificate of Participation

*This is to certify that **Deepmoni Brahma** has presented an Oral entitled “Synthesis of ternary canial-layered double hydroxide as a potential adsorbent and its effective removal of congo red dye from aqueous solution” in the International Conference on Emerging Trends in Nanomaterials Science and Technology (ICETNMST-2022) held during 27-29 Jan, 2022 organized by the Department of Science and Humanities, National Institute of Technology Nagaland, India.*

Dr. S. Venugopal
Patron

Dr. Jyoti Prasad Borah
Convenor

Dr. Amrit Puzari
Convenor



SLC (University of Delhi)
SHYAM LAL COLLEGE
NAAC ACCREDITED A++ & NIRF 68th

International Conference
on
Current Trends in Chemical Sciences for Sustainable Living
Certificate

*This is to certify that Prof./Dr./Mr./Ms. **Deepmoni Brahma** from **Bodoland University, Assam** has participated/presented paper/poster/delivered Invited Lecture on **Coconut Husk Ash Modified CoAl-Layered Double Hydroxide Composite and its Application in Dye Remediation from Aqueous Solution in the “INTERNATIONAL CONFERENCE on CURRENT TRENDS IN CHEMICAL SCIENCES FOR SUSTAINABLE LIVING”** organized by Department of Chemistry under the aegis of IQAC, Shyam Lal College, University of Delhi on 4-5th April 2024.*

Prof. Kusha Tiwari
IQAC, Director

Dr. Reeta Sharma
Convenor

Prof. Rabi Narayan Kar
Principal

**International e-Poster Conference on Current
Outlook in Material Science and Engineering
(COMSE-2k20)
from 15-16th May 2020**

**Organized by
Bodoland University
in Association with
Tripura University, ADP College, Nagaon & MIT Aurangabad
On Facebook**

Certificate of Achievement

*This is to certify that Dr./Mr./Ms. **Deepmoni Brahma** of Department of Chemistry, Bodoland University, Kokrajhar has presented his/her paper entitled as "Synthesis of Layered double hydroxide derived CuAlO mixed metal oxide" in "International e-Poster Conference on Current Outlook in Material Science and Engineering (COMSE-2k20)" on 15-16th May 2020.*



Dr. Dhruba J. Haloi

(Convener)



Dr. Subhendu Bhandari

(Co-Convener)



Dr. Bishnu Prasad Koiry

(Convener)



Dr. Lakshmi K. Singh

(Co-Convener)